APPSBX 38 1–234 (1984)
ISSN 0570-4898

Plasma Polymerization and Plasma Treatment

Editor:
H. K. Yasuda

Journal of Applied Polymer Science: Applied Polymer Symposia
an Interscience® Publication

published by JOHN WILEY & SONS
New York • Chichester • Brisbane • Toronto • Singapore

DISCLAIMER NOTICE

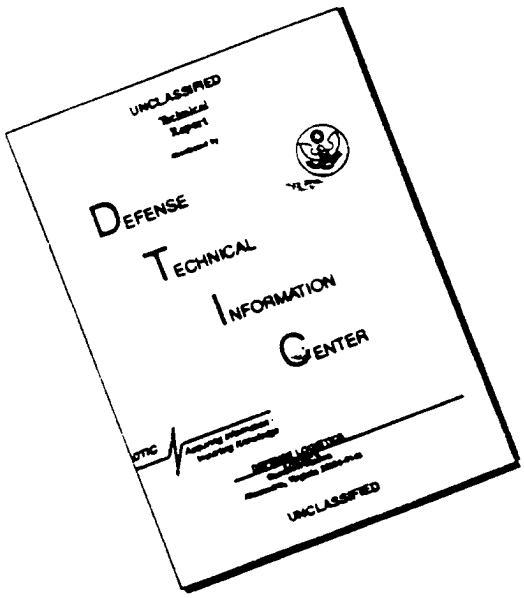

THIS DOCUMENT IS BEST QUALITY AVAILABLE. THE COPY FURNISHED TO DTIC CONTAINED A SIGNIFICANT NUMBER OF PAGES WHICH DO NOT REPRODUCE LEGIBLY.

JOURNAL OF APPLIED POLYMER SCIENCE
Applied Polymer Symposium 38

Plasma Polymerization and Plasma Treatment

Editor:
H. K. Yasuda
Graduate Center for Materials Research
University of Missouri-Rolla
Rolla, Missouri 65401-0249

an Interscience® Publication
published by JOHN WILEY-& SONS

JOURNAL OF APPLIED POLYMER SCIENCE
Applied Polymer Symposia

Professor H. K. Yasuda has been appointed Editor for this Symposium by the Board of Editors of the *Journal of Applied Polymer Science*.

Published by John Wiley & Sons, Inc., this Symposium constitutes a part of the subscription to the *Journal of Applied Polymer Science*, Vol. 29, and as such is supplied without additional charge to the subscribers. This Symposium appears in one volume; additional sets may be purchased from the Subscription Department, John Wiley & Sons, Inc.

Subscription price, *Journal of Applied Polymer Science*, Vol. 29 (1984): $420.00. Postage and handling outside U.S.A.: $54.00 by surface; $255.00 by air. Please allow four to six weeks for processing a change of address. Back volumes, microfilm, and microfiche are available for previous years. Request price list from publisher.

Printed in the United States of America.

Contents

Preface

At the September 1982 National Meeting of the American Chemical Society, held in Kansas City, Missouri, the Organic Coatings and Applied Polymer Science Division sponsored a three-day symposium on "Plasma Polymerization and Plasma Treatment."

A similar symposium was sponsored by the Polymer Division at the Miami Meeting in 1978, organized by Dr. Mitchel Shen. During this four-year period, the scientific community of "Plasma Polymerization" has lost two outstanding scientists, Drs. Mitchel Shen and John Hollahan, who have contributed so much to the research and development of plasma polymerization and its related technology. The symposium at the Kansas City Meeting was dedicated to these two pioneers in this field. The meeting was opened by a moment of silent prayer proposed by the session chairman, Dr. E. Hellmuth, and followed by the tributes to Drs. Shen and Hollahan by Dr. Alex Bell, who himself is one of the leading pioneers and who had the closest association with Drs. Shen and Hollahan.

The symposium consisted of six invited lectures and thirty contributed papers. The six invited lecturers covered a wide range of plasma polymerization. Dr. A. Bell reviewed the latest development in "Plasma-initiated Polymerization of Methyl Methacrylate." Dr. S. Hattori discussed a new emerging technology of the "Application of Plasma Polymerized Film to Electron Beam Lithography." Dr. A. Dilks lectured on "Characterization of Plasma-polymerized Materials by Modern Spectroscopic Techniques." Dr. E. Kay reviewed the inter-related phenomena of polymer formation and etching in plasma under the title of "Fluorocarbon Plasma with Simultaneous Etching and Polymerization." Dr. K. Hayashi was invited to lecture on reaction mechanisms of "Radiation, Photo, and Plasma Induced Polymerization." Unfortunately, due to his illness, Dr. Hayashi could not come to the meeting, and Dr. H. Yasuda delivered a lecture on "Radiation-induced Polymerization" based on Dr. Hayashi's review article. H. Yasuda also reviewed fundamental aspects of "Growth Mechanisms of Polymerization in Vacuum Deposition of Polymers."

The total number of papers presented steadily increased from sixteen at Philadelphia (1975), to twenty at Miami (1978), and to thirty-six at Kansas City (1982), indicating the growing interest in plasma polymerization. The noteworthy shift in the contents of papers may also indicate that plasma polymerization has reached the stage where laboratory curiosity becomes realistic process. More than 50% of papers presented in the previous symposia were mainly concerned with kinetic and mechanistic aspects of plasma polymerization. In contrast to this situation, more than 50% of papers presented at this symposium were focused on properties of plasma polymers and their applications. This trend can also be

Journal of Applied Polymer Science: Applied Polymer Symposium 38, v–vi(1984)

viewed as an indication of healthy growth of plasma polymerization and plasma treatment.

This volume is the result of the collaborative effort by the participants of the symposium. Not all papers presented at the symposium are included in this volume. Some papers had been submitted to publication elsewhere.

As the organizer of the symposium, I hope that this volume will serve as a source of stimulating information for further growth of plasma polymerization and plasma treatment.

H. K. YASUDA
University of Missouri–Rolla

A Tribute to Mitchel Shen and John Hollahan

Mitchel Shen and John Hollahan were well known to many researchers in the field of plasma chemistry. Each was responsible for the publication of a large number of papers and edited volumes, and for the organization of many conferences and symposia. Their efforts helped to shape and define the field, and to gain prominence for it in the eyes of both industrial and academic researchers. It is, therefore, fitting that this symposium be dedicated to their memory and that a few words be said to recall their careers and contributions.

Mitchel Shen was born in Tienjin, China, and emigrated with his parents to Taiwan at the end of World War II. In 1955, he came to the U.S. to begin his undergraduate education in chemistry at St. Francis College in Pennsylvania. He received his B.S. degree in 1959 and then moved to Princeton University for his graduate studies. In 1962, he was awarded an M.S. degree, and the following year, a Ph.D. degree, both in physical chemistry. After completing his Ph.D. work, he stayed on for an additional year at Princeton to work as a postdoctoral fellow with his research director, Professor Tobolsky.

In 1964, Mitchel Shen joined the technical staff of the Chemical Physics Group at the North American Rockwell Science Center in California and began work on a series of projects concerning polymers for the aerospace industry. Following a five-year period at Rockwell, he accepted an invitation to join the Department of Chemical Engineering at the University of California, Berkeley. Appointed initially as an associate professor, he advanced rapidly to the rank of full professor in 1973. Professor Shen remained at Berkeley until his death in 1979.

Mitchel Shen had a broad interest in polymer physical chemistry and was known for his contributions to several areas. His program encompassed work on rubber elasticity, rheology of entangled liquids, membrane properties, polymer alloys, and plasma-deposited polymers. The results of this research were described in over 100 research papers. Professor Shen also coauthored a book entitled "Introduction to Polymer Viscoelasticity" and coedited five other volumes, two of which are on the subject of plasma polymerization. In addition to his many writing and teaching activities, he also found the time to serve on a variety of professional committees and editorial boards, and to serve as Vice Chairman of the Department of Chemical Engineering at Berkeley, from 1976 to 1979. I should also note that Professor Shen was responsible for organizing the first two ACS symposia on plasma polymerization held in 1975 and 1978.

John Hollahan was a native of Seattle, Washington. He received his B.S. degree in Chemistry from the University of Washington in 1958, and his Ph.D. from the same university in 1964. Following his graduate studies he worked with Professor Klemperer at Harvard University, as a postdoctoral fellow. He

Journal of Applied Polymer Science: Applied Polymer Symposium 38, vii–viii(1984)

then moved back West and took employment at LFE, a division of Tracerlab. It was there that he began his involvement with plasma chemistry. LFE was one of the first industrial groups to bring out equipment for plasma ashing and was eager to find applications for its units in other areas. Hollahan's assignment was to assess the technical and commercial feasibility of using low pressure plasma processes for surface treatment of solids and for the deposition of thin polymer films.

In 1968, Hollahan left LFE and joined Boeing Scientific Research Laboratories in Seattle. After a three year period there, he accepted a position as a Senior Resident Research Associate at the NASA Ames Research Center at Moffett Field, California. In 1973, he joined the Tegal Corporation to serve as Director of R&D in the area of plasma technology. After three years with Tegal, he was hired by Perkin-Elmer Ultek Division to become Senior Staff Scientist for Advanced Development. He held this position until his death in late 1981.

Throughout his professional career, John Hollahan did a great deal to advance the science of plasma chemistry and to educate the scientific community regarding the potentials of plasma technology. At the time of his death he had published 31 research papers and had coedited three books relating to plasma chemistry. Perhaps the best known of these was the book entitled "Techniques and Applications of Plasma Chemistry." Dr. Hollahan was also instrumental in initiating the Gordon Conferences on Plasma Chemistry (1971) and was the Chairman for the First International Symposium on Plasma Chemistry, held in Kiel, Germany, in 1973. Both of these conferences have continued since their inception and are today regarded as the principal meetings in the field of plasma chemistry and technology.

With the deaths of Mitchel Shen and John Hollahan, the world lost two very important scientists, and I might add, two very fine individuals. Each in his own way contributed to establishing the foundations for research in the area of plasma polymerization, and to the furtherment of interest in plasma chemistry. The results of their work have not been lost, and I am certain that their papers and books will continue to educate future generations of scientists, and to serve as the point of departure for new research.

ALEXIS T. BELL
Department of Chemical Engineering
University of California
Berkeley, California
June 24, 1983

PYROLYSIS AS A MEANS OF STRUCTURAL STUDIES ON PLASMA-POLYMERIZED ORGANOSILICONES

M. GAZICKI,* A. M. WRÓBEL, and M. KRYSZEWSKI
Department of Polymer Physics, Centre of Molecular and Macromolecular Studies, Polish Academy of Sciences, Boczna 5, 90-362 Łódź, Poland

SYNOPSIS

Two techniques involving pyrolysis were used to investigate the structure of plasma-polymerized organosilicone materials. Low-temperature pyrolysis (300°C) coupled with gas chromatography and mass spectrometry was applied to the analysis of the oligomeric fraction of plasma polymers, whereas high-temperature pyrolysis (550–750°C) coupled with gas chromatography was used in order to examine the hydrocarbon part of the highly crosslinked polymers. The results obtained for two different groups of plasma polymers, i.e., plasma-polymerized methylsilazanes and plasma-polymerized methylsiloxanes, indicated significant structural differences, showing that silazanes exhibit much more diversity in their chemical structure, especially in terms of bridges and crosslinkages. The mechanism of plasma polymerization of methylsilicone monomers was also proposed based on the results of pyrolysis experiments as well as on the results of IR spectroscopy.

INTRODUCTION

Pyrolysis is not used very frequently to investigate plasma polymers. There are only a few cases reported in the literature where authors utilize pyrolysis coupled either with gas chromatography [1,2] or with mass spectrometry [3,4] in structural studies of these materials. One of the reasons for such limited interest in this technique is, no doubt, the fact that generally relatively little is known about the structure of plasma polymers, which makes it extremely difficult to interpret the results of any pyrolysis experiment. Nevertheless, the recent work of Dilks and co-workers [4,5] proves that pyrolysis may be a very useful tool in structural studies of plasma-polymerized hydrocarbons, especially when used

*Present address: Graduate Center for Materials Research, University of Missouri-Rolla, Rolla, MO 65401.

Journal of Applied Polymer Science: Applied Polymer Symposium 38, 1–19 (1984)

CCC 0570-4898/84/010001-19$04.00

along with other modern analytical techniques such as magic-angle solid-state NMR and the application of isotope-labeled materials. All the references cited above are dealing, however, with plasma-polymerized hydrocarbons; to our knowledge no one so far has used pyrolysis for structural investigations of plasma-polymerized organosilicones.

It is known that plasma-polymerized organosilicones prepared under mild energetic conditions contain a certain amount of low-molecular-weight, soluble fraction. The results of a study on such a fraction in plasma-polymerized hexamethylcyclotrisilazane performed by means of extraction in carbon tetrachloride followed by gas chromatographic/mass spectrometric analysis have already been reported elsewhere [6]. The thermogravimetric data of such soluble fraction containing films indicate, however, thermal behavior different from that of completely insoluble films. A thermogram typical of hexamethylcyclotrisilazane plasma polymerized under low-energy conditions is shown in Figure 1. As is seen, thermal decomposition of this material occurs in three stages, with the appearance of stage I, the low-temperature decomposition being characteristic only of films containing soluble fraction. In other words, low-temperature decomposition does not occur in the case of films prepared under higher-energy conditions which are completely insoluble. On the other hand, when the soluble fraction is extracted from material prepared under low-energy conditions, the residue does not exhibit stage I decomposition either. All of these findings indicate that the low-temperature decomposition is attributed to the liberation of low-molecular-weight fraction, essentially the same as soluble fraction, from the polymer network. The components of this fraction trapped (but not chemically bonded) in the crosslinked network during deposition are volatile enough to be liberated at relatively low temperature. Low-temperature pyrolysis/gas chromatography/mass

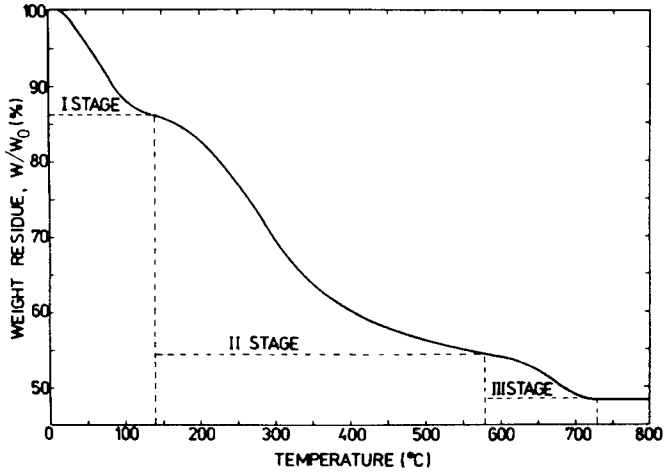

FIG. 1. Typical thermogram of plasma-polymerized hexamethylcyclotrisilazane deposited in low-energy conditions (p = 0.3 torr, i = 1 mA/cm^2, t = 30 s).

spectrometry experiments with plasma-polymerized hexamethylcyclotrisilazane fully confirm this hypothesis. The composition of the volatile phase is very similar to the composition of the soluble phase, both containing low-molecular-weight, oligomeric products, the majority of which are detected in both experiments. All the above findings lead to the conclusion that low-temperature pyrolysis coupled with gas chromatography and mass spectrometry is an excellent tool for the examination of oligomeric products present in plasma-polymerized organosilicone materials. Not only is this technique simpler and faster (it avoids several-hours-long extractions), but it is also more direct and can possibly detect species which may not be stable enough to be followed by means of the extraction method.

When the pyrolysis of the unsoluble or extracted or finally previously decomposed in low-temperature plasma-polymerized organosilicones is performed in the high-temperature (corresponding to stage II or stage III in Fig. 1) hydrocarbons appear to be the only products. Considering the structure of all organosilicone compounds, which are built of two levels, i.e., organic (usually methyl) groups sticking out of inorganic framework of either Si—O—Si or Si—NH—Si type, it is natural to conclude that high-temperature pyrolysis splits off organic portions of the material, leaving behind the glasslike residue, in an action comparable to lawn mowing. It has been shown, indeed, that the inorganic content of plasma-polymerized organosilicones increases dramatically with increasing temperature and time of pyrolysis, and hardly any organic residue is left after heating at 800°C for 30 min [7,8]. Since methyl groups are not the only hydrocarbon groups present in plasma-polymerized organosilicones, the careful examination of high-temperature pyrolysis products may provide a considerable amount of valuable information concerning the organic part of these materials.

The concept of this work was, therefore, to utilize the pyrolysis in two different regimes in the structural investigations of plasma-polymerized organosilicones: (i) low-temperature pyrolysis/gas chromatography/mass spectrometry to investigate oligomeric products; (ii) high-temperature pyrolysis/gas chromatography to examine the organic (hydrocarbon) part of the crosslinked polymer network. The main goal is to point out the differences, if any, between plasma-polymerized organosiloxanes (Si—O compounds) and plasma-polymerized organosilazanes (Si—N compounds), as well as to distinguish between products obtained from linear monomers and those obtained from cyclic monomers.

EXPERIMENTAL

Five monomers were chosen for this study, two silazanes (linear hexamethyldisilazane and cyclic hexamethylcyclotrisilazane) and three siloxanes (linear hexamethyldisiloxane, cyclic hexamethylcyclotrisiloxane, and octamethylcyclotetrasiloxane). Plasma polymerizations were carried out in a stationary bell jar system with internal electrodes. In all experiments initial pressure of monomer $p_0 = 0.3$ torr, discharge frequency $f = 20$ kHz, current density $j = 1$ mA/cm^2, and discharge duration $t = 30$ s were used. These relatively mild energetic

conditions resulted in a sufficiently high content of oligomeric fractions in each case.

The analyses were carried out using polymer samples of about 0.2 mg removed from the electrodes. They were pyrolyzed in a Jeol model 727 pyrolyzer in helium atmosphere. Low-temperature pyrolysis was carried out at 300°C for 30 s. Preliminary experiments showed that this temperature, although slightly higher than the stage I decomposition temperature, provided the best sensitivity without any substantial changes in the volatile fraction composition. In this regime, the pyrolysis products were fed directly into the GC–MS system built out of Jeol JGC 1100 gas chromatograph (2-m × 3-mm stainless-steel column with 10% OV101 on 80/100 mesh Varaport) and LKB model 2091 mass spectrometer operating at a standard electron beam energy of 70 eV. High-temperature pyrolysis was performed at either 550 or 750°C for 15 s, and the hydrocarbons were separated using 1-m × 3-mm stainless-steel column filled with 5A 60/80 molecular sieve. Analysis of retention times with the utilization of standard hydrocarbon samples used both ways, externally and internally, was applied in this case instead of mass spectrometric analysis.

LOW-TEMPERATURE PYROLYSIS

Low-temperature pyrolysis of all five plasma-polymerized organosilicone materials was performed with the assumption that the low-molecular-weight products detected in the analysis were resulting from the plasma reactions only, and thermal treatment did not influence their structure. This assumption was made based on the results obtained with plasma-polymerized hexamethylcyclotrisilazane, in which case it proved to be true. Indeed, a number of oligomeric products have been detected in each case, some of them being definitely predominant. Figure 2 presents gas chromatograms of volatile fractions of all the five plasma-polymerized organosilicones. A group of peaks appearing at the very beginning of each chromatogram and marked with the letter X corresponds to a not completely resolved mixture of light hydrocarbons and methylsilanes and is, therefore, difficult to interpret. All the remaining significantly abundant peaks, however, marked by letters A, B, C, and so on, have been identified on the basis of both their mass spectra and their gas chromatograms. Three identification methods were used: (1) comparison of the mass spectra with the literature data; (2) application of the standard compounds and comparison of both mass spectra and retention times; and (3) in cases in which the former two sources were not available the structural formula was proposed based on analysis of the mass spectrum with regard to fragmentation patterns typical of organosilicones, as well as to the possible plasma reactions leading to the corresponding structures. It should be stated here that in each case the chemical formula derived from the mass spectrometric data was verified by comparison of the observed and calculated relative intensity values for the first and second isotope peaks of most abundant $(M - CH_3)^+$ ion peak. The difference between the observed intensity values and those calculated on the basis of the accepted chemical formula stayed

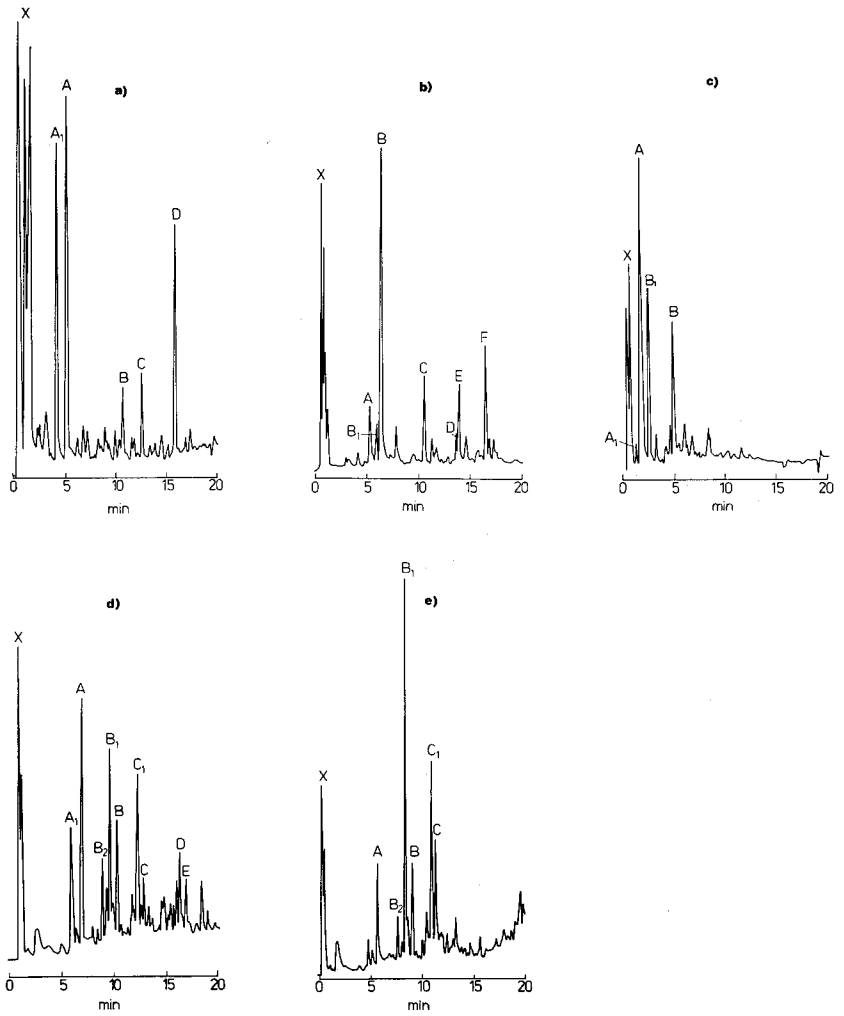

FIG. 2. Gas chromatograms of the oligomeric products liberated during low-temperature pyrolysis (300°C) of (a) plasma-polymerized hexamethyldisilazane, (b) plasma-polymerized hexamethylcyclotrisilazane, (c) plasma-polymerized hexamethyldisiloxane, (d) plasma-polymerized hexamethylcyclotrisiloxane, (e) plasma-polymerized octamethylcyclotetrasiloxane.

within the limits of reproducibility in each case. Organosilicone compounds are especially suitable for verification of isotopic abundances since silicone itself contains high concentrations of its natural isotopes, Si^{29} 4.7% and Si^{30} 3.1%.

Table I presents a summary of the identification work, the structures of all the main compounds liberated from the respective materials. For the sake of brevity the mass spectra corresponding to these products are not presented here, and only a general description of the fragmentation behavior of particular groups of oligomers is given. A detailed discussion of the mass spectra themselves, as

TABLE I

Oligomeric Products Liberated from Plasma Polymers of Methylsilazane and Methylsiloxane Monomers by Low-Temperature Pyrolysis

MONOMER	OLIGOMERIC PRODUCTS
$Me_3Si-NH-SiMe_3$ HEXAMETHYLDISILAZANE (HMDSN)	$HMe_2Si-NH-SiMe_3$ (A_1); $Me_3Si-NH-SiMe_3$ (A); $Me_3Si-NH-SiMe_2-NH-SiMe_3$ (B); 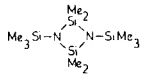 (C); 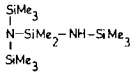 (D)
HEXAMETHYLCYCLOTRISILAZANE (HMCTSN)	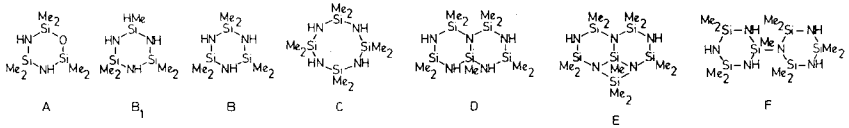 A, B_1, B, C, D, E, F
$Me_3Si-O-SiMe_3$ HEXAMETHYLDISILOXANE (HMDSO)	$HMe_2Si-O-SiMe_3$ (A_1); $Me_3Si-O-SiMe_3$ (A); $HMe_2Si-O-SiMe_2-O-SiMe_3$ (B_1); $Me_3Si-O-SiMe_2-O-SiMe_3$ (B)
HEXAMETHYLCYCLOTRISILOXANE (HMCTSO)	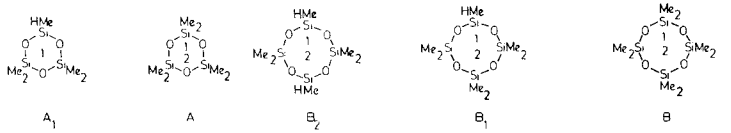 A_1, A, B_2, B_1, B
OCTAMETHYLCYCLOTETRASILOXANE (OMCTSO)	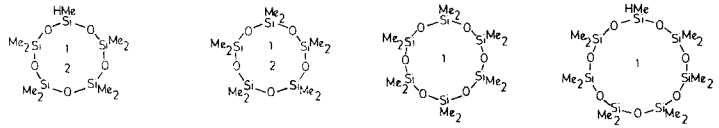 C_1, C, D, E

[1]Products of HMCTSO.

[2]Products of OMCTSO.

well as the reaction mechanisms proposed for the formation of each of the oligomeric structure are presented elsewhere [9].

It can be seen in Table I that one of the volatile products is the respective monomer in each case. This finding is in full agreement with the concept of trapping of some of the gas-phase molecules into the polymer network during the deposition process. There are also structures present in which one or two methyl groups have been replaced by hydrogen atoms, and these compounds are marked by the corresponding letters with the subscript of 1 or 2. The mass spectra of these structures are analogous to the mass spectra of the corresponding methyl derivatives with the shift of most of the peaks toward lower masses by a factor of either 14 (one substitution) or 28 (two substitutions). The fragmentation $(M - H)^+$ ion peaks also appear in all their spectra, further evidence for the presence of Si—H groups.

The main features of the mass spectrometric fragmentation patterns of oligomeric products liberated from each plasma-polymerized organosilicone material are now presented.

Plasma-Polymerized Hexamethyldisilazane

Monomer A and its monohydroderivative A_1 are the first two out of the five main components of the volatile fraction in this case. The structures of the remaining three products B, C, and D do, though, need some discussion of their verification.

The general pattern of linear methyl silazane and siloxane fragmentation is such that the parent-ion M^+ peak is very weak (less or about 1%), the most abundant peak is due to a $(M - CH_3)^+$-type fragmentation ion [10,11]. The appearance of the doubly charged $(M - 2CH_3)^{2+}$ ion peaks is also very characteristic of this group of compounds [11]. The molecular peaks of compounds B, C, and D are, indeed, very weak, being 0.8% (m/e = 234, compound B), 1.1% (m/e = 290, compound C), and 0.9% (m/e = 306, compound D), and the corresponding $(M - CH_3)^+$ peaks are the most abundant in all of the three spectra (m/e = 219 for compound B, m/e = 275 for compound C, and m/e = 291 for compound D). Doubly charged ion peaks have also been detected in each case, appearing at m/e = 102, 130, and 138, respectively. The loss of methane and/or ammonia from the $(M - CH_3)^+$ ion is the most characteristic feature of methyl silazane fragmentation patterns [12,13]. The loss of ammonia indicates, however, the presence of —NH— units in the structure of the parent ion. Peaks corresponding to all three kinds of fragmentation ions, $(M - CH_3 - CH_4)^+$, $(M - CH_3 - NH_3)^+$, and $(M - CH_3 - CH_4 - NH_3)^+$ have been found in the spectra of compounds B and D (m/e = 203, 202, and 186, respectively, for compound B and m/e = 275, 274, and 258, respectively, for compound D). In the spectrum of compound C, however, both peaks due to the loss of ammonia are absent, whereas peak corresponding to the loss of methane only is still present (m/e = 259). This indicates that although all of these three compounds are of silazane structure, compound C does not contain

imine groups; i.e., nitrogen atoms have to be trifunctional with respect to silicone. Consequently compounds B and D have to be linear, whereas compound C is very likely cyclic.

Plasma-Polymerized Hexamethylcyclotrisilazane

Out of seven main compounds found in the oligomeric, volatile phase of this material one is monomer (structure B), one is its monohydro derivative (structure B_1), and three have been found in the soluble fraction of this polymer (structures, A, C, and F) and are discussed elsewhere [6]. The remaining structures D and E were thus subjected to mass spectrometric verification. In their mass spectra the parent ion peaks appear at $m/e = 349$ (0.8%) and $m/e = 405$ (0.8%) and the base peaks at $m/e = 334$ and $m/e = 390$ for compounds D and E, respectively. Peaks corresponding to fragmentation ions $(M - CH_3 - CH_4)^+$, $(M - CH_3 - NH_3)^+$, and $(M - CH_3 - CH_4 - NH_3)^+$ have been found at $m/e = 318$, 317, and 301 for compound D and at $m/e = 374$, 373, and 357 for compound E. Finally, doubly charged $(M - 2CH_3)^{2+}$ ion peaks appear at $m/e = 159.5$ for compound D and at $m/e = 187.5$ for compound E. The methylsilazane character of product D and its molecular formula $Si_5C_9H_{31}N_5$ deduced from its mass spectrum determine its bicyclopentasilazane structure as shown in Table I. No other alternative structure the formation of which would be more probable can fit the above data. As far as compound E is concerned, it is clear that it has to be a derivative of compound D in which two hydrogen atoms have been replaced by a dimethylsilyl group. All the singly charged peaks in this compound's mass spectrum are shifted toward higher m/e values by a factor of 56 compared with the mass spectrum of compound D, whereas the doubly charged peak is shifted by half of this value, i.e., by the factor of 28. By substituting two hydrogen atoms in the structure of compound D with the dimethylsilyl group one ends up with two isomeric tricyclic structures, one of which is shown in Table I. The other possibility is the structure in which all the three rings are six membered.

Plasma-Polymerized Hexamethyldisiloxane

As is shown in Table I, the components of the volatile fraction of this polymer consist of monomer A, its monohydroderivative A_1, octamethyltrisiloxane B, and its monohydroderivative B_1. Fragmentation patterns of linear siloxanes indicate that parent ion peaks are usually very weak, mainly below 0.05%, the abundant peaks being $(M - CH_3)^+$, the base peak, and $[Si(CH_3)_3]^+$, $m/e = 73$, with the intensity usually close to 100% [14]. These two peaks are, indeed, the two most abundant in the spectrum of compound B, $(M - CH_3)^+$ being the base peak at $m/e = 221$ and $[Si(CH_3)_3]^+$ an ion peak with relative abundance about 94.5%. According to the prediction the parent ion peak $m/e = 236$ is not detected at all. The typical fragmentation ions of linear siloxanes [14], the ions $(M - 2CH_3)^{2+}$, $[M - CH_3 - (CH_3)_2SiO]^+$, $(M - CH_3 - C_2H_6)^+$, and $(M - CH_3 - CH_4)^+$ show up in the mass spectrum of compound B at ratios

m/e = 103, 147, 191, and 205, respectively. As far as compound B_1 is concerned, it shows a spectrum typical of monohydroderivative, with the shift of some peaks by the value of 14 and the appearance of a $(M - H)^+$ ion peak as well as the corresponding fragmentation peaks.

Plasma-Polymerized Hexamethylcyclotrisiloxane and Plasma-Polymerized Octamethylcyclotetrasiloxane

As is seen in Table I, the oligomeric products liberated from both of the above polymers are of the same nature, being exclusively monocyclic methylsiloxanes of various ring size. Six- to 14-membered rings have been found for plasma-polymerized hexamethylcyclotrisiloxane and 6- to 10-membered rings for plasma-polymerized octamethyltetrasiloxane. Similarily to the monomers the corresponding oligomers are marked in Table I by the numbers 1 or 2 inside the cycles. Some of these products are monohydro (structures A_1, B_1, C_1, and E) or dihydro (structure B_2) substituents. The structure of most of the oligomers has been verified mass spectrometrically and gas chromatographically with the application of the respective standard samples. That is why the discussion of their spectra is limited to the main peaks only.

The main mass spectrometric property of 6- and 8-membered cyclic methylsiloxanes is the base peak at m/e = 73 due to the $[Si(CH_3)_3]^+$ ion and the second most abundant peak arising from the doubly charged $[M - 2CH_3]^{2+}$ ion [11]. In the mass spectra of compounds A_1, A, B_2, B_1, and B, the base peak appears always at m/e = 73, indeed, and the second most intense peaks are found at m/e = 89, 96, 119, 126, and 133, respectively. As far as higher oligomers are concerned, the cyclic methylsiloxanes of rings sized from 8 to 14 are characterized by the base peak at m/e = 73 again, with a very intense peak due to the $[M - CH_3 - Si(CH_3)_4]^+$ type of fragmentation [11]. The peaks corresponding to such fragmentation ions have been found at m/e = 253, 267, 341, and 401 in the mass spectra of compounds C_1, C, D, and E, respectively. In each case also the base peak has arisen at m/e = 73. The shift by 14 mass units toward lower m/e values noted for some of the ion peaks in the spectra of compounds A_1, B_1, and C_1 as compared with those of A, B, and C indicates the presence of one hydrogen substituent. A similar shift, but by 28 mass units, in the spectrum of compound B_2 compared with that of B indicates the presence of two hydrogen substituents. More supporting evidence is found in the appearance of peaks due to $(M - H)^+$ ions in the spectra of all these products.

HIGH-TEMPERATURE PYROLYSIS

When subjected to the high-temperature regime of pyrolysis, all the five plasma-polymerized organosilicone materials behaved in a very similar way, evolving light hydrocarbons only, the main part of which consisted of methane, ethane, and ethylene. A typical gas chromatogram of gaseous pyrolysis products is shown in Figure 3 for plasma-polymerized hexamethylcyclotrisilazane. It has been shown before [7] that high-temperature decomposition of this material

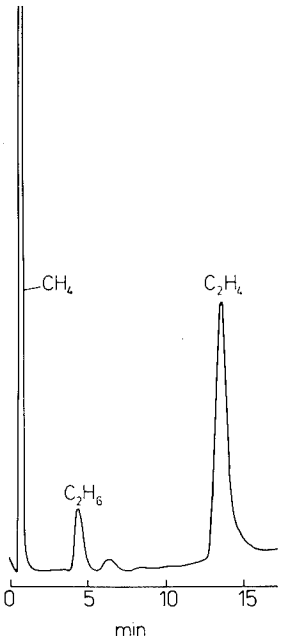

FIG. 3. Gas chromatogram of the high-temperature pyrolysis (550°C) products of plasma-polymerized hexamethylcyclotrisilazane.

involves a rapid decay of $SiCH_3$, SiH, and NH groups according to the following dissociation reactions:

$$\geqslant Si{-}CH_3 \longrightarrow \geqslant Si^{\cdot} + {}^{\cdot}CH_3$$

$$\geqslant Si{-}H \longrightarrow \geqslant Si^{\cdot} + {}^{\cdot}H$$

$$(\geqslant Si)_2N{-}H \longrightarrow (\geqslant Si)_2N^{\cdot} + {}^{\cdot}H$$

and the residue is mainly inorganic. Methyl and hydrogen radicals are thus the main (but not only, as we shall see) primary products of this lawn-mowing-type, high-temperature pyrolysis of plasma-polymerized organosilicones. These radicals are converted in the gaseous phase into numerous products according to the schemes [15]

$$CH_3^{\cdot} + H^{\cdot} \longrightarrow CH_4$$

$$2CH_3^{\cdot} \longrightarrow C_2H_6$$

$$C_2H_6 + CH_3^{\cdot} \longrightarrow C_2H_5^{\cdot} + CH_4$$

$$C_2H_5^{\cdot} \longrightarrow C_2H_4 + H^{\cdot}$$

$$C_2H_6 + H^{\cdot} \longrightarrow C_2H_5^{\cdot} + H_2$$

$$2C_2H_5^{\cdot} \longrightarrow C_2H_6 + C_2H_4$$

The rates of the above reactions strongly depend on pyrolysis temperature, as do the equilibria between particular products. As it turns out, in the range of temperatures used (above 500°C) the most favorable is the formation of hydrogen, methane, and ethylene [15]. Hydrogen does not appear in gas chromatograms of pyrolysis products simply because it is not detected by this method.

If, however, methyl radicals were the only primary hydrocarbon products of high-temperature pyrolysis, the composition of the gaseous pyrolazate would depend on pyrolysis conditions only but not on the structure of the material. In other words, the amount of the mowed off methyl radicals would vary for pyrolysis of materials plasma polymerized under various energetic conditions, but ratios of different hydrocarbon content in the pyrolazate should remain constant. For the above to be fairly true, the assumption has to be made that the ratio of methyl group and hydrogen atom content for polymers deposited under different condition is constant, which is not far from reality in the case of plasma-polymerized silazanes. The concentrations of both CH_3 groups and NH groups in plasma-polymerized organosilazanes decreases with increasing glow-discharge energy, the contribution of SiH groups still being negligible [16].

In order to check whether the composition of hydrocarbon products of high-temperature pyrolysis is independent of the polymer structure, thermal decomposition of plasma-polymerized hexamethylcyclotrisilazane samples obtained at various glow-discharge current densities was performed. Figure 4 shows the plots of ethylene/methane and ethane/methane concentration ratios in gaseous

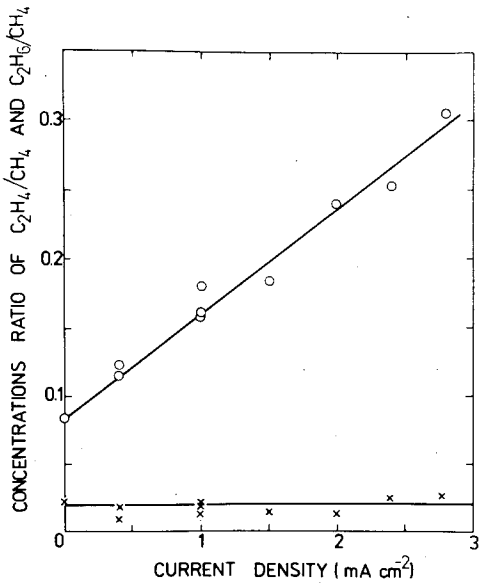

FIG. 4. Concentration ratios of C_2H_4/CH_4 (○) and C_2H_6/CH_4 (×) in high-temperature pyrolysis (750°C) products of plasma-polymerized hexamethylcyclotrisilazane as a function of glow-discharge current density.

pyrolyzates versus glow-discharge current density of sample preparation. It is seen that the C_2H_4/CH_4 ratio rises with increasing current density, whereas the C_2H_6/CH_4 ratio remains constant; the values at zero current density correspond to the respective ratios for monomer pyrolysis. The constancy of the C_2H_6/CH_4 ratio in the pyrolyzate indicates its independence of polymer structure and indicates that methyl groups are the only primary hydrocarbon species for the formation of ethane. On the other hand, the ethylene/methane ratio does not remain constant under these conditions, leading to the conclusion that along with the reactions shown above there must be another, essentially primary source of ethylene. The dependence of C_2H_4/CH_4 ratio on polymer structure indicates strongly that the additional amount of ethylene is evolved straight from this structure. IR analysis of plasma-polymerized organosilicones indicates that there are ethylene bridges between silicone atoms present in these materials (Fig. 5). Thus, ethylene may be evolved from the polymer structure through the decomposition of disilyethylene linkages according to the simplified reaction

$$\geqslant Si{-}CH_2{-}CH_2{-}Si\leqslant \longrightarrow 2(\geqslant Si^{\cdot}) + C_2H_4$$

This type of reaction has been reported by Blazso et al. [17], who were studying thermal decomposition of conventional polydimethylsilethylene-siloxane and

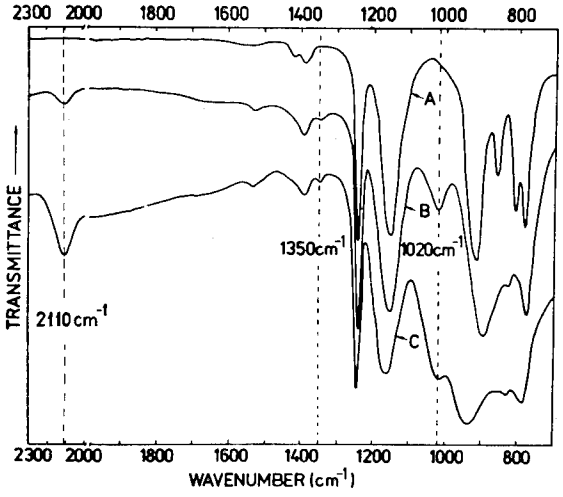

FIG. 5. IR spectra of plasma-polymerized hexamethylcyclotrisilazane samples obtained at 0.3 torr and 30 s at various discharge current densities: (A) spectrum of the monomer, (B) i = 1 mA/cm, (C) i = 2 mA/cm^2. The marked bands correspond to 1020 cm^{-1}: ω (CH_2) vibration in disilymethylene and disilyethylene bridges; 1350 cm^{-1}: δ symmetric (CH_2) vibration; and 2110 cm^{-1}: ν (SiH) vibration.

TABLE II
Relative Contents of Gaseous Products of High-Temperature (550°C) Pyrolysis of Plasma Polymers Obtained from Methylsilazane and Methylsiloxane Monomers, and Relative Pressure Increase in Polymerization Reactor after Glow Discharge

Monomer	Relative content of pyrolysis products		Pressure increase $\Delta p/p_0$ (%)
	C_2H_4/CH_4	C_2H_6/CH_4	
Hexamethyldisilazane	0.85	0.06	26
Hexamethylcyclotrisilazane	0.40	0.05	33
Hexamethyldisiloxane	1.20	0.06	23
Hexamethylcyclotrisiloxane	1.15	0.05	6
Octamethylcyclotetrasiloxane	1.16	0.06	9

polydimethylsilpropylene-siloxane. They have found the elimination of hydrocarbon segments located between silicon atoms and subsequent evolution of ethylene and propylene, respectively.

Referring back to the C_2H_4/CH_4 ratio shown in Figure 4 we note that the rise of the ratio with increasing current density results from the increased concentration of disilyethylene linkages in the polymer structure. The extrapolation of the line to zero current density yields exactly the C_2H_4/CH_4 value found for monomer. This value corresponds to the relative content of ethylene in the decomposition products due to secondary reactions with methyl radical as the primer.

Since the concentration of disilyethylene bridges in plasma-polymerized hexamethylcyclotrisilazane and consequently the ratio of ethylene/methane contents in its gaseous pyrolazate vary with the polymerization conditions, they should also be different for the polymers obtained from different monomers, which very possibly exhibit different tendencies toward formation of such bridges. As has been said before, all the plasma-polymerized organosilicones investigated in this work evolved light hydrocarbons, mainly methane, ethylene, and ethane. The corresponding ratios for each of the five polymers are shown in Table II. Again, the ethane/methane ratio does not depend on the structure of the pyrolyzed material, which is more proof for the finding that ethane is formed only in secondary reactions. The ethylene/methane ratio, however, varies significantly among the cited materials, and the difference between plasma-polymerized siloxanes and plasma-polymerized silazanes is here evident. The relative ethylene contents in gaseous pyrolazates of plasma-polymerized methylsiloxane materials are up to three times higher than the corresponding values for plasma-polymerized methylsilazanes, indicating that the former polymers contain significantly higher amounts of disilyethylene bridges. This finding agrees well with the fact that silazane polymers undergo crosslinking mainly via formation of the tertiary nitrogen Si—N bonds, the formation of disilyethylene bridges being a side effect

[16]. Since siloxane polymers are lacking such possibility, they consequently contain more disilyethylene bridges.

DISCUSSION

It is quite obvious that knowing the structure of low-molecular-weight products of plasma polymerization one is much better equipped to speculate about the structure of the polymer itself as well as about the chemistry of polymerization reactions. The nature of the chemical processes leading to the formation of oligomers is very likely similar to those leading to polymer deposition, and structural features of these oligomers are supposedly copied and multiplied in the structure of the polymer.

A comparison between oligomeric products of methylsiloxanes and methylsilazanes results in several findings. The most general one is that methylsiloxanes have fewer possible reaction pathways available under plasma conditions than methylsilazanes, which leads to less diversity among their products. Plasma polymerization of linear siloxanes yields only linear oligomers in the volatile fraction, whereas plasma polymerization of linear silazanes brings about all the possibilities, i.e., linear, branched, and cyclic oligomers. The same is true for cyclic monomers. Oligomers liberated from plasma-polymerized monocyclic siloxanes turn out to be monocyclic siloxanes only. In contrast, a number of different monocyclic, bicyclic, and tricyclic structures have been found in the volatile fraction of plasma-polymerized monocyclic silazane. This finding led us to conclude that, in general, the chemical structure of plasma-polymerized siloxanes is supposed to be more uniform, containing fewer different groups, branches, and crosslinkages compared with the structure of plasma-polymerized silazanes. This is not completely surprising when it is taken into consideration that the trifunctionality of the nitrogen atom offers more possible reaction pathways than the bifunctionality of oxygen. In other words, silazanes can be substituted, branched, and crosslinked through nitrogen atom, whereas the oxygen atom in siloxanes does not provide such possibilities.

The reaction mechanisms can be written for the formation of each of the oligomeric products presented in Table I with the assumption that the plasma behavior of particular monomers is similar to that in the ionization chamber of the mass spectrometer with only a difference in pressure. Higher pressure under plasma conditions increases the probability of bimolecular reactions, which of course have to be involved in the formation of oligomers. A large number of such reactions based on the cationic mechanisms with the precursor ion $(M—CH_3)^+$ similar to that obtained under mass spectrometric conditions has been proposed elsewhere [9]. Although we are not going to present all of these schemes here, it is worthwhile to cite two such reactions leading to the two different kinds of dimers. The first one is an addition reaction leading to the formation of double-membered monocyclic dimer out of two monocyclic monomer molecules, an example of which is the formation of product D from hexamethylcyclotrisiloxane:

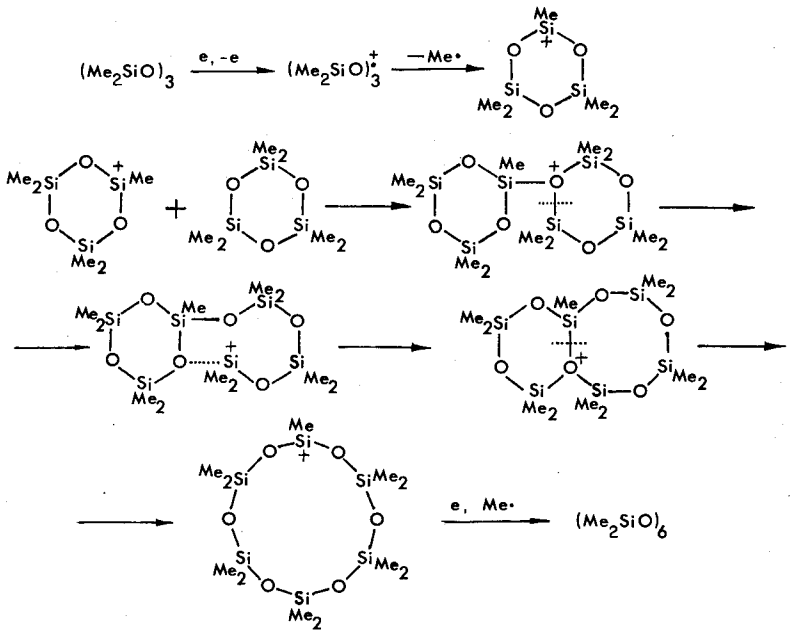

In contrast, the reaction leading to the bicyclic dimer from two monocyclic monomer units is a substitution reaction. The formation of product F from hexamethylcyclotrisilazane is an example of this alternative:

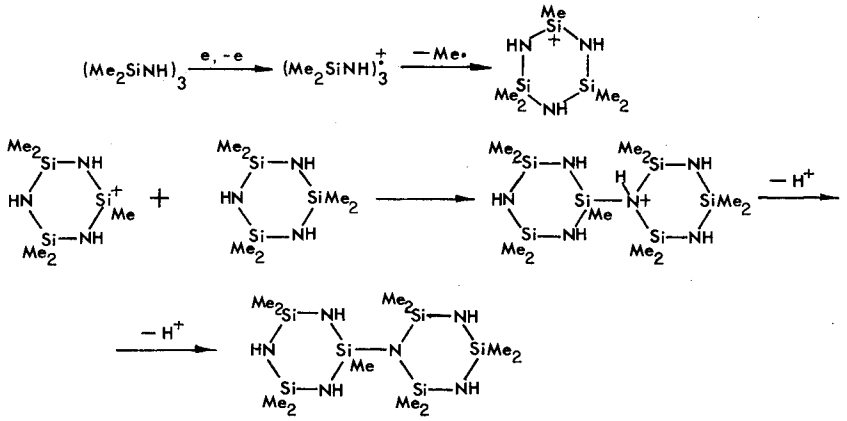

Both the above schemes are hypothetical, but we do not need complete confirmation of the mechanism to state that there is a significant difference between formations of monocyclic and bicyclic dimers in terms of possible by-products. The two reactions can be schematically represented by the overall equations

2 Monomer ⟶ Dimer (monocyclic) (siloxane)

2 Monomer ⟶ Dimer (bicyclic) + CH_4 (silazane)

The first reaction yields only dimer with no by-product, whereas the second one always involves the formation of by-product (in this case it is a molecule of methane).

Interesting conclusions concerning pressure changes during plasma polymerization can thus be drawn from comparison of the above equations. The addition reaction leading to monocyclic dimer results in a pressure drop, whereas in the substitution reaction leading to bicyclic dimer, the pressure remains constant. The above statement is, of course, true only when both reactions occur in the gas phase. These pathways are certainly not the only reactions taking place during plasma polymerization of the respective monomers, and the total pressure effect is different. If, however, addition reactions are predominant in plasma polymerization of hexamethylcyclotrisiloxane and substitution reactions dominate plasma polymerization of hexamethylcyclotrisilazane, the total pressure effects for both of these processes should be different. Results presented in Table II show that the pressure effect is positive in each case; i.e., glow discharge always brings about an increase in pressure for the organosilicones under study. There is, however, a striking difference in relative pressure increase for plasma polymerization of cyclic siloxanes and plasma polymerization of cyclic silazane. The very low ratio of pressure increase in the case of hexamethylcyclotrisiloxane ($\Delta p/p_0 = 6\%$) as well as in the case of octamethylcyclotetrasiloxane ($\Delta p/p_0 = 9\%$) support strongly the suggestion that addition reactions rather than substitution are responsible for the increase in molecular mass in their polymerization. On the other hand, polymerization of hexamethyltrisilazane is accompanied by the greatest pressure increase ($\Delta p/p_0 = 33\%$), supporting the suggestion that substitution reactions predominate in this case. In view of the above, one may find it surprising that plasma polymerization of linear siloxane brings about significant pressure increase ($\Delta p/p_0 = 23\%$, almost as high as for linear silazane, 26%). The linear molecule, however, does not offer the possibility of addition reactions unless it is equipped with multiple bonds. Any dimerization of molecules such as hexamethyldisiloxane or hexamethyldisilazane has to go through substitution reactions with the evolution of by-product.

The above dimerization reactions are considered to result from the bombardment of electrons present in plasma and explained on the basis of cationic mechanism. The results of relative pressure changes indicate that they occur (at least partly) in the gas phase. The probability that further oligomerization processes will take place in the gas phase drops significantly with the increasing molecular mass of the oligomers simply because of their growing tendency toward adsorption and condensation. It is also evident from the structure of the respective oligomers that these reactions, although possibly leading to the branched and crosslinked polymer structures in the case of silazanes and perhaps linear siloxanes, can yield only monocyclic polymers in the case of cyclosiloxanes. On the other hand, it is well known that all of these materials are highly crosslinked; it follows that some other crosslinking processes must also appear in this case.

As has been shown before [18], the structure of plasma-polymerized organosilicones is not quite homogeneous but rather consists of two regions. The

top oligomeric layer of thickness about 500 Å covers the more dense, bulk, highly crosslinked part of the polymer. At the same time our high-temperature pyrolysis experiments supported by IR analysis of the highly crosslinked polymers showed the presence of disilylethylene bridges, linkages absent in the structure of oligomers. It seems therefore to be very probable that oligomers primarily formed in cationic reactions are then crosslinked with the formation of disilylethylene (and presumably disilylmethylene, the presence of which has been also shown by means of IR) bridges. Such crosslinking reactions are known in the chemistry of conventional organosilicone polymers as initiated by UV irradiation and following the radical mechanism [19]

$$\geqslant Si{-}CH_3 \xrightarrow{h\nu\ (UV)} \begin{cases} \longrightarrow \geqslant Si^{\cdot} + {}^{\cdot}CH_3 \\ \longrightarrow \geqslant Si{-}\dot{C}H_2 + {}^{\cdot}H \end{cases}$$

$$\geqslant Si{-}CH_3 + {\cdot}Si\leqslant \longrightarrow \geqslant Si{-}CH_2^{\cdot} + HSi\leqslant$$

$$\geqslant Si{-}CH_3 + {\cdot}CH_3 \longrightarrow \geqslant Si{-}CH_2^{\cdot} + CH_4$$

$$\geqslant Si{-}CH_3 + {}^{\cdot}H \longrightarrow \geqslant Si{-}CH_2^{\cdot} + H_2$$

$$\geqslant Si{-}CH_2^{\cdot} + {\cdot}Si\leqslant \longrightarrow \geqslant Si{-}CH_2{-}Si\leqslant$$

$$\geqslant Si{-}\dot{C}H_2 + {\cdot}H_2C{-}Si\leqslant \longrightarrow \geqslant Si{-}CH_2{-}CH_2{-}Si\leqslant$$

The above set of free-radical reactions leads not only to the formation of disilyethylene and disilymethylene bridges and consequently to the crosslinking of the polymer, but also clearly explains the formation of SiH bonds, the presence of which has been detected in both oligomeric fraction by means of mass spectrometry (Table I) and crosslinked polymer by means of IR analysis (Fig. 5). Very recently Wertheimer confirmed the role of UV irradiation in crosslinking of plasma-polymerized organosilicone film in a very simple and appealing experiment [20]. Fresh sample obtained after a very short deposition time was divided in two and the halves subjected separately to two simulated possible crosslinking agents, electron bombardment and UV irradiation. UV irradiation caused shrinkage of the sample, indicating the presence of crosslinking, whereas no changes were observed in the material after exposure to electron bombardment.

Finally, the relatively smaller amount of disilyethylene bridges detected by means of high-temperature pyrolysis in plasma-polymerized silazanes and especially hexamethylcyclotrisilazane should also be discussed in the light of the mechanism proposed above. The oligomeric products of hexamethylcyclotrisilazane (bicyclic and tricyclic oligomers) are definitely more ordered and consequently less flexible than the conformational multimembered monocyclic siloxane oligomers. It follows that in the case of cyclosilazanes it takes lower concentrations of intermolecular bridges to make the whole system rigid enough not to accept any further crosslinking only on the basis of conformational mobilities of the segments. Paradoxically this does not necessarily mean that the degree of crosslinking is higher in the case of plasma-polymerized siloxanes.

The total degree of crosslinking may be comparable in both cases but silazanes require fewer bridges simply because some of their oligomers are already "cross-linked."

CONCLUSION

In order to summarize the above work, first of all one should point out the fact that the carefully controlled pyrolysis of plasma polymers appears to be extremely useful technique for structural studies on these hard to handle materials. For the obvious reasons the low-temperature pyrolysis, giving insight into the structure of the oligomeric products is of special importance. Although the usefulness of this technique has been shown in the case of plasma-polymerized organosilicone materials only, there is no particular reason preventing its use in structural studies of any other plasma polymers.

As far as plasma-polymerized organosilicones are concerned the general picture drawn from the pyrolysis results is such that cationic oligomerization reactions resulting from the electron bombardment of the monomer and presumably taking place in both gas and solid phases are followed by UV-initiated cross-linking, which takes place exclusively in the solid phase and brings about the final product.

REFERENCES

[1] M. Seeger, E. M. Barall II, and M. Shen, *J. Polym. Sci. Polym. Chem. Ed., 13,* 1541 (1975).
[2] M. Seeger, R. J. Gritter, J. M. Tibbitt, M. Shen, and A. T. Bell, *J. Polym. Sci. Polym. Chem. Ed., 15,* 1403 (1977).
[3] M. Venugopalan, I.-Sioun Lin, and M. Grenda, *J. Polym. Sci. Polym. Chem. Ed., 18,* 2731 (1980).
[4] A. Dilks, and S. Kaplan, presented at 184th National American Chemical Society Meeting, Kansas City, 1982.
[5] A. Dilks, S. Kaplan, and R. Crandall, unpublished.
[6] M. Gazicki, A. M. Wróbel, and M. Kryszewski, *J. Appl. Polym. Sci., 21,* 2013 (1977).
[7] A. M. Wróbel and M. Kryszewski, in *Plasma Polymerization,* Am. Chem. Soc. Symp. Ser. 108, M. Shen and A. T. Bell, Eds., Am. Chem. Soc., Washington, DC, 1979, Chap. 14.
[8] A. M. Wróbel, J. Kowalski, J. Grębowicz, and M. Kryszewski, *J. Macromol. Sci. Chem., 17*(3), 433 (1982).
[9] A. M. Wróbel, M. Kryszewski, and M. Gazicki, *J. Macromol. Sci. Chem., 20,* (5 and 6), 583 (1983).
[10] M. R. Litzow and T. R. Spalding, in *Mass Spectrometry of Inorganic and Organometallic Compounds,* Elsevier, Amsterdam, 1973, Chap. 7.
[11] J. E. Coutant and R. J. Robinson, in *Analysis of Silicones,* A. L. Smith, Ed., Interscience, New York, 1974.
[12] A. G. Sharkey, R. A. Friedel, and S. H. Langer, *Anal. Chem., 29,* 770 (1957).
[13] J. Silbiger, C. Lifshitz, J. Fuchs, and A. Mandelbaum, *J. Am. Chem. Soc., 89,* 4308 (1967).
[14] V. Yu. Orlov, *Zh. Obsch. Khim., 37,* 2300 (1967).
[15] K. J. Laider and L. F. Loucks, in *Comprehensive Chemical Kinetics,* C. H. Bamford and C. F. H. Tipper, Eds., Elsevier, Amsterdam, 1972, Vol. 5.

[16] A. M. Wróbel, M. Kryszewski, and M. Gazicki, *Polymer, 17,* 678 (1976).
[17] M. Blazso, G. Garzo, K. A. Andrianov, and L. M. Volkova, *J. Organomet. Chem., 54,* 105 (1973).
[18] A. M. Wróbel, M. R. Wertheimer, J. Dib, and H. P. Schreiber, *J. Macromol. Sci. Chem., 14,* 321 (1980).
[19] A. D. Dellman, M. Landy, and B. B. Simms, *J. Polym. Sci. A-1, 7,* 3375 (1969).
[20] M. R. Wertheimer, private communication.

EVALUATING THE ADHESION CHARACTERISTICS OF GLOW-DISCHARGE PLASMA-POLYMERIZED FILMS BY A NOVEL VOLTAGE CYCLING TECHNIQUE

MICHAEL F. NICHOLS and ALLEN W. HAHN
John M. Dalton Research Center, University of Missouri, Columbia, Missouri 65211

WILLIAM J. JAMES, ASHOK K. SHARMA, and H. K. YASUDA
Graduate Center for Materials Research, University of Missouri, Rolla, Missouri 65401

SYNOPSIS

Many thin-film epoxy and polymeric coatings are available as electrical insulating materials. Most of these films exhibit excellent bulk electrical properties; however, their electrical insulating characteristics are compromised or diminished at interfacial boundaries when they are submerged in conductive solutions. The loss of insulative properties is generally associated with the loss of adhesion to the underlying substrate. We have developed a voltage cycling technique using a modified form of cyclic voltammetry to stress this interfacial region under accelerated end use conditions. We have found that this technique was preferable to conventional ones (i.e., pull tests) in that we could observe the synergistic effects of water, ions, and electric fields on the rate of adhesive loss of the insulating films to their underlying substrates. Improvements in the adhesion of Parylene films to platinum substrates by the use of primer coatings of glow-discharge polymers is also verified by this technique.

INTRODUCTION

Many organic films have bulk properties which make them desirable candidates as electrical insulators for metal substrates. Unfortunately, many of these films simply oppose and do not readily adhere to their underlying substrates. When placed in an aqueous environment, these films become detached from the substrate, compromising their insulative nature. Work in our laboratories has focused

Journal of Applied Polymer Science: Applied Polymer Symposium 38, 21–33 (1984)

CCC 0570-4898/84/010021-13$04.00

on altering surface characteristics so that these two dissimilar solids (metal/polymer) may maintain adhesion at the interfacial regions under a variety of environmental stresses.

The adhesion of polymers to metals occurs because of surface forces and perhaps some chemical bonding. Although the exact nature of the surface forces is not clear, they can arise from [1] van der Waals forces and/or [2] electrostatic forces [1,2,5]. A wide variety of qualitative and quantitative tests exist to determine how well two substances will adhere to each other. Each of these tests attempts to disrupt either one or all of the above-mentioned forces. For example, direct tests of mechanical properties by pull and shear tests exist for the determination of cohesive and/or adhesive strengths of thin polymeric films in wet and dry environments [6–8]. Although the results of these tests performed on relatively large substrates such as pull rods may be applicable to polymeric films formed on other substrates, the tests are, for the most part, substrate and geometry dependent. Therefore one cannot apply them to coatings on micron-size wire probes such as might be used for stimulating and/or recording neural electrodes. Comparative measures of adhesive strength can also be made by immersing coated metal samples in boiling saline solutions for varying periods of time and then examining the surfaces optically or with scanning electron microscopy (SEM) [7,8]. However, it is known that organic coatings may exhibit good dry and wet adhesion but when subjected to electrical potentials and salt solutions be quickly detached from the metal surface, thus negating their insulating characteristics [9].

For several years, we have been engaged in the study of adhesion of polymer films to metal substrates. Our principal means of improving this adhesion has been by using glow-discharge polymerization techniques. The chemical and physical properties of these films, including adhesive and cohesive strengths, are very sensitive to kinetic factors which in turn are related to the reactor operating parameters, e.g., power, flow rate, system pressure, temperature, etc. Considerable time can be expended in determining the combination of these parameters that results in a film with the desired chemical, mechanical, and adhesive properties. Therefore we explored the use of a testing technique which would disrupt the mechanical and/or chemical forces acting at the interface by the creation of channels, formation of high-gas-pressure sites, and dissolution products in an accelerated testing protocol. Accordingly, we decided to use a voltage cycling technique (VCT) modified from cyclic voltammetry to determine the comparative quality of adhesion of polymer films to platinum wires under the synergistic effects of water, ions, and electric fields.

EXPERIMENTAL

Working Cell and Apparatus

The apparatus is illustrated schematically in Figure 1. A modified H cell with three-electrode geometry is arranged such that the counterelectrode is driven by

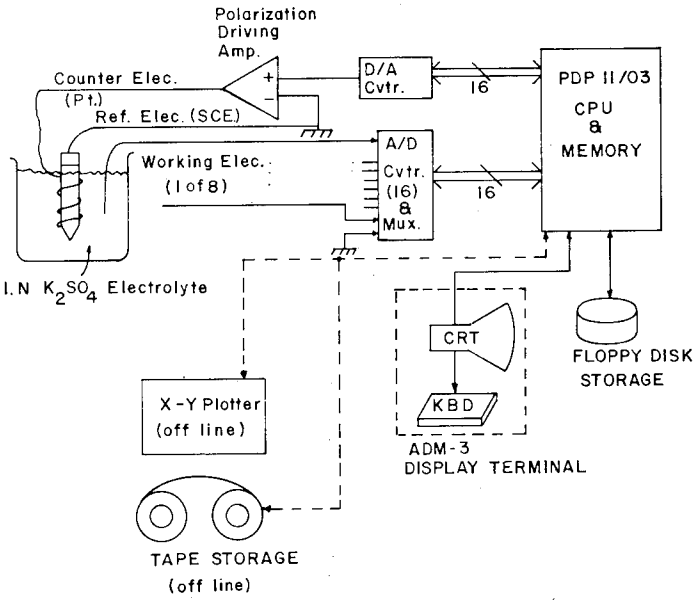

FIG. 1. Apparatus and multichannel data acquisition system.

a low-impedance amplifier from the digital-to-analog (D/A) converters. Current through each working electrode is monitored by an amplifier whose voltage output is proportional to input current. This output voltage is then sampled by the analog-to-digital (A/D) converters for digital presentation to the computer data collection system. The cell geometry is such that the working electrodes (coated or uncoated samples) are arranged concentrically 18 mm from the saturated calomel reference electrode (SCE). A counterelectrode of uncoated 250-μm-diam platinum wire is helically wound around the reference electrode concentrically disposed to, and equidistant from, the working electrodes.

A solution of 1.0*N* potassium sulfate (75-mmho/cm conductivity) was chosen as the electrolyte in preference to physiological saline solution because of the instability of the current generated in the anodic region, possibly as a consequence of chloride/platinum oxide interaction [3] and platinum dissolution. It was also used to avoid the complexity of secondary reactions involving absorption of chloride as noted by others [4,10].

The experiments were initially done manually on individual electrodes using a laboratory potentiostat, and the resulting voltammograms were then correlated with the results of SEM examination of films subjected to varying periods of soaking in the electrolyte media. Earlier results on collodion-coated platinum wire are described elsewhere [11].

Each of these experiments was very time consuming when multiple sweeps were required. Also, the consecutive processing of the individual experimental runs led to high variability because it was not possible to simultaneously cycle coated and uncoated electrodes.

To remedy these problems, we constructed a unique eight-channel, three-electrode system which was connected to a PDP 11/03 microcomputer (Digital Equipment Corporation, Maynard, MA.) (Fig. 1). Software was written to control the testing and recording of data simultaneously from eight working electrodes. This allowed us to compare the *V-I* waveforms from coated and uncoated electrodes within the same experimental cycle. Sampling and storage of data from all eight channels were possible during operator-selected portions of the cycling experiment. This allowed us to recover particular cycles or portions of them for further study.

The outputs from the D/A converter (Fig. 1) provided the triangular waveform through a polarization driving amplifier which biased the working electrodes between the limits of +3 and −2 V. Figure 2(a) illustrates the relationship of

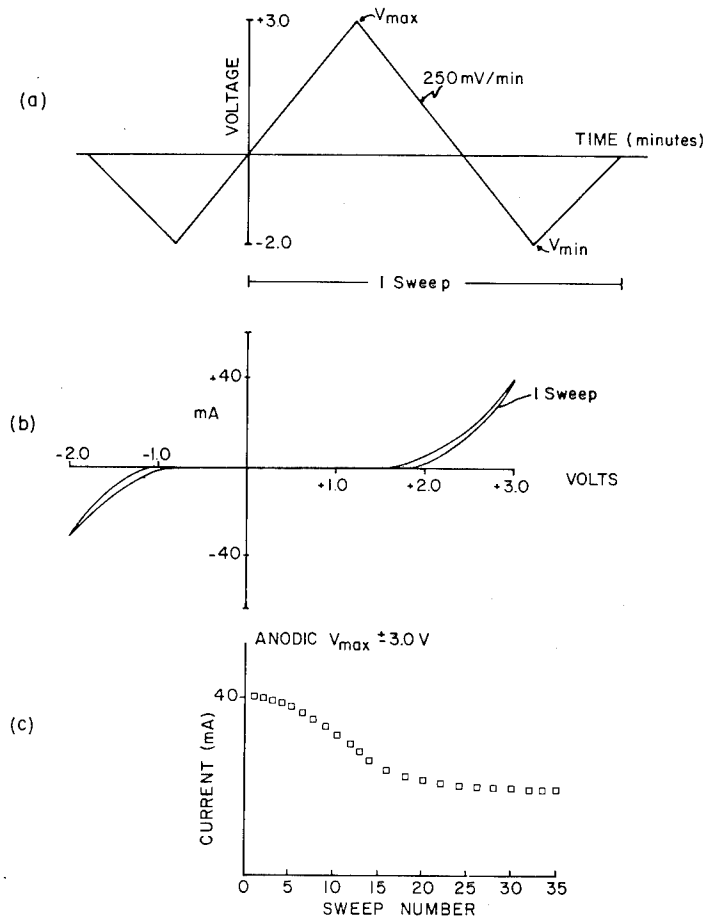

FIG. 2. Waveforms and plotted data produced and recorded by electrochemical data acquisition system.

the maxima and minima of the triangular waveform to the generated currents at a fixed potential on single-sweep voltammograms [Fig. 2(b)] and subsequent to a plot of these maximum currents at +3 V dc versus the number of sweeps or cycles [Fig. 2(c)]. Each box in Figure 2(c) represents the current measured at the maximum potential (+3 V dc) at the end of each sweep.

Calibration Studies

Previous studies using manually operated equipment demonstrated that prolonged cycling (up to 80 cycles) resulted in increased current from wires with poorly adhering polymer films as judged from SEM results [12]. However, if the film was not entirely removed from the wire, the changes in the voltammogram between −1.5 and −2.0 V dc were not sufficiently sensitive to detect small changes in areas where increased reduction or oxidation currents could take place. From an examination of the micrographs after cycling, we decided to investigate the relationship between the measured current and exposed area of the wire substrates. The area/current relationship was measured at several voltages to determine the sensitivity and repeatability of the experiments. A calibrated micromanipulator (each step exposing an area of 0.007 cm^2) was used to hold each sample and submerge it into the electrolyte a known distance. The platinum wires were cleaned by ultrasound in solutions of detergent and nitric acid, with intermediate rinsing in glass-distilled water. The electrodes were then stored dry.

Figure 3(a) shows the results of an experiment using four platinum electrodes following the precleaning procedure. The lack of sensitivity at −1.5 V (vs. SCE) is evidenced by the fact that a tenfold increase in exposed area resulted in only an average twofold increase in current. In contrast, at −2.0 V this same increase in area resulted in a fivefold increase in current due to electrochemical reactions.

Figure 3(b) shows that at anodic voltages of +2.0 V, no appreciable change in current could be seen even for a tenfold increase in area. Increasing the applied voltage to +3.0 V resulted in an increase in current density very similar in sensitivity to that measured at −2.0 V (cathodic) on the bare substrates shown in Figure 3(a). These data provided the optimal parameters for the maximum and minimum sweep voltages for the experiments.

Polymer Coatings

The substrates used in this study were 250-μm-diam, 2.5-cm-long platinum wires which had electrochemically etched (sodium cyanide bath) surfaces. The polymer films were glow discharge polymers of methane (GDP-M), tetrafluoroethylene (GDP-TFE), or tetramethyldisiloxane (GDP-TMDSiO) deposited in a bell jar reactor operating at a frequency of 10 kHz. The conditions of polymerization are given in Table I. All substrates were argon etched for 5 min at a power of 70 W, a flow of 2 cm^3 (STP)/min, and pressure of 37 mtorr.

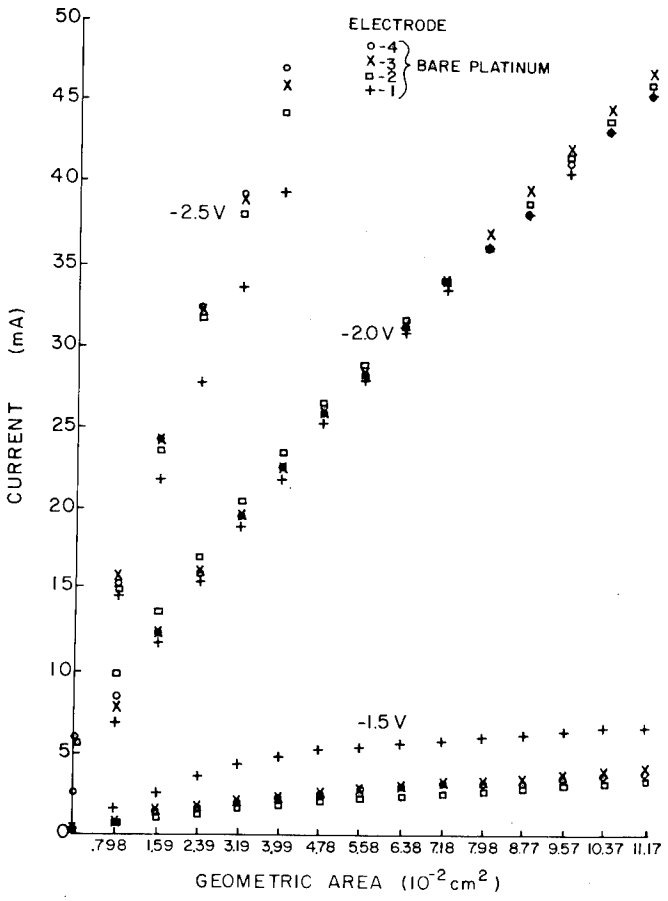

FIG. 3a. Cathodic currents as a function of geometric areas and applied voltage on uncoated Pt wires (250-μm diam).

TABLE I
Glow Discharge Polymerization Conditions

Polymer	Power (W)	Flow [cm^3(STP)/min]	Deposition rate (Å/min)	Thickness (kÅ)
GDP-M	82	0.5	40	2
GDP-TFE	21	1.28	137	2
GDP-TMDSiO	133	1.99	350	10

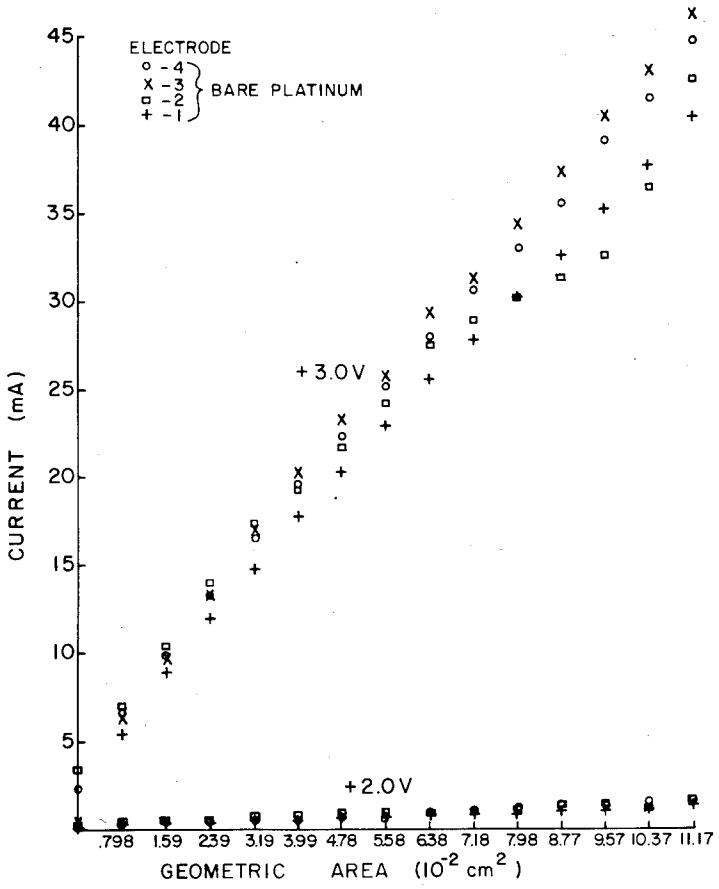

FIG. 3b. Anodic currents as a function of geometric areas and applied voltage on uncoated Pt wires (250-μm diam).

To determine whether the glow discharge coatings could improve the adhesion of other polymer films, composite coatings were also synthesized on identical substrates. The composite coatings consisted of an initial 300-Å layer of a glow-discharge-polymerized film placed on the bare platinum substrates as described above. On top of the film was placed a coating of either poly(*p*-xylylene) or poly(chloro-*p*-xylylene) by the Gorham method [13]. These polymers are commercially named Parylene N and Parylene C (Union Carbide Company, San Diego, CA.) and were chosen because they are considered to be good electrical insulators in thin-film applications. However, long-term applications have been limited by adhesive loss to the underlying substrates at interfacial junctions or mechanically formed microcracks through the surface of the films.

For these tests an interfacial region at the tip of the electrode was artificially created by cutting the tip with a sharp scalpel blade or exposing the tip by discharging a capacitor-stored voltage from the electrode to an appropriately positioned ground plane. The details of this system are found in [14].

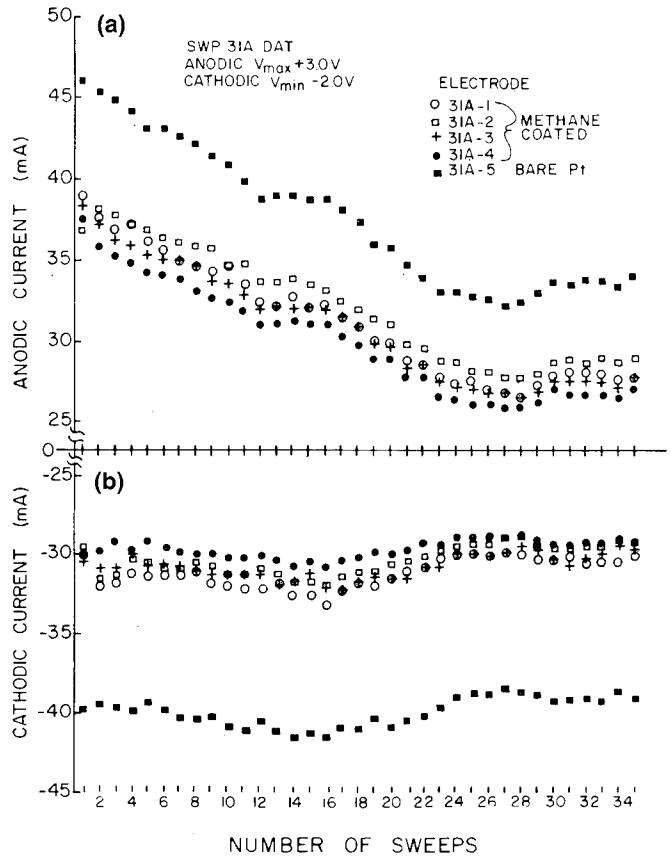

FIG. 4. Anodic (a) and cathodic (b) currents observed on 2000-Å GDP-M-coated Pt wires.

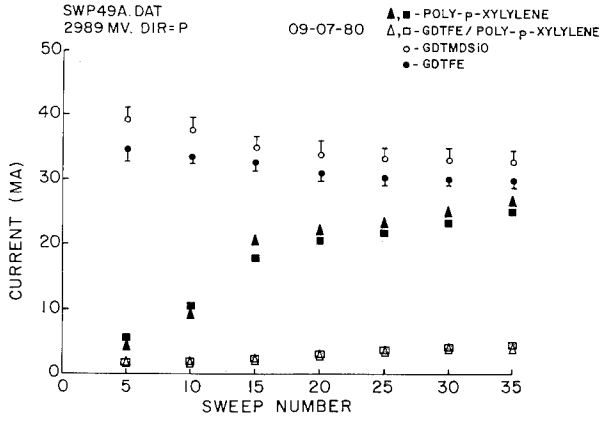

FIG. 5. Average (± standard deviation) anodic currents observed for five electrodes during cycling for GDP-TFE and GDP-TMDSiO films. Two electrodes coated with a combination of GDP-TFE (2000 Å) and poly(*p*-xylylene) (2.5 μm) are shown for comparison.

RESULTS AND DISCUSSION

Although we feel this technique will be most beneficial studying the adhesion of coatings of 1 μm or greater, we have tested ultrathin 2000-Å GDP-M, 10,000-Å GDP-TMDSiO, and 2000-Å GDP-TFE coatings. The results of these tests are shown in Figures 4 and 5, which indicate that the reproducibility of the technique is excellent and that a consistent electrochemical process over a well-defined constant area is taking place. During the anodic potential sweeps, there appears to be passivation of the wire surface as indicated by the decreasing currents for both the bare and coated wires [see Fig. 4(a)]. Note that there are no sharp deviations from the differential currents of the bare and coated electrodes between sweeps 1 and 35 in either Figure 4(a) or 4(b), indicating that not only is the

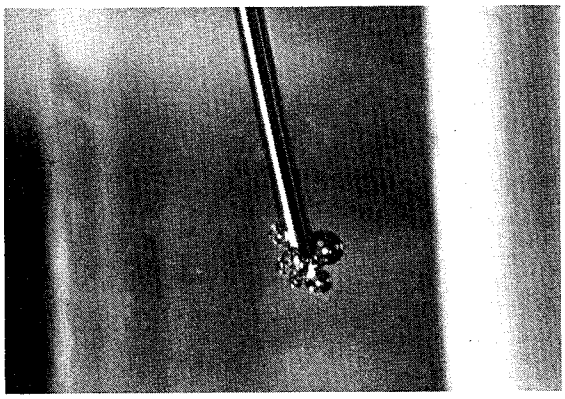

(a)

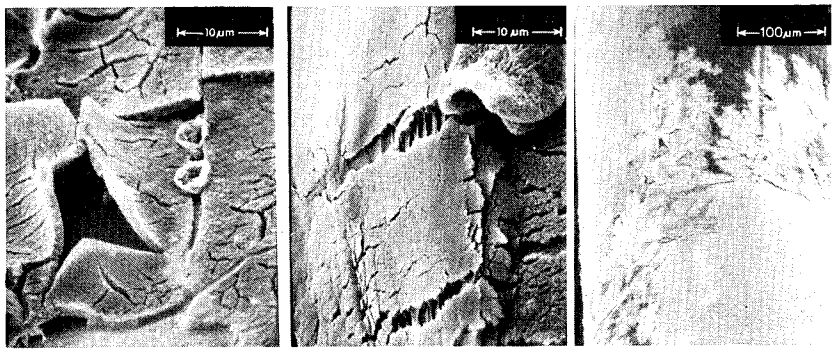

(b) (c) (d)

FIG. 6. Light and scanning electron micrographs (SEMs) of voltage-cycled electrodes: (a) light micrograph of a 250-μm platinum wire coated with GDP-TFE/poly(*p*-xylylene) during the first five voltage sweeps, (b) SEM of a substrate coated with poly(*p*-xylylene) after 70 voltage cycles, (c) SEM of a composite-coated [GDP-TFE/poly(*p*-xylylene)] substrate after 70 voltage cycles, (d) same as (b) but showing actual detachment of film from surface.

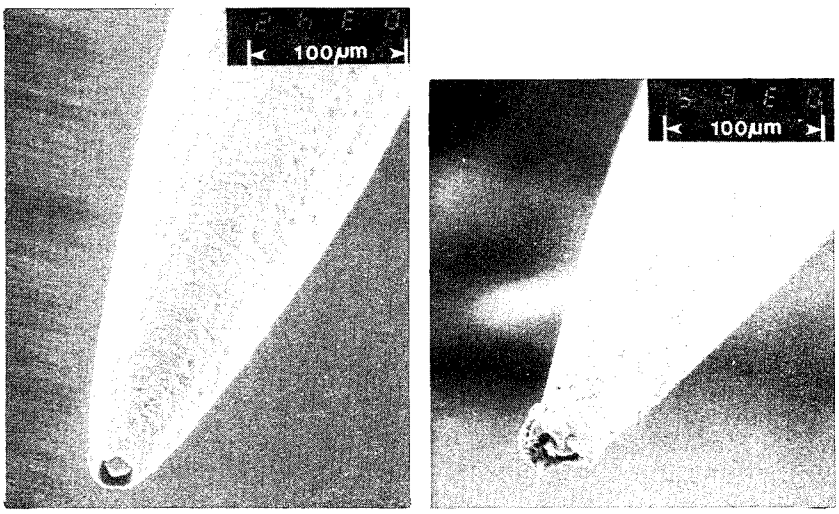

FIG. 7. SEM of electrodes coated with a composite GDP-M/Parylene C film: (a) after exposing the tip by corona discharge and before voltage cycling, (b) after voltage cycling for 105 sweeps.

coating acting as a diffusion barrier but that the film is not rupturing or exposing new areas of fresh platinum. Such changes would be indicated by increases in current in proportion to the newly exposed areas, as shown in the calibration studies of Figures 3(a) and 3(b) minus the decrease in current attributable to the anodic passivation current.

The results shown in Figure 5 indicate that both GDP-TFE and GDP-TMDSiO behave similarly to GDP-M and that even the thicker 10,000-Å GDP-TMDSiO films were not removed by cycling.

Included in Figure 5 are the results for poly(*p*-xylylene) and GDP-TFE/poly(*p*-xylylene)-composite-coated electrodes. As the number of cycles increases, the current rises for both groups, indicating that portions of the coating are being removed. However, the final currents for the composite-coated electrodes were only 10% of the current for the noncomposite poly(*p*-xylylene) films. Further examination of these electrodes was carried out by light and scanning electron microscopy as shown in Figures 6(a)–(d). Figure 6(a) shows the intact coating during the early stages of cycling. Note the bubbles forming only at the tip. The electrode shown in Figure 6(d) had most of the poly (*p*-xylylene) coating removed from the submerged area by the 70th sweep. Although sliding of the coating laterally along the surface occurred with the composite GDP-TFE/poly(*p*-xylylene) coating [Fig. 6(c)], actual lifting or detachment as in the noncomposite [Fig. 6(b)] was not found.

Further voltage cycling studies were done on wires in which the glow discharge polymer of methane (GDP-M) was used as a primer coating for the insulating overcoat of Parylene C. Figure 7(b) shows that this combination of coatings

tolerated the voltage cycling to 105 sweeps without any untoward effects on the film's protective structure. The currents measured for these electrodes were in the microampere region and remained constant during the cycling procedure. This can be compared with the data in Figure 5 (ordinate is in milliamperes), where even the best combination of coatings [GDP-TFE/poly(*p*-xylylene)] showed increases in current to several milliamperes after 35 sweeps.

Comparative Testing

To confirm whether the method was sensitive to the adhesion improvements shown in Figures 6 and 7, we carried out additional tests on these film combinations with an Instron pull tester. Brass rods 1 cm in diameter were mechanically polished with alumina and then electroplated with 3 μm of platinum. The average pull strength of the platinum deposits was 22.9×10^6 Pa after 2 h of boiling in saline solution. Results for the poly(*p*-xylylene) (Parylene N) and the composite GDP-TFE/Parylene N under accelerated boiling conditions are shown in Figure 8. The composite film appears to adhere better to the substrate than the noncomposite film as judged by the absolute magnitude of pull strength at each interval of boiling time. However, the decreasing rate of pull strength with boiling of the composite is no better than the Parylene N film alone. By comparing these results with those in Figures 5 and 6, one can see that some loss of adhesion is evident from both techniques.

The sensitivity of the method to the improvements shown in Figure 7 for the combination of glow discharge methane (GDP-M) and Parylene C is shown in Figure 9. The change in pull strength with hours of boiling for the composite is negligible when compared with the noncomposite film. These results were also demonstrated electrically by the low-microampere current throughout cycling and visually in Figure 7.

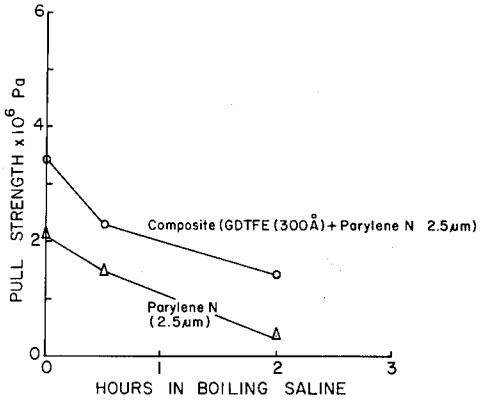

FIG. 8. Adhesion of Parylene N and GDP-TFE/Parylene N composite coatings under accelerated boiling conditions.

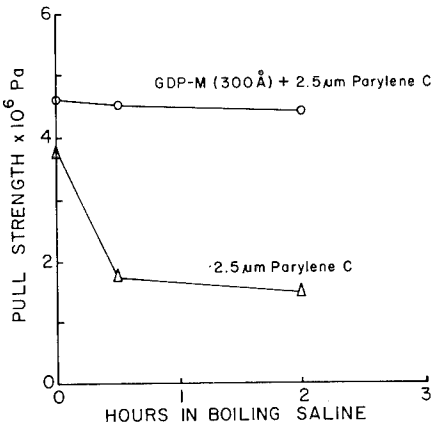

FIG. 9. Adhesion of Parylene C and GDP-M/Parylene C composite coatings under accelerated boiling conditions.

CONCLUSION

A new voltage cycling technique for monitoring the adhesion of organic films to their underlying substrates has been presented and compared with the conventional pull testing protocol with excellent agreement in detecting the rate of loss of adhesion. We conclude that in evaluating materials whose end use will be as insulators, the voltage cycling technique has many advantages over other techniques. Most important is the technique's ability to simultaneously stress the coating in the electrical, electrochemical, and mechanical modes independent of substrate size or geometry.

The authors would like to thank Ms. Victoria Watts, Mr. Charles Jorgenson, and Mr. Richard Lee for their superb technical assistance. We would also like to thank Dr. Darrel Kinden, Director of the Electron Microscope Laboratory of the College of Veterinary Medicine, UMC, for his outstanding help in obtaining quality micrographs. The authors would also like to thank the reviewers for their helpful comments. This work was supported in part by Contracts No. N01-NS-8-2393 and N01-NS-1-2382 from the National Institute of Neurological and Communicative Disorders and Stroke, NIH, Bethesda, MD 20205.

REFERENCES

[1] J. Yasuda, in *Proceedings of the Symposium on Adhesion Aspects of Polymeric Coatings,* Electrochemical Society Meeting, Minneapolis, May 1981, Plenum, New York, 1982.
[2] H. K. Yasuda, A. K. Sharma, E. B. Hale, and J. W. James, *J. Adhes., 13,* 269 (1982).
[3] J. Kruger, *Corrosion and Degradation of Implant Materials,* ASTM STP 684, B. C. Syrett and A. Acharya, Eds., American Society for Testing Materials, Philadelphia, 1979, pp. 107–127.
[4] S. B. Brummer, J. McHardy, and M. J. Turner, *Brain Behav. Evol., 14,* 10 (1977).
[5] N. C. Wake, *Polymer, 19,* 291 (1978).

[6] H. W. White, L. M. Goodwin, and T. Wolfram, *Adhesion, 9,* 237 (1978).
[7] R. K. Sadhir, W. J. James, H. K. Yasuda, A. K. Sharma, M. F. Nichols, and A. W. Hahn, *Biomaterials, 2,* 239 (1981).
[8] K. Bhasin, D. B. Jones, S. Sinhardy, and W. J. James, *Thin Solid Films, 45,* 195 (1977).
[9] M. Joly and J. Laout, in *Proceedings of the Third International Conference on Organic Coatings,* G. D. Parfitt and A. V. Patsis, Eds., Science and Technology, 1978, pp. 208–220.
[10] S. B. Brummer and M. J. Turner, *IEEE Trans. Biomed. Eng., 24,* 59 (1977).
[11] M. F. Nichols, A. W. Hahn, W. J. James, A. K. Sharma, and H. K. Yasuda, *Biomaterials, 2,* 161 (1981).
[12] Fifth Quarterly Progress Report, Contract No. N01-NS-8-2353, National Institutes of Health, October 1, 1979–December 31, 1979.
[13] W. F. Gorham, *J. Polym. Sci. A-1, 4,* 3027 (1966).
[14] G. E. Loeb, M. J. Bak, M. Salcman, and E. M. Schmidt, *IEEE Trans. Biomed. Eng., 23*(2), 121 (1977).

AN ATOMIC ASPECT OF PLASMA POLYMERIZATION: THE ROLE OF ELEMENTAL COMPOSITION OF THE MONOMER

M. GAZICKI and H. YASUDA
Department of Chemical Engineering and Graduate Center for Materials Research, University of Missouri, Rolla, Missouri 65401

SYNOPSIS

Seventeen monomers belonging to four different groups were polymerized. These groups were hydrocarbons, fluorocarbons, organosilicones, and sulfur-containing compounds. The specific tendency toward plasma polymerization expressed as deposition yield was studied as a function of elemental composition and the role of the particular atoms present in the monomer structure was followed. Deposition yields were found to be determined by elemental composition rather than molecular structure of the monomer. The abnormal deposition rate behavior of some monomers as well as pressure changes during polymerization were explained on the basis of the CAP (competitive ablation and polymerization) model of plasma polymerization.

INTRODUCTION

In discussions of a possible mechanism of plasma polymerization, two general routes are usually considered. One is a chain propagation mechanism similar to the conventional polymerization reactions and sometimes called plasma-induced polymerization or simply molecular polymerization [1]. All of the existing kinetic models of the process (such as the models proposed by Denaro, Owens, and Crawshaw [2], Lam, Baddour, and Stancell [3], and Poll, Artz, and Wickleder [4]) assume such a propagation scheme. On the other hand, the continuum of stepwise reactions leading to the deposition of solid is also being considered; this, by contrast, is called atomic polymerization [1]. The particular reactions in this continuum may be of a very various nature, i.e., excitation, ionization, homolitic bond splitting, molecular fragmentation, as well as bimolecular reactions of all kinds with all species involved. The number of such reactions is

Journal of Applied Polymer Science: Applied Polymer Symposium 38, 35–44 (1984)

CCC 0570-4898/84/010035-10$04.00

not, of course, infinite and each of them exhibits a particular probability; consequently, some of them are much more likely than others. Although, however, there are predominant reactions in such schemes they are not chain reactions. It has to be stressed here that monomer molecule fragmentation is a significant part of the atomic model, which, of course, does not mean that each molecule is split up among the participating atoms. It is called atomic only in contrast to the molecular model [1].

Therefore, it is quite understandable that in the first of the mechanisms the molecular structure of a monomer should play a predominant role, whereas in the atomic model it is rather the monomer atomic composition which should determine its tendency toward deposition. In order to examine the role of elemental composition four different groups of monomers have been investigated in this study: hydrocarbons, organosilicones, fluorocarbons, and sulfur-containing compounds. Some of the monomers also contained either oxygen or nitrogen. Low-energy conditions of plasma polymerization have also been chosen since such conditions are more favorable as far as the molecular model is concerned. Thus, if this model cannot be applied under low-energy conditions of plasma polymerization, it will not be applicable for any other conditions.

EXPERIMENTAL

The plasma polymerization equipment used in this study was the bell jar flow system with internal electrodes. Each of the two electrodes was equipped with a series of static magnets attached to its external surface in the circle mode. The role of the magnetic field was to focus plasma in the circle geometry (donut-shaped pattern). The system was applied by af power supply consisting of an HP 200 ABR audio oscillator, Crown M600 power amplifier, and NWL 25674 40V/2000V transformer. This supply system was operated at 10 kHz and provided a power range of 0 to about 100 W. The energy input per mass unit for this power range varied between 10^7 and 5×10^9 J/kg and these energetic conditions were considered to be quite moderate. The flow rate of each monomer was controlled by an MKS Baratron 254 flow control system, whereas glow discharge current and voltage were measured by using HP 3435A multimeters and these measurements were used to calculate the power. The system pressure was recorded by means of an MKS Baratron 220 pressure gauge and the deposition rates were monitored by a Kronos QM 301 thickness monitor along with the RI 100 deposition rate indicator. The thickness sensor was an oscillating quartz crystal which operated proportionally to the mass of the material deposited and was located stationary halfway between the electrodes. For any sample preparation, however (samples for dielectric measurements, for instance), a sample holder rotating halfway between the electrodes at frequency 1 c/s was used.

Seventeen monomers have been investigated in this study; they were representatives of four different groups. Hydrocarbons: propylene, isobutylene, cyclohexane, cyclohexene, and methane; organosilicones: 1,1,3,3-tetramethyldisilazane, hexamethylcyclotrisilazane, 1,1,3,3-tetramethyldisiloxane, hexa-

methylcyclotrisiloxane, and 2,4,6,8-tetramethylcyclotetrasiloxane; fluorocarbons: tetrafluoroethylene and perfluorocyclobutane; sulfur-containing monomers: carbon disulfide, carbonyl sulfide, thiophene, thiazole, and tetrafluoro-1,3-dithietane.

RESULTS

Deposition Rates

The first, qualitative observation was that the deposition rates of all species investigated were set at two levels, differing by about an order of magnitude. Most of the monomers showed rates in the tens of angstroms per minute, whereas hydrocarbons only (whether saturated like methane or unsaturated) exhibited rates in the range of angstroms per minute. In order to present a comparative picture of all the monomers' tendencies toward deposition the results were plotted in DR/*FM* vs. *W*/*FM* coordinates where DR is the deposition rate, *F* is the feed-in flow rate, *M* is the molecular weight of monomer, and *W* is the total power input. The first of the parameters (DR/*WM*) corresponds to the yield of the deposition, whereas the second one, *W*/*FM*, corresponds to the energy input per mass unit of monomer; plotting the deposition rate results of many different compounds in these coordinates gives rise to the most objective comparison of their tendencies toward deposition. Figure 1 shows the result of this plotting. It can be seen that the two tendencies are sharply distinguishable in this diagram. The lower broad line consists only of the results obtained for hydrocarbons; significantly, methane behaves here in exactly the same way as all the unsaturated hydrocarbons. The remaining three groups of monomers contribute to the upper, broad line. Although, unfortunately, the results here are sufficiently scattered to make it very difficult to distinguish among the three groups, it is worth noticing that the very left-hand edge of this line almost exclusively composed organosilicone results, with no fluorocarbon points. First of all, however, it is clear that hydrocarbons show behavior significantly different from that of any other type

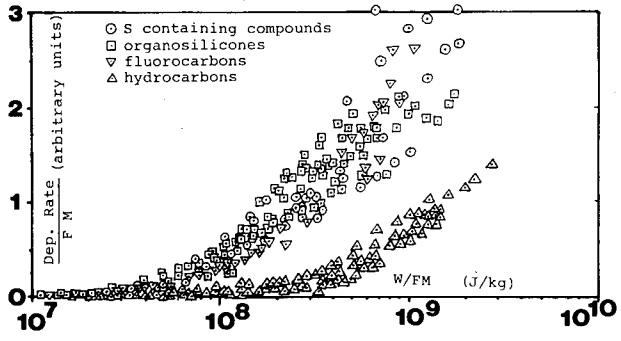

FIG. 1. Deposition rate over *FM* (deposition yield) vs. *W*/*FM* (energy input per mass unit) for four groups of monomers studied: (⊙) sulfur-containing compounds, (⊡) organosilicones, (▽) fluorocarbons, (△) hydrocarbons.

of monomer, requiring an order of magnitude higher energy input per mass to come up with comparable yield, and that their molecular structure is not a decisive factor here.

The results of two monomers only were not shown in Figure 1. These monomers were carbonyl sulfide and tetrafluoro-1,3-dithietane; the relationships of their deposition rates to power, shown in Figures 2 and 3, respectively, require more comment. All of the monomers with the exception of these two showed typical deposition rate dependences on power. Rising with increasing power, these characteristics stabilized and saturated at different levels, higher for higher flow rates. In the case of carbonyl sulfide, however, the deposition rates increase rapidly, reaching distinct maxima in different power regions for different flow rates, and then begin to decrease rapidly (Fig. 2). This behavior is a good example of the competitive polymerization and ablation (CAP) model of plasma polymerization [5]. For a low level of energy input the polymerization is dominant, which results in deposition rate increasing with power. Above certain levels of energy, however, the ablation process becomes significant enough to contribute to the overall picture and this contribution increases with power, resulting in decreasing deposition rate. Carbonyl sulfide contains oxygen, and it is known that such compounds show a tendency to evolve reactive oxygen atoms from their structure causing ablation [6]. It is thus not surprising that carbonyl sulfide is a good example of the CAP model.

Another even more sophisticated example of competitive ablation and polymerization is the case of tetrafluoro-1,3-dithietane, for which deposition rates versus power are shown in Figure 3. The relationships have been taken for three different flow rates (0.33, 1.0, and 3.0 sccm), and at first view each of them seems to show a completely different behavior. The interrupted lines in these curves indicate regions where deposition rates became negative, as found by decreasing numbers of thickness monitor readouts. The curve obtained for 1.0 sccm consists of two (at least) positive regions, the first with the distinct peak

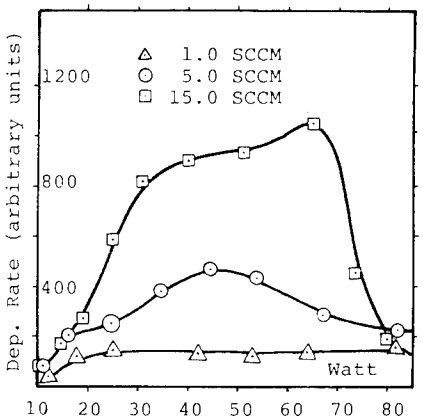

FIG. 2. Deposition rate versus power for carbonyl sulfide: (△) 1.0, (⊙) 5.0, (⊡) 15.0 sccm.

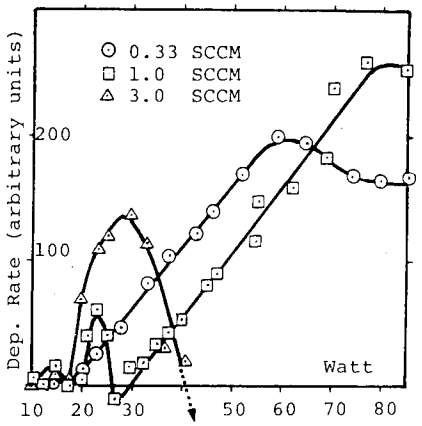

FIG. 3. Deposition rate versus power for tetrafluoro-1,3-dithietane: (⊙) 0.33, (⊡) 1.0, (△) 3.0 sccm.

at about 23 W and the second with deposition rate increasing linearly to reach saturation; these positive regions are interrupted by a negative region. The 3.0-sccm curve reaches a peak at about 30 W, then decreases to reach negative values over 40 W, with no tendency to reverse within the power range used. The 0.33-sccm curve, however, shows typical, positive behavior, i.e., linear increase with power and the saturation level, and has no tendency to become negative in the same range. It seems likely that the 3.0-sccm characteristic corresponds to the first positive region only, while the 0.33-sccm characteristic corresponds to the second positive region only. This behavior strongly suggests that in the case of tetrafluoro-1,3-dithietane two different mechanisms are active in the respective W/FM regions and the exchange of these mechanisms is accompanied by ablation temporarily taking over. As a matter of fact, fluorine is known as the second element (besides oxygen) showing a significant tendency to cause ablation [7], such behavior is not surprising.

System Pressure

In a given flow system for a given monomer the system pressure is established at constant temperature as a function of two factors only. These factors are the feed-in flow rate (subject to automatic control in our case) and the pumping rate of the monomer. Any change in the flow rate results in a subsequent change of pressure. In other words, the higher the flow rate of a given gas, the higher is the pressure of its flow, which is called p_0 here (initial pressure of the system). This situation changes dramatically when the monomer is subjected to a glow discharge. The system pressure under glow discharge conditions, p_G, is a function of monomer flow rate, the pumping rate of the leaving gases, and the glow discharge reactions. In the first approximation, we neglect the influence of pumping rates; in other words we assume that pumping rates of monomer and

leaving gases are equal. The pressure change under glow is then the result of the reactions taking place only. Let us now consider the CAP model again and extend the term ablation to all phases present in the system, i.e., ablation of the solid phase and fragmentation of the gas-phase species. The competitiveness in CAP model should now be reflected in pressure changes. Ablation in this sense consists of all processes contributing to the pressure increase, whereas polymerization is responsible for the pressure drop. The glow discharge pressure p_G is a result of the competition between the two. In other words, in a rough approximation, if polymerization dominates p_G should be lower than p_0 and p_G/p_0 should be lower than unity, and when ablation dominates p_G/p_0 should be higher than unity.

In most of the cases reported in this work, significant pressure changes were observed when the system was subjected to the glow discharge. The following

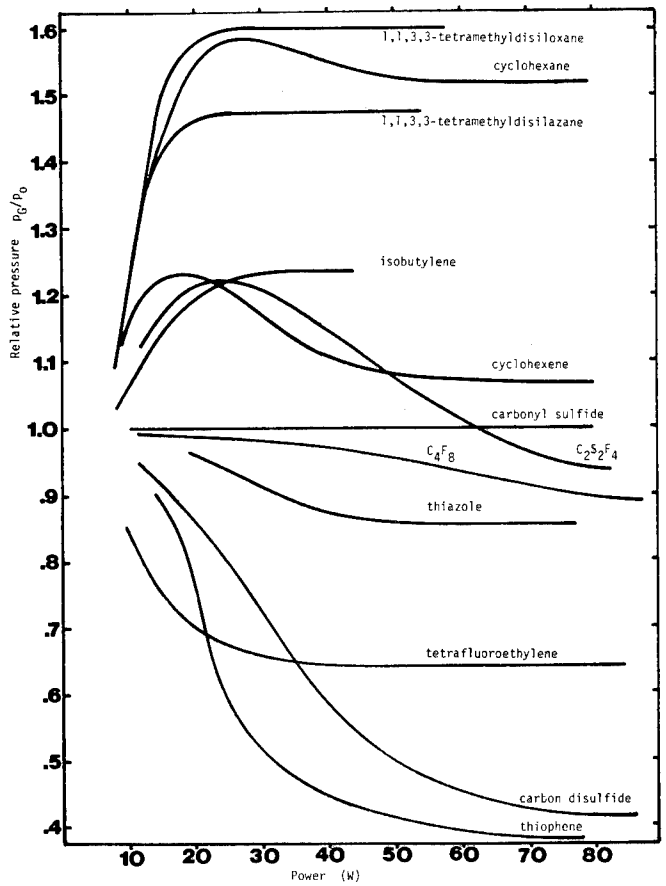

FIG. 4. Relative pressure p_G/p_0 versus power for most of the investigated monomers. Feed-in flow rate $F = 1$ sccm in each case.

trends should be stressed. All the hydrocarbons and organosilicones showed positive pressure changes which increased until the power reached saturation levels similar to those of the deposition rates. Fluorocarbons as well as most of the sulfur-containing compounds showed negative pressure changes. Carbonyl sulfide and tetrafluoro-1,3-dithietane are exceptional here too. Figure 4 presents the pressure changes against power for most of the monomers at a flow rate of 1 sccm. A few monomers are not included in this figure either because their low vapor pressure results in flow rates lower than 1 sccm (as in the cases of hexamethylcyclotrisilazane and 2,4,6,8-tetramethylcyclotetrasiloxane) or because their value of p_G/p_0 exceeds the scale of the figure (as in the case of hexamethylcyclotrisiloxane, for which the saturation level is $p_G/p_0 = 2.15$). The tendencies are, however, the same in each case and the generalization discussed below concerns all the monomers, including those not presented in the figure.

In comparison of the pressure-change results with the deposition rate data for the respective groups of monomers the following general observations should be stressed. Hydrocarbons, which have a lesser tendency than other monomers toward polymerization, exhibit positive pressure changes, whereas fluorocarbons as well as most sulfur monomers, showing higher polymerization yields, exhibit negative pressure changes. Methane is an exceptional hydrocarbon with respect to pressure since it does not undergo any significant changes. The methane molecule does not provide, however, very many possibilities for fragmentation, and despite its low deposition rates, pressure changes are negligible in this case. Generally, however, the results for hydrocarbons, fluorocarbons, and sulfur monomers are consistent with the CAP model, which predicts positive pressure changes for slow depositions and negative pressure changes for fast depositions. In this context, the case of organosilicones requires more explanation since despite high polymerization yields they exhibit significant positive pressure changes during the discharge. To understand this behavior, one should take into consideration the structure of all the organosilicones. This structure is built up on two levels: the organic side groups (methyl groups in our case) are attached to the inorganic framework (Si—O—Si or Si—NH—Si chains or rings [8]). The pressure increase during the plasma polymerization of such systems is always due to the splitting off of organic groups, whereas the inorganic part of the molecules does not undergo significant fragmentation in the deposition process. As both ablation and polymerization processes, dealing with different parts of the molecule, occur at the same time with high yields, they are simultaneous rather than competitive here and this explains the abnormal behavior of organosilicone monomers with respect to the CAP model.

DIELECTRIC PROPERTIES OF PLASMA-POLYMERIZED THIN FILMS

Since the elemental composition of the monomers plays a significant role in their tendencies toward deposition, it is also interesting to find out how the properties of the polymers depend on this composition. The dielectric properties

TABLE I
Dielectric Parameters of Plasma-Polymerized Thin Films

Monomer	Flow rate (sccm)	Power (W)	W/FM (J/kg)	Deposition rate (Å/min)	Dielectric constant	Dissipation factor (%)
Propylene	15	30	6.4×10^7	3.9	2.40	0.4
Isobutylene	10	27	6.5×10^7	2.6	3.01	0.5
Cyclohexane	10	41	6.5×10^7	6.2	1.87	0.4
Cyclohexene	5	20	6.5×10^7	5.5	2.18	0.3
1,1,3,3-Tetramethyldisilazane	5	40	8×10^7	63	2.90	0.9
Hexamethylcyclotrisilazane	0.21	26	7.6×10^8	11	5.14	9.8
1,1,3,3-Tetramethyldisiloxane	5	40	8×10^7	59	2.54	0.7
Hexamethylcyclotrisiloxane	1	33	2×10^8	46	2.70	0.3
2,4,6,8-Tetramethylcyclotetrasiloxane	0.5	18	2×10^8	38	4.28	0.4
Tetrafluoroethylene	15	72.5	6.5×10^7	55	4.98	0.3
Perfluorocyclobutane	7.5	72.5	6.5×10^7	56	2.60	0.4
Carbon disulfide	5	70	2.5×10^8	31	4.27	0.55
Carbon sulfide	5	70	3×10^8	22	3.09	1.1
Thiophene	6	75	2×10^8	38	2.42	0.9
Thiazole	6	75	2×10^8	62	3.07	1.6
Tetrafluoro-1,3-dithietane	1	42	3×10^8	7	4.44	1.0

have been chosen in this study and the results (at room temperature and $f = 100$ Hz) are presented in Table I. As can be immediately seen, no significant differences in dielectric parameters were found between films of different elemental composition. As a matter of fact, the differences in dielectric constants are sometimes higher within one group than between groups. The only noticeable tendency concerns slightly higher dissipation factors found for sulfur-containing compounds than for any other film. This result is consistent with the data published by Bradley and Hammes [9], who reported plasma-polymerized sulfur-containing films as exhibiting the highest values of conductivities among different groups of plasma polymers. The dissipation factor of the film is a function of its conductivity and thus the result is not surprising. Generally, however, the dielectric parameters of plasma-polymerized films are not characteristic for the materials of different elemental composition. It seems to us that it is rather the general property of plasma polymers that owing to their high concentration of such dipole groups as carbonyl and hydroxyl groups they exhibit significantly higher dissipation factors than their conventional unpolar correspondents; this fact dominates other possible differences in this parameter due to the elemental composition.

CONCLUSION

This study indicates that even under relatively low-energy-input conditions, where molecular polymerization might play a role, it can be observed that the nature of the elements present in the monomer molecule seems far more important than the order in which these elements are added to the monomer's structure. It has been found, for instance, that hydrocarbons, saturated or unsaturated, show a much lesser specific tendency toward deposition than other organic compounds. It has also been shown that the presence of some elements such as oxygen or fluorine in some instances leads to seemingly abnormal behavior. The competitive ablation and polymerization (CAP) model of plasma polymerization predicts, however, such behavior; in any case it is only the specific tendency to ablation exhibited by particular elements which brings about the anomalies. The CAP model is a phenomenological representation of the atomic type of deposition and there is no doubt that this model approximates the process much better than molecular models based on conventional chain-type polymerization reactions.

REFERENCES

[1] H. Yasuda, *J. Polym. Sci. Macromol. Rev., 16,* 199 (1981).
[2] A. R. Denaro, P. A. Owens, and A. Crawshaw, *Eur. Polym. J., 4,* 93 (1968).
[3] D. K. Lam, R. F. Baddour, and A. F. Stancell, in *Plasma Chemistry of Polymers,* M. Shen, Ed., Dekker, New York, 1976.
[4] H. U. Poll, M. Artz, and K. H. Wickleder, *Eur. Polym. J., 12,* 505 (1976).
[5] H. Yasuda and T. Hsu, *Surf. Sci., 76,* 232 (1978).

[6] H. Yasuda, presented at the IUPAC International Round Table on Plasma Polymerization and Plasma Treatment, Limoges, France, 1977.
[7] E. Kay, presented at the IUPAC International Round Table on Plasma Polymerization and Plasma Treatment, Limoges, France, 1977.
[8] A. M. Wróbel, M. Kryszewski, and M. Gazicki, *Polymer, 17*, 678 (1976).
[9] A. Bradley and J. P. Hammes, *J. Electrochem. Soc., 110*(1), 15 (1963).

PLASMA-INITIATED SOLUTION POLYMERIZATION AND ITS APPLICATION TO IMMOBILIZATION OF ENZYMES

YOSHIHITO OSADA, YU IRIYAMA, MITSUO TAKASE, YASUHIRO IINO, and MASARU OHTA
Department of Chemistry, Ibaraki University, Mito 310, Japan

SYNOPSIS

Plasma-initiated solution polymerization of 2-hydroxyethyl methacrylate, acrylamide, and 2-acrylamido-2-methyl-1-propanesulfonic acid (AMPS) was carried out in water, ethanol, DMSO, and DMF by exposing the monomers to radio-frequency cold plasma for 60 s, followed by the post-polymerization at 25°C. It was found that the polymerization takes place very rapidly in water regardless of the monomer species to give an extremely high-molecular-weight polymer. Crosslinked polymer gels prepared by the plasma-initiated copolymerization of AMPS and acrylamide in the presence of *N,N*-methylene-bisacrylamide in water were found to exhibit high-water-adsorption abilities. This polymerization method was applied to immobilize invertase on various organic and inorganic porous substrates. Electrons generated from the plasma were found to be trapped by solvated 2,2-diphenyl-1-picrylhydrazyl and the rate of electron liberation from the plasma was estimated.

INTRODUCTION

Plasma-initiated polymerization of vinyl monomers to give ultrahigh-molecular-weight polymers with linear structure has been developed recently by Osada et al. [1–3]. It was also found that organic and inorganic cyclic monomers such as single-crystalline trioxane, tetraoxane [4,5], phosphazenes [6,7], and siloxanes [8] undergo ring-opening polymerization in the course of the same plasma initiation procedure. In this article we present solution polymerization of water-soluble vinyl monomers such as acrylamide (AAM), 2-hydroxyethyl methacrylate (HEMA), and 2-acrylamido-2-methyl-1-propanesulfonic acid (AMPS). It was found that these monomers polymerize exceedingly rapidly in water, resulting in polymers with very high molecular weight. The technique of this polymerization was applied to the immobilization of enzymes. The principle of

Journal of Applied Polymer Science: Applied Polymer Symposium 38, 45–54 (1984)

CCC 0570-4898/84/010045-10$04.00

this novel immobilization method is based on the entrapment of enzyme proteins in the extremely high-molecular-weight polymers prepared at low temperature and short plasma duration. A one-electron plasma reduction of solid and solvated viologens and other electron scavengers was also found. The concentration of electrons liberated in the plasma and subsequently diffused to the liquid phase was estimated.

EXPERIMENTAL

The experimental apparatus and procedure used in this investigation were essentially identical with those described previously [1–3,6–8]. Liquid monomers and solvents were purified by vacuum distillation under argon. AAM, 2,2-diphenyl-1-picrylhydrazyl (DPPH), and 2,2′-azobisisobutyronitrile (AIBN) were recrystallized from an appropriate solvent.

Photopolymerization was carried out by irradiation from high-pressure mercury lamp (400 W) at a distance of 50 cm throughout the polymerization. Invertase entrapped was of commercial origin (concentrate from yeast, stabilized with 50% glycerine, Wako Chemical). Saccharose was used as a substrate. The rate of hydrolysis of a 10 wt % solution of the substrate was assayed polarimetrically with a JASCO DIP 140 polarimeter in the acetate buffer (pH 4.6) at 25°C.

A spongelike immobilized enzyme was prepared by exposing plasma for 60 s on 2–5 mL of 50 vol % aqueous HEMA solution containing 1–2 mL of invertase. Immobilization was also performed on porous organic and inorganic substrates such as polyacrylonitrile fibers having 2.5–5.0-μm pores, silica particles, and molecular sieve 4A. These substrates were first immersed in 2 mL of invertase and 6 mL of water for 1 h *in vacuo* at room temperature, followed by mixing with 2–4 mL of HEMA *in vacuo*. Plasma was exposed for 90 s in a separable flask (35 mm i.d.) and postpolymerized for 24 h at 25°C. The reaction mixture was washed thoroughly with a large amount of water to remove free invertase, monomer, and polymer. The activity of the enzymes while being stirred was tested in a 5-mL Erlenmeyer flask. The stability of the immobilized enzyme was studied on "resting" the enzyme in acetic acid–acetate buffer solution in the absence of the substrate at room temperature. The aliquot was taken every 7 days and tested the activity change.

RESULTS AND DISCUSSION

Effects of Water on Rate of Polymerization

Figure 1 shows typical time–conversion curves for the plasma-initiated polymerization of AAM, HEMA, and AMPS in water, ethanol, DMSO, and DMF. It is apparent that these monomers can polymerize exceedingly rapidly in water compared with the polymerization in the organic solvents. The rate of polymerization of AAM in water was calculated as 4800 times higher than that in DMF. Similar results were obtained for other monomers such as acrylic and

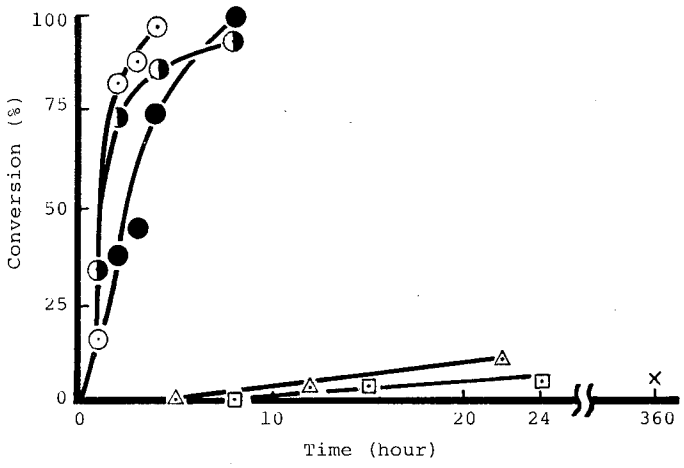

FIG. 1. Time–conversion relationships for the plasma-initiated polymerization of HEMA half-filled (◑), AMPS (●), AAM (⊙) in water, and AAM in ethanol (△), DMSO (⊡), and DMF (×); plasma: 100 W, 60 s; HEMA, 4.15 mol/L (50% v/v); AAM, 4.15 mol/L; AMPS, 2.08 mol/L; 25°C postpolymerization.

methacrylic acids and *N*-hydroxymethyl-acrylamide [9]. Since no such strong solvent effects were obtained by photoinitiated or chemically initiated radical polymerization [9–11], the results obtained are apparently the result of plasma-initiated polymerization. Figure 2 shows the dependence of monomer concentration on the rate of polymerization of HEMA [12]. The apparent rate of polymerization strongly depends on water content, with a maximum value obtained at 50% v/v. It was reported before that the polymerization is sustained by free radical propagation from the results of the tacticity distribution and the monomer–copolymer relationship [1–3]. Therefore, the obtained result is quite unusual for the radical polymerization since it should maintain a first-order relationship with regard to monomer concentration [13].

The polymers obtained in water were found to have extremely high molecular weight. For example, plasma exposure for 60 s and the postpolymerization for 5–8 h at 25°C resulted in poly-AAM and poly-AMPS with conversion higher than 95% and intrinsic viscosities 22.6 and 15.5 dL g^{-1}, respectively. In contrast, AAM and AMPS were polymerized to only 59 and 46% conversion by H_2O_2 (1 mol % to monomer) after 24 h at 50°C, and their intrinsic viscosities were 4.3 and 9.7 dL g^{-1}. The molecular weight of plasma-polymerized poly-AAM was approximately estimated to be 9.0×10^6 from the viscosity–molecular weight relationship [14].

Formation of a long-living radical is another unique feature of plasma-initiated polymerization. This living radical was used successfully to prepare block copolymers [9]. It should be noted that rapid polymerization of alkyl esters of acrylic and methacrylic acid occurred in water when the monomer was emulsified with an appropriate amount of surfactant such as sodium salt of dodecylbenzene

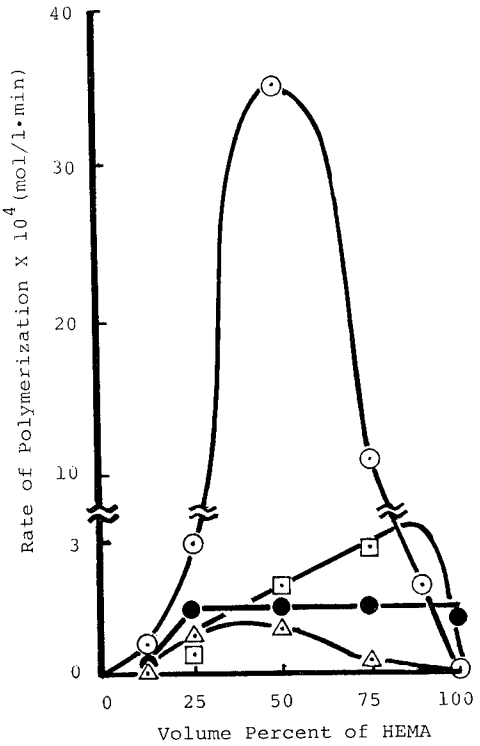

FIG. 2. Monomer concentration dependences of the rate of polymerization of HEMA by plasma and UV exposures. Plasma (100 W, 60 s; 25°C postpolymerization): water (⊙), ethanol (△), DMSO (⊡). UV: (400-W mercury lamp, 25°C in-source polymerization): water (●).

sulfonic acid [15]. It had been believed that no acrylate esters were subject to plasma-initiated polymerization [3].

Water and Metal-Ion Adsorption Behaviors of Gels

We have found that crosslinked polymer gels prepared by the plasma-initiated copolymerization of AMPS and AAM in water exhibit an extremely high-water-adsorption ability. The degree of water or artificial urine adsorption, which is defined as $(W - W_0)/W_0$ (where W and W_0 are the weights of gels in swollen and dry states), attained 1750 and 120 as shown in Figure 3 [16]. As is well known, a variety of superabsorbant polymer gels were developed recently [17,18], but to our knowledge the obtained values of water and artificial urine adsorption seem to be some of the highest cases ever reported. This high absorbance is considered to be related to the extremely long macromolecular chain of these polymer gels and their marked entanglement since polymer gels prepared by radical initiators such as H_2O_2 and $K_2S_2O_8$ showed less pronounced absorbance abilities both for water and artificial urine.

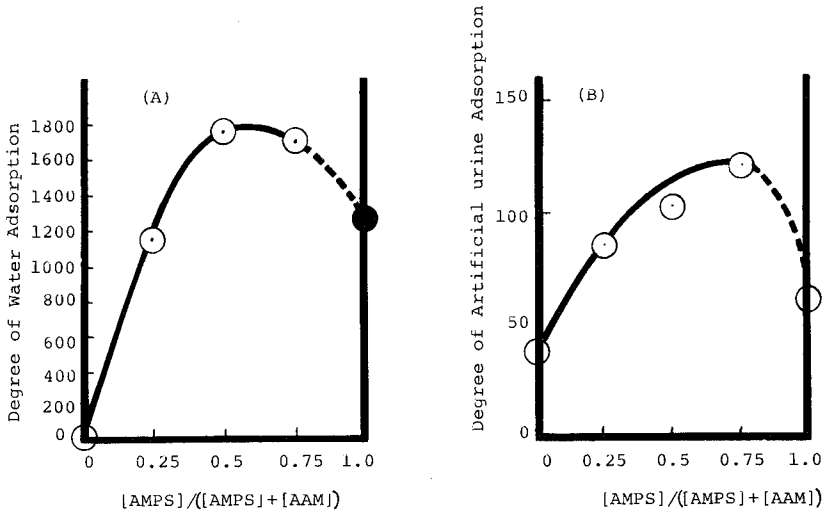

FIG. 3. Relationship between degree of water (A) and artificial urine (B) adsorptions on the mole fraction of AMPS unit in AMPS–AAM copolymer; molar ratio of *N,N*-methylene-bisacrylamide to monomer was 10^{-4} (●) and 10^{-5} (⊙).

We have also found that the poly-AMPS gels prepared by plasma initiation have very large ion-binding constants K against Cr^{3+}, Co^{2+}, and Cu^{2+}; K (mol/L) was determined as 35.9 for Cr^{3+} and 30.0 for Co^{2+}, whereas those of the gels prepared by the radical initiator were 17.6 for Cr^{3+} and 6.25 for Co^{2+} [16].

Immobilization of Enzymes

Extremely rapid polymerization of monomers in water was applied to immobilize enzymes [19]. Plasma is essentially a surface reaction, and a host of chemically active species such as electrons, ions, and radicals in the gas plasma cannot penetrate into the medium more than a few microns [20]. In fact, prolonged plasma exposure scarcely damped invertase activity, as shown in Figure 4.

The following are typical characteristics of enzyme immobilization by use of plasma-initiated polymerization: (i) practically no penetration of energetic plasma into medium, (ii) brief exposure of plasma, (iii) rapid polymerization at low temperature, (iv) little leakage of enzymes due to ultrahigh-molecular-weight polymers, (v) pure system containing no initiator. Three types of immobilization were performed: One is the polymerization of an aqueous AAM or HEMA containing invertase [and *N,N*-methylene-bisacrylamide (MBAA) in the case of AAM] in the ampule to give a spongelike pellet-type enzyme. The other one was the thin film prepared in the common plasma reactor. The monomer–enzyme solution on a slide glass was exposed to plasma, followed by postpolymerization at room temperature. The relative activities of the immobilized enzymes were

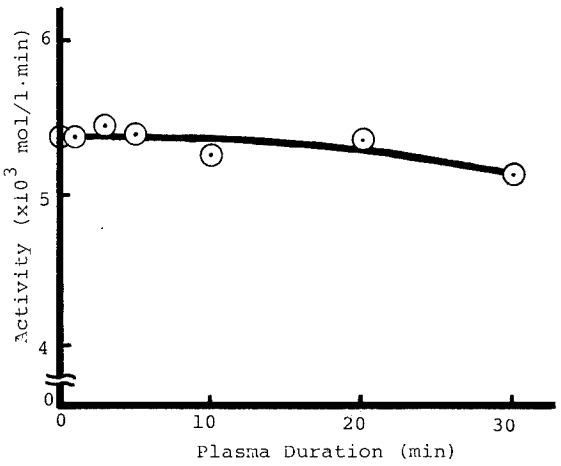

FIG. 4. Influence of plasma duration on activity of invertase. Plasma was sustained in an ampule of 10 mm diameter containing 0.02 mL of invertase and 10 mL of buffer solution. Hydrolysis was carried out using 10 wt % saccharose solution.

found to be about 40–60% for the pellets and 20% for the thin films [19]. In addition, the immobilization was also performed on porous organic and inorganic substrates. Figure 5 shows the activities of immobilized invertase entrapped in the porous polyacrylonitrile fibers, on silica particles with 3 mm diameter, and on molecular sieve 4A. It is seen that the porous fibers can maintain high activity through repeated use. The fiber-entrapped enzyme and the spongelike immobilized enzyme from poly-HEMA were employed in a continuous system in the

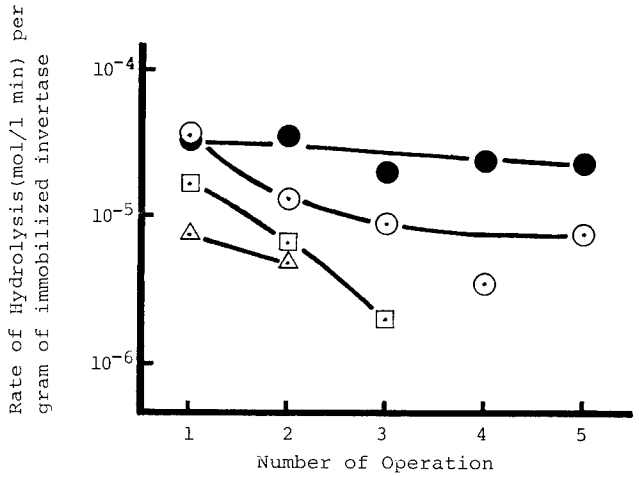

FIG. 5. Changes in activity of invertase immobilized on the various porous substrates by repeated use: (⊙) porous polyacrylonitrile fiber, 35.5 denier; (●) porous polyacrylonitrile fiber, 75 denier; (⊡) molecular seive 4A, cylinder 3 mm diameter and 6 mm long; (△) silica sphere 3 mm in diameter.

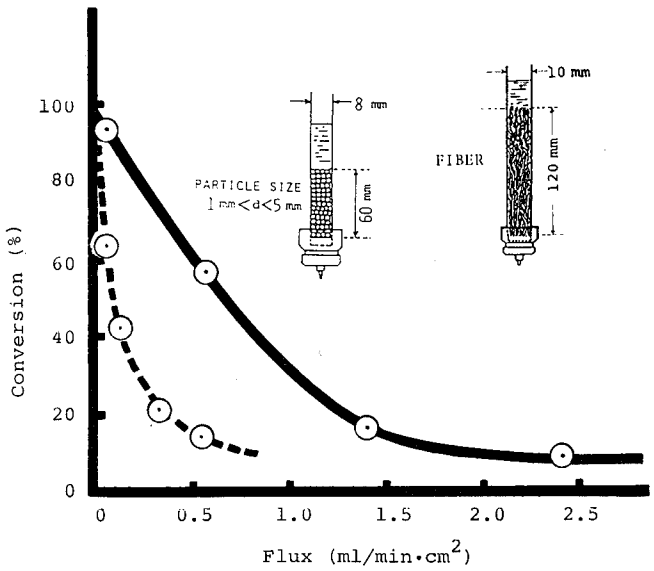

FIG. 6. Effect of flow rate on percent conversion of hydrolysis of saccharose by the fiber-entrapped invertase (—⊙—) and pellet-type immobilized invertase (--⊙--), fiber (35.5 denier)-entrapped invertase: 0.17 g; pellet-type immobilized invertase: 0.7 g; saccharose: 10 wt %, pH 4.6.

column. As shown in Figure 6, the degree of conversion of the saccharose into product is a function of the flow rate, with conversion x expressed as

$$x = 1 - \exp(-K/F)$$

where K is the apparent rate constant (min^{-1}) and F is the flux (mL/min cm^2) for the given column length. The long-term stability of invertase in the particle in the column has been tested on "resting" the enzyme in the absence of the substrate at room temperature. So far the invertase immobilized is providing about 70% of initial activity after 10 months of rest. The technique of entrapment of enzymes by the plasma-initiated polymerization is simple and can potentially be applied to many proteins, cells, and bacteria.

Plasma Reactions with Electron and Radical Scavengers

It should be emphasized here again that the rate of polymerization of monomers was negligibly low in DMF, as shown in Figure 1. An interesting feature in connection with this phenomenon is the fact that a DMF solution of viologen compounds is reduced very quickly by plasma exposure to give cation radicals [21]. For example, the transparent DMF solution of benzylviologen (1,1′-dibenzyl-4,4′-dipyridinium dichlorides; BV^{2+}) changed to a deep blue color as soon as the plasma was exposed. The spectra in Figure 7 are in good agreement with the reported spectra of photochemically reduced viologens, showing the monotonous increase of the intensity with the plasma duration [21]. The char-

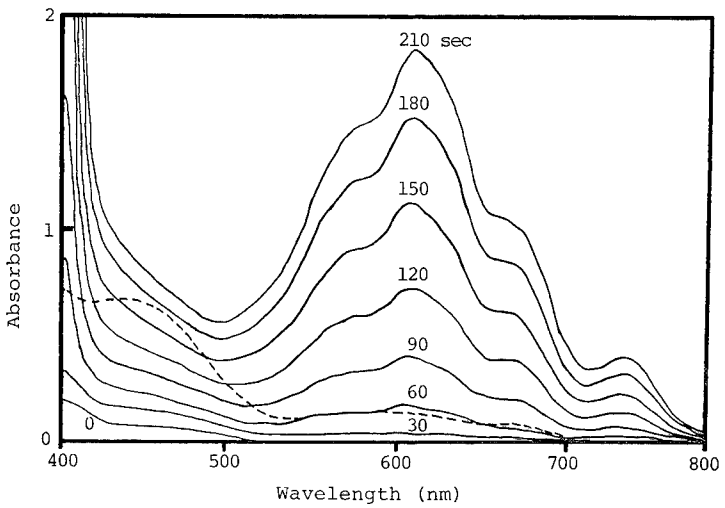

FIG. 7. Progressive spectral changes of benzylviologen with plasma duration; figures denote plasma duration; benzylviologen, 4.88×10^{-4} mol/L in DMF; plasma, 100 W; (---) after air quenching.

acteristic absorptions at 402 and 607 nm clearly show the formation of corresponding cation radical $BV^{+\bullet}$ [22,23]. The spectrum disappeared on exposure to air, but reappeared with repeated plasma exposure. This fact suggests that the reduction occurred via a one-electron process [24].

From experiments at different concentrations and different plasma powers, the rate of plasma reduction of BV^{2+} was found to be expressed as follows:

$$d[BV^{+\bullet}]/dt = K[BV^{2+}]^{0.5}(\text{Plasma power})^{1.0}$$

where K is a constant depending on the plasma reactor.

In addition to the DMF solution of BV^{2+}, a solid sample of BV^{2+}, poly(xylylviologen dichloride)s, methylene blue, iodine, and other organic and inorganic compounds were found to be reduced in DMF. The reduction also took place when BV^{2+} was mixed with DMF which had been exposed to plasma a few days prior to mixing. It was also found that plasma-exposed DMF is capable of initiating polymerization when vinyl monomers were mixed instead of BV^{2+}. These experimental facts imply that the reaction products generated within the plasma are sufficiently long-lived to induce "postreduction" and "postpolymerization" in DMF. The stabilized active species in DMF should result in a lower activity for the polymerization, and this assumption is consistent with the results presented in Figures 1 and 2.

It was found that the presence of a small amount of BV^{2+} strongly inhibits polymerization. This fact indicates that the electrons diffused into the liquid could be considered at least as a transient intermediate for subsequent radical polymerization. Furthermore, active species (electron or radical) responsible for the polymerization induced by plasma in DMF or DMSO were found to be

efficiently trapped by DPPH. The progressive spectral changes of DPPH with plasma duration are shown in Figure 8(A). Similar spectral changes were obtained when DMF had initially been exposed to plasma, followed by subsequent mixing with DPPH. Figure 8(B) shows the spectral changes of DPPH when AIBN was thermally decomposed, forming 2-cyano-2-propyl radicals in the presence of DPPH [25,26]. It is seen that the rate of spectral changes due to AIBN decomposition is significantly slower than that caused by the plasma. The rate of DPPH consumption was calculated as 3.3×10^{-5} mol/L s per 1 cm^2 of liquid surface for plasma at 100 W and 2.5×10^{-9} mol/L for 10^{-3} mol/L of AIBN decomposition at 50°C. The obtained value for the rate of AIBN decomposition is consistent with the literature [27]. Supposing that the rate of electron (radical) consumption induced by plasma is proportional to the scavenger's concentration, one can roughly estimate that the concentration of electrons liberated in the plasma at 100 W and diffused through 1 cm^2 of liquid surface to be about 13,000 times higher than that caused by the decomposition of 10^{-3} mol/L of AIBN at 50°C in DMF. This result indicates that enormous numbers of electrons (radicals) are generated within a very short duration of plasma and can diffuse readily through the liquid monomer surface, subsequently initiating polymerization. Finally, it should be mentioned, however, that the following unique and inter-

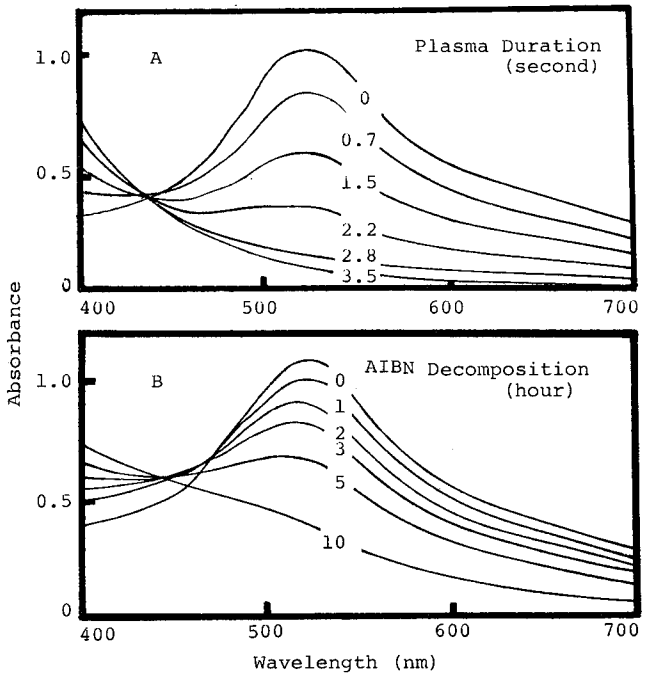

FIG. 8. Progressive spectral changes of DPPH in DMSO by plasma exposure (A) and by thermal decomposition of AIBN at 50°C (B); DPPH, 10^{-4} mol/L; AIBN, 10^{-3} mol/L; plasma, 100 W; figures denote plasma duration in seconds (A) and decomposition time of AIBN in hours (B).

esting features of plasma-initiated polymerization remain unsolved pending further investigation: Why are the radicals sufficiently long-lived to induce post-polymerization, and how are they formed? Why is the polymerization so selective toward monomer species? Why is the process of polymerization so strongly affected by the solvent? What is the role of water in the polymerization?

REFERENCES

[1] Y. Osada, A. Bell, and M. Shen, *J. Polym. Sci. Polym. Lett. Ed., 16,* 309 (1978).
[2] D. Johnson, Y. Osada, A. Bell, and M. Shen, *Macromolecules, 14,* 118 (1981).
[3] Y. Osada, A. Bell, and M. Shen, in *Plasma Polymerization, Am. Chem. Soc. Symp. Ser. No. 108,* M. Shen and A. T. Bell, Eds., Am. Chem. Soc., Washington, DC, 1979, p. 253.
[4] Y. Osada, M. Shen, and A. Bell, *J. Polym. Sci. Polym. Lett. Ed., 16,* 669 (1978).
[5] A. Odajima, Y. Nakase, Y. Osada, A. Bell, and M. Shen, in *Plasma Polymerization, Am. Chem. Soc. Symp. Ser. No. 108,* M. Shen and A. T. Bell, Eds., Am. Chem. Soc., Washington, DC, 1979, p. 263.
[6] Y. Osada, M. Hashidzume, E. Tsuchida, and A. Bell, *Nature* (London), *286,* 693 (1980).
[7] Y. Osada, Y. Iriyama, and M. Hashidzume, *Kobunshi Ronbunshu, 38,* 635 (1981).
[8] Y. Osada and M. Hashidzume, *J. Polym. Sci. Polym. Lett. Ed., 19,* 369 (1981).
[9] Y. Osada, Y. Iriyama, and M. Takase, *Kobunshi Ronbunshu, 38,* 629 (1981).
[10] T. Alfrey, Jr., and C. C. Prince, *J. Polym. Sci., 2,* 101 (1947).
[11] C. H. Bamford, A. D. Jenkins, and R. Johnson, *Trans. Faraday Soc., 55,* 418 (1959).
[12] Y. Osada, M. Takase, and Y. Iriyama, *Polym. J., 15,* 81 (1983).
[13] P. J. Flory, *Principles of Polymer Chemistry,* Cornell U. P., Ithaca, NY, 1953, Chap. 4.
[14] W. Sholten, *Makromol. Chem., 14,* 169 (1954).
[15] Y. Osada and M. Takase, *J. Polym. Sci. Polym. Lett. Ed., 21,* 643 (1983).
[16] Y. Osada and M. Takase, *Nippon Kagaku Kaishi,* 439 (1983).
[17] G. F. Fanta, M. D. Weaver, and W. M. Doane, *Chemtech,* 675 (1974).
[18] L. A. Gugliemelli, M. O. Weaver, C. R. Russel, and C. E. Rist, *J. Appl. Polym. Sci., 13,* 2007 (1969).
[19] Y. Osada, Y. Iino, and Y. Iriyama, *Chem. Lett.,* 171 (1982).
[20] For example, *Techniques and Applications of Plasma Chemistry,* J. R. Hollahan and A. T. Bell, Eds., Wiley, New York, 1974, p. 116.
[21] Y. Osada and Y. Iriyama, *J. Am. Chem. Soc., 104,* 2925 (1982).
[22] E. M. Kosower and J. L. Cotter, *J. Am. Chem. Soc., 86,* 5524 (1964).
[23] C. S. Johnson, Jr., and H. S. Gutowsky, *J. Chem. Phys., 39,* 58 (1963).
[24] C. L. Bird and A. T. Kuhn, *Chem. Soc. Rev., 10,* 49 (1981).
[25] H. W. Melville and W. F. Watson, *Trans. Faraday Soc., 44,* 886 (1948).
[26] G. S. Hammond, J. N. Sen, and C. E. Boozer, *J. Am. Chem. Soc., 77,* 3244 (1955).
[27] C. E. Bawn and S. F. Mellish, *Trans. Faraday Soc., 47,* 1216 (1951).

BIOCOMPATIBILITY OF GLOW-DISCHARGE-POLYMERIZED FILMS AND VACUUM-DEPOSITED PARYLENE

ALLEN W. HAHN, DONALD H. YORK, MICHAEL F. NICHOLS, and GEORGE C. AMROMIN
John M. Dalton Research Center, University of Missouri, Columbia, Missouri 65211

H. K. YASUDA
Graduate Center for Materials Research, University of Missouri, Rolla, Missouri 65401

SYNOPSIS

Since glow discharge and vacuum-deposited polymers are formed without catalysts, their potential use as acceptable implant materials for animals or people is encouraging. We have evaluated the tissue response of six different glow-discharge-formed polymers and the vacuum-formed polymers of paraxylylene. The tissues examined for response were skeletal muscle tissue of rats and the cerebral cortical tissue of rabbits. Both quantitative and qualitative results are reported. Results of our studies show that, in general, the tissue response to glow discharge polymers is acceptable as is the cortical response to the chlorinated form of paraxylylene (Parylene C). Adverse responses were seen most often in brain tissue. Tissue response, in both tissues, was a graded one. We conclude that both types of polymers hold substantial promise for implant use as either protective or interfacial materials.

BACKGROUND

One of the major problems of implantation of electrical circuits and recording and stimulating electrodes in animals (including humans) has been the lack of a suitable insulating coating. This coating must protect the circuit or lead wire material and at the same time be compatible or at least tolerated by the body or body parts in which it is implanted. Many present-day materials meet several but frequently not all of the criteria necessary for long-term implantations.

Journal of Applied Polymer Science: Applied Polymer Symposium 38, 55–64 (1984)

CCC 0570-4898/84/010055-10$04.00

Our earlier studies with glow-discharge-polymerized films led us to believe that these films held promise as materials which could serve as insulating coatings for devices and electrodes and could also be engineered to meet the compatibility requirement of the tissue in which they were to be implanted. Results of our earlier implantation studies in the skeletal muscle of rats showed that the reaction elicited by the body was relatively minimal, especially when compared with a commonly used material, dimethylsiloxane (Silastic) [1]. We have since extended these studies to implantation of both glow-discharge-polymerized films and vacuum-deposited films of poly(p-xylylene) (Parylene) in the central nervous system (cortex and meninges) of rabbits. We have found some differences between the reactivity in these tissues and those in skeletal muscle. This article reports the results of these later studies and reports a synopsis of our former studies on the effect of implantation on the body tissues in contact with particular materials.

EXPERIMENTAL

Synthesis of Glow-Discharge (or Plasma)-Polymerized Films

Glow discharge films were synthesized in both tubular and bell jar reactors. The plasma was maintained by either a radio-frequency (rf) discharge at 3.9 MHz or an audio-frequency (af) discharge between 10 and 20 kHz. The films used in our initial study (skeletal muscle implantation) were thicker than those used in our later studies on neural implantations. The thicker films (0.5 μm) were formed over Silastic rods that were 1 mm in diameter and 7 mm long. In these studies we used the glow discharge polymers of ethylene (GDP-E), styrene (GDP-S), and chlorotrifluoroethylene (GDP-CTFE). These films were deposited in a tubular reactor according to the procedure outlined by Mayhan et al. [2]. The initial reactor was evacuated to 13 mPa and prepurified argon gas was fed to the system until a pressure of 1.33 Pa was obtained. The monomeric gas of choice was then introduced and a rf power input level (3.9451 MHz) was adjusted to 6 W.

Thinner (0.1–0.3 μm) glow discharge polymer films of methane, TFE, and tetramethyldisiloxane (TMDSO) were later obtained on 250-μm-diam by 2.5-cm-long platinum wire. The platinum wire was used as a substrate for implantation in neural tissue. In addition to the glow discharge films, we also synthesized vacuum deposited films of poly(*p*-xylylene) in both the nonsubstituted and chlorosubstituted forms (Parylene N and Parylene C). These films were synthesized in a specially designed reactor built to allow synthesis of both glow-discharge films and vacuum-deposited films.

Skeletal Muscle Implantation

After sterilization in ethylene oxide gas and appropriate out-gassing, coated Silastic rods were implanted into the paravertebral muscles of male Wistar rats.

Seventy-eight rats were used for the entire study, 26 for each of the three polymers with four implantation sites in each rat. Using aseptic surgical techniques, the two implants placed cranially consisted of uncoated Silastic tubing as controls and the two caudal locations contained the glow-discharge-polymerized coatings on top of the Silastic tubings. After the surgical implantation, 75 of the rats were divided into five groups for necropsy at 2, 4, 8, 12 and 24 weeks. In order to determine long-term effects, the remaining three animals were necropsied at 75, 77, and 84 weeks.

Central Nervous System (CNS) Implantation

Material synthesized on platinum wire substrates (250 μm diam, 2.5 cm length) consisted of the glow discharge polymers of methane (M), tetrafluoroethylene (TFE), and tetramethyldisiloxane (TMDSO) and Parylene N and Parylene C vacuum-deposited films. These substrates were sterilized in ethylene oxide gas and air washed for approximately 3 days. The implantations were made in the cranium of 20 New Zealand white rabbits of both sexes, along with an uncoated platinum wire as a control. Four wires were placed in a transmeningeal location in each rabbit and the preparation allowed to incubate for 8 weeks. The animals were then humanely killed and their brains immediately perfused with an appropriate fixative solution. The brains were removed and sectioned for later staining and histopathologic examination. On histopathologic examination, the amount of gliosis, neuronal changes, edema, and chronic inflammatory cells present was noted. These changes were compared with changes noted around the control wire and a rating then made (1 mild to 5 severe) based on the comparison.

RESULTS

Skeletal Muscle Implantations

Gross and histopathologic examination of the tissue removed from the skeletal muscle sites were subjected to both qualitative and quantitative examination. Histologically, we examined and recorded the size of the fibrous tissue capsule that had developed around the implanted material and also counted the number of reactive cells as an indication of the severity and form of the foreign body reaction. These counts are represented from a grade of zero for less than one inflammatory cell per high-power field (IC/hpf) to a grade of three for greater than 10 IC/hpf. These data (capsule thickness in micrometers and number of inflammatory cells) were accumulated and are presented in Figures 1 and 2 for the ethylene, styrene, and chlorotrifluoroethylene glow discharge polymers. Note that in these figures there is an initial response that is more severe than that of the implanted Silastic control. However, note also that at steady state the materials come to a level that does not differ significantly from that of the control.

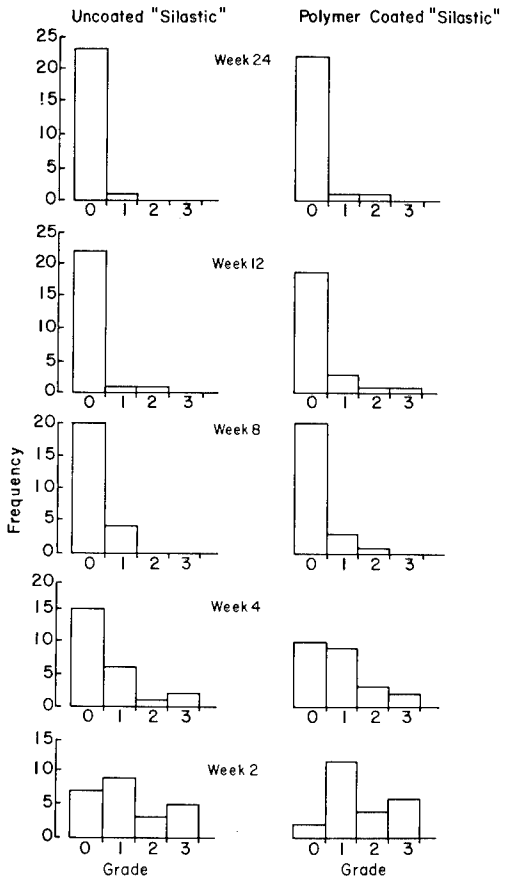

FIG. 1. Distribution of the assigned grades demonstrating the reactivity adjacent to the implant site as a function of time. Studies done in paravertebral muscles of rats.

CNS Implantation

Our data are interesting but much less extensive on implantations in the cerebral cortex of rabbits. The reaction of the cortex to the glow discharge polymers of M, TFE, and TMDSO have been examined. We consider the response to M and TFE to be satisfactory and a relatively mild reactivity, while the reaction to TMDSO is considered to be relatively severe. Figure 3 is a photomicrograph showing the typical reactivity surrounding a control wire (bare platinum). For all ratings, a section around the control wire was compared with a section around the polymeric coated wire in the same animal. Figure 4 illustrates the reactivity surrounding an electrode coated with GDP-M. Figure 5 illustrates the reactivity seen around the GDP-TFE polymer. The GDP-M polymer elicited a very minimal reactivity (graded 1 on a scale of 5) and the GDP-TFE-coated one grades approximately

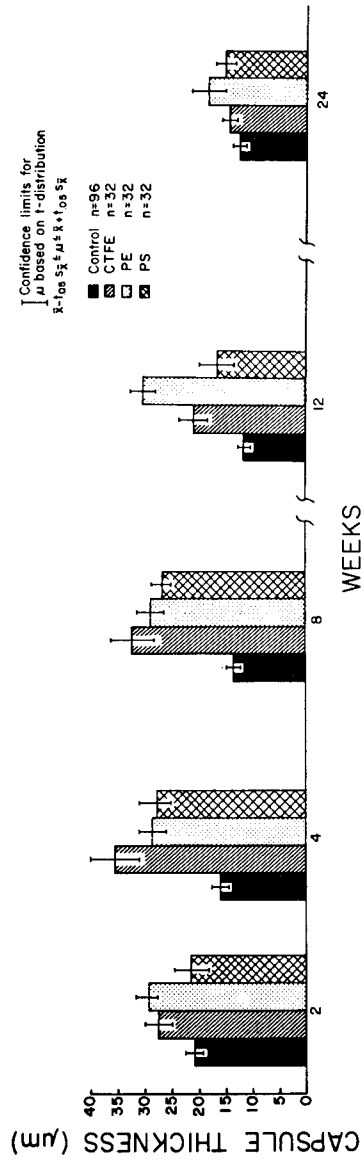

FIG. 2. Capsule thickness measured at four equidistant sites surrounding the implant in the paravertebral muscles of rats. Results for controls are pooled for the three groups.

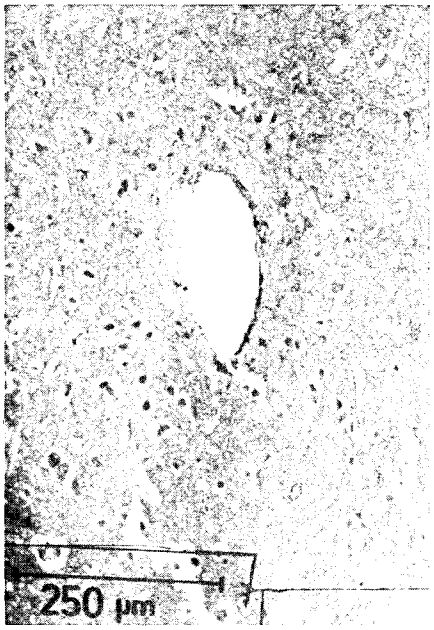

FIG. 3. Reactivity of rabbit cerebral cortex tissue to a bare platinum wire (control). A few reactive astrocytes are demonstrated by the Cajal staining procedure.

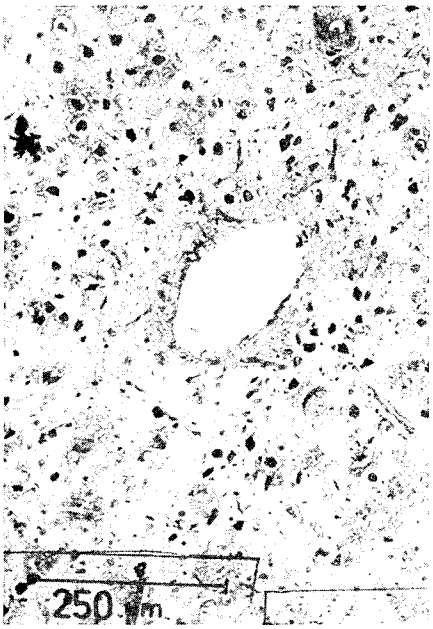

FIG. 4. Reactivity of the cortical tract surrounding a wire coated with the glow discharge polymer of methane (GDP-M). A Cajal stain for fibrillary and reactive astrocytes was used. Ranked as 1 on a scale of 5 (when compared with the reactivity around a bare control wire in the same animal).

FIG. 5. Histologic section (Holtzer glial stain) of the cortical tract surrounding an electrode coated with the glow discharge polymer of TFE. Ranked 2 on a scale of 5. Scale and magnification as in Fig. 4.

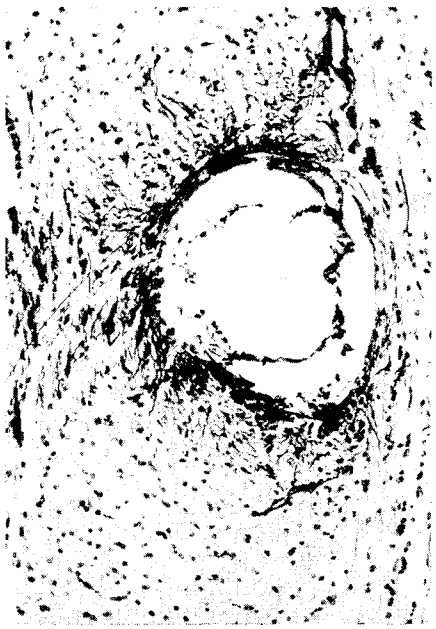

FIG. 6. Cortical tissue reactivity surrounding a wire coated with the glow discharge polymer of TMDSO. Ranked 4 on a scale of 5. Scale and magnification as in Fig. 4.

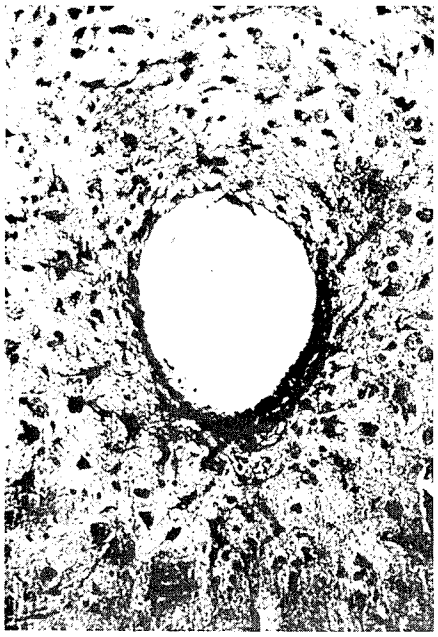

FIG. 7. Histologic section (Holtzer glial stain) of the tract surrounding an electrode coated with Parylene N. Ranked 5 on a scale of 5. Scale and magnification as in Fig. 4.

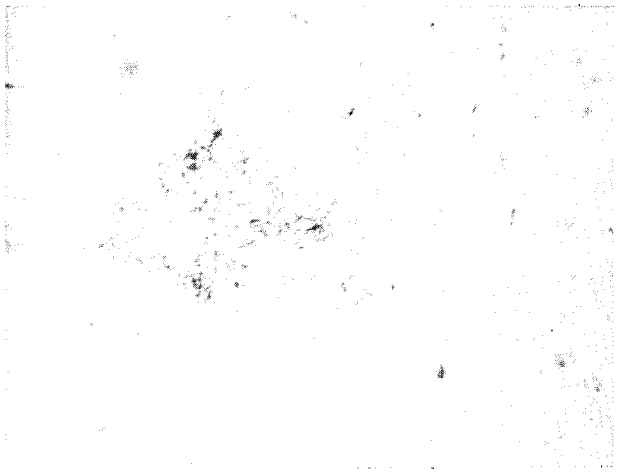

FIG. 8. Representative section of the cortical reactivity around a Parylene-C-coated wire. Ranked 3 on a scale of 5. Magnification 2.5×.

3 on a scale of 5. Figure 6 is the reactivity around the GDP-TMDSO-coated wire (4 on a scale of 5) and is considered relatively severe.

We have found the cortical reaction to the vacuum-deposited parylenes more severe than originally expected [3]. Figure 7 is a photomicrograph of the implantation site surrounding the Parylene N polymer. The capsule thickness is quite extensive and there are reactive cells around this site. There was infiltration of reactive cells in and around the implantation site and also fibrous tissue which presumably has grown down from the meninges. We consider this reactivity to be severe (grade 5 on a scale of 1 to 5).

Figure 8 is a photomicrograph taken around the implant site of a wire coated with the monochlorosubstituted form of poly(*p*-xylylene) (Parylene C). This form is more commonly used for biological applications. There is some edema around the cells and also the presence of some reactive cells. We would consider this to rank as 3 on a scale of 1 to 5.

A summary of these reactions is shown in Table I.

TABLE I
Summary of CNS Reactivity to Implanted Polymers

Histological Description	Biocompatibility Rating Scale	GDP - TFE	GDP - TMDSIO	GDP - Methane	Parylene-C	Parylene-N
a) Gliosis - Nil b) Neuronal changes - Nil c) Edema - Nil d) Chronic inflammatory cells - Nil	1			✓		
a) a few glial cells present b) <10% degenerating neutrons counted/slide	2	✓				
a) diffuse glial fibers present b) 10%-50% degenerating neurons present c) several areas of edema present d) lymphocytes and monocytes present	3		✓		✓	
a) thick glial fiber band around tract b) >50% degenerating neurons counted c) larger areas of edema near tract d) present of lymphocytes, monocytes	4		✓			
a) dense glial band 30-50 μm, plus presence of numerous glial cells b) 80% of degenerating neurons counted c) edema up to 200 μm surrounding tract d) large number of lymphocytes, monocytes	5					✓

DISCUSSION

From our studies, several points seem to be apparent. First, the biological reactivity to any foreign material is a function of time and tends to resolve to steady state in about eight weeks after implantation. This appears to be the length of time when transient reactions disappear from the host animal.

It also seems clear that the skeletal muscle reactivity of rats to various forms of glow discharge polymers is of approximately the same order of magnitude as that of the Silastic control material after steady state is reached. On the other hand, the reactivity of the central nervous system (specifically the cortex) of rabbits seems to be very dependent upon the particular type of polymer implanted and may vary along the length of the tract. Our studies have shown minimal reactivity with the glow discharge polymer of methane. Glow-discharge-polymerized TMDSO is more reactive in the cortex than GDP-TFE, and GDP methane appears to be the least reactive. Parylene C seems to elicit a cortical reactivity of about the same order of magnitude as GDP-TFE, while Parylene N-coated wires elicited the most severe reactivity of any polymers thus far examined by these methods. Studies by others [3] of the reactivity to the chlorosubstituted parylene (Parylene C) have shown it to be a very nonreactive type of material. To our knowledge, no implantation studies on Parylene N have been reported.

We cannot yet explain the large difference seen in the cortical reactivity of the two forms of Parylene. Whether or not the presence (or absence) of chlorine in the ring or the synthesis mode is responsible is yet to be determined.

It does appear that by tailoring and "engineering" the external coating material, one can overcome problems with reactivity to certain polymers that might have very adequate insulating characteristics but inadequate biocompatibility.

Our present and future studies are and will be devoted to solving this problem in order that, ideally, any type of material could be implanted in any particular organ provided the suitable reactivity parameters of that organ to implantation are known.

The authors thank Ms. Victoria Watts and Mr. Charles Jorgenson for their technical assistance. This work was supported in part by contracts N01-NS-8-2392 and N01-NS-1-2382, NINCDS, NIH, Bethesda, MD 20205.

REFERENCES

[1] M. F. Nichols, A. W. Hahn, J. R. Easley, and K. G. Mayhan, *J. Biomed. Mater. Res., 13*(3), 229 (1979).

[2] K. G. Mayhan, A. W. Hahn, M. R. Havens, and B. W. Peace, *Natl. Bur. Stand. Sp. Publ., 415*, 1 (1975).

[3] G. E. Loeb, M. J. Bak, M. Salcman, and E. M. Schmidt, *IEEE Trans. Biomed. Eng. BME-24*(2), 121 (1977).

SEMICONTINUOUS PLASMA POLYMERIZATION COATING ONTO THE INSIDE SURFACE OF PLASTIC TUBING

YASUO MATSUZAWA and H. YASUDA
Department of Chemical Engineering and Graduate Center for Materials Research, University of Missouri, Rolla, Missouri 65401

SYNOPSIS

A semicontinuous, rf capacitively coupled plasma polymerization apparatus was designed and constructed to coat the internal surface of a small-diameter plastic tubing. The glow zone was restricted to a small area to obtain a uniform coating of plasma polymer over the entire length of tubing (13 m long). It was found that a uniform coating can be achieved by maintaining the glow discharge parameters and velocity of moving substrate. In such a reactor, it was found that the deposition rates obtained for plasma polymers of tetrafluoroethylene, hexafluoroethane, and hexafluoroethane/hydrogen were very high compared with those polymerized in a conventional plasma polymerization apparatus. Special attention was needed to avoid deposition of an excessively thick coating, which was found to damage the barrier characteristics of the coating.

INTRODUCTION

The advantageous features of plasma polymers [1] (glow discharge polymers) when they are used as the ultrathin layers which contact with blood are (i) The surface modification can be achieved without altering bulk properties of substrate material. (ii) It is possible to cover the surface at very low levels of coating thickness. (iii) The layer adheres well to the substrate material. (iv) The plasma-polymerized layer consists of amorphous material. (v) Because of its ultrathin thickness and good adhesion, the coating layer can be made highly flexible and tough. (vi) Macroscopic topography of the surface can be kept unaffected by the coating.

The last feature might be particularly important in the practical evaluation of the surface–blood interaction. Many other methods of surface modification such

Journal of Applied Polymer Science: Applied Polymer Symposium 38, 65–74 (1984)

CCC 0570-4898/84/010065-10$04.00

as graft copolymerization tend to alter the surface topography as well as the surface chemical properties. Thus, it is generally difficult to separate chemical and physical factors in the properties of the modified surface in the evaluation of blood–surface interaction.

By changing monomers and by controlling the conditions of plasma polymerization, it is possible to provide chemically different surfaces without changing the macroscopic physical properties of the substrate surface. Thus, the method provides a unique possibility to investigate the effect of chemical and physical aspects of the surface on the blood–surface interaction independently of each other.

Although the precise chemical nature of plasma polymers is complex and not well defined, gross chemical effects can be controlled by the relative amounts of elements which constitute the surface material. In search of nonreactive surfaces, such as the nonthrombogenic surface (surface with the least interaction with blood), the ambiguity of chemical structure of the surface does not seem to be a drawback.

The physicochemical nature of the glow discharge polymer is controlled by the type of monomer used and the plasma polymerization conditions. Thus, surfaces with a wide range of physicochemical properties can be attained by plasma polymerization.

However, as far as the use of plasma polymer as a biomaterial is concerned, the many biological testing procedures that require test surfaces of various sizes and geometries present practical difficulties. For example, one test procedure requires a flat and transparent test specimen, whereas another requires that the surface be an internal surface of small-diameter tubing.

It is easy to coat a relatively small disk or film with the types of plasma polymerization apparatus that have been widely used. However, it is almost impossible to uniformly coat an inner surface of a small-diameter plastic tubing with the conventional apparatus.

For example, when a small-sized tubing, e.g., 3–6 mm i.d. and the ratio of length to inner diameter of 100 or greater, is placed in a large plasma reactor, plasma does not penetrate the tubing. The plasma quenches itself near the ends of the tubing and only small portions near the ends are coated. In order to force plasma to penetrate into the tubing, a small glass tube reactor can be used [1]. By this means, it was shown that considerable lengths of tubing, e.g., 1 m or longer, can be coated. On the other hand, it was also shown that uniformity of coating along the length of the tubing in thickness as well as the chemical nature of plasma polymer were not as good as hoped for. This is due to the inherent difficulty of supply of monomer and the relative location of glow discharge in the monomer flow, associated with the small-tube reactor [2–4]. Because of the small volume of the reactor, glow generally extends along a considerable length of tube. This appears beneficial at first glance; however, most polymerization occurs at the tip of the glow against the monomer flow and not enough monomer can be supplied to the downstream portion of the tube. In plasma treatments [5] in which the consumption of gas is negligible this is not a serious problem.

However, in plasma polymerization, in which the quantitative consumption of the monomer is a mandatory condition for the uniformity of coating, this is an inherent drawback to such an approach.

In this study, a semicontinuous system has been constructed to achieve a uniform coating on the inner surface of the plastic tubing by plasma polymerization. The operational parameters for the plasma polymerization process as well as the chemical nature of the plasma polymers deposited on the internal surface of the plastic tubing are discussed.

EXPERIMENTAL

The new glow discharge reactor used in this study has two independent vacuum systems, as shown in Figure 1. The first, consisting of two glass cross vessels connected by one-half-in.-diam Vycor silicon glass tube, is pumped down and maintained at 10^{-3} torr throughout the process. The second system consists of a plastic tubing to be coated which is connected to the monomer pressurized-

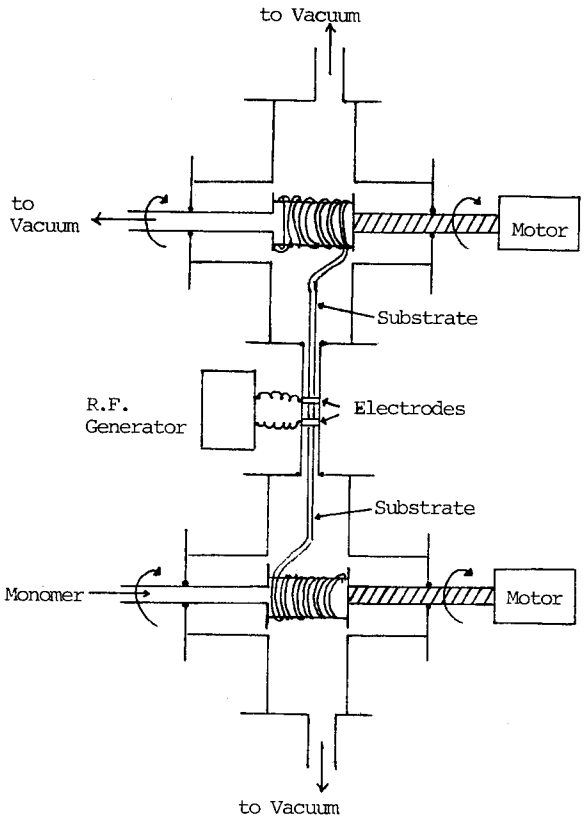

FIG. 1. Schematic representation of glow discharge reactor.

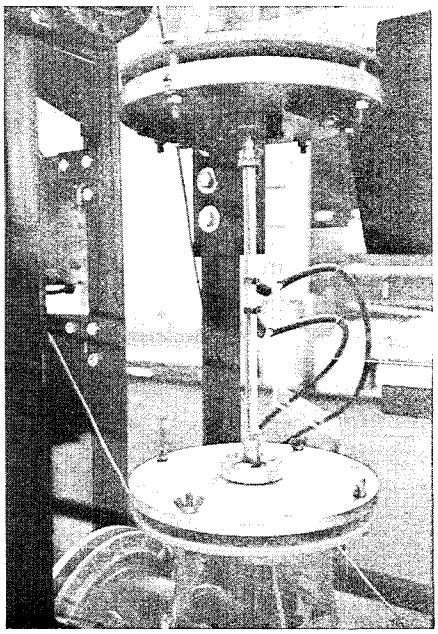

FIG. 2. A restricted glow discharge inside the Silastic tubing.

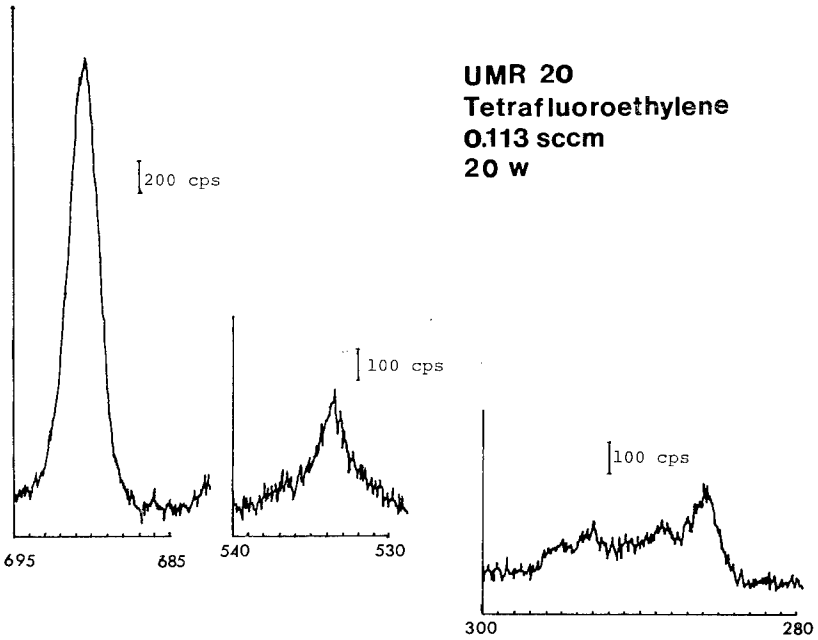

FIG. 3. ESCA spectra for F_{1s}, O_{1s}, and C_{1s}.

cylinder inlet system on one end and to a pump on the other end. The second system is also pumped down to 10^{-3} torr initially; then the monomer gas is allowed to flow at low pressure through the tubing.

The tubing is wound on an electric-motor-driven spool in the lower glass cross vessel, then threaded through the Vycor tube to a second electric-motor-driven spool in the upper glass cross vessel. Two copper electrodes 2 cm apart are attached to the Vycor tube and connected to a 13.56-MHz radio-frequency power generator. A glow discharge is set up inside the monomer-filled Silastic tubing between the electrodes. As the Silastic tubing is drawn upward at constant speed, it passes through the glow discharge zone and the inner surface is coated with a continuous, uniform layer of plasma polymer. Since the outside of the Silastic tubing is being pumped down by a pump, the glow discharge can be restricted to only the inside of the Silastic tubing (Figure 2). However, it is possible to coat both sides of the tubing by introducing the same or another monomer in the first vacuum system and creating glow discharge on both sides.

Monomers used in this study are tetrafluoroethylene (TFE), hexafluoroethane (Freon 116), and a mixture of hexafluoroethane and hydrogen. The monomers are introduced to the Silastic tubing through a commercial mass flow controller.

RESULTS AND DISCUSSION

Chemical Structure of Deposited Polymers Studied by Electron Spectroscopy for Chemical Analysis (ESCA)

The ESCA spectra of tetrafluoroethylene plasma polymer prepared under the following conditions, i.e., discharge power of 20 W and monomer flow rate of 0.113 sccm, are shown in Figure 3. The C_{1s} spectra shown in Figure 3 have peaks at 295, 293, 288.5, and 286 eV which can be assigned to CF_3, CF_2, CF, and C, respectively. The TFE plasma polymer has a strong fluorine peak at 690 eV and relatively weak oxygen peak at 533.5 eV. No significant shift was observed in the peaks of F_{1s} and O_{1s} for the TFE plasma polymers obtained under different plasma polymerization conditions. The elemental ratios F_{1s}/C_{1s} and O_{1s}/C_{1s} are summarized in Table I. There is no significant change in the elemental ratio O_{1s}/C_{1s} as the composite plasma polymerization parameter [6] W/FM (where W is the discharge power, F is the monomer flow rate, and M is the monomer molecular weight) varies, whereas a fluctuation in the elemental ratio of F_{1s}/C_{1s} is observed as the W/FM value changes.

The ESCA spectra obtained for the hexafluoroethane plasma polymers are very similar to those for tetrafluoroethylene plasma polymers under the plasma polymerization conditions used in this study. The elemental ratios F_{1s}/C_{1s} and O_{1s}/C_{1s} for the hexafluoroethane plasma polymers prepared under different glow discharge powers (10, 15, and 25 W) are summarized in Table II. The hexafluoroethane plasma polymer obtained at low discharge power demonstrates higher fluorine and lower oxygen atom content than the plasma polymers prepared at higher discharge power.

TABLE I
Summary of ESCA Results for Tetrafluoroethylene Plasma Polymer Deposited on Silastic Tubing

UMR#	Substrate#	Monomer	Flow Rate (SCCM)	Coating Time (seconds)	Power (watts)	W/FM (J/kg)	Corrected Peak Intensity $\times 10^4$ counts·eV O_{1s}	C_{1s}	F_{1s}	Elemental Ratio O_{1s}/C_{1s}	F_{1s}/C_{1s}
18	101-2	Tetrafluoro-ethylene	0.113	8.6	10	1.19×10^9	0.859	3.51	2.45	0.245	0.698
19	101-5	"	"	4.4	10	1.19×10^9	0.859	3.14	1.02	0.274	0.516
20	102-12	"	"	10.0	20	2.38×10^9	0.910	4.35	3.37	0.209	0.775
22	104-23	"	0.115	14	14	1.63×10^9	0.814	3.74	3.49	0.218	0.933
23	104-24	"	"	5	14	1.63×10^9	0.843	3.77	2.33	0.224	0.618
24	105-35	"	0.331	3	10	4.05×10^8	0.827	3.68	2.88	0.225	0.783
25	105-41	"	"	3	6	2.40×10^8	0.814	3.68	2.32	0.221	0.630

Under the plasma polymerization conditions used in this study, plasma polymers which have a moderate fluorine atom content and relatively low oxygen atom content are formed from the tetrafluoroethylene and hexafluoroethane monomers.

On the other hand, when the plasma polymer is formed from a mixture of hexafluoroethane and hydrogen, especially at higher discharge power (30 W), the polymer formed exhibits a quite different chemical nature, as shown in Figure 4. The spectra represent a weak fluorine peak at 690 eV and a relatively strong and sharp oxygen peak at 533.5 eV. The C_{1s} spectrum for this polymer has a singlet peak at 286 eV with a wide shoulder on the high-binding-energy side, whereas plasma polymers of TFE, hexafluoroethane, or hexafluoroethane/hydrogen prepared at the low discharge power (4 W) have four peaks for the C_{1s} at 295, 293, 288.5, and 286 eV.

Although the difference in the amount of fluorine and oxygen atoms is not very great, this system may provide a good candidate surface which is characterized by (i) higher oxygen content and (ii) low fluorine content when compared with the TFE or hexafluoroethane plasma polymers examined in this study.

TABLE II
Summary of ESCA Results for Hexafluoroethane Plasma Polymer Deposited on Silastic Tubing

UMR#	Substrate#	Monomer	Flow Rate (SCCM)	Coating Time (seconds)	Power (watts)	W/FM (J/kg)	Corrected Peak Intensity $\times 10^4$ counts·eV O_{1s}	C_{1s}	F_{1s}	Elemental Ratio O_{1s}/C_{1s}	F_{1s}/C_{1s}
12	82-7-12-3	Hexafluoro-ethane	0.266	4	25	9.13×10^8	0.814	2.87	1.89	0.284	0.658
14	82-7-12-2	"	"	"	15	5.48×10^8	1.04	3.55	2.51	0.293	0.707
13	82-7-12-1	"	"	"	10	3.65×10^8	0.865	3.66	3.42	0.236	0.934

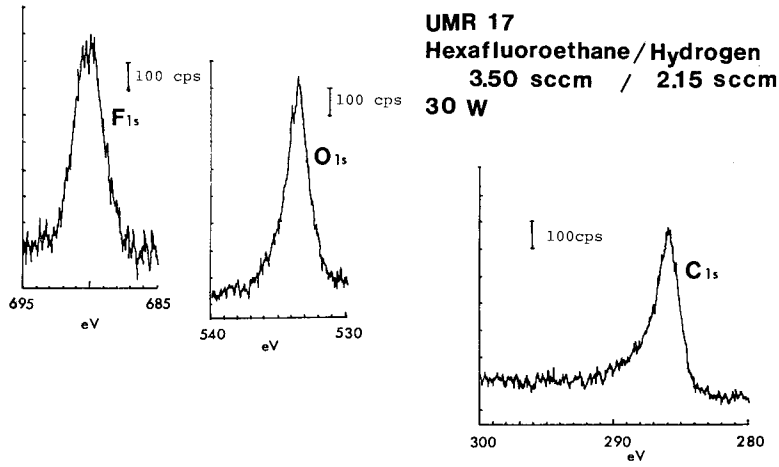

FIG. 4. ESCA spectra for F_{1s}, O_{1s}, and C_{1s}.

It is interesting to note that these results obtained by such a small-tube reactor are completely opposite to results found with large-volume reactors [7]. In large-volume reactors, it was generally found that (i) hexafluoroethane does not polymerize well by plasma, and (ii) the addition of H_2 is needed to form polymer from hexafluoroethane and the polymers formed are similar to plasma polymers of TFE polymerized under high-W/FM conditions, i.e., small F content and high O content. This discrepancy may be due to the facts that in such a small reactor (3 mm i.d. by 20 mm long) the ratio of surface to volume is much greater than in the larger-volume reactor and that the entire surface consists of substrate material which contains sufficient amounts of hydrogen atoms to be split off by plasma.

Thus, it appears that the effect of surface (of substrate tubing) in the overall plasma polymerization is much more important in such a small-volume reactor in which the plasma-containing surface is the substrate surface than in plasma polymerization of the same monomer in a larger-volume reactor.

Deposition Thickness

Deposition thicknesses of plasma polymers were obtained by observing the edge of the coated Silastic tubing in their SEM pictures. The deposition rates obtained for TFE, hexafluoroethane, and hexafluoroethane/hydrogen plasma polymers are shown in Table III.

It is seen that very high deposition rates have been obtained with this semicontinuous system as compared to those obtained by the conventional system. These faster deposition rates, 0.02, 0.006, 0.002 μm/s, are easily anticipated since the glow zone is restricted to small volume (3.3 mm i.d. × 20 mm long). If we assume 100% yield of polymerization in the glow region, a calculated

TABLE III
Deposition Rate of Plasma Polymers for Tetrafluoroethylene, Hexafluoroethane, and a Mixture of Hexafluoroethane and Hydrogen

Monomer	Flow Rate (sccm)	Power (watts)	W/FM (J/kg)	Deposition Rate (μm/s)
Tetrafluoroethylene	1.75	16.5	1.26×10^8	0.02
Hexafluoroethane	1.99	12	5.86×10^7	0.006
*Hexafluoroethane/ Hydrogen	3.09/2.67	4	1.24×10^7	0.002

*Mixture of hexafluoroethane and hydrogen (% of hexafluoroethane: 53.6%).

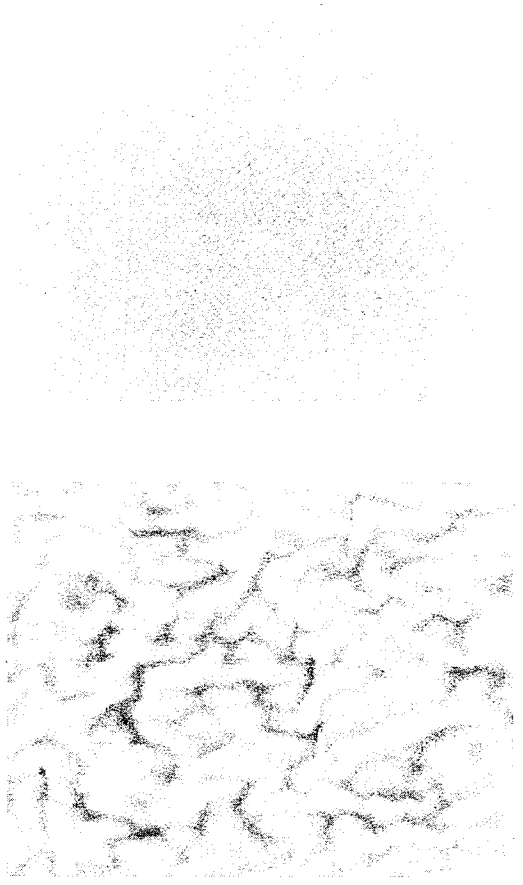

FIG. 5. SEM photographs of the internal surface of the Silastic tubing.

deposition rate of 27 μm/s could be expected for tetrafluoroethylene plasma polymerization [flow rate 1 cm^3 (STP)/min; assumed density 1.3 g/cm^3]. Actual deposition rates obtained are not as high as this value. Nevertheless, an extremely high deposition rate is one of the important characteristics of plasma polymerization in a small volume. Because of the fast deposition rate, either dilution of monomer by adding non-polymer-forming gas or faster movement of the tubing may be necessary to obtain the thicknesses desired for biomedical applications, 0.01–0.05 μm.

Surface Morphology

Figure 5 represents the internal surface of the Silastic tubing before coating. The photographs taken at magnifications of 100 and 1000 times depict a ridgelike structure on the surface. Straight lines appearing in the photographs are seen on the original surface, and are not due to handling.

When the coating with any of the monomers used in this study has been put on the tubing, the surface shows a knitted fibrous structure on the original surface of the Silastic tubing depending on the residence time and glow discharge conditions. For example, Figure 6 shows how the surface has been altered by plasma polymerization coating of hexafluoroethane as the residence time varies. It is clearly seen that the surface coated for 6.3 s has the knitted fibrous structure [Fig. 6(b)], while the surface for shorter residence time closely resembles the original surface structure [Fig. 6(a)]. It has also been found that a thicker coating causes a flaw or crack on the surface [Fig. 6(c)] which can be easily detected by means of a dye test (an oil-soluble dye, Sudan red, was used). In other words, when the coated surface has a smooth knitted fibrous structure it is not stained at all by the dye solution. However, the original uncoated surface or a coated surface with flaws or cracks is easily stained and will show a deep red color. It is anticipated that the cracks will be formed when the thickness of coating exceeds a critical value which is dependent on plasma polymerization conditions, due to the buildup of internal stress in the plasma polymer [8].

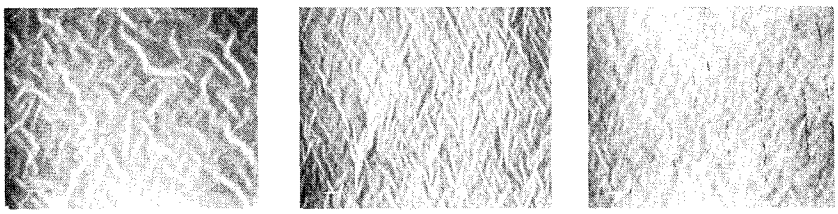

(a) (b) (c)

FIG. 6. SEM surface pictures for hexafluoroethane plasma polymer; magnification, 1000×, discharge power, 11 W; hexafluoroethane flow rate, 0.355 sccm; residence time (a) 3.6, (b) 6.3, (c) 27 s.

Thus, in order to obtain flawless coating layer, it is necessary to shorten the residence time to the order of a few seconds.

CONCLUSION

(i) By the construction of a plasma polymerization reactor in which the substrate tubing moves continuously while plasma is restricted to a relatively small volume (2 cm of inner space of a tubing), it is possible to coat the inner surface of small (3 mm i.d.) tubing for a considerably longer length (e.g., 13 m) than had been obtained in a stationary-substrate system.

(ii) In such a small-volume reactor, extremely high deposition rates are generally obtained and there is a tendency for an excessively thick coating to form unless special care is taken to control the deposition rate.

(iii) By selection of plasma polymerization conditions, it was shown that a very thin layer of plasma polymer coating can be placed in such a manner that the surface topography has not been changed significantly from that of the original uncoated surface, yet the chemical nature can be modified to that of the coating. Such a layer exhibited a perfect barrier to oil-soluble dye (Sudan red) solution, indicating complete coverage of the surface as well as its changed physicochemical nature.

REFERENCES

[1] H. Yasuda and N. Morosoff, NIH Annual Report No. NIH-NO1-HV-3-2913-7.
[2] H. Yasuda and T. Hirotsu, *J. Polym. Sci. Polym. Chem. Ed., 16,* 229 (1978).
[3] H. Yasuda and T. Hirotsu, *J. Polym. Sci. Polym. Chem. Ed., 16,* 313 (1978).
[4] H. Yasuda and N. Morosoff, *J. Appl. Polym. Sci., 23,* 1003 (1979).
[5] K. Hatada, H. Kobayashi, and M. Asai, *Org. Coat. Appl. Polym. Sci. Proc., 47,* 391 (1982).
[6] H. Yasuda and T. Hirotsu, *J. Polym. Sci. Polym. Chem. Ed., 16,* 2587 (1978).
[7] T. Masuoka and H. Yasuda, *J. Polym. Sci. Polym. Chem. Ed., 20,* 2633 (1982).
[8] H. Yasuda, T. Hirotsu, and H. G. Olf, *J. Appl. Polym. Sci., 21,* 3179 (1977).

STUDY OF THE EFFECT OF ION IMPLANTATION ON POLYMER TO METAL ADHESION

G. SURENDRAN and W. J. JAMES
Department of Chemistry and Graduate Center for Materials Research, University of Missouri, Rolla, Missouri 65401

W. BREARLEY and E. B. HALE
Department of Physics and Graduate Center for Materials Research, University of Missouri, Rolla, Missouri 65401

SYNOPSIS

In an effort to improve adhesion of plasma-formed organotin coatings to aluminum and stainless-steel surfaces, ion implantation was effected in two ways. The metal substrates were placed in a rf inductively coupled reactor and a tetramethyltin monomer was polymerized in the glow discharge onto the metal surfaces. The coated surfaces were then bombarded with nitrogen ions (100 keV, 10^{16} ions/cm^2) and then recoated in the plasma reactor. The second approach involved bombardment of the metal surfaces by Sn ions prior to plasma coating. The resulting films were characterized by SEM and their adhesive strength was determined by boiling in saline solution and/or by mechanical testing. The results of this preliminary study indicate the first approach to be effective in improving adhesion.

INTRODUCTION

Good adhesion is important to any application of polymer coatings to metals. Three factors which influence adhesion are wetting, adsorption, and interdiffusion. The first two are often varied by controlling surface roughness and contamination. Our approach to improve adhesion focuses on the promotion of nonequilibrium "interdiffusion" and creation of nucleation sites at the interface. This is referred to as atomic interfacial mixing (AIM) [1]. To accomplish AIM, the polymer coating is produced in a glow discharge and the interface is treated by ion implantation.

Implanted ions may become nucleation sites for the polymer if they are close

Journal of Applied Polymer Science: Applied Polymer Symposium 38, 75–81 (1984)

CCC 0570-4898/84/010075-07$04.00

enough to the metal surface. In fact, mechanical, optical, magnetic, and other electronic properties are all affected and influenced by the insertion of foreign atoms. Ion implantation provides a way to distribute these foreign atoms where conventional techniques fail [2]. A reasonable choice of an ion species is one that will bond well with the polymers, e.g., carbon. Alternatively, inert atoms such as nitrogen and argon can be used to drive atoms contained in a thin film previously deposited on the metal surface into the interface. This is called recoil implantation.

Since metals and organic polymers have drastically different electronic properties, interfacial bonding is not readily affected by conventional coating techniques. The problem is especially difficult if the interfacial bonding is to withstand the effects of water diffusion through the polymer coating. Since water is a strong hydrogen bonding agent, it tends to destroy secondary bonds including van der Waals forces at the metal–polymer interface.

Two mechanisms are involved in glow discharge polymerization. If the monomer contains unsaturated bonds, the plasma can induce polymerization in the conventional manner in which polymerization is initiated by a reactive species created in the electrical discharge. Second, reactive species consisting of fragments of varying size and charge can be produced from the monomer which upon condensation will produce products which may be very different in structure and stoichiometry from the conventionally formed polymers. As a consequence of this latter mechanism, it is not necessary to have unsaturated bonds in the starting monomer since the exciting plasma will create the necessary active fragment, i.e., radicals. The characteristics of the plasma-formed films—adhesion, extent of crosslinking, etc. [3]—are dictated by the choice of kinetic formation parameters—rf power, plasma pressure, and choice of starting material.

In this study we have chosen to combine the techniques of plasma polymerization and ion implantation. Tetramethyltin (TMT) was chosen as the starting monomer because it is saturated and cannot undergo plasma-induced polymerization. The tin to carbon ratio can be tailored by appropriate choices of the reactor-operating parameters [3]. Prior studies of plasma polymerization of TMT on aluminum surfaces suggest some primary bonding at the interface through oxygen bridging, Al—O—Sn [4]. In addition, ion implantation should further enhance AIM.

EXPERIMENTAL

The plasma polymerization was carried out using a rf inductively coupled tubular reactor which has been thoroughly described in the literature [5]. Two metal substrates were chosen: 316L stainless steel and aluminum. The former was chosen because it does not readily oxidize, whereas the latter always contains an oxide layer. Furthermore, previous studies [4] had shown good adhesion of plasma-formed organotin polymers to these metal surfaces.

The samples were polished, cleaned with distilled water, and air dried. They

TABLE I
Preparation of Organotin Polymers on Aluminum and Stainless Steel by Plasma Deposition[a]

Ar^+ cleaning	15 min, 30 W
Monomer flow	5×10^{-3} cm^3/s
Pressure	35 mtorr
Power	2.5–6 W
SWR	3–4
Duration	2–160 min
Thickness	100–2000 Å

[a]Film thicknesses were determined by using Nomarski interferometry. For film thicknesses of less than 700–800 Å, calculated deposition rates were used to estimate the thicknesses.

were subjected to an argon ion plasma for a period of 10–15 min prior to introduction of the organotin monomer. The parameters used in polymer film formation are given in Table I.

Two approaches were used for the ion implantation. Thin films (<100 Å) were deposited on the metal surface via glow discharge. These were then bombarded with N_2^+ ions at 100 keV to a dose of ca. 10^{16} cm^{-2} over part of their area (ca. 1 cm^2). Following the implantation the samples were again coated with plasma-formed organotin polymers to provide a thicker film (ca. 2000 Å) with a higher tin content.

In the second approach, the metal surfaces were first bombarded with Sn^+ ions at the same energy and dosage as for N_2^+. The resulting samples were then thick film coated as above.

Adhesion testing was done by two methods: immersion in boiling saline solution and tensile pull measurements. The saline testing involved boiling the samples in a 1% solution for 1 h and then examining the surface with a scanning electron microscope (SEM) for signs of film damage or rupture. They were then boiled again and reexamined, up to a maximum of 8 h.

The pull tests were performed using an Instron tensile tester; the technique is well described in the literature [6]. The pressure at which interface failure occurred was recorded.

RESULTS AND DISCUSSION

The implanted and unimplanted regions of the stainless-steel samples behaved quite differently in the saline test depending on the ratio of Sn to C. When the Sn/C ratio exceeded 2, the implanted film was intact and undamaged after 8 h of solution exposure, whereas carbon-rich samples were destroyed in less than 1 h. However, films of the same composition on nonimplanted aluminum showed little difference in condition after 4 h of testing. Clearly, the choice of substrate, polymer composition, and ion treatment are very important to adhesion. Similar results in prior studies suggest that the oxide on aluminum provides the greater adhesive strength [4].

As regards the direct and recoil methods of implantation, Figures 1 and 2

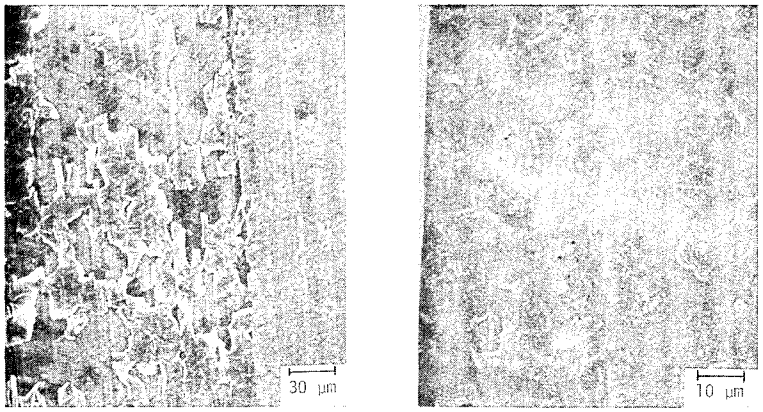

FIG. 1. Polymer on aluminum. SEM micrographs taken after 4 h exposure to boiling saline solution. The boundary between the recoil implantation (right) side and unimplanted (left) side is shown in (a); (b) shows more detail of the implanted area, where only small flaws are seen.

clearly show that the recoil method of implantation (bombardment of thin polymer films followed by redeposition of plasma-formed polymer) improves adhesion on both aluminum and stainless steel. In Figure 1(a) the nonimplanted area has many large holes and the boundary of the implanted region is clearly defined. Figure 2 presents implanted stainless-steel samples after recoil implantation. After 1 h of the boiling test, the film in the unimplanted region has separated from the metal. However, the implanted region is unaffected even after 2 h of exposure.

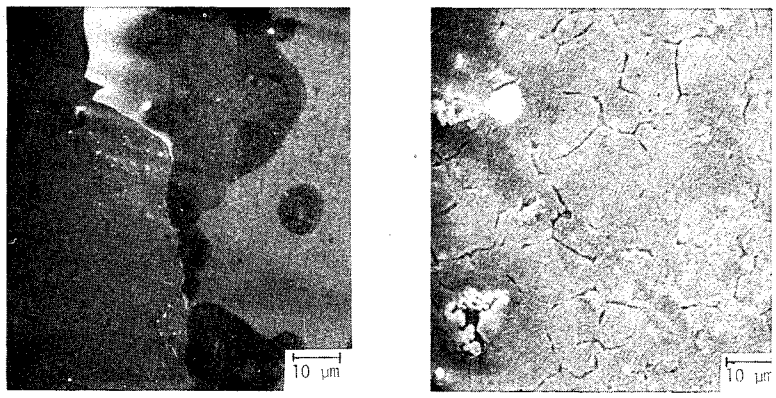

FIG. 2. Polymer on stainless steel. (a) After only 1 h in boiling test and shows that polymer has completely separated from unimplanted (left) side. After 2 h exposure (b) shows the film basically unchanged, but flaws are beginning to develop.

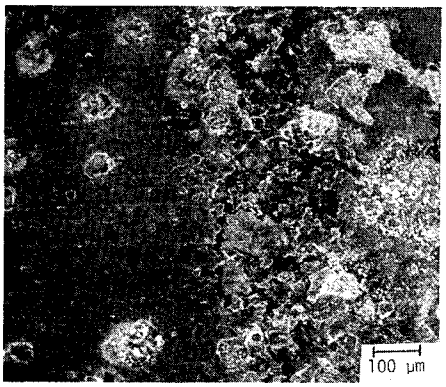

FIG. 3. Polymer on aluminum. After 4 h in the boiling test, the directly implanted Sn^+ region on the right is clearly much more deteriorated. (Note also reduced magnification.)

Further evidence of the superiority of the recoil method over direct implantation is shown in Figures 3 and 4. Figure 3 is a SEM micrograph of the plasma-polymerized TMT on an aluminum substrate which was implanted with Sn^+ prior to polymerization and then boiled in saline solution for 4 h. The directly implanted region (on the right) has clearly deteriorated more than the unimplanted region on the left.

Figures 4(a) and 4(b) are SEM micrographs of the same polymer on stainless steel. Figure 4(a) shows the unimplanted region after 8 h of boiling in saline solution. Although the surface is flawed, there is no pronounced detachment of the polymer from the stainless-steel surface. However, in the regions implanted

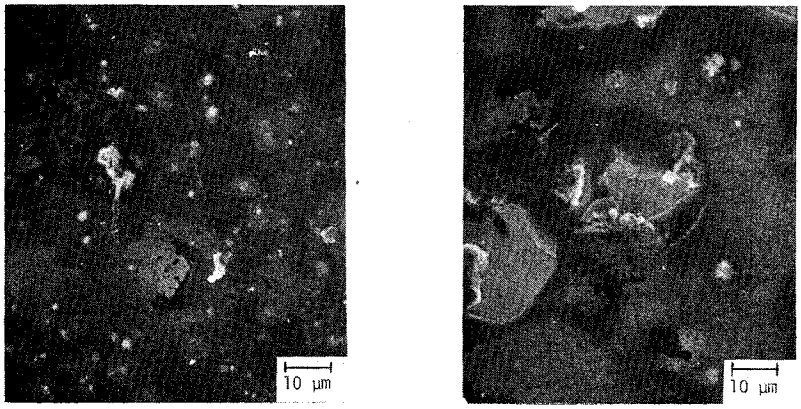

FIG. 4. Polymer on stainless steel. After 8 h in boiling test, the unimplanted case in (a) is flawed, but still reasonably good; (b) shows that the polymer on the Sn^+-implanted sample developed large holes and is clearly worse than the unimplanted case.

TABLE II
Failure Strengths (psi) Before and After Implantation[a]

	Direct implantation of Sn^+		Recoil implantation	
	Al	SS	Al	SS
Unimplanted	494	4850	414	2377
		>5500[b]	963	3290
			2210	2846
Implanted	3790	2241	3877	>5500[b]
		3408	>5500[b]	>5000[b]
				>5500[b]

[a]Each table value is an average of at least five measurements (±200 psi). Different values in same column correspond to different polymer deposition conditions.

[b]Failure occurred in the epoxy layer, so the adhesive strength of the polymer/metal interface exceeds this value.

by means of the direct method, the polymer film has been detached to a considerable degree and deterioration of the film is clearly more pronounced than in the unimplanted region.

The pull test measurements are in accord with the boiling tests in that appreciable increases in the pull strengths are recorded for both metal substrates when the recoil implant technique is used (see Table II). In the case of stainless steel, the effect of direct implantation with Sn^+ prior to plasma polymer deposition would appear on the basis of this limited study to diminish the adhesive strength.

CONCLUSIONS

Recoil implantation improves adhesion of plasma-formed organotin polymers to metal substrates of stainless steel and aluminum as measured by pull tests and evidenced by SEM micrographs of implanted and nonimplanted surfaces after boiling in saline solutions.

The recoil technique of ion implantation appears to be clearly superior to that of the direct technique as evidenced by the SEM micrographs. This conclusion is further confirmed by the pull tests carried out on the stainless-steel samples. However, the failure strengths obtained for the aluminum samples show a marked improvement in adhesion by either implantation technique although the limited pull test data do not distinguish the two implantation techniques when applied to plasma-polymerized TMT on aluminum.

REFERENCES

[1] H. K. Yasuda, A. K. Sharma, E. B. Hale, and W. J. James, *J. Adhes.*, *13*, 269 (1982). Also, E. B. Hale, W. J. James, A. K. Sharma, and H. K. Yasuda, in *Modification of the Surface Properties of Metals by Ion Implantation*, R. P. M. Proctor and V. Ashworth, Eds. Pergamon, Oxford, 1982, p. 167.

[2] J. K. Hirvonen, *Ion Implantation, Treatise on Materials Science and Technology,* Vol. 18, Academic, New York, 1980.
[3] E. Kny, L. L. Levenson, W. J. James, and R. A. Auerbach, *J. Vac. Sci. Technol., 16*(2), 359 (1979).
[4] E. Kny, L. L. Levenson, W. J. James, and R. A. Auerbach, *J. Phys. Chem., 84,* 1635 (1980).
[5] R. K. Sadhir, W. J. James, H. K. Yasuda, A. K. Sharma, M. F. Nichols, and A. W. Hahn, *Biomaterials, 2,* 239 (1981).
[6] R. Jacobson and B. Kruse, *Thin Solid Films, 15,* 71 (1973); R. Jacobson, *Thin Solid Films, 34,* 191 (1976).

CHEMICAL PROPERTIES OF METALLATED PLASMA POLYMERS

N. MOROSOFF and D. L. PATEL
Research Triangle Institute, P. O. Box 12194, Research Triangle Park, North Carolina 27709

P. S. LUGG and A. L. CRUMBLISS
Department of Chemistry, Duke University, Durham, North Carolina 27706

SYNOPSIS

Transition-metal-containing plasma polymers and plasma deposits were formed by plasma-polymerizing pentacarbonyliron(0) or cyclopentadienyldicarbonylcobalt(I) either as sole monomers or as one component of a mixture with a C_2 hydrocarbon (ethane, ethylene, or acetylene). The iron-containing plasma polymers were extensively characterized (FTIR, ESCA, Mössbauer spectroscopy, electron microscopy, and electron diffraction) and found to contain Fe^{3+} as iron oxide (crystals of 20 Å diameter) and iron carboxylate. Such iron-containing plasma polymers and plasma deposits were found to be redox active and to promote adhesion of electrochemically deposited Prussian blue. Cobalt-containing plasma polymer was characterized by FTIR. At low *W/FM* a trimeric cobalt cluster compound is formed.

INTRODUCTION

Metal-containing plasma polymers were among the earliest plasma polymers to be studied [1], but have only recently received wide attention [2–7]. This report is an overview of our recent investigations of the preparation and characterization of transition-metal-containing plasma polymers and plasma deposits. The transition metals were introduced into the plasma as the volatile organometallic compounds pentacarbonyliron(0) [$Fe(CO)_5$] and cyclopentadienyldicarbonylcobalt(I) [$CpCo(CO)_2$]. They were copolymerized with C_2 hydrocarbons and were also plasma polymerized with no comonomer. The plasma polymers were characterized by deposition rate measurements and Fourier transform in-

Journal of Applied Polymer Science: Applied Polymer Symposium 38, 83–97 (1984)

CCC 0570-4898/84/010083-15$04.00

frared spectroscopy (FTIR). Some iron-containing plasma polymers were also analyzed by means of x-ray photoelectron spectroscopy (ESCA), cyclic voltammetry, Mössbauer spectroscopy, transmission electron microscopy, and electron diffraction [14].

EXPERIMENTAL

Plasma polymerizations were carried out in the inductively coupled cylindrical reactor previously described [8] with a modified (2 mm i.d.) orifice for monomer introduction. Plasma reactions were carried out using 50 or 100 W of rf power (13.56 MHz) in most cases. The metal complexes were used as received, stored in the dark at −78°C, and warmed to room temperature [$CpCo(CO)_2$] or 0°C [$Fe(CO)_5$] during plasma polymerizations. $Fe(CO)_5$ and $CpCo(CO)_2$ were obtained from the Aldrich Chemical Company and the Strem Chemical Company, respectively. Purified aluminum foil was obtained from the J. T. Baker Chemical Company.

Deposition rates were obtained gravimetrically. Infrared spectra were obtained by using a Nicolet 7199 FTIR spectrometer. The plasma polymers were deposited on aluminum foil which was pressed against a 45° KRS-5 internal reflection element (ATR).

ESCA spectra were obtained using a Physical Electronics PHI model 548 instrument with a MgK_α x-ray source equipped with a model 15-5226 precision electron energy detector. Plasma polymer was deposited on Al foil blanks.

Carbon rods (0.3 cm × 3.8 cm; Ultracarbon, Bay City, MI) were extracted with hot CH_3CN for 18 h and mounted in the reactor for direct deposition of the metallated polymer. Characterization by cyclic voltammetry was performed by using a Bioanalytical Systems CV-1B triangular wave generator and a cell equipped with the metallated-plasma-polymer-coated carbon electrode, a Ag/AgCl reference electrode, and a platinum working electrode. All voltammograms were obtained in aqueous solution containing 0.1*M* KNO_3 at room temperature.

RESULTS AND DISCUSSION

Iron-Containing Plasma Polymer; Preparation and Characterization

Iron-containing plasma polymers and deposits were formed at the conditions given in Table I. Deposition rates were obtained gravimetrically as a function of distance along the length of the reactor and are expressed in Figure 1 as yield (%) per centimeter-wide strip around the circumference of the reactor [14]. The data in Figure 1 indicate that for all hydrocarbons a much more even rate of polymer deposition is achieved in the absence of $Fe(CO)_5$. Increasing the ratio *W/F*, for either 10 or 50% $Fe(CO)_5$, increases the integrated deposition rate.

Deposition rates obtained for the plasma deposit formed when $Fe(CO)_5$ is used as the sole monomer or in combination with hydrogen are also given in Figure 1. The same preferential deposition close to the monomer inlet is observed for

TABLE I
Experimental Conditions of Plasma Polymerizations[a]

Row	Monomer feed	ΣF (cm^3/min)	F_{Fe} (cm^3/min)	rf power (W)	W/FM (J/kg × 10^{-8})	P_g[b] (mtorr)	P_m (mtorr)
1	Hydrocarbon	0.45	0	50	53	— 28	
						= 15	20
						≡ 3	
2	Hydrocarbon, $Fe(CO)_5$	0.45	0.045	50	33	— 28	
						= 12	20
						≡ 5.5	
3	Hydrocarbon, $Fe(CO)_5$	0.21	0.021	100	142	— 10.5	
						= 9	20
						≡ 4.5	
4	Hydrocarbon, $Fe(CO)_5$	0.45	0.225	50	13	— 48	
							20
						≡ 53	
5	Hydrocarbon, $Fe(CO)_5$	0.10	0.05	50	60	— 7	2.4
						≡ 7.2	9.2
6	$Fe(CO)_5$		0.10	50	34	17.6	3.5
7	Hydrogen, $Fe(CO)_5$	0.10	0.05	50	68	8.9	3.8

[a]ΣF is the total flow rate, F_{Fe} the $Fe(CO)_5$ flow rate, W the rf power, P_m the pressure in the plasma reactor prior to initiation of glow discharge, P_g the pressure in glow discharge, and M the molecular weight (or mole-average molecular weight).

[b](—) ethane (single bond), (=) ethylene (double bond), (≡) acetylene (triple bond).

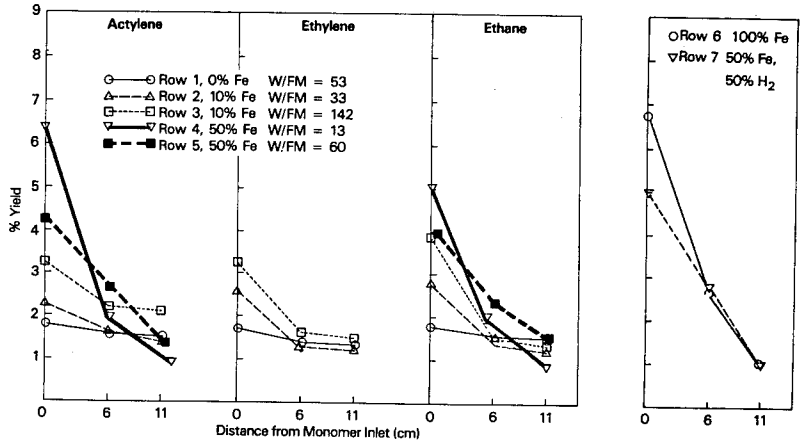

FIG. 1. Deposition rates as a function of distance from the monomer inlet for plasma polymerizations of $Fe(CO)_5$ with or without C_2 hydrocarbons. Deposition rates are expressed as yield (%) per 1-cm-wide strip on reactor circumference (area 12.6 cm^2). 10% Fe refers to 10 mol % of $Fe(CO)_5$ in the monomer mix. Plasma polymer designations refer to rows in Table I. Units for W/FM are 10^8 J/kg.

these cases as is obtained to a lesser degree for the row 2–5 plasma polymerizations.

The identification of the preferred deposition rate with the presence of iron in the plasma polymer is bolstered by the ESCA results (from the surface) shown in Figure 2. The figure shows that for a given preparation the deposit formed nearest the monomer inlet contains the greatest Fe/C ratio. The O/C ratios fall in the same sequence, for the various preparation conditions, as the Fe/C ratios. This suggests that oxygen from the $Fe(CO)_5$ is incorporated in the plasma deposit.

Infrared spectra obtained for the row 6 [Table I, 100% $Fe(CO)_5$] and row 5 [50% $Fe(CO)_5$, 50% ethane] plasma polymerizations are given in Figure 3. The most prominent features of the spectrum are three broad peaks at approximately 1565, 1400, and 1040 cm^{-1}. The peaks at 1565 and 1400 cm^{-1} are the most intense and correspond in position to intense absorption peaks assigned to the carboxylate ion (ca. 1570 and 1400 cm^{-1}) [9–11]. The spectrum obtained for iron formate (KBr pellet) is shown at the bottom of Figure 3 for comparison.

The peak at approximately 1040 cm^{-1} which is present in the IR spectrum for the $Fe(CO)_5$ plus ethane plasma polymer may be caused by C—OH (alcohol), or iron oxide. It may be noted that an alcohol should also show an OH in-plane deformation in the region 1300–1400 cm^{-1} and an OH stretch in the region 3200–3700 cm^{-1}. The broad peak at around 3300 cm^{-1} seen for both the row 5 and row 6 preparations may indicate an alcohol hydroxyl, a hydroxyl bonded to iron, or water. The presence of C—H groups in the row 5 plasma polymer is denoted by small peaks at 2925 and 2865 cm^{-1} (C—H stretch).

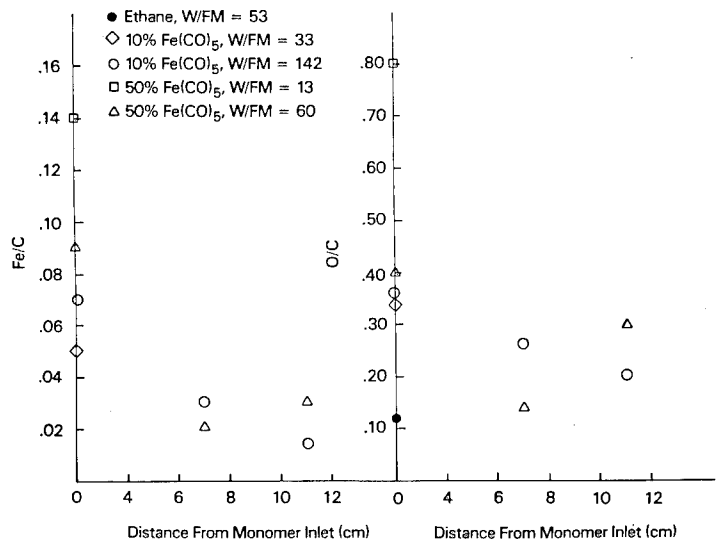

FIG. 2. Elemental ratios obtained from ESCA spectra for plasma polymer made using various ethane/$Fe(CO)_5$ monomer mixtures. Plots are against position in the reactor. Units for W/FM are 10^8 J/kg.

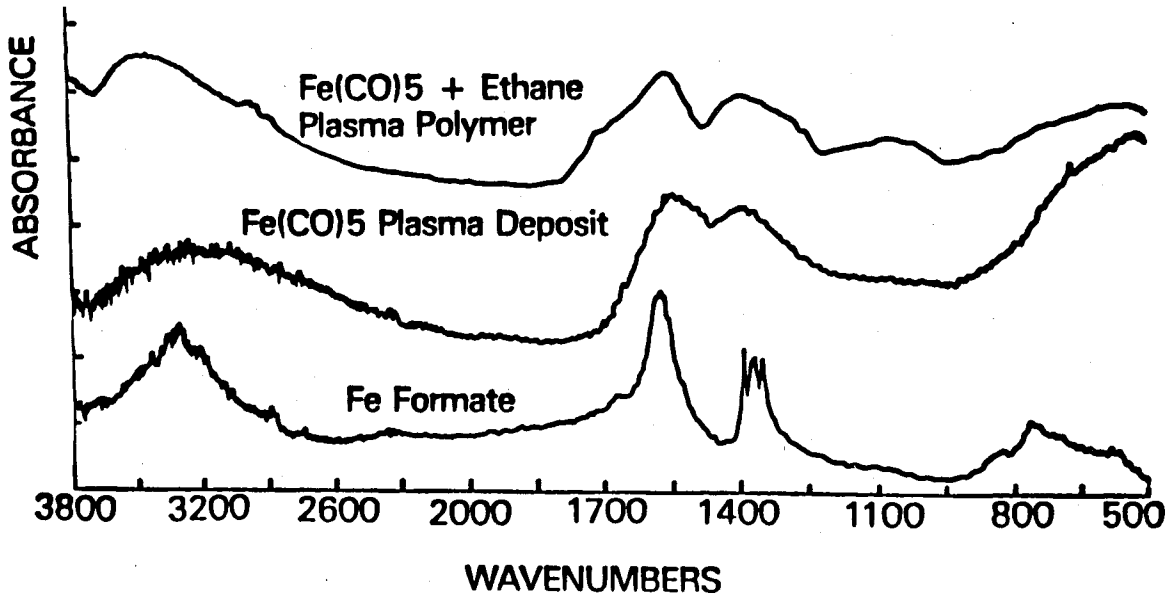

FIG. 3. FTIR absorbance spectra obtained using ATR technique for row 5 (Table I) plasma polymer (top), row 6 plasma deposit (middle) as deposited under the monomer inlet, and a spectrum of iron formate (bottom) obtained by the transmission method.

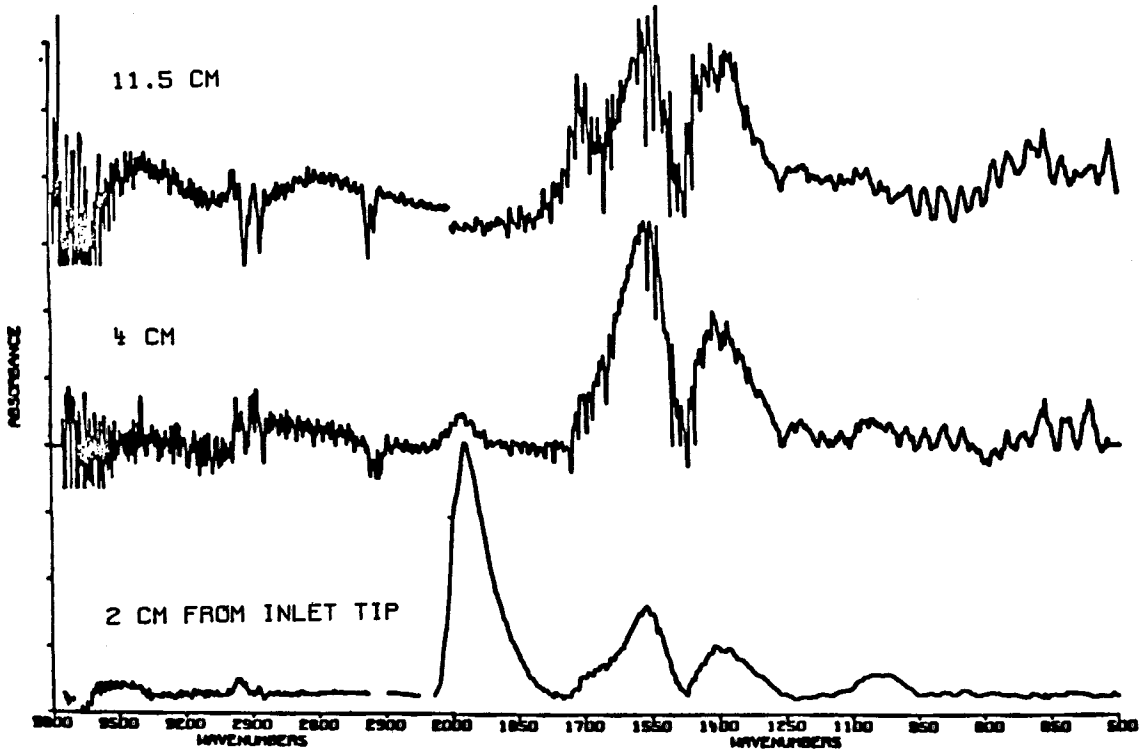

FIG. 4. FTIR absorbance spectra obtained for row 4 (Table I) plasma polymer near the monomer inlet (bottom), 4 cm from the monomer inlet (middle), and 11.5 cm from the monomer inlet (top). Spectra have been baseline straightened and therefore show only relatively sharp peaks.

Spectra obtained for the same molar ratio of ethane to $Fe(CO)_5$ (1:1), but at a lower *W/FM* (row 4, Table I), are shown in Figure 4. In addition to the features previously seen in Figure 3, a peak at 1900–2000 cm^{-1} is assigned to metal-complexed carbon monoxide. This peak is extremely broad, extending to 1850 cm^{-1}, consistent with the presence of some bridging carbonyls. This feature decreases in intensity for plasma polymer deposited at greater distances from the monomer inlet. An additional peak is noted at 1700 cm^{-1} for the plasma polymer deposited 11.5 cm from the monomer inlet. This is assigned to the C=O stretch for a ketone, aldehyde, or carboxylic acid. Infrared spectra obtained for plasma polymers deposited using a molar ratio of 10% $Fe(CO)_5$ (rows 2 and 3 of Table I) are essentially a superposition of the top spectrum of Figure 4 on the spectrum obtained for the plasma polymer deposited using any of the C_2 hydrocarbons as the sole monomer. In these spectra the peak at 1700 cm^{-1} is the more pronounced the more saturated the C_2 hydrocarbon comonomer. In some cases [10% $Fe(CO)_5$] a peak at 2200 cm^{-1} similar to that observed for adsorption of carbon monoxide on metal oxides is noted [12,13].

Transmission electron micrographs were obtained for row 5 plasma polymer for films of 1-, 5-, and 10-$\mu g/cm^2$ thickness. These showed the presence of dense particles of 20–30 angstrom diameter not found in electron micrographs of similarly prepared films made using ethane as the sole monomer. The electron diffraction pattern was consistent with that expected for iron oxide.

Mössbauer spectra were obtained for row 5 and row 4 plasma polymers and were consistent with a single-component, high-spin iron(III) for the row 5 plasma polymer; and two-component, high-spin iron(III) plus iron in an organometallic complex for the row 4 plasma polymer. A more complete description of the characterization of these iron-containing plasma polymers is to be published elsewhere [14].

Electrochemical Analysis of Iron-Containing Plasma Polymer

Cyclic voltammetry was used to study the electrochemical activity of iron-containing plasma polymer and deposit [15]. The coating of graphite electrodes was carried out under the conditions of row 5 and row 6 in Table I. The graphite electrodes were placed along the cylindrical axis of the reactor with the end of the electrode to be exposed to the electrolyte at a distance of 5 mm from the monomer inlet. Scanning electron micrographs of the electrodes showed them to be rough-surfaced. Thicknesses are therefore expressed as nominal, i.e., the thickness of the coating that would be present if the electrode surface were smooth.

Cyclic voltammograms obtained using electrodes coated with row 5 plasma polymer or row 6 plasma deposit and an aqueous 0.1*M* KNO_3 electrolyte exhibit a cathodic peak at -1.0 V and anodic peak at -0.55 V (vs. Ag/AgCl) [see Fig. 5(a)]. In an effort to see if iron in the coating would bind to hexacyanoferrate, electrodes coated with row 5 plasma polymer or row 6 plasma deposit were exposed to cyclic voltammetry in an aqueous solution 0.1*M* in KNO_3 and 0.005*M*

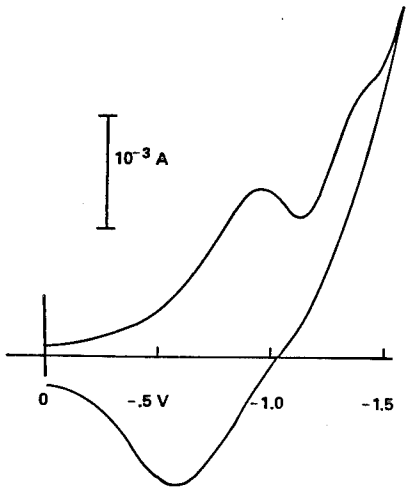

(a)

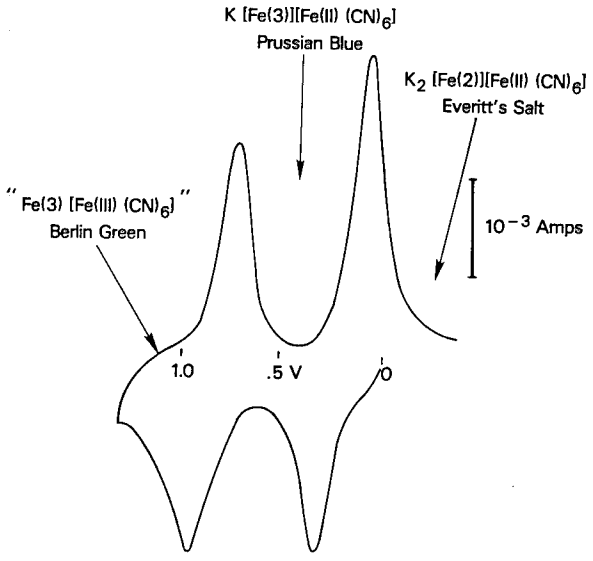

(b)

FIG. 5. (a) Cyclic voltammogram obtained in 0.1*M* KNO_3 using a row 5 (Table I) iron-containing plasma-polymer-coated electrode. Scan rate 100 mV s^{-1}. (b) Cyclic voltammogram obtained in 0.1*M* KNO_3 using a row 5 (Table I) iron-containing plasma-polymer-coated electrode which was preconditioned by being placed in a 5m*M* hexacyanoferrate(III) solution at 0.0 V (vs. Ag/AgCl) (i.e., method II) for 2.25 h followed by rinsing. Scan rate 100 mV s^{-1}.

in $K_3Fe(CN)_6$. It was discovered that cycling from -0.2 to $+1.2$ V (method I) in this solution caused binding of Prussian blue to the electrode. Such binding could also be effected by maintaining the electrode at a potential of 0.0 V (Ag/AgCl reference), in such a solution, for a period of time with stirring (method II). In either case, a cyclic voltammogram typical of Prussian blue is obtained [16] and is observed even if the electrode is removed from the solution, washed, and then redox cycled in an aqueous 0.1*M* KNO_3 solution containing no hexacyanoferrate. A cyclic voltammogram obtained for such bound Prussian blue is presented in Figure 5(b).

It is believed that the high-spin iron in the Prussian blue {i.e., $Fe(3)^+$ in $KFe(3)[Fe(II)(CN)_6]$} is generated by oxidation of the hexacyanoferrate ion in solution. Two pieces of evidence support this. First, exposure of an electrode coated with 5 $\mu g/cm^2$ (nominal thickness) of row 5 plasma polymer to an aqueous 0.1*M* KNO_3 solution at 0.0 V (Ag/AgCl reference) for 2.25 h, with stirring, resulted in leaching of only 0.2% of the iron in the coating to the solution (analysis by atomic absorption). (It may be noted that under the same conditions 25% of the iron in the row 6 plasma deposit is leached to the solution). The leaching measured for the row 5 plasma polymer corresponds to only 1.2% of the amount of $Fe(3)^+$ present in Prussian blue deposited under the same conditions but with 0.005*M* $K_3Fe(CN_6)$ also present in the cell (i.e., method II, 2.25 h). Second, the auxiliary electrode is at a potential of $+1.6$ V when the primary electrode is at 0.0 V and isolation of this electrode from the other components in the cell by use of a salt bridge results in no deposition of Prussian blue by

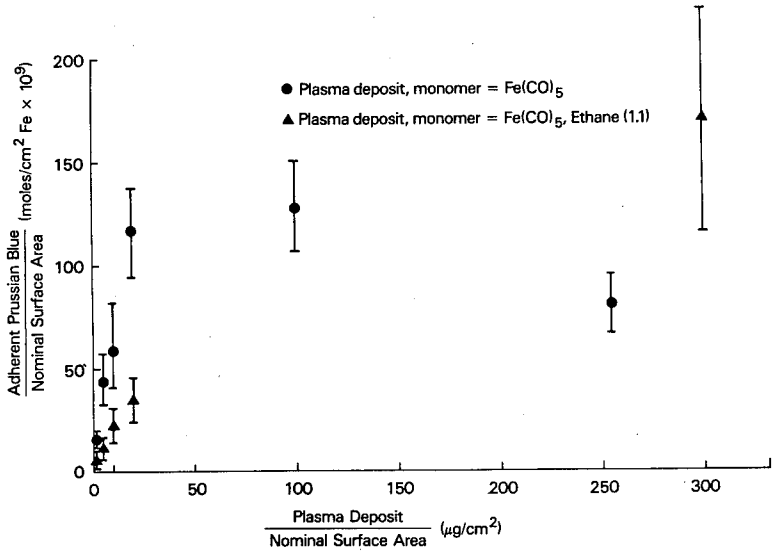

FIG. 6. Plot of amount of high-spin iron in adherent Prussian blue versus nominal thickness of plasma polymer coating, when plasma-polymer-coated electrode has been preconditioned by method II for 2.25 h. Amount of adherent Prussian blue is obtained from area under cyclic voltammogram peak at 0.2 V.

method II. The potential of the auxiliary electrode is such as to allow oxidation of the hexacyanoferrate ion.

Cyclic voltammograms have been observed for Prussian blue deposited on electrodes by other means [16,17]. However, the deposit we observe differs in presenting well-defined peaks [Fig. 5(b)], in persisting for over 1000 redox cycles in a neutral aqueous solution of KNO_3, and in accessibility to sodium as well as potassium ions.

The amount of Prussian blue deposited on the electrode (deduced from area under the cyclic voltammogram peaks) increases (for a given set of conditions) with the amount of iron-containing plasma deposited on the electrode. This is shown in Figure 6 for plasma-deposit-coated electrodes subsequently coated with Prussian blue by method II for 2.25 h. It may be noted that a plateau is reached for both methods, at a lower degree of plasma deposit coverage for row 6.

The results described here for rough-surfaced graphite electrodes could not be reproduced exactly when plasma polymer was deposited on a smooth-surfaced platinum electrode. Although electrochemical evidence of persistent binding of hexacyanoferrate ion to a row-5-plasma-polymer-coated electrode was obtained, the details of the cyclic voltammograms differed from those presented here. Investigation of this area is being pursued.

Plasma Polymerization of Cyclopentadienyldicarbonylcobalt (I)

Deposition rates as a function of distance from the monomer inlet are presented in Figure 7 for plasma polymerizations involving $CpCo(CO)_2$ as monomer or comonomer. It may be noted that the cobalt-containing plasma polymer is more evenly distributed over the reactor than is the iron-containing plasma polymer.

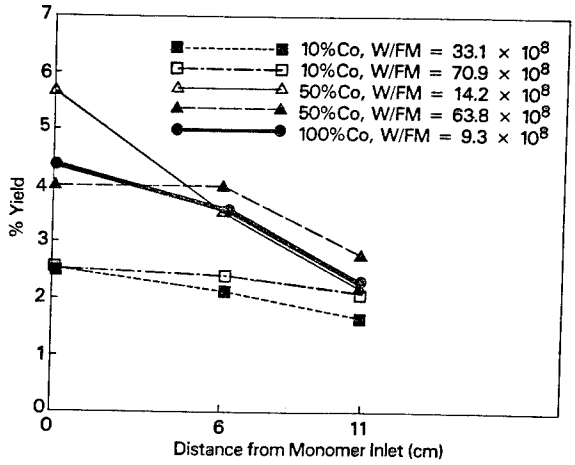

FIG. 7. Deposition rate as a function of distance from monomer inlet for $CpCo(CO)_2$ polymerizations expressed as in Fig. 1. Rf power was 50 W for all plasma polymerizations. Units for W/FM are J/kg.

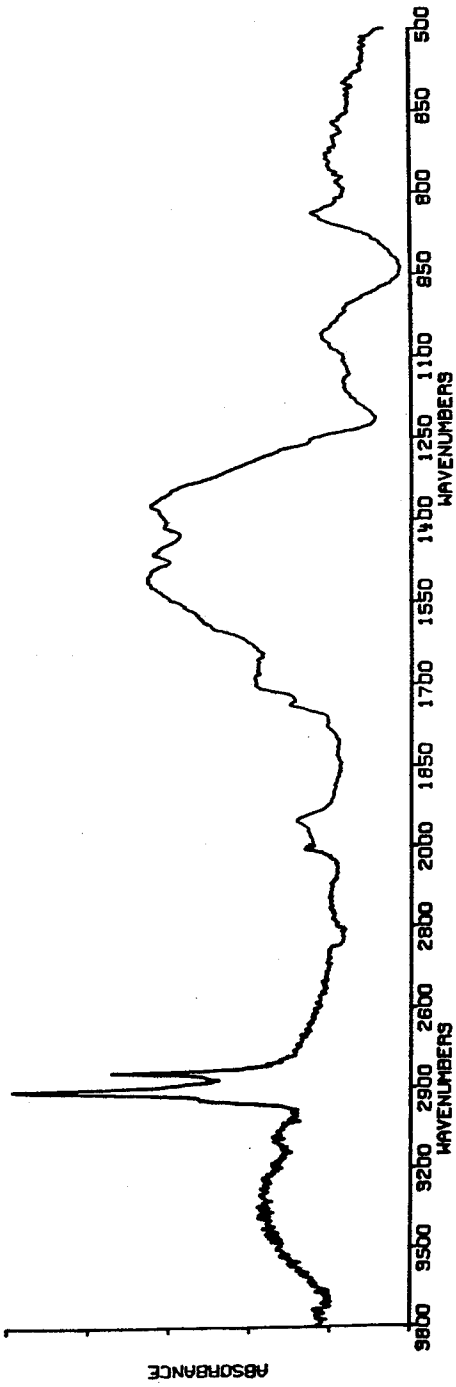

FIG. 8. Infrared spectrum obtained for plasma polymer of cyclopentadienyldicarbonylcobalt deposited 4 cm from the monomer inlet using $F = 0.39$ cm^3/min, 50 W of rf power, $p_s = 7$ mtorr.

This may be caused by the tighter binding of the cyclopentadienyl ligand relative to the carbonyl. The polymerization rate (rate of generation of involatile species) is therefore greater for plasma polymerizations involving $Fe(CO)_5$ than for $CpCo(CO)_2$.

Infrared spectra were obtained for plasma copolymerization of $CpCo(CO)_2$ with ethane and for plasma polymerization of the metal complex alone. The IR spectrum obtained for the latter is shown in Figure 8. Note may be taken of the C—H stretch region of the spectrum. The IR spectrum of the monomer exhibits a peak at 3100 cm^{-1} [18]. A small broad peak in that region is noted in the spectrum of the plasma polymer. Two intense peaks at 2930 and 2870 cm^{-1} indicate that rearrangement of the cyclopentadienyl moiety has taken place. Peaks at 2015 and 1951 cm^{-1} are characteristic of carbon monoxide complexed to metals. They are displaced from the positions found for the monomer (2028 and 1967 cm^{-1}) and lie on a broad peak, suggesting a variety of environments for the carbonyl group [19]. The broad peak at 3400 cm^{-1} suggests a hydroxyl group. The plasma polymer was prepared at an rf energy to flow rate ratio W/FM of 9×10^{-8} J/kg. Plasma polymers prepared using $CpCo(CO)_2$ and ethane

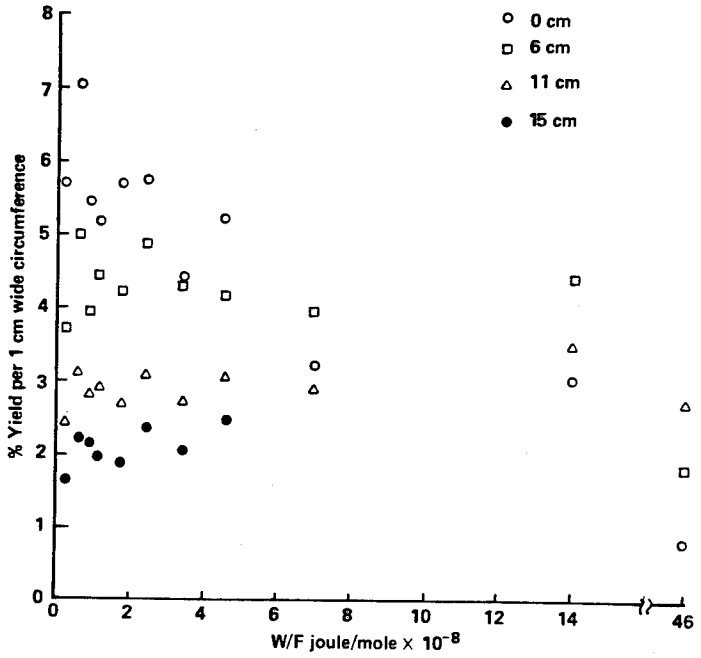

FIG. 9. Plot of deposition rate versus W/F for $CpCo(CO)_2$ plasma polymerization. The deposition rate (expressed as % yield) was obtained at four locations within the reactor. Plasma polymerizations were carried out by keeping power at 50 W and varying flow rate or keeping flow rate at 0.28 cm^2/min and varying power. The pressure prior to initiating glow discharge (P_m) was 20 mtorr for all but one plasma polymerization (see Fig. 10).

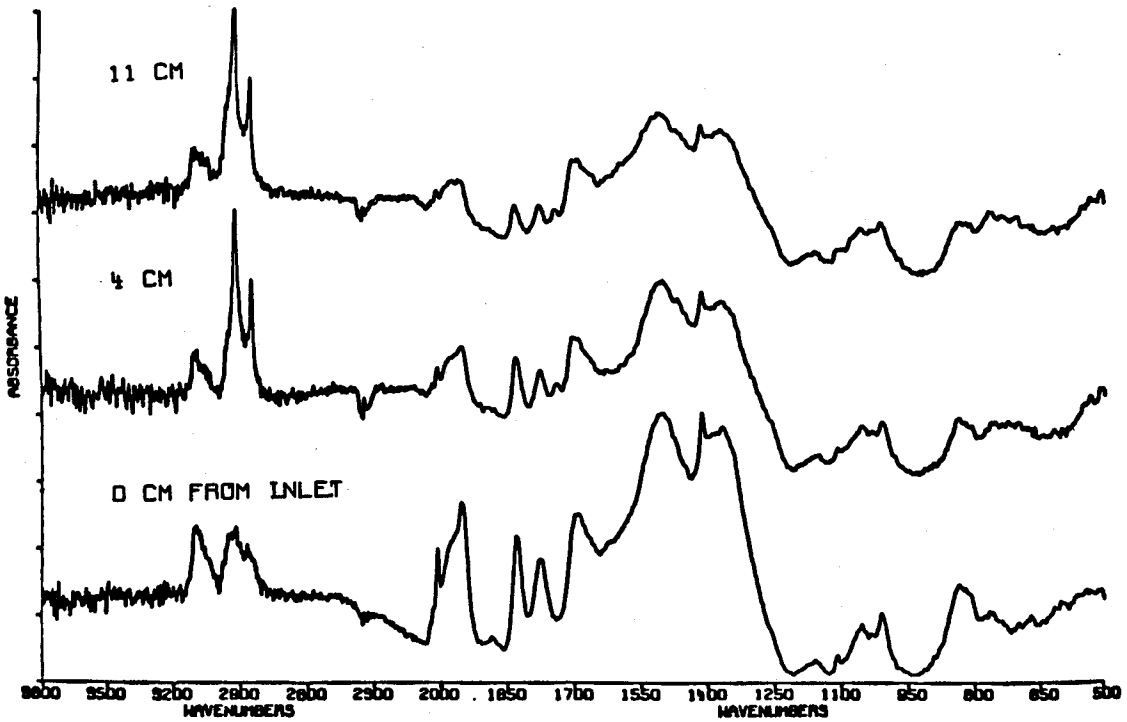

FIG. 10. Infrared spectra of $CpCo(CO)_2$ plasma polymers deposited at various sites within the reaction chamber. Plasma polymerization conditions were $W/F = 0.25$, $F = 0.272$ cm^3 (STP)/min, power 5 W, $P_m = 7.9$ mtorr, $P_g = 19.6$ mtorr.

as comonomers were made at somewhat higher levels of W/FM [(14–64) $\times$ 10^{-8} J/kg] and exhibited no peaks at 2000 or 3100 cm^{-1}.

For $CpCo(CO)_2$ as sole monomer, deposition rate data were obtained as a function of the parameter W/F (Fig. 9) [20]. There is a pronounced nonuniformity in the distribution of deposition rates at low W/F, with the highest deposition rate under the monomer inlet. This is reminiscent of the situation with $Fe(CO)_5$ and occurs for the same reason, precipitation of involatile species. The IR spectra obtained for low W/F are shown in Figure 10 and exhibit peaks due to bridging carbonyls at 1830, 1775, and 1675 cm^{-1}. This is consistent with the formation of the trimeric cluster compound tris(cyclopentadienylcarbonylcobalt) [21] $[CpCo(CO)]_3$, which codeposits with the cobalt-containing plasma polymer [20]. To our knowledge this is the first report of the preparation of a transition-metal cluster compound via plasma techniques.

CONCLUSIONS

(i) Plasma polymers made using $Fe(CO)_5$ plus a C_2 hydrocarbon as comonomers result in more uneven deposition in a tubular reactor than those formed under similar conditions but with no $Fe(CO)_5$ in the monomer mix. This is due to the more rapid generation of involatile species in the presence of $Fe(CO)_5$ than when the C_2 hydrocarbons are used as sole monomer.

(ii) Plasma polymers made with $Fe(CO)_5$ as comonomer contain iron oxide and iron carboxylate. They differ chemically from the plasma deposit resulting from the use of $Fe(CO)_5$ as the sole monomer in the presence of C—H bonds and in an IR absorption peak at ca. 1000 cm^{-1} attributed to iron oxide. They differ from those made with C_2 hydrocarbon as a sole monomer in the presence of a peak at 1700 cm^{-1} attributed to an aldehydic or ketonic carbonyl. The latter is the more intense the more saturated the monomer. Some of the iron in plasma polymers made under row 5 conditions is in the form of small crystallites of 20–30 angstrom diameter.

(iii) The iron-containing plasma polymer is redox active as shown by cyclic voltammetry. In addition, it promotes electrodeposition of an adherent Prussian blue coating from a potassium hexacyanoferrate solution. Prussian blue deposited in this way is distinguished by well-defined redox peaks in the cyclic voltammogram, adherence for over 1000 redox cycles in neutral electrolyte solution, and accessibility to sodium and potassium ions. The amount of Prussian blue deposited for a given set of conditions increases with the amount of iron-containing plasma polymer on the electrode but appears to require a thin or discontinuous coating of the plasma polymer on the electrode. This may be due to the fact that the plasma polymer will not swell in water.

(iv) Although iron-containing plasma deposits prepared with or without C_2 hydrocarbons in the monomer stream behave similarly in the electrochemical experiments (both are redox active, both promote adhesion of Prussian blue), the one prepared with 50 mol % ethane (row 5) shows negligible leaching of iron to the electrolyte solution; the other (row 6) leaches iron readily to the electrolyte solution.

(v) Iron-containing plasma polymer prepared at sufficiently low *W/FM* contains iron complexed to carbon monoxide.

(vi) At relatively high *W/FM*, plasma polymers prepared by using $CpCo(CO)_2$ as a monomer or comonomer display a relatively uniform distribution of deposition rate. The rate of generation of involatile species is therefore not as rapid as is the case with $Fe(CO)_5$. Carbon monoxide complexed to cobalt is observed when $CpCo(CO)_2$ is used as sole monomer but not when it is introduced into the reactor together with a C_2 hydrocarbon.

(vii) At low *W/FM* with $CpCo(CO)_2$ as sole monomer, preferred deposition close to the monomer inlet of a trimeric cluster compound is observed. This is the first report of the preparation of a transition-metal cluster compound by means of plasma chemistry.

The authors gratefully acknowledge the experimental work of George Cessna, who prepared some of the iron-containing plasma polymer samples and obtained their IR spectra. The ESCA spectra were obtained by Dieter Griffis and X. B. Cox, Department of Chemistry, University of North Carolina at Chapel Hill. Electron microscopy was carried out by Dr. Alan R. White, presently at the University of Colorado, Boulder, Mössbauer spectra were provided by Professor D. B. Brown, University of Vermont. This work was made possible by NSF Grant No. CPE-8006805.

REFERENCES

[1] A. Bradley and J. P. Hammes, *J. Electrochem. Soc., 110,* 15 (1963).
[2] E. Kay and A. Dilks, *J. Vac. Sci. Technol., 18,* 1 (1981).
[3] E. Kny, L. L. Levenson, W. J. James, and R. A. Auerbach, *J. Vac. Sci. Technol., 16,* 359 (1979).
[4] R. Liepins, M. Campbell, J. S. Clements, J. Hammond, and R. J. Fries, *J. Vac. Sci. Technol., 18,* 1218 (1981).
[5] D. Shuttleworth, *J. Phys. Chem., 84,* 1629 (1980).
[6] R. J. Nowak, F. A. Schultz, M. Umana, R. Lam, and R. W. Murray, *Anal. Chem., 52,* 315 (1980).
[7] M. F. Dautartas and J. F. Evans, *J. Electroanal. Chem., 109,* 301 (1980).
[8] H. Yasuda and C. E. Lamaze, *J. Appl. Polym. Sci., 17,* 1519 (1973).
[9] C. N. R. Rao, *Chemical Applications of Infrared Spectroscopy,* Academic, New York, 1963, pp. 194, 199.
[10] L. J. Bellamy, *The Infrared Spectra of Complex Molecules,* Wiley, New York, 1958.
[11] *Polymer Spectroscopy,* D. O. Hummel, Ed., Verlag Chemie, Weinheim, 1974.
[12] P. S. Braterman, *Metal Carbonyl Spectra,* Academic, New York, 1975, p. 179.
[13] R. P. Eischens and W. A. Pliskin, *Adv. Catal., X,* 1 (1958).
[14] N. Morosoff, D. L. Patel, A. R. White, D. B. Brown, M. Umana, P. S. Lugg, and A. L. Crumbliss, *Thin Solid Films,* to appear.
[15] A. L. Crumbliss, P. S. Lugg, D. L. Patel, and N. Morosoff, *Inorg. Chem., 22,* 3541 (1983); J. W. Childers, A. L. Crumbliss, P. S. Lugg, R. A. Palmer, N. Morosoff, and D. L. Patel, *J. Phys., 44,* C6-285 (1983); and A. L. Crumbliss, P. S. Lugg, and N. Morosoff, *Inorg. Chem.,* to appear.
[16] D. Ellis, M. Eckoff, and V. D. Neff, Jr., *Phys. Chem., 85,* 1225 (1981).
[17] K. Itaya, T. Ataka, and S. Toshima, *J. Am. Chem. Soc., 104,* 4767 (1982).
[18] T. S. Piper, F. A. Cotton, and G. Wilkinson, *J. Inorg. Nucl. Chem., 1,* 165 (1955).
[19] J. R. Blackborow and D. Young, *Metal Vapour Synthesis in Organometallic Chemistry,* Springer, New York, 1979, p. 76.
[20] N. Morosoff, D. L. Patel, P. S. Lugg, and A. L. Crumbliss, *Inorg. Chim. Acta, 83,* 137 (1984).
[21] F. A. Cotton and J. D. Jamerson, *J. Am. Chem. Soc., 98,* 1272 (1976).

SYNTHESIS OF ORGANOGERMANIUM FILMS BY GLOW DISCHARGE POLYMERIZATION

R. K. SADHIR
Research Laboratories, Westinghouse R&D Center, Pittsburgh, Pennsylvania 15235

W. J. JAMES
Department of Chemistry and Graduate Center for Materials Research, University of Missouri, Rolla, Missouri 65401

R. A. AUERBACH
Lord Corporation Fellowship, Carnegie–Mellon Institute of Research, 4400 Fifth Avenue, Pittsburgh, Pennsylvania 15213

SYNOPSIS

Organogermanium films were deposited on glass substrates via glow discharge polymerization of tetramethyl germanium. Films of organogermanium were also prepared by introducing oxygen as a nonpolymerizing reactive gas during the glow discharge polymerization. The variation in deposition rate, conductivity, and composition of films prepared under the different conditions is discussed. The C/Ge ratios, determined by ESCA, vary as a function of the reactor parameters.

INTRODUCTION

In recent years there has been considerable effort expended in the synthesis of inorganic thin films by glow discharge. This subject has been reviewed in detail by Hollahan and Rosler [1]. In our laboratory [2–6], we have done an exhaustive study of the glow discharge polymerization of organotin monomers. Thin (150–2000 Å) films have been deposited on a variety of substrates with resulting sheet conductivities as high as 10^4 $(\Omega\ \text{cm})^{-1}$. Kny et al. [2] have prepared semiconducting organotin films by glow discharge polymerization of tetramethyl tin. Since germanium and tin are in the same group of the Periodic

Journal of Applied Polymer Science: Applied Polymer Symposium 38, 99–104 (1984)

CCC 0570-4898/84/010099-06$04.00

Table, it appeared reasonable that semiconducting films of organogermanium could be prepared.

Spear and LeComber [7] have reported the synthesis of Ge and Si specimens by decomposition of germane and silane, respectively, in a radio-frequency (rf) glow discharge. The specimens were doped with small amounts of phosphine or diborane to obtain *n*- or *p*-type semiconductors. Anderson and Spear [8] also prepared amorphous germanium carbide by decomposition of a mixture of germania and ethylene in a rf glow discharge. The substrates were held at a temperature between 400 and 800 K during deposition. They observed a systematic variation of the dc conductivity with deposition temperature. Kuppers, Koenings, and Wilson [9] have discussed the codeposition of glassy silica and germania inside a tube using plasma-activated CVD. The deposition was effected at 1000°C in a microwave discharge from a mixture of $SiCl_4$, $GeCl_4$, and O_2.

In this article, we report on the preparation and properties of organogermanium films prepared by glow discharge polymerization of tetramethyl germanium.

EXPERIMENTAL

A rf, inductively coupled, glow discharge reactor was used for the preparation of the organogermanium films. The reactor design has been discussed elsewhere [6]. The system is evacuated by means of a rotary and oil diffusion pump in the millitorr range. The monomer gases or vapors are introduced by one leak valve and a nonpolymerizing gas (oxygen) is introduced through another valve at a desired flow rate. The parameters used for the deposition of the organogermanium films are given in Table I. The starting material was tetramethyl germanium. The substrates, precleaned glass slides, were exposed to a plasma of Ar gas at

TABLE I
Parameters for the Glow Discharge Polymerization of Tetramethyl Germanium

Experiment	Experiment 1	Experiment 2
Starting compound	Tetramethyl germanium	Tetramethyl germanium
Flow rate of monomer (STP) cm^3/sec	9.6×10^{-3}	1.2×10^{-2}
Flow rate of O_2 (STP) cm^3/sec	-	3.6×10^{-4}
rf Power (watts)	4.0	4.5
SW* ratio	3.0	2.6
System pressure (mtorr)	55	57
Duration (sec)	2950	7600
Maximum Deposition Rate Å/sec	1.42	.78
Film appearance	Golden colored semi-transparent	Reflective, metal-like

*Standing wave ratio.

a pressure of 50 mtorr prior to the deposition of the film. After the Ar ion cleaning, the monomer was introduced into the reactor at the desired flow rate. The glow discharge polymerization of tetramethyl germanium yielded a golden semitransparent film close to the monomer inlet and transparent films in all other regions of the reactor. The position of the substrate is taken as its distance from the monomer inlet of the reactor. In another experiment (No. 2 in Table I), the films were prepared in a mixed plasma of oxygen and tetramethyl germanium. These films were reflective and metallic in appearance but exhibited semiconducting behavior.

Film thicknesses were determined by the Nomarsky interference method [10] using a Reichert Wien polarization interferometer. The scanning electron micrographs were taken with a JEOL scanning electron microscope. The conductivity of the films was determined by a four-probe method. A PHI ESCA/Auger 549 spectrometer was used to determine the composition of the films. XPS were recorded using a pass energy of 100 eV and a MgK_{α} x-ray source.

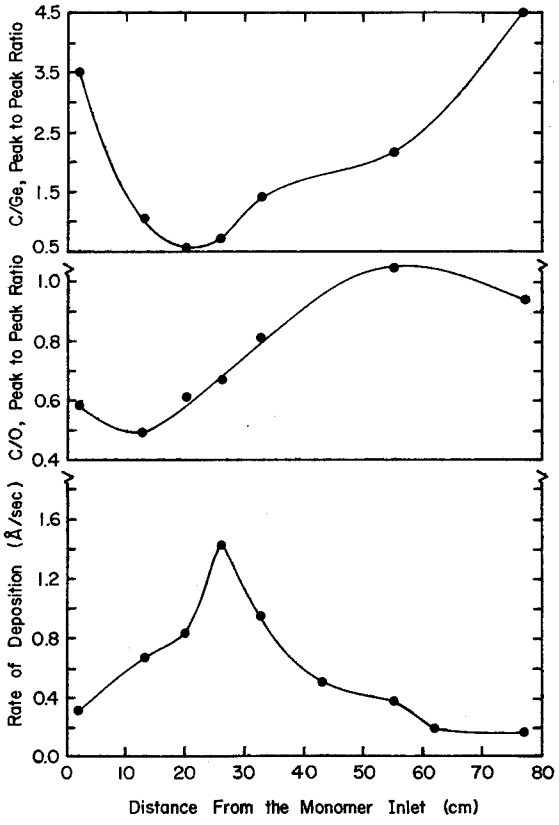

FIG. 1. Rate of deposition and composition of organogermanium film (ca. 25 Å of film removed by argon sputtering).

RESULTS AND DISCUSSION

Figure 1 shows the rate of deposition, and the composition of the organogermanium films along the length of the reactor. The maximum deposition rate is observed at about 26–30 cm from the monomer inlet. Figure 2 depicts the rate of deposition and the composition of the films prepared in the presence of oxygen. In general, the rate of deposition is lower when the glow discharge polymerization is effected in the presence of oxygen. This can be attributed to the ablative action of oxygen. In the process of glow discharge polymerization, the process of polymer formation can be represented by competitive ablation and polymerization [11]. When the polymer deposits, non-polymer-forming gaseous by-products result from the reactive intermediates. Because polymer-forming species leave the gas (plasma) phase as the polymer is deposited, the major portion of the gas consists of the product gas when a high conversion ratio of starting material to polymer is obtained. The characteristics of the product gas plasma are the predominant factors in determining the extent of the ablation process. A drastic ablation effect is observed in the glow discharge polymerization of fluorine- or oxygen-containing compounds [12]. A negative rate of deposition is obtained in these compounds due to the etching effects of fluorine and oxygen produced as

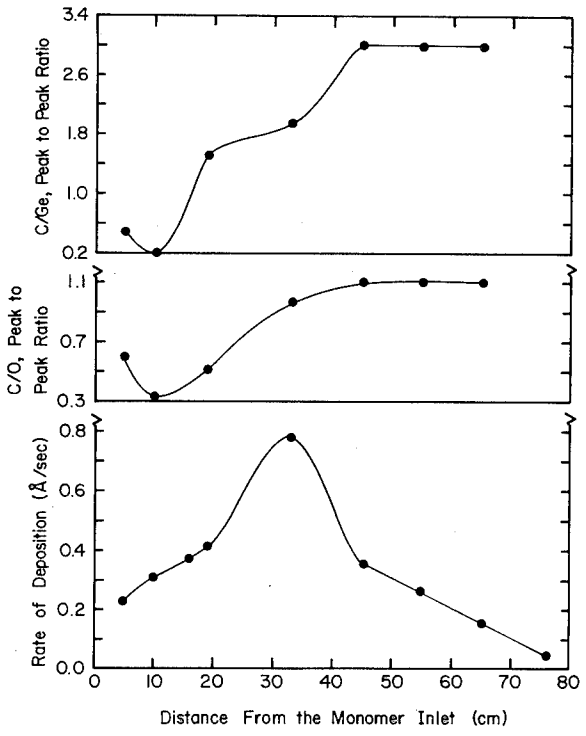

FIG. 2. Rate of deposition and composition of organogermanium films prepared in the presence of oxygen (ca. 25 Å of film removed by argon sputtering).

product gases during the process of polymerization. In this study, oxygen was introduced to extract C as CO and CO_2. Because of this ablative action of oxygen, the rate of deposition of the organogermanium films was lowered as expected. Figures 1 and 2 provide evidence that films with higher germanium content are obtained when the deposition is effected in the presence of oxygen.

ESCA examination of these films reveals (Figs. 1 and 2) that the stoichiometry of the starting monomer, tetramethyl germanium, is not retained. The C/Ge ratio was determined by comparing the peak heights of the C_{1s} and Ge Auger 422 peaks. The C/O ratio was determined by considering the relative heights of the C_{1s} and the O_{1s} peaks. The films of higher germanium content are deposited 10–25 cm from the monomer inlet. Films of highest germanium content (C/Ge ratio 0.21) were obtained at a distance of 10 cm under the conditions used in experiment 2 (Table I). The composition of the films on the surface is different from that of those in the bulk. After deposition of the film ceases, some unreactive monomer and other reactive species become attached to the active sites of the film. Moreover, when the films come in contact with air, a thin layer of germanium oxide forms and carbon dioxide can be adsorbed on the surface. Usually several hours elapse between the time of sample preparation and ESCA analysis. Because of this, we consider the actual carbon content to be that measured after 20–50 angstrom of the film has been removed by sputtering with argon ions. The carbon content then remains essentially constant throughout the bulk. After

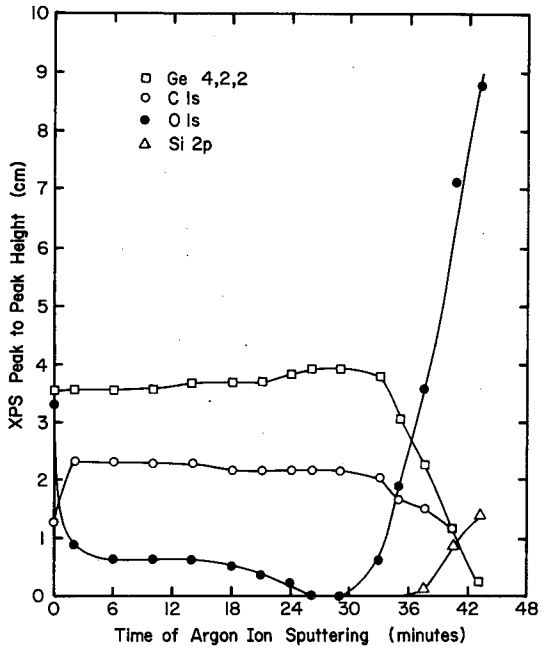

FIG. 3. Depth profile of the organogermanium film.

sputtering 20–25 Å of film, the peak height of oxygen is reduced drastically (by a factor of ca. 8) and the peak height of Ge increases.

Figure 3 shows a depth profile of the film deposits at a distance of 16 cm from the inlet of the monomer. The sputtering was done with Ar ions at 2 kV and 30-mA current. It is observed that the Ge content is less on the surface than in the bulk and that the O content is less in the bulk of the film. This particular film sputtered at a rate of 26 Å/min. The sputtering rates vary as the composition is varied and appear to increase as the C/Ge ratio increases.

The sheet conductivity of the film deposited in the presence of oxygen at the 10-cm position in the reactor is 1.8×10^{-6} $(\Omega\ \text{cm})^{-1}$. At other positions, the conductivity was lower than this but could not be measured accurately by the method used. Experiments are in progress to determine the structural and electronic properties of polymer films prepared by varying kinetic parameters (flow rate, power, etc.).

REFERENCES

[1] J. R. Hollahan and R. S. Rosler, in *Thin Film Processes,* J. L. Vossen and W. Kern, Eds., Academic, New York, 1979.
[2] E. Kny, W. J. James, L. L. Levenson, and R. A. Auerbach, presented at the Annual Meeting of the Materials Research Society, Cambridge, MA, 1979; *Thin Solid Films, 85,* 23 (1981).
[3] E. Kny, L. L. Levenson, W. J. James, and R. A. Auerbach, *Thin Solid Films, 64,* 395 (1979).
[4] E.Kny, L. L. Levenson, W. J. James, and R. A. Auerbach, *J. Vac. Sci. Technol., 16*(2), 359 (1979).
[5] E. Kny, L. L. Levenson, W. J. James, and R. A. Auerbach, *J. Phys. Chem., 84,* 1635 (1980).
[6] R. K. Sadhir, W. J. James, and R. A. Auerbach, *Thin Solid Films, 97,* 17 (1982).
[7] W. E. Spear and P. G. LeComber, *Philos. Mag., 33,* 935 (1976).
[8] D. A. Anderson and W. E. Spear, *Philos. Mag., 35,* 1A (1976).
[9] D. Kuppers, J. Koenings, and H. Wilson, *J. Electrochem. Soc., 123,* 1079 (1976).
[10] G. Nomarsky and A. R. Weill, *Rev. Met.* (Paris), *55,* 121 (1955).
[11] H. K. Yasuda, in *Plasma Polymerization,* Am. Chem. Soc. Symp. Ser. No. 108, M. Shen and A. T. Bell, Eds., Am. Chem. Soc., Washington, DC, 1978, p. 37.
[12] H. K. Yasuda, presented at the International Round Table on Plasma Polymerization and Treatment, IUPAC Symposium on Plasma Chemistry, Limoges, France, 1977.

CHARACTERIZATION OF PLASMA-POLYMERIZED MATERIALS BY MODERN SPECTROSCOPIC TECHNIQUES

S. KAPLAN and A. DILKS*
Xerox Corporation, W-114 Webster, New York 14580

SYNOPSIS

The structures of a number of insoluble, intractable films deposited in a radio-frequency plasma have been investigated with magic-angle spinning ^{13}C nuclear magnetic resonance (^{13}C-NMR). Infrared, combined pyrolysis–gas chromatography–mass spectrometry, or ESCA measurements were also employed in order to corroborate and extend the NMR conclusions. Spectroscopic data are presented for polymers prepared from ethane, ethylene, acetylene, toluene, tetrafluoroethylene, and octafluorotoluene. In the case of toluene, specific isotopic labeling was used to map the destinations of individual carbon atoms and to identify likely gas-phase mechanisms leading to film formation.

INTRODUCTION

Polymer films produced by a glow discharge often possess chemical and physical properties that are superior to conventionally polymerized materials [1–3]. They are prepared by a totally dry vapor-phase deposition process and may be conformally coated onto virtually any substrate. The rapid growth in recent years of technological applications for plasma-polymerized coatings has stimulated efforts to characterize the polymers in terms of their chemical structures and the primary routes to their formation. Because of the large number of reaction pathways available during plasma excitation, polymers formed in plasmas generally have complex, highly crosslinked structures that render them insoluble [1–3]. Thus, analytical techniques have been limited to those for which solid samples can be studied. For plasma-polymerized fluorocarbons the most detailed structural information has been derived from x-ray photoelectron spectroscopy (ESCA) [2–7], which provides quantitative chemical information from thin-film

*Present address: Shell Thornton Research Center, P. O. Box 1, Chester, England.

Journal of Applied Polymer Science: Applied Polymer Symposium 38, 105–125 (1984)

CCC 0570-4898/84/010105-21$04.00

samples *in situ*. This technique, however, is of little use for hydrocarbons because of their extremely small chemical shifts [8]. The most widely used spectroscopic technique for determining structure and bonding in plasma-polymerized hydrocarbons has been infrared (IR) spectroscopy [1–3,9–11], which exhibits high sensitivity to particular structural features. Quantitative analysis by IR has been problematic because of the difficulties in determining accurate band absorbances and the absence of extinction coefficient data associated with the variety of structural environments in the polymer. Mass-spectrometric determination of the pyrolysis products of the films has also been used to investigate the polymer structure [10,12]. Although mass spectrometry is useful in detecting the presence of certain functional groups, differential cross sections for electron impact ionization of various species make quantitative analysis difficult. In separate experiments, pyrolysis–gas chromatography has been used to deduce information about the polymer structure [2,12–14].

Recent measurements of plasma-polymerized materials by high-resolution solid-state ^{13}C nuclear magnetic resonance (NMR) spectroscopy have demonstrated that NMR is complementary to other spectroscopic techniques and, furthermore, capable of providing unique structural information [15–17]. NMR spectra generally give a uniform representation of the entire bulk structure without bias toward particular structural features, as is the case for infrared and mass spectrometry. Thus, it is possible with NMR to determine the relative contribution of each observed functional group to the total polymer structure. On the other hand, the sensitivity of NMR is considerably lower than other techniques, thus necessitating large sample volumes and long-term signal averaging. Nevertheless, ^{13}C-NMR is a viable characterization tool for plasma polymers. In this paper we describe current efforts to exploit the NMR technique, along with corroborative IR, combined pyrolysis–gas chromatography–mass spectrometry, and ESCA analyses, to investigate the structure of a number of plasma-polymerized materials.

The ability of solution NMR to give structural information at the molecular level is attributed to the very high chemical shift resolution attainable. Unlike solution NMR, where linewidth resolution of better than 0.5 Hz is readily achieved, ^{13}C-NMR in the solid-state is hampered by ca. 30-kHz lines, broadened by large dipolar interactions and chemical shift anisotropies. The proton-enhanced ^{13}C method with high-power proton decoupling [18] combined with magic-angle spinning [19] has largely overcome this problem and has been successful in characterizing the structure of organic solids and polymers [20]. The resolution of 1–20 Hz achieved in rigid organic solids and crystalline polymers has been limited by insufficient decoupling power and residual ^{13}C–^{13}C interactions [21,22]. In amorphous polymers, however, the distribution of isotropic chemical shifts, presumably from local differences in microstructure, conformation, and chain packing, limits resolution to ca. 3 ppm [20,22]. For plasma-polymerized materials broad resonance lines due to the overlap of peaks from many chemically inequivalent environments are expected. Still, resolution of ^{13}C spectral features is sufficient to permit comparison of structural parameters in a number of deposited polymer films [15–17].

Furthermore, since the ^{13}C isotope occurs only 1% in natural abundance, labeling the injected vapor at a specific chemical site offers the attractive possibility of tracing the destiny of particular carbon atoms in the plasma process. Toluene has been chosen as the monomer for such a study because it is one of the simplest molecules having two distinct carbon types (i.e., saturated and unsaturated) for which isotopically labeled analogs are readily available [17].

EXPERIMENTAL

Film Preparation

Plasma-polymerized films were deposited in an inductively coupled radio-frequency system operating at 13.56 MHz. The plasma reactor consisted of a Pyrex glass tube 7.5 cm in diameter and 30 cm long, with the inlet and outlet constricted to 1.5 cm (see Fig. 1). The system was pumped by a Welch Co. model 1402 mechanical pump via a liquid-nitrogen-filled cold trap and had a base pressure of $<10^{-3}$ torr. The radio-frequency power, supplied by a Tegal Corporation RFG 300 generator with a Heathkit HM 102 power meter and SWR bridge, was coupled to the plasma with a copper coil (eight turns over 10 cm) wound on the reactor tube. The pressure in the system was monitored by an MKS Baratron 222 capacitance manometer, and, for injected gases, the flow rate was determined by a bubble flow meter. For toluene and octafluorotoluene, the required supply pressure was maintained by heating the liquid reservoir and inlet lines to 60°C, and the flow rate was approximated from the time to use up a given volume of liquid. Polymer deposition rates were measured in separate experiments with a Sloan DTM 200 quartz-crystal thickness monitor mounted at the exit to the coil region of the reactor.

The ethane, ethylene, and acetylene used in this study were obtained from Union Carbide Linde Division. Because the acetylene was dissolved in acetone, a dry ice/acetone trap was included in the high-pressure line to prevent solvent from entering the plasma system. Reagent-grade toluene was obtained from Baker Chemical Co. (Phillipsburg, NY). Ninety percent methyl ^{13}C-enriched toluene was obtained from KOR Isotopes (Cambridge, MA) and 90% phenyl ^{13}C-1-enriched toluene from US Services, Inc. (Prochem) (Summit, NJ). The enriched

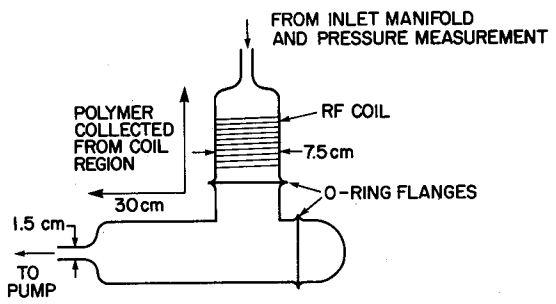

FIG. 1. Radiofrequency plasma reactor used in this work.

materials were mixed with the natural-abundance toluene in order to given the desired isotopic dilution. All of the toluene mixtures were thoroughly degassed by freeze–thaw cycling in a vacuum system which had a base pressure $<10^{-4}$ torr. Tetrafluoroethylene and octafluorotoluene were obtained from PCR Research Chemicals, Inc. (Gainesville, FL) and were handled in the same way as their hydrocarbon analogs. Bulk polymer samples were collected within the coil region of the reactor, which was opened under a dry nitrogen atmosphere. Air exposure was avoided because plasma-polymerized materials oxidize rapidly in the atmosphere owing to the relatively high concentration of free spins remaining in their structures [1,11,23,24]. Elemental analysis of the hydrocarbon polymers was carried out at Galbraith Labs. (Knoxville, TN) after air exposure, and they were found at that stage to contain 5–10% oxygen by weight.

Important parameters that pertain to the preparation of the hydrocarbon films are listed in Table I. The change in pressure in the reactor subsequent to exciting a plasma indicates whether a gas or vapor fragments or polymerizes [25]. In the present work ethane shows a pressure increase, ethylene shows no change, and acetylene shows a pressure decrease. Therefore, ethane predominantly fragments, acetylene predominantly polymerizes, and ethylene fragments and polymerizes to a similar degree. The deposition rates in Table I are consistent with this argument. Table I also shows the H/C stoichiometries of the bulk polymers. The polymers are hydrogen deficient compared with the injected gases and have compositions similar to those previously reported for these materials. The conditions used in preparation of the fluorocarbon films, adjusted prior to initiating the plasmas, were pressure, 0.2 torr; flow rate, 4 cm^3 min^{-1} (STP); and power, 20 W.

Nuclear Magnetic Resonance

^{13}C spectra were obtained at 22.63 MHz on a Bruker CXP spectrometer equipped with an external deuterium time-shared field lock. Applied pulse sequences included the proton (and fluorine) -enhanced single-contact cross-polarization experiment with high-power decoupling [18] and magic-angle spinning

TABLE I
Plasma Parameters and Film Stoichiometries

Injected gas	Flow rate (cm^3 m^{-1}, STP)	Pressure (torr)		Power (W)	Deposition rate (g cm^{-2} min^{-1})	H/C ratio in polymer
		Plasma off	Plasma on			
Ethane	4	0.10	0.12	10	9×10^{-7}	1.3
Ethylene	4	0.10	0.10	10	18×10^{-7}	1.3
Acetylene	4	0.10	0.07	10	33×10^{-7}	0.9
Toluene	3.5	0.15	0.09	20	—	1.0

[19] as well as the delayed-decoupling variant to suppress detection of the protonated carbon spins [26]. Cross-polarization was achieved with a contact time of 1 ms and resonant radio-frequency fields of 8 and 32 G for proton and carbon nuclei, respectively. During observation of the carbon free-induction decay, the proton power was stepped up to 12 G (15 G for fluorine) for decoupling. In the delayed-decoupling experiment a 40- or 60-μs delay without rf was inserted between the cross-polarization and signal acquisition periods. During this delay, strong ^{13}C-^{1}H dipolar couplings provide a mechanism for the loss of magnetization of those carbons with directly attached hydrogens. Rapid methyl group motions, however, partially suppress the dipolar interactions, resulting in incomplete suppression of methyl peaks in delayed-decoupling spectra [26]. Data accumulation with quadrature detection used a cycle of eight acquisitions, which included sequential application of four carbon rf phases [27,28] and proton spin-temperature alternation [29] with appropriate data routing, to eliminate spectral artifacts.

Separate NMR probes were used for carbon–proton and carbon–fluorine experiments. Both probes had a doubly tuned single coil [30] and accomplished magic-angle spinning with a nitrogen-driven Beams-type turbine. The carbon–proton system, modeled after the design of Fyfe et al. [31], employed hollow Kel-F rotors filled with ca. 20 mg of each plasma polymer and achieved spinning speeds of 2.2–2.4 kHz. The carbon–fluorine system was a modified Bruker probe which could accommodate ca. 50 mg of sample in a Delrin rotor and spin up to 3 kHz.

The integrated areas in the ^{13}C spectra are believed to be a measure of the contributions of the various carbon types to the polymer structure [15]. Primary sources of error for a quantitative treatment of the data include the possibility of loss of unsaturated carbon peak intensity to spinning sidebands, and distortions due to differential cross-polarization times for carbons in different environments. These potential pitfalls have been considered for the hydrocarbon polymers and are believed not to cause severe errors in the data [15]. A deconvolution of overlapping bands was achieved by fitting the line shapes measured in the delayed-decoupling experiment for the nonprotonated and methyl carbon peaks to the full spectra. Subtracting these fitted peaks from the full spectra gave the contributions of the remaining peaks.

Other Spectroscopic Measurements

For IR analysis each plasma polymer was pressed into a KBr pellet 1 mm thick at a concentration of 0.5% w/w. Spectra were recorded with a Beckman IR 4240 spectrophotometer between 4000 and 400 cm^{-1}, scanning at a speed of 300 cm^{-1} min^{-1} or with a Digilab FTS-15C Fourier transform spectrometer operating at a resolution of 4 cm^{-1}. The spectra for all of the plasma polymers derived from hydrocarbon monomers were similar to those obtained by other workers [9–11,24,32].

ESCA spectra of the perfluorinated polymers were recorded with an AEI ES200B spectrometer. $Al_{K\alpha}$ exciting radiation was employed, and the instrument was operated in the fixed analyzer transmission mode. Under these conditions the Au $4f_{7/2}$ core-level signal, at a binding energy of 84.0 eV, of a clean gold foil used for calibration purposes had a full width at half-maximum of 1.2 eV. All binding energies quoted in this work are referenced to the C_{1s} core level, at 285.0 eV, of the hydrocarbon contamination which builds up on a sample surface after it has remained in the spectrometer for many hours.

Sequential pyrolysis/GC/MS analysis of the plasma-polymerized toluene polymers was accomplished using a Perkin–Elmer 3920 gas chromatograph attached to a Nuclide 12-90G magnetic sectored mass spectrometer. A few micrograms of polymer in a direct-insertion probe were pyrolyzed at 550°C for 20 s or heated to 150°C to remove trapped volatiles. Helium was used as a carrier gas and the GC column consisted of 5% SP 2100 supported on 100/120 mesh Supelcoport JO5655. The column temperature, initially held at 125°C for 4 min, was ramped at 8°C min^{-1} to 225°C and then held constant. The mass spectrum of GC effluent from 14 to 500 amu was recorded every 7 s and stored digitally on disk as mass/intensity pairs by a DA/CS I.2 data system. A typical analysis time required 500 scans (1 h).

RESULTS AND DISCUSSION

Plasma-Polymerized Ethane, Ethylene, and Acetylene

Figure 2 shows (a) ^{13}C cross-polarization spectra with magic-angle spinning of plasma-polymerized ethane, ethylene, and acetylene formed under the conditions described above, and (b) the corresponding spectra acquired by the delayed-decoupling experiment. The full cross-polarization spectra are reminiscent of those typically obtained for coals and oil shales in which two broad bands, assigned to saturated and unsaturated carbons, are resolved [33,34]. Using the

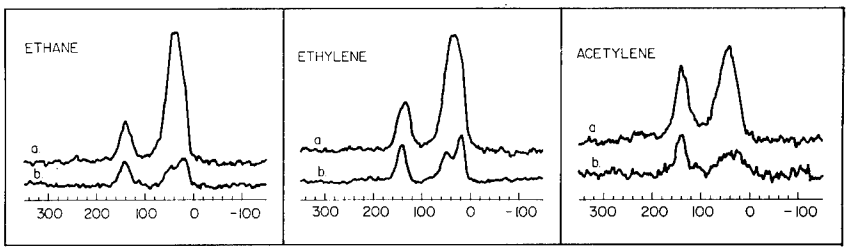

FIG. 2. ^{13}C spectra of polymers prepared from plasmas of ethane, ethylene, and acetylene. (a) Full spectra obtained with the cross-polarization NMR technique. Spin speed = 2.2 kHz, cross-polarization time = 1 ms, ^{1}H decoupling power = 12 G, repetition time/number of scans 1 s/25,000; 1 s/20,000, and 0.4 s/100,000 for 20-mg samples of ethane, ethylene, and acetylene, respectively. (b) Delayed-decoupling spectra under identical conditions as in (a) but with a 40-μs delay without rf power inserted between the cross-polarization mixing pulse and the signal acquisition period. Horizontal scale units are ppm from TMS.

line shapes of the nonprotonated and methyl carbon resonances in the delayed-decoupling spectrum of plasma-polymerized ethylene, one can deconvolute the full cross-polarization spectra in Figure 2 into five regions. They are assigned to (I) unsaturated nonprotonated, (II) unsaturated CH and CH_2, (III) quaternary, (IV) methine and methylene, and (V) methyl carbons. The chemical shifts for each carbon type agree with the range of shifts normally observed in hydrocarbons [35].

The contribution of each of these functionalities to the total polymer structure is given in Table II. The foremost observation from the data presented here is the ranking, according to increasing unsaturated character of the polymers formed from ethane (19%), ethylene (24%), and acetylene (38%). This ranking can be rationalized in terms of processes that occur in the gas phase or at the forming polymer surface. The reaction of acetylene by a mechanism analogous to free-radical, chain-growth polymerization will result in the incorporation of carbon–carbon double bonds in the polymer [36]. Clearly, this mechanism will be particularly important to the plasma excited in acetylene itself, but from mass spectrometry studies [9,37–40] it has been shown that acetylene is also formed in significant amounts in an ethylene plasma and to a lesser extent in an ethane plasma. Double bonds, however, may also be formed by the elimination of hydrogen during the interaction of the forming polymer surface with active species (ions and metastables) or the vacuum UV radiation emitted from the plasmas [41]. These reactions, however, may be reversed by hydrogenation of the unsaturated structures, a process that becomes more favorable as the partial pressure of hydrogen increases. Because the quantity of hydrogen in the plasma is expected to be greatest for ethane and least for acetylene [25], the anticipated trend in unsaturated character of the polymers is in the same direction as our findings.

The second important conclusion from Table II is that, although in the polymers derived from ethane and ethylene approximately 1 in 5 carbon atoms are methyl carbons, the corresponding figure of 1 in 16 for the plasma-polymerized acetylene is much lower. The incorporation of methyl groups in the polymer can be described by reactions of CH_3 and CH_2 radicals [36,42]. The formation of CH_3 and CH_2 radicals is primarily by carbon–carbon bond cleavage reactions, which

TABLE II
Relative Areas in the ^{13}C-NMR Spectra of Plasma-Polymerized C_2 Hydrocarbons[a]

	Peak				
Injected gas	I $=C<$	II $=CH + =CH_2$	III $>C<$	IV $>CH + >CH_2$	V $-CH_3$
Ethane	9	10	17	47	17
Ethylene	12	12	12	43	21
Acetylene	17	21	16	40	6

[a]Data reproducibility ± 15%.

lead to relatively high partial pressures of these radicals in the ethane and ethylene plasmas. Indeed, the importance of the CH_2 radical in the ethylene discharge was reported in a mass spectrometric investigation of the plasma effluent species [40]. For the acetylene plasma there are no simple reaction pathways that lead to the formation of CH_3 or CH_2 radicals [43], thus explaining the low methyl content in the polymer.

Infrared spectroscopy can be used to determine the ranking of the three polymers both in terms of unsaturation, from absorbances due to C=C stretching bands between 1600 and 1680 cm^{-1}, and methyl content, from the absorbance at 1370 cm^{-1} due to the methyl C—H bending mode. Consistent with a previously published IR analysis of the polymers [9], the intensities of these bands in our IR spectra reveal trends in agreement with the NMR data of Table II.

Finally, from the NMR data in Table II we can see that, for the three polymers compared here, approximately half of the unsaturated carbons and one-fifth of the saturated carbons have no directly bonded hydrogen. This information is not readily obtained from an IR analysis [10] and suggests a high degree of branching or crosslinking for the films prepared in this study. A determination of crosslink densities can be carried out as follows. A fully saturated hydrocarbon polymer without crosslinking or cyclic structures will have an H/C ratio of ca. 2. For each carbon that is unsaturated or involved in a crosslink or cyclic structure, the number of hydrogens is reduced by one, thus lowering the H/C ratio. A simple calculation based solely on the measured elemental ratios (Table I) and degrees of unsaturation (Table II) in the polymers yields roughly 1 crosslink and/or cyclic structure per four to five carbon atoms in the ethane- and ethylene-derived polymers, whereas the corresponding figure for plasma-polymerized acetylene is one per three carbon atoms. At such levels of crosslinking, these plasma polymers must be considered highly complex, three-dimensional networks.

Plasma-Polymerized Toluene

Figure 3 depicts the magic-angle spinning cross-polarization (a) and the delayed-decoupling (b) spectra of plasma-polymerized toluene prepared under the conditions of this work. The delayed-decoupling experiment clearly identifies the peaks at 141 and 128 ppm as nonprotonated unsaturated and protonated unsaturated carbons, respectively. The delayed-decoupling spectrum reveals only a small contribution from quaternary and methyl carbons to the overall polymer structure. Therefore the saturated carbon region of the full spectrum is comprised mainly of methylene and/or methine carbons. No acetylenic or allenic structures were detected in the polymer, as evidenced by the lack of spectral intensity in the ranges 63–90 and 200–214 ppm, respectively. Contributions from terminal olefins are also ruled out because, aside from the high-field tail of the unsaturated carbon resonances, there is little signal intensity in the 102–120 ppm region [35,44–46].

From peak intensities in the spectrum in Figure 3(a), the calculated contributions to the total polymer structure are unsaturated nonprotonated, 27%; un-

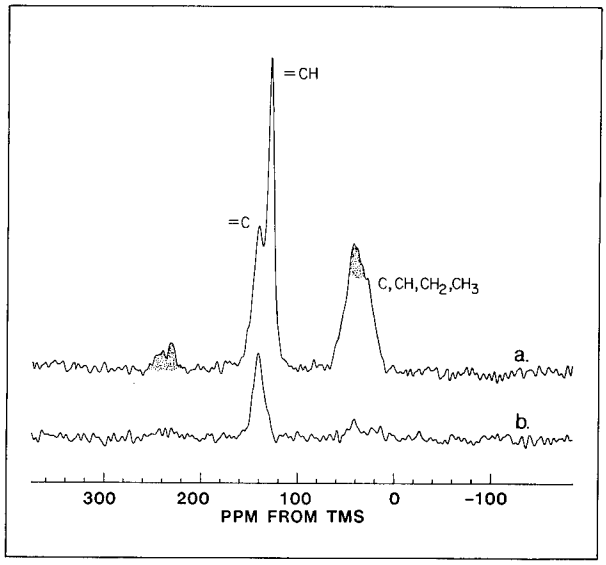

FIG. 3. Magic-angle spinning ^{13}C-NMR spectra of polymer prepared from a toluene plasma. (a) Full spectrum obtained with the cross-polarization NMR technique. Spin speed = 2.3 kHz, cross-polarization time = 1 ms, ^{1}H decoupling power = 12 G, repetition time = 1 s, number of scans = 98,000. (b) Delayed-decoupling spectrum under identical conditions as in (a) but with a 60-μs delay without rf power inserted between the cross-polarization mixing pulse and the signal acquisition period. Shaded peaks are spinning sidebands.

saturated protonated, 33%; and saturated, 40%. In order to account for the quantitative differences in the structural features of the polymer as compared with toluene, molecule reorganization must occur during plasma polymerization. In particular, the data require a net saturation of ca. 30% of the toluene double bonds and a net displacement of hydrogen by carbon on ca. 20% of the toluene protonated ring carbons.

A more comprehensive picture of the structure of plasma-polymerized toluene emerges when we consider the ^{13}C-NMR spectra of polymers formed from isotopically labeled starting materials. From such spectra it is possible to determine the polymer sites into which individual toluene carbons are incorporated. Figure 4 shows the spectra of the plasma polymers prepared from 18.6% $^{13}CH_3$- and 19.5% phenyl ^{13}C-1-labeled toluene. The gross differences between the features in these spectra reflect major differences in the carbon environments in the polymer derived from the methyl and phenyl C-1 carbon atoms. Thus, the identities of the specific toluene carbons are essentially preserved in the plasma and complete carbon scrambling, i.e., loss of carbon-atom positional identity (discussed below), or severe fragmentation of the monomer does not occur.

Increased peak intensities in the spectra of the labeled materials relative to those of the natural-abundance polymer are a consequence of the incorporation of methyl carbons primarily into saturated environments and phenyl C-1 carbons primarily into unsaturated environments in the polymer. Concomitant, though

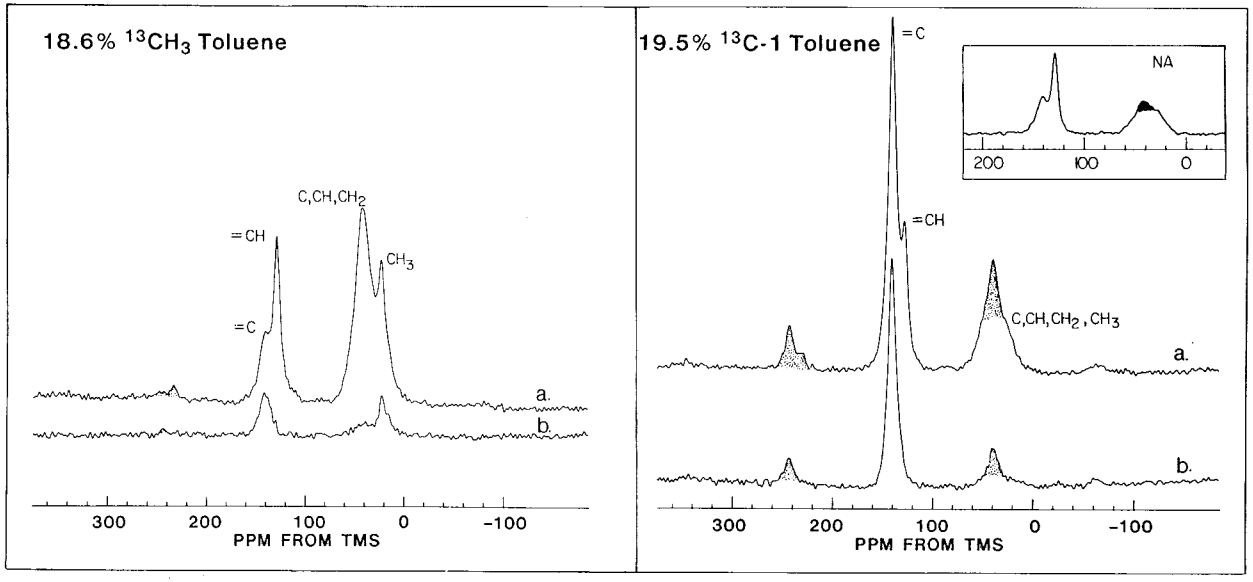

FIG. 4. (a) ^{13}C-NMR spectra of polymer prepared from 18.6% methyl-enriched toluene. Conditions as in Fig. 3 except number of scans = 30,000. (b) ^{13}C spectra of polymer prepared from 19.5% phenyl ^{13}C-1 toluene. Conditions as in Fig. 3 except number of scans = 20,000. Inset shows the natural-abundance (NA) plasma-polymerized toluene spectrum of Fig. 3 plotted to scale for a direct comparison of intensities.

smaller, increases in the other resonances reveal a significant crossover of toluene methyl carbons and phenyl C-1 carbons into unsaturated and saturated polymer environments, respectively. The destiny of a particular toluene carbon atom can be quantified by plotting the ^{13}C-NMR component signal intensities as a function of enrichment level. Figure 5 shows such plots of the total intensity of the spectrum and the intensities of the unsaturated and saturated carbon regions versus enrichment for polymers derived from both $^{13}CH_3$- and ^{13}C-1-labeled starting materials. The linearity of these plots testifies to the accuracy of the data in spite of the long-term nature of the measurements. For a given labeled carbon, the relative slopes, normalized to 100% for the slope of the total signal intensity, represent the distribution of polymer environments derived from that carbon. The data in Figure 5 reveal that 24% of the toluene methyl carbons become unsaturated and 20% of the toluene phenyl C-1 carbons become saturated during polymer formation.

An important conclusion can be derived from the slope of the total signal intensity versus enrichment, in Figure 5, for each labeled site. If a particular toluene carbon is incorporated into the polymer in proportion to its relative abundance in toluene, the total spectral intensity will increase by 1/7% for each 1% in ^{13}C enrichment. Because the slopes for both the methyl and phenyl C-1 sites are ca. 1/7, these carbons are proportionally incorporated, and it logically follows that all of the toluene carbons are uniformly incorporated into the polymer structure. This conclusion precludes the selective loss of particular carbon atoms in the gas phase and suggests that toluene does not fragment appreciably during polymer formation. The potential polymerization mechanisms and film structures are, therefore, likely restricted to those in which toluene itself or other precursors retaining all seven carbon atoms are involved.

More specific mapping of the toluene carbon destinies is achieved by a deconvolution of overlapping bands. For both labeled polymers, we can separate the contributions to the unsaturated resonances into protonated and nonprotonated carbons, and for the polymer derived from $^{13}CH_3$-enriched toluene it is also possible to resolve a methyl component. Figure 6 displays the plots of these component intensities versus enrichment level, and again the normalized slopes represent the percentage of a carbon type which ends up in a particular polymer environment. The results are summarized in Table III.

A dominant contribution to the polymer spectrum, accounting for 73% of the toluene C-1 carbons, is the unsaturated nonprotonated resonance at 141 ppm. The very large fraction of C-1 carbons remaining in a C-1 environment in the polymer supports a hypothesis that the dominant gas-phase precursors are those which preserve the C-1 structure, such as toluene itself or the benzyl radical. This observation precludes a dominant contribution from seven-membered-ring isomers of toluene, such as cycloheptatriene or cycloheptatrienyl radical, because these structures would not retain the C-1 carbon identity. Furthermore, the chemical shift of 141 ppm is consistent with the C-1 shift for the benzyl functionality [47]. The contention that benzyl groups are important in the polymer structure is further supported by the major peak at 43 ppm in Figure 4(a), ascribed largely

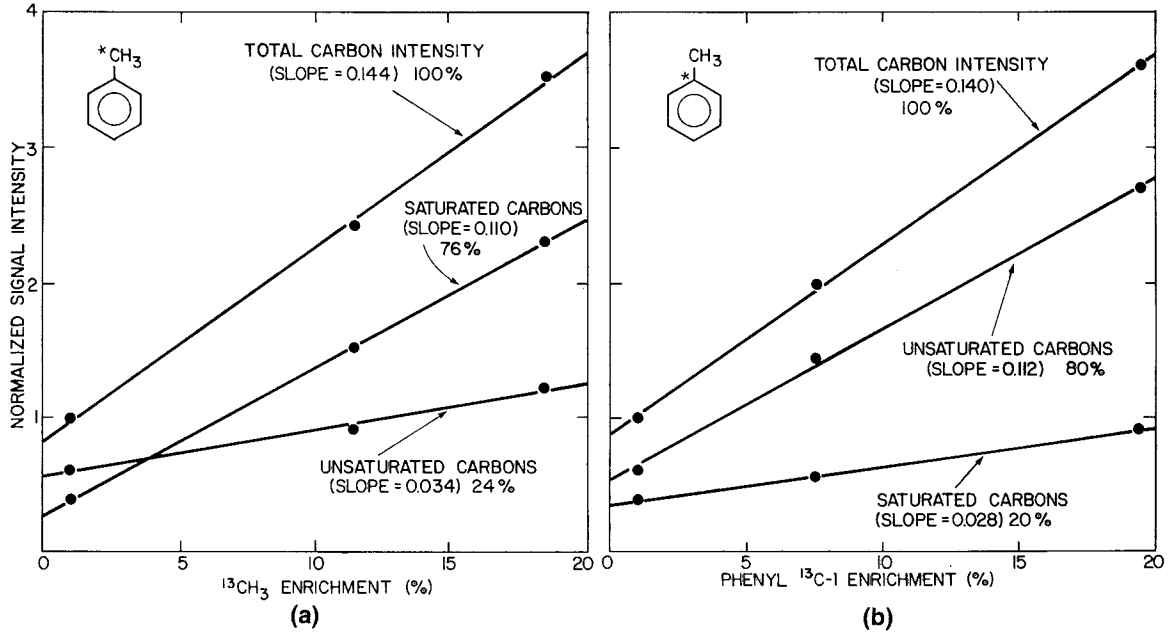

FIG. 5. Integrated areas of the unsaturated and saturated carbon peaks in the polymer spectra are plotted as a function of enrichment level of the $^{13}CH_3$ (a) and phenyl ^{13}C-1 (b) -labeled toluenes. The relative slopes, normalized to 100% for the slope of the total carbon intensity, represent the distribution of polymer environments derived from the labeled carbon.

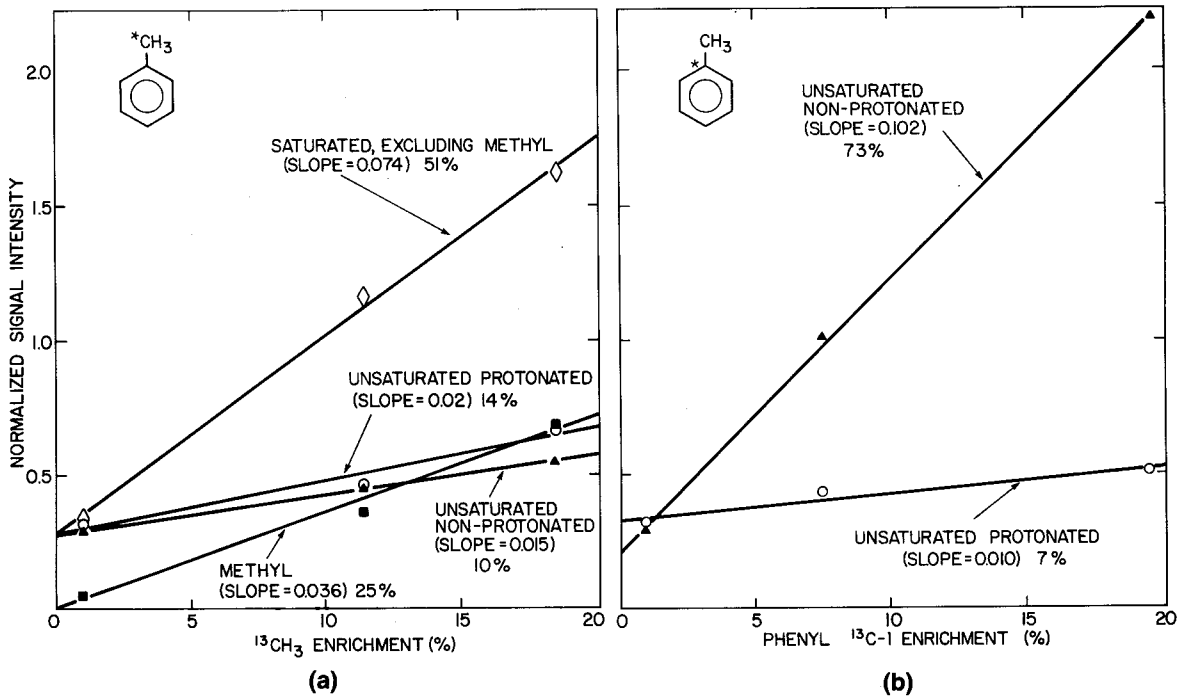

FIG. 6. Integrated areas of carbon peaks of the polymer versus toluene enrichment level as in Fig. 5 except here the unsaturated band has been further deconvoluted into protonated and nonprotonated resonances, and for the $^{13}CH_3$-enriched toluene, the methyl-group contribution has been separated from that of the other aliphatic carbons.

TABLE III
Distribution of Toluene Carbons in the Plasma Polymer[a]

Toluene carbons	Structural type in polymer			
	=C	=CH	C,CH,CH_2	CH_3
All[b]	27	33	40	
CH_3[c]	10	14	51	25
C-1[c]	73	7	20	
C2–C6[d]	21	42	37	

[a]Numbers represent percentage of a particular toluene carbon (or average percentage of several carbons) ending up in the specified structural type in the polymer. Data accuracy ± 15%.

[b]The average destination in the polymer of all toluene carbons is derived directly from the relative peak areas in Fig. 3.

[c]The destination of toluene methyl and phenyl C-1 carbons is determined from the relative slopes of the plots of Figs. 5 and 6.

[d]The average destination of the toluene protonated ring carbons is determined from the appropriate weighted averaging of the previous three rows of data.

to benzyl methylene carbons and accounting for half of the original toluene methyl carbons. The sharp methyl resonance at 20 ppm is a consequence of 25% of the toluene methyl carbons remaining as methyl groups in the polymer (see Table III). Thus, while the benzyl radical appears to be the major precursor, the retention of methyl groups in the polymer may well occur via direct attachment of a ring carbon in toluene itself to a surface or gas-phase radical.

The ^{13}C peaks of the polymer are not due entirely to benzyl and tolyl groups, but to many structures with a range of chemical shifts. The low-field tail of the nonprotonated unsaturated resonance (144–147 ppm) may have contributions from polystyrene-like phenyl C-1 carbons attached directly to disubstituted sp^3 hybridized carbons [45,47], although these structures are not as important as has been suggested in an earlier study of a similar film [48]. From empirical shift calculations [35,45] and a survey of model compounds [35,44–46,49], other possible structures within an acceptable shift range for the nonprotonated unsaturated carbon are substituted cyclohexenes and cyclohexadienes (i.e., partially saturated benzyl and tolyl analogs), which are likely to be present since ca. 30% of the toluene double bonds saturate during polymerization. Ring-opened structures are largely discounted for the following reasons. Ring opening processes are likely to generate acetylenic, allenic, or terminal olefinic structures, none of which are detected in the ^{13}C spectra. More importantly, the strong driving force to maintain aromaticity will result in short lifetimes for ring-opened intermediates in the gas phase, and reformation of the energetically more favorable aromatic structure should occur rapidly before further collisions with other molecules or the polymer surface.

The foregoing discussion reveals that the major precursors are toluene itself and benzyl radical. Based on this conclusion, the elemental analysis, and the distribution of carbon environments measured for the polymers as summarized

in Table III, we propose the following representation for the structure of the plasma-polymerized toluene prepared in this study.

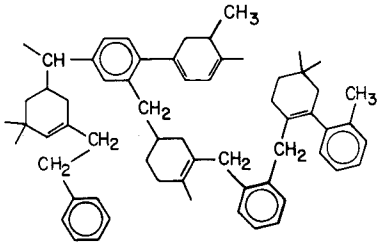

Initiating a plasma in toluene vapor inevitably results in the production of the molecular radical cation, which may undergo a variety of unimolecular reactions [50]. Sufficient energy of the impacting electron causing ionization can result in skeletal rearrangements and C—H bond cleavage. In addition to the toluene radical cation and benzyl cation, the cycloheptatriene radical cation and tropylium cation are formed; both of these seven-membered-ring intermediates can scramble the positional identity of individual carbon atoms. In order to investigate the possibility of carbon-atom scrambling as well as the presence of seven-membered rings in the polymer structure, it is useful to perform sequential pyrolysis–gas chromatography–mass spectrometry measurements [51]. From such an experiment, a total ion chromatogram, i.e., a histogram of the total ion current measured in the mass spectrometer as a function of the GC elution time, can be constructed. Figure 7 shows a chromatogram for the polymer derived from natural-abundance ^{13}C toluene. Comparison with model system elution times, as well as analysis of the mass spectrum at a given chromatogram peak, allows assignment of the components in Figure 7. Besides A, which is benzene, all of the identified products contain benzyl or tolyl groups, supporting the contention that these groups are prevalent in the gas phase during plasma excitation of toluene. It is

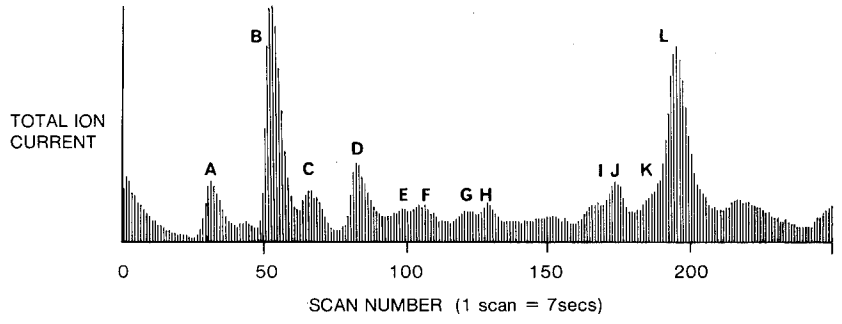

FIG. 7. Pyrolysis–GC–MS total ion chromatogram of plasma-polymerized toluene. Components are (A) benzene, (B) toluene, (C) ethylbenzene and xylene, (I) biphenyl, (J) diphenylmethane, (K) methyl biphenyl, and (L) bibenzyl. Assignments of peaks D–H have not been determined. T = 550°C for 20 s.

necessary, however, to exercise caution in interpreting these data in terms of the polymer structure. First, the materials detected in the mass spectrometer may have undergone reaction in the GC column, resulting in recombination of radicals produced by the pyrolysis. Second, since the cross section for electron impact ionization to produce the parent ion is very much larger for unsaturated species than for saturated species [52], the results are heavily biased toward the unsaturated portion of the polymer structure.

Mass spectra fragmentation patterns for phenyl-containing pyrolysis products of the methyl-labeled polymer differ significantly from predictions based solely upon the increased incidence of ^{13}C at the methyl site. These differences can only be explained by a scrambling process which exchanges methyl and ring carbons. The assumption that no new rings are created from the elements is supported by the very small number of benzene derivatives observed in a mass chromatogram of plasma-polymerized ethylene. The results of statistical calculations based on the methyl enrichment of 18.6% are shown in Figure 8 for the biphenyl product, whose parent ion M appears at 154 amu. The calculations predict the M + 1 peak (155 amu), which is derived from the fraction of biphenyl molecules having one ^{13}C atom (ignoring the small contribution from the deuterium isotope of hydrogen), to have an intensity relative to the M peak of 0.135 and 0.497 for 0 and 100% scrambling, respectively, of the carbon atoms in the original toluene molecules. An average of several measurements yielded a value of 0.24 ± 0.02 for (M ± 1)/M, corresponding to ca. 32% scrambling of toluene carbons prior to polymer formation. In a separate experiment the 550°C pyrolysis was replaced by heating at 150°C in order to measure the mass chromatogram of trapped volatiles in the polymer. In this experiment the biphenyl fragment gave the same scrambling value as did the high-temperature pyrolysis. The fact

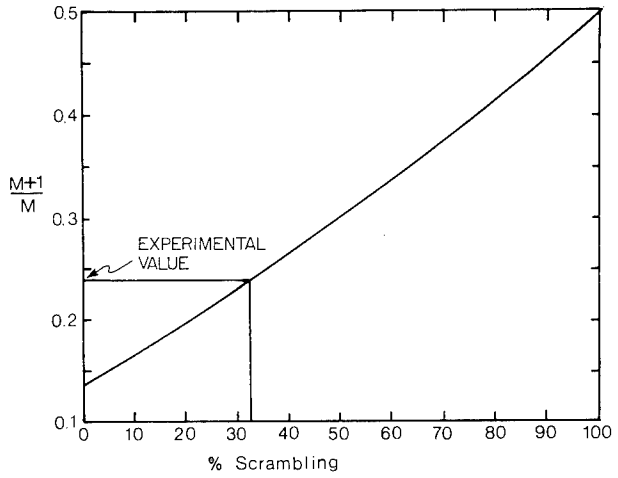

FIG. 8. Predicted (M + 1)/M ratio for the biphenyl pyrolysis product of plasma-polymerized $^{13}CH_3$-labeled toluene versus the degree of carbon atom scrambling, based on 18.6% methyl enrichment. The experimentally observed ratio of 0.24 ± 0.02 corresponds to ca. 32% scrambling.

that significant scrambling is observed in phenyl-containing volatiles derived from the polymer suggests that large internal energies of the polymer precursors, subsequent to ion neutralization, result in the rearrangement of cycloheptatriene and tropyl radical to the energetically favored toluene and benzyl radical isomers, respectively. We therefore expect, as depicted above in the representative structure of the polymer, that six-membered rings predominate.

Scrambling of the toluene methyl carbon into the ring could fully account for those methyl carbons which, according to the NMR data, end up unsaturated in the polymer. The saturation of toluene C-1 carbons can be attributed, in part, to the scrambling of this carbon into the methyl position, but a more important process involves scrambling to a protonated ring position and the subsequent saturation of that site by a free-radical mechanism. The majority of the polymer structure, however, is formed from material which has not undergone scrambling. Direct formation of the benzyl radical by electron-impact-induced C—H bond cleavage is a relatively low-energy process, and these radical precursors, as well as unreacted toluene precursors, give rise to the large number of toluene C-1 carbons remaining nonprotonated unsaturated in the polymer.

Since the NMR data show that over one-quarter of the carbon atoms in the polymer are nonprotonated unsaturated, many such sites must have been created during the polymerization process. A probable mechanism is ring substitution in which a benzyl or other radical substitutes on an aromatic ring at the forming polymer surface, or a free radical at the surface substitutes on the ring of a toluene molecule [36]. Saturation most likely occurs at the polymer surface by reactions involving addition of atomic hydrogen present in the plasma to produce cyclohexadienyl radical intermediates [36]. The excess energy generated in this exothermic reaction can dissipate into the surrounding lattice and thus not eject the attached hydrogen. The surface radical produced in this process may then react with a benzyl radical or toluene molecule. The diene structures may become further saturated by an initial addition of either a hydrogen atom or benzyl radical. Polymerization thus proceeds by ring substitutions and hydrogen atom and radical additions to form a highly crosslinked network structure.

Plasma-Polymerized Fluorocarbons

Previous characterization of plasma-polymerized fluorocarbons has employed ESCA spectroscopy [2–7]. Although ESCA observes only the topmost ca. 50 Å of surface, for plasma-polymerized fluorocarbons the measured structural features are believed to be representative of the bulk structure [7]. Figure 9 shows the ESCA C_{1s} core-level spectra of polymer prepared from two very different monomers, tetrafluoroethylene and octafluorotoluene. The salient features of these spectra are the overlapping CF_3, CF_2, CF, and C bands from high to low binding energy. The signal centered at 285 eV arises from a small amount of hydrocarbon contamination. An additional peak at 295.6 eV in the spectrum of plasma-polymerized octafluorotoluene is 6.6 eV lower in kinetic energy than the CF component, and is most likely a shakeup satellite associated with the $\pi \rightarrow \pi^*$

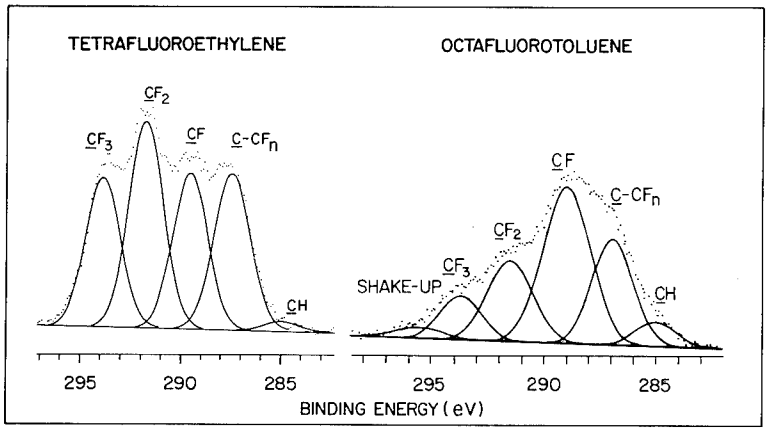

FIG. 9. ESCA C_{1s} core-level spectra of plasma-polymerized tetrafluoroethylene and octafluorotoluene.

transitions accompanying photoionization of unsaturated CF sites [7]. The binding-energy assignments are well documented and the deconvoluted band areas are a measure of the relative contributions of each structural type. The large CF_2 carbon peak for the tetrafluoroethylene polymer is consistent with the importance of a free-radical chain growth polymerization mechanism [40]. For plasma-polymerized octafluorotoluene, CF carbons are the largest component of the polymer structure.

Analogous to the ^{13}C-NMR spectra acquired on hydrocarbon polymers, we have performed magic-angle spinning fluorine-enhanced cross-polarization experiments on plasma-polymerized fluorocarbons [53]. Although the fluorine experiment is in principle identical to that for protons, the far greater spread of fluorine chemical shifts (ca. 200 ppm) necessitates higher decoupling power to obtain natural carbon linewidths (<1 ppm) from crystalline polymers. This requirement is somewhat relaxed, however, in amorphous polymers, since the distribution of chemical environments often limits achievable resolution to several ppm.

The ^{13}C spectra of plasma-polymerized tetrafluoroethylene and octafluorotoluene are shown in Figure 10. Unlike the ESCA carbon core-level spectra, NMR spectra can resolve saturated and unsaturated chemical shifts, and consequently, the spectra are more complex, consisting in the case of tetrafluoroethylene of six bands. The assignments of these bands, determined by chemical shifts of model perfluorinated compounds [54–56] and aided by the delayed-decoupling spectra, are (from low to high field) (I) unsaturated CF and CF_2, (II) unsaturated CF and nonfluorinated, (III) trifluoromethyl, (IV) difluoromethylene, (V) fluoromethine, and (VI) quaternary carbons. The unsaturated CF carbons occur over a wide range of chemical shifts but primarily contribute to regions I and II.

Although the unsaturated carbon region of plasma-polymerized octafluorotoluene is poorly resolved, its large intensity in the full cross-polarization spec-

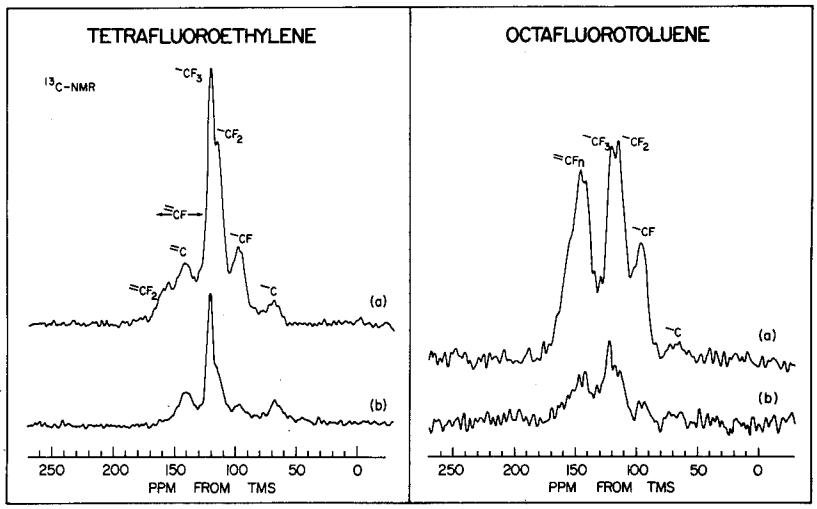

FIG. 10. Solid-state ^{13}C magic-angle spinning spectra of plasma-polymerized tetrafluoroethylene and octafluorotoluene. (a) Full spectra obtained with the cross-polarization technique with spin speed = 2.8 kHz, cross-polarization time = 1 ms, ^1H decoupling power = 15 G, number of scans = 100,000, repetition time = 1 s. (b) Delayed-decoupling spectra under identical conditions as in (a) but with a 60-μs delay without rf power inserted between the cross-polarization mixing pulse and signal acquisition period.

trum and strong attenuation in the delayed-decoupling experiment suggest the importance of unsaturated fluorinated carbons. This conclusion is consistent with the observation of strong ESCA CF shakeup peak. Therefore, like its hydrocarbon analog, the octafluorotoluene aromatic ring structure is partly retained in the polymer. Interestingly, the degrees of unsaturation, as measured from the NMR spectra, are similar to those of the hydrocarbon analogs—ca. 25 and 40% for the tetrafluoroethylene and octafluorotoluene plasma polymers, respectively.

CONCLUSION

Polymers deposited under plasma conditions are quite complex, and determination of the precise structure of a plasma-polymerized material is a formidable task. From the examples shown here, we see that solid-state NMR is a useful tool for determining structural features and gas-phase mechanisms. For the polymers formed from ethane, ethylene, and acetylene gases, ^{13}C spectra have revealed that plasma-polymerized acetylene has the highest unsaturated character and crosslink density but the lowest methyl content. These trends were explained in terms of likely processes occurring in the gas phase during film formation. For plasma-polymerized toluene, NMR and combined pyrolysis–gas chromatography–mass spectrometry measurements on polymers formed from ^{13}C-labeled monomers have led to a proposed structure dominated by benzyl and tolyl functionalities. Finally, preliminary NMR and ESCA data of the polymers

formed from tetrafluoroethylene and octafluorotoluene have revealed similarities in structure with their respective hydrocarbon analogs.

REFERENCES

[1] M. Millard, in *Techniques and Applications of Plasma Chemistry*, J. R. Hollahan and A. T. Bell, Eds., Wiley, New York, 1974, and references cited therein.

[2] M. Shen and A. T. Bell, Eds., *Plasma Polymerization*, Am. Chem. Soc. Symp. Ser. 108, Am. Chem. Soc., Washington, DC, 1979, and references cited therein.

[3] H. Yasuda, *J. Polym. Sci. Macromol. Rev., 16,* 199 (1981), and references cited therein.

[4] D. T. Clark, in *Physicochemical Aspects of Polymer Surfaces,* K. L. Mittal, Ed., Plenum, New York, 1982, and references cited therein.

[5] D. T. Clark, A. Dilks, and D. Shuttleworth, in *Polymer Surfaces,* D. T. Clark and W. J. Feast, Eds., Wiley, London, 1978.

[6] D. T. Clark and D. Shuttleworth, *J. Polym. Sci. Polym. Chem. Ed., 18,* 407 (1980), and references cited therein.

[7] A. Dilks, in *Developments in Polymer Characterization—2,* J. V. Dawkins, Ed., Applied Science, Barking, England, 1980.

[8] D. T. Clark and H. R. Thomas, *J. Polym. Sci. Polym. Chem. Ed., 16,* 791 (1978).

[9] M. Kobayashi, A. T. Bell, and M. Shen, *Macromolecules,, 7,* 277 (1974).

[10] J. M. Tibbitt, M. Shen, and A. T. Bell, *J. Macromol. Sci. Chem., 10,* 1623 (1976).

[11] H. Yasuda, M. O. Bumgarner, H. C. Marsh, and N. Morosoff, *J. Polym. Sci. Polym. Chem. Ed., 14,* 195 (1976).

[12] M. Venugopalan, I.-S. Lin, and M. S. Grenda, *J. Polym. Sci. Polym. Chem. Ed., 18,* 2731 (1980).

[13] M. Seeger, E. M. Barrall II, and M. Shen, *J. Polym. Sci. Polym. Chem. Ed., 13,* 1541 (1975).

[14] M. Seeger, R. J. Gritter, J. M. Tibbitt, M. Shen, and A. T. Bell, *J. Polym. Sci. Polym. Chem. Ed., 15,* 1403 (1977).

[15] A. Dilks, S. Kaplan, and A. VanLaeken, *J. Polym. Sci. Polym. Chem. Ed., 19,* 2987 (1981).

[16] S. Kaplan and A. Dilks, *Thin Solid Films, 84,* 419 (1981).

[17] S. Kaplan and A. Dilks, *J. Polym. Sci. Polym. Chem. Ed., 21,* 1819 (1983).

[18] A. Pines, M. G. Gibby, and J. S. Waugh, *J. Chem. Phys., 59,* 569 (1973).

[19] E. R. Andrew, *Prog. Nucl. Magn. Reson. Spectrosc., 8,* 1 (1971).

[20] J. Schaefer, E. O. Stejskal, and R. Buchdahl, *Macromolecules, 10,* 384 (1977).

[21] J. S. Waugh, in *NMR and Biochemistry*, S. J. Opella and P. Lu, Eds., Dekker, New York, 1979, p. 203.

[22] W. L. Earl and D. L. VanderHart, *Macromolecules, 12,* 762 (1979).

[23] H. Yasuda and T. Hsu, *J. Polym. Sci. Polym. Chem. Ed., 15,* 81 (1977).

[24] H. Yasuda, H. C. Marsh, M. O. Bumgarner, and N. Morosoff, *J. Appl. Polym. Sci., 19,* 2845 (1975).

[25] H. Yasuda, M. O. Bumgarner, and J. J. Hillman, *J. Appl. Polym. Sci., 19,* 531 (1975).

[26] S. J. Opella, M. H. Frey, and T. A. Cross, *J. Am. Chem. Soc., 101,* 5856 (1979).

[27] D. I. Hoult and R. E. Richards, *Proc. R. Soc. London Ser. A, 344,* 311 (1975).

[28] E. O. Stejskal and J. Schaefer, *J. Magn. Reson., 14,* 160 (1974).

[29] E. O. Stejskal and J. Schaefer, *J. Magn. Reson., 18,* 560 (1975).

[30] M. E. Stoll, A. J. Vega, and R. W. Vaughan, *Rev. Sci. Instrum., 48,* 800 (1977).

[31] C. A. Fyfe, H. Mossbruger, and C. S. Yannoni, *J. Magn. Reson., 36,* 61 (1979).

[32] K. Bieg, *Thin Solid Films, 84,* 411 (1981).

[33] V. J. Bartuska, G. E. Maciel, J. Schaefer, and E. O. Stejskal, *Fuel, 56,* 354 (1977).

[34] H. A. Resing, A. N. Garroway, and R. N. Hazlett, *Fuel, 57,* 450 (1978).

[35] F. W. Wehrli and T. Wirthlin, *Interpretation of Carbon-13 NMR Spectra,* Heyden, Philadelphia, 1978.

[36] D. C. Nonhebel and J. C. Walton, *Free Radical Chemistry,* Cambridge U. P., Cambridge, 1974.
[37] S. I. Ivanov, S. H. Fakirov, and D. M. Svirachev, *Eur. Polym. J., 14,* 611 (1979).
[38] G. Smolinsky and M. J. Vasile, *Int. J. Mass. Spectrom. Ion Phys., 21,* 171 (1976).
[39] M. J. Vasile and G. Smolinsky, *Int. J. Mass. Spectrom. Ion Phys., 21,* 263 (1976).
[40] A. Dilks and E. Kay, *Macromolecules, 14,* 855 (1980).
[41] D. T. Clark and A. Dilks, *J. Polym. Sci. Polym. Chem. Ed., 15,* 2321 (1977).
[42] J. Hine, *Divalent Carbon*, Ronald, New York, 1964.
[43] M. J. Vasile and G. Smolinsky, *Int. J. Mass. Spectrom. Ion Phys., 24,* 11 (1977).
[44] G. C. Levy, R. L. Lichter, and G. L. Nelson, *Carbon-13 Nuclear Magnetic Resonance Spectroscopy,* Wiley, New York, 1980.
[45] E. Breitmaier and W. Voelter, ^{13}C *NMR Spectroscopy,* Verlag Chemie, New York, 1978.
[46] J. B. Stothers, *Carbon-13 NMR Spectroscopy,* Academic, New York, 1972.
[47] D. F. Ewing, *Org. Magn. Reson., 12,* 499 (1979).
[48] F. J. Dinan, S. Fridmann, and P. J. Schirmann, in R. F. Gould, Ed., *Chemical Reactions in Electrical Discharges,* Am. Chem. Soc., Washington, DC, 1969.
[49] F. Bohlmann, R. Zeisberg, and E. Klein, *Org. Magn. Reson., 7,* 426 (1975).
[50] F. W. McLafferty and F. M. Buckhoff, *J. Am. Chem. Soc., 101,* 1783 (1979), and references cited therein.
[51] A. Dilks, S. Kaplan, and R. Crandall, in preparation.
[52] R. M. Silverstein, G. C. Bassler, and T. C. Morrill, *Spectrometric Identification of Organic Compounds,* Wiley, New York, 1981.
[53] W. W. Fleming, C. A. Fyfe, J. R. Lyerla, H. Vanni, and C. S. Yannoni, *Macromolecules, 13,* 460 (1980).
[54] D. W. Overall and J. J. Chang, *J. Magn. Reson., 25,* 361 (1977).
[55] N. Ishikawa and M. Maruta, *Nippon Kagaku Kaishi, 10,* 1411 (1977).
[56] M. A. Hamza, G. Serratrice, and J.-J. Delpuech, *Org. Magn. Reson., 16,* 98 (1981).

APPLICATION OF PLASMA-POLYMERIZED FILM TO ELECTRON BEAM LITHOGRAPHY

SHUZO HATTORI, MASAO YAMADA, JUNJI TAMANO, and MASAYUKI IEDA

Department of Electrical Engineering, Nagoya University, Chikusa-ku, Nagoya 464, Japan

SHINZO MORITA, KATSUMI YONEDA, SUSUMU IKEDA, and SHINTARO ISHIBASHI

Department of Electrical Engineering, Meijo University, Tempaku-ku, Nagoya 468, Japan

SYNOPSIS

For completion of vacuum lithography, a delineable and dry-developable electron beam resist film was formed by the plasma polymerization method. Methyl methacrylate (MMA) and hexafluorobutyl methacrylate (6FBMA) were polymerized downstream of an argon glow discharge. Resistivity to plasma etching was improved by copolymerization with styrene for both monomers. The sensitivity of the resist was enhanced by doping tin atoms into the resist using tetramethyl tin (TMT). Plasma etching using a microwave discharge was effective in forming fine patterns. The effect of graft polymerization of styrene on the pattern-delineated resist is discussed.

INTRODUCTION

Dry process technologies become key technologies for very large-scale integrated-circuit (VLSI) fabrication. Dry resist coatings and dry pattern developing become especially important processes, because homogeneous thin coatings of high-molecular-weight polymers are difficult to obtain by spinning. Furthermore, swelling of the resist in an etching solvent deforms a fine pattern. In order to realize dry process technologies, a plasma-polymerized film is proposed as an electron beam resist which is developable by a dry method [1–3]. The system of these new dry processes is referred to as vacuum lithography. In this article,

Journal of Applied Polymer Science: Applied Polymer Symposium 38, 127–135 (1984)

CCC 0570-4898/84/010127-09$04.00

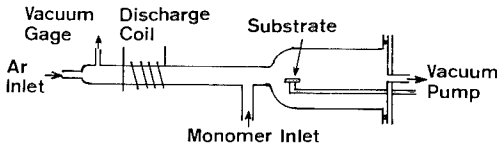

FIG. 1. Argon flow-type reactor.

the possibility and problems of plasma-polymerized resist coatings will be discussed in relation to vacuum lithography.

EXPERIMENTAL

Plasma polymerization was effected by using an argon-flow-type reactor as shown in Figure 1 [4]. The monomer was introduced into the tail flame of an argon glow discharge and the resist film was formed on a chromium-coated glass substrate located further downstream of the discharge. Monomers of methyl methacrylate (MMA), dimethyltetrafluoropropyl methacrylate (D4FPMA), hexafluorobutyl methacrylate (6FBMA), heptafluoropentyl methacrylate (8FBMA), styrene (St), and tetramethyl tin (TMT) were used. For infrared (IR) spectra measurements, a NaCl crystal was used as the substrate. For comparison, spin-coated poly(methyl methacrylate) (PPMMA) film (Tokyo-oka, OEBR-1000) was also investigated. A pattern of lines and spaces was delineated by an electron beam of 4×4 μm^2 using an electron beam patterning machine (Elionix, ELS-2A) at an acceleration voltage of 20 kV and a dose of 1–1000 $\mu C/cm^2$.

Plasma etching was performed using two types of apparatus. One is a sputtering machine which contains parallel-plate electrodes of diameter 100 mm with spac-

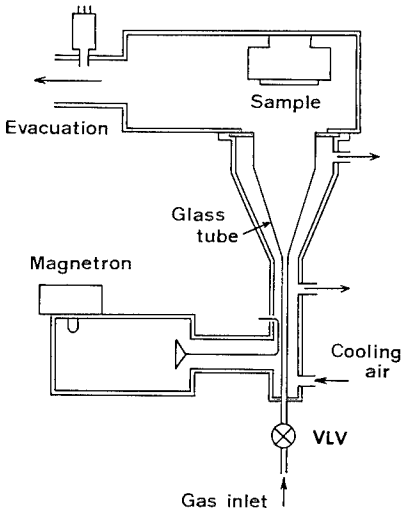

FIG. 2. Microwave discharge etching reactor (2.45 GHz).

ing of a few centimeters and operated at a frequency of 13.56 MHz, a power level of 100 W, and a pressure of 2–3 mtorr using as etching gas an Ar—O_2 mixture or hydrogen. Another is a microwave discharge machine as shown in Figure 2. It was operated at a frequency of 2.45 GHz, discharge power up to 1 kW, and pressure ranging from a few millitorr to a few torr of oxygen.

RESULTS

The optimum plasma polymerization conditions were selected from the degree to which the IR spectrum of the polymerized film resembled that of a conventional polymer. In the case of the argon-flow-type reactor, IR spectra of the plasma-polymerized methyl methacrylate (PPMMA) showed that the deviation of polymer structure from that of conventional PMMA became significant with increasing discharge power level or with decreasing argon flow rate as shown in Figure 3. The significant point of change is observed at 1730 cm^{-1}, and a few peaks near 1140 cm^{-1} were attributed to —COO— structure in MMA. The change may result from the decomposition of monomer in the high-intensity discharge, and the polymer begins to resemble that of oxidized polyethylene. Optimum plasma polymerization for all of the monomers was performed at an argon flow rate of 60–70 cm^3 (STP)/min, a monomer flow rate of 6–10 cm^3 (STP)/min, a discharge power level of about 10 W, and a gas pressure of 0.7–1.0 torr [3].

A hollowed pattern was usually formed on the positive resist by electron beam delineation. Temperature rise in the electron-beam-delineated part is estimated to exceed 100°C even at about 10 $\mu C/cm^2$. This means that hollowed-pattern formation will be referred to the evaporation of a small molecule formed by scission of the polymer at the elevated temperature. This phenomenon is termed self-development [5,6].

When the resist dose-contrast properties were evaluated by plasma-etching development using the sputtering machine, the sensitivity and γ value of the PPMMA resist were better than those of conventional PMMA [4]. The etching rate of PPMMA was smaller than that of conventional PMMA, but the sensitivity of PPMMA to electron beam delineation was lower than that of PMMA. Thus, it is concluded that the crosslinking of the polymer increases the etching resistance and improves the quality of the resist. When styrene was plasma copolymerized with MMA, the quality of the resulting resist was greatly improved, as shown in Figure 4.

Physical or chemical effects must be considered in the mechanism of plasma etching. In order to obtain some insight into the mechanism, oxygen and hydrogen plasma etching were performed on PPMMA. As shown in Figure 5, the plasma-etching selectivity was improved by using a hydrogen plasma instead of an oxygen plasma [2]. An oxygen plasma is usually more chemically active than a hydrogen plasma. The experimental results suggest that the physical effect of the plasma is useful for the development, much like an electron beam delineation phenomenon, but the pattern was usually damaged after the development.

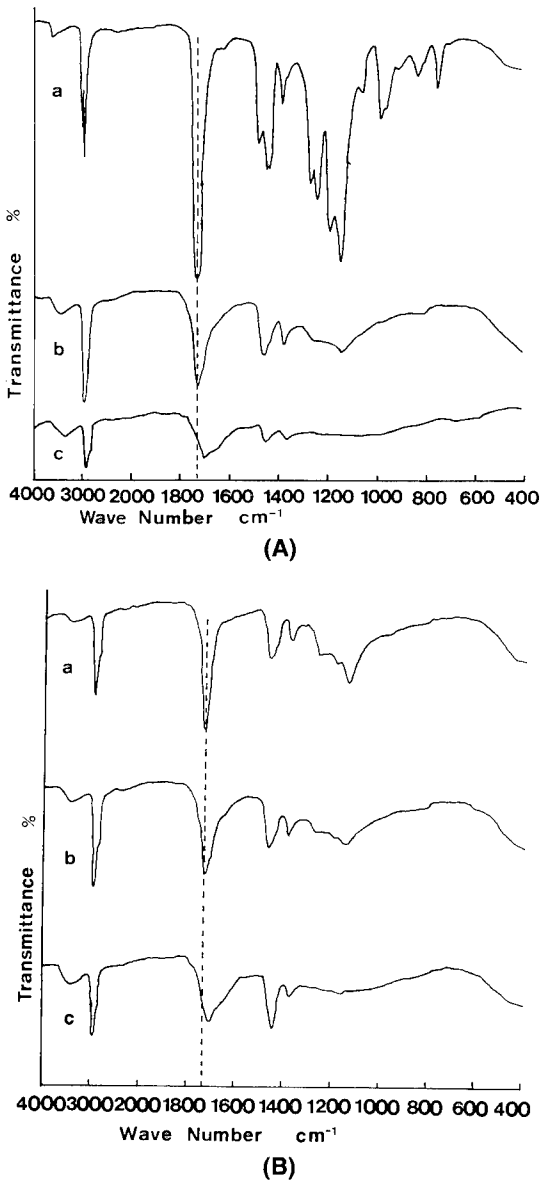

FIG. 3. IR spectra of PMMA. (A) Effect of discharge power level: (a) conventional PMMA, (b) PPMMA formed at 10 W, (c) PPMMA formed at 30 W; 0.7 torr, 63 cm^3 (STP)/min (Ar), 6.3 cm^3 (STP)/min (MMA). (B) Effect of argon flow rate: (a) 77, (b) 63, (c) 42 cm^3 (STP)/min; 0.7 torr, 10 W.

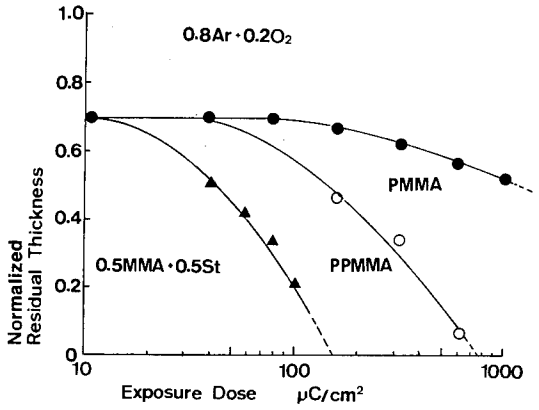

FIG. 4. Normalized residual thickness versus exposure dose.

A clear pattern was developed without damage due to ion bombardment using microwave plasma etching with O_2 in Figure 6, where the PPMMA resist was delineated at 400 $\mu C/cm^2$. The relative plasma-etching rate at a high dose rate was dependent on the gas pressure as shown in Figure 7. These differences have been attributed to differences in plasma state [7]. At 2 mtorr, the highest degree of ionization was observed, and the floating potential was at a lower level in our experiments. This means that the microwave plasma is gentle, but is highly ionized near 2 mtorr.

In order to improve the sensitivity of the resist, a metal-doped polymer was formed by copolymerizing TMT into PPMMA, because it was expected that scission of the polymer chain would be increased by electrons scattered from the metal atom. Actually, the pattern could be formed at a lower dose rate for the metal-doped resist [2,6].

Fluoroalkyl methacrylate was plasma polymerized to provide a more sensitive resist. The sensitivity of plasma-polymerized 6FBMA was higher than that of PPMMA. However, no improvement of resist quality was observed for the two

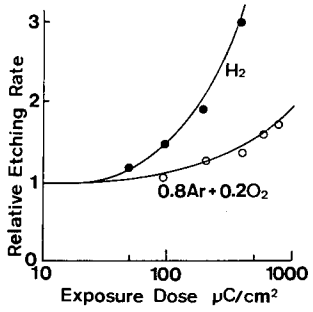

FIG. 5. Effect of plasma etching gas on resist properties.

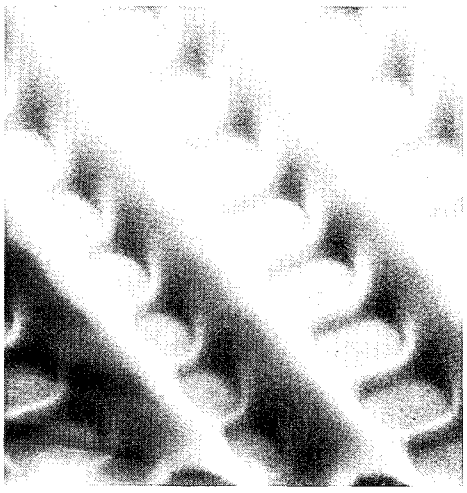

FIG. 6. SEM picture of pattern developed by oxygen plasma etching on PPMMA.

resists formed from D4FPMA and 8FPMA. Sometimes the resist showed a negative pattern when developed thermally in vacuum. From IR spectra (Fig. 8), absorption peaks due to CH bond structure are very weak for polymers from D4FPMA and 8FPMA compared with those from 6FBMA. This means that the polymers are crosslinked much more than PP6FBMA.

Plasma-copolymerized 6FBMA with styrene and/or TMT showed improvement of quality (Figs. 9 and 10). This means that the high sensitivity of about 10 $\mu C/cm^2$ was obtained by a vacuum lithography.

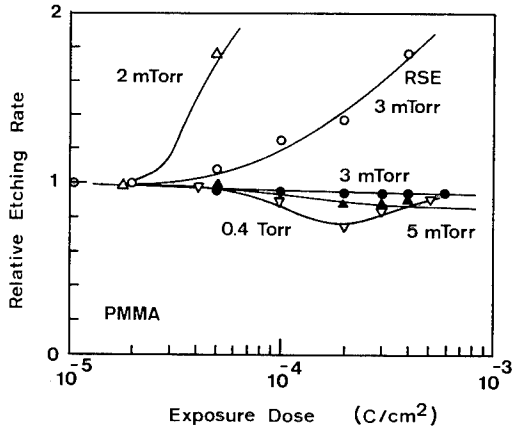

FIG. 7. Effect of gas pressures on microwave plasma etching of PMMA.

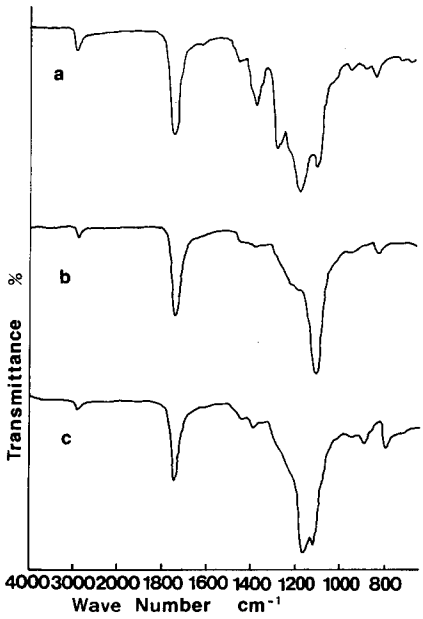

FIG. 8. IR spectra of plasma-polymerized films: (a) 6FBMA, (b) D4FPMA, and (c) 8FPMA.

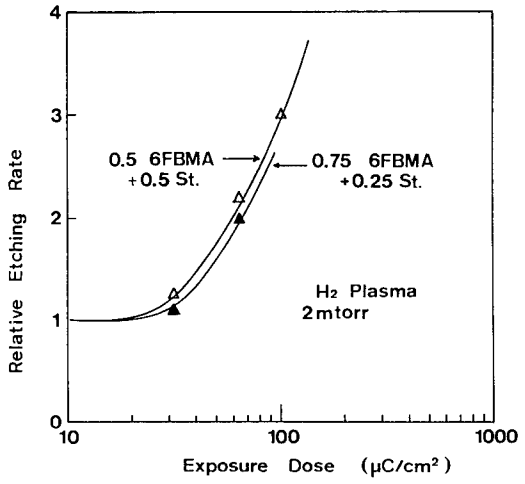

FIG. 9. Relative etching rate versus exposure dose.

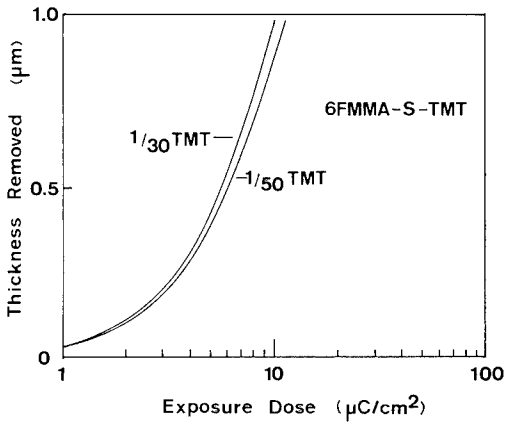

FIG. 10. Thickness removed versus exposure dose.

DISCUSSION

To realize vacuum lithography, problems in the dry development process for plasma-polymerized resist films must be solved theoretically and experimentally. In the wet process, the scissored polymer chain need not be as short, because the development is greatly enhanced by increased molecular motion, which enhances the counterdiffusion of solvent molecules into the solid polymer film and finally makes possible the folding of the macromolecule into the solvent. But, for dry development, the formation of a volatile molecule is most important.

For a degradative polymer, dissociation will propagate along the polymer chain by initiation of scission under proper conditions and a dissociated molecule will be vaporized [8]. The phenomenon of self-development can be explained by this dissociation. Under the usual conditions of electron beam delineation, however, the propagation of dissociation is limited. Therefore, an additional process is necessary to complete the development.

In the case of development by plasma etching, chemical and physical etching must be considered. If the volatile molecule is fabricated by chemical erosion along the polymer chain, the scission of a conventional polymer chain will enhance the plasma-etching rate. But for the plasma-polymerized resist film, the scissored number of the polymer chain has little significance because the degree of crosslinking and branching in the polymer is significant. If the vaporization of a scissored polymer arises from a thermal mechanism, e.g., ion and/or electron bombardment onto the resist surface, it is impossible to obtain a similar or sufficient sensitivity for the plasma-polymerized resist film in comparison to wet development, because a large dose rate is necessary to form a volatile small polymer by scissoring the polymer chain.

According to our theoretical analysis, if a fairly long polymer chain is formed by plasma polymerization, the breadth of the initial molecular weight distribution is not important for dry development [9]. However, a specially synthesized resist

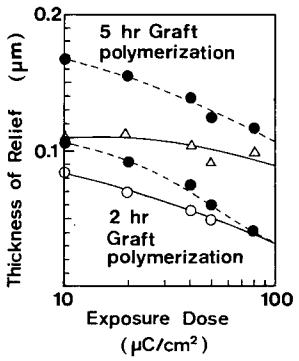

FIG. 11. Thickness of relief versus electron dose: (—) after graft polymerization; (---) after oxygen microwave plasma etching at 700 W, 2 mtorr for 10 min.

film must be formed for a higher sensitivity and a higher resolution. Accordingly, a monomer which formed a plasma-etching-resistive polymer was grafted onto the plasma-polymerized resist, where a pattern was delineated by an electron beam. As shown in Figure 11, styrene was grafted successfully onto PPMMA. The thickness of the grafted film is proportional to the dose rate on the film.

REFERENCES

[1] S. Morita, J. Tamano, S. Hattori, and M. Ieda, *J. Appl. Phys., 51,* 3938 (1980).
[2] S. Hattori, J. Tamano, M. Yamada, M. Ieda, S. Morita, K. Yoneda, and S. Ishibashi, *Thin Solid Films, 83,* 189 (1981).
[3] S. Morita, S. Hattori, M. Ieda, J. Tamano, and M. Yoneda, *Kobunshi Ronbunshu, 38,* 657 (1891).
[4] J. Tamano, S. Hattori, S. Morita, and K. Yoneda, *Plasma Chem. Plasma Proc., 1,* 261 (1981).
[5] L. F. Thompson and M. J. Bowden, *J. ELectrochem. Soc., 120,* 1702 (1973).
[6] M. Yamada and S. Hattori, *Jpn. J. Appl. Phys., 20,* 1969 (1981).
[7] M. Yamada, J. Tamano, S. Hattori, and S. Morita, unpublished.
[8] M. Tsuda, Y. Nakamura, et al., *Photo. Sci. Eng., 23,* 290 (1979).
[9] M. Yamada, S. Hattori, and S. Morita, *J. Electrochem. Soc., 129,* 2598 (1982).

ELECTRICAL PROPERTIES OF GLOW-DISCHARGE POLYMERS, PARYLENES, AND COMPOSITE FILMS

E. J. CHARLSON and E. M. CHARLSON
Department of Electrical Engineering, University of Missouri–Columbia, Columbia, Missouri 65211

A. K. SHARMA and H. K. YASUDA
Graduate Center for Materials Research, University of Missouri–Rolla, Rolla, Missouri 65401

SYNOPSIS

Dielectric constants and volume resistivities have been measured for a group of glow discharge and thermally deposited polymers intended for use as the insulating coating of chronically implanted neural electrodes. Both single-layer and composite structures were investigated, with the latter consisting of a glow discharge thin precoat (600 Å) to promote good adhesion to noble metals, followed by a thick outer layer of poly(p-xylylene) (Parylene). The thickness of the precoats and their tendency to have irregular surfaces required an unconventional test device. A new miniature version of a Hg probe is described along with a protocol to accommodate saline soak tests, simulating implantation. Measurements were obtained for precoats of methane, TFE, and TMDSiO. Precoat dielectric constants were two times higher than those of thick polymers, while volume resistivities were 1–1.5 orders lower. Soak tests in saline revealed a cyclic variation with time of ± 20% change in dielectric constant and as much as one order change in resistivity. A peak in the imaginary part of the dielectric constant was encountered for as-synthesized material, indicating a relaxation loss mechanism which disappears after several months of dry aging.

INTRODUCTION

This article describes measurements of electrical parameters of a special group of polymers for potential use as the insulating coating of chronically implanted neural electrodes or devices. Because of the strongly ionic environment where the implants need to function, it is particularly important that the polymers be relatively impervious to liquid water. The exclusion of liquid water minimizes

Journal of Applied Polymer Science: Applied Polymer Symposium 38, 137–148 (1984)

CCC 0570-4898/84/010137-12$04.00

electrochemical reactions that liberate gaseous products at the electrode–polymer interface. These gases tend to separate the insulating coating from the electrode, which ultimately destroys the film structurally and electrically.

Several of the currently available polymers [e.g., Parylenes, i.e., poly(p-xylylene) and its derivatives] which are sufficiently dense to accommodate the leakage requirement have been found to have poor adhesion to the noble metal electrodes required in this application. Therefore, the approach taken to overcome this deficiency involves synthesizing a composite structure, a well-adhering precoat of a highly crosslinked glow discharge polymer coupled with a dense, thicker overcoat film of Parylene or other such polymers. Precoat materials that adhere well to the electrode have been found to adhere well to the overcoat.

The techniques used in preparing the precoat materials makes these polymers rather unique, a subject covered by several authors in the literature under the heading glow discharge or plasma polymerization. The precoat polymer structure is typically not a uniform thin layer but rather exhibits a coarse-textured surface. Thus, the interpretation of the electrical characteristics is complicated by the uncertainty in the exact structure, and an accurate direct measurement of the thickness for the precoat materials is required. In addition, the excessively rough surface of the films dictates that a new approach to making contacts for electrical measurements be developed.

EXPERIMENTAL

Coating Procedure

Glow discharge polymer coatings used as the precoat material were deposited in a magnetron bell jar reactor operated at an audio frequency of 10 kHz. The details of the equipment used and the method of polymerization are described elsewhere [1]. The substrates to be coated were moved on a circular disk, which was rotated vertically through the center of the electrodes by magnetic coupling. The discharge was initiated by feeding the reactor with the monomer vapors and applying power from an audio amplifier. A thickness monitor (OM-300, Veeco Instruments, Inc.) placed adjacent to the rotating disk in the reactor was used to estimate the thickness of polymer deposited on the substrate. The monomers used in this study included methane, tetrafluoroethylene, and tetramethyldisiloxane. A glow discharge polymer of methane (called GDPM or polymethane) was deposited at a monomer flow rate of approximately 1.0 cm^3/min and power greater than 70 W [2,3]. Methane polymerizes quite slowly (20 Å/min) under these conditions and deposition of coatings greater than 0.2 μm in thickness was not feasible without interrupting the deposition for time periods of around 30 min to allow for cooling of the electrodes.

Parylenes (both Parylene N and its chloro derivative, Parylene C) were deposited by a pyrolytic vapor decomposition polymerization method originally developed by Gorham [4]. Parylenes are conventional polymers in many respects, but like glow discharge polymers their synthesis is accomplished at low pressures

and the polymers possess residual radical activity. These polymers are very attractive because of their superior insulating characteristics and insolubility in most known organic solvents. A 2.5-μm-thick film of Parylene C can be deposited in less than an hour by passing vapors of about 5 g of chloroxylylene dimer through a furnace maintained at 650°C. The thickness of the polymer film can be changed by changing the weight of dimer. To deposit thicker films of Parylene N polymer, the reactor was fed with argon gas at a pressure ranging from 40 to 100 mtorr.

The composite structures consisted of a precoat, i.e., an ultrathin (0.02 μm) film of a glow discharge polymer, and an overcoat of a thicker film of the Parylene polymer. The composites reported in this article were formed by depositing the precoat in the bell jar reactor and the Parylene in a Parylene reactor, although we currently have a system which allows composite structures of this kind to be synthesized in one reactor.

Thickness Measurement

The typical 600-Å thickness of the precoat films is intermediate between the range usually considered appropriate for an ellipsometer (<100 Å) and that for the Tolansky step method involving interference fringes (>2000 Å with an accuracy of ±200 Å). We determined that for this range, a thickness profilometer provided the most convenient and most accurate measurements. This method involves the movement of a mechanical stylus over a step made in the film to be measured. The stylus is mechanically connected to the core of a counterwound linear differential transformer which outputs a differential phase between two reference signals. The overall system produces a dc signal proportional to the thickness. The major problem encountered in using this method was the creation of an appropriate step from substrate to polymer. The high energy inherent to the coating process itself ensured gradual transition on film edges, disallowing the use of internal masking to produce the step.

Several scribing methods to produce an abrupt step were investigated. The best was found to involve the use of a semiconductor wafer scribing machine equipped with a special scribing tool. Typically, the substrates used for thickness testing were either glass slides or flat aluminum engraving plates. To avoid scribing the substrate itself, a plastic scribe tool softer than the substrate was fashioned. In some cases, for films which tended to be "sticky," a thin slurry of Linde B in water was used as a scribe medium. The profilometer was then used to determine the required number of scribe strokes and static weight necessary to produce a good step. Removal of the polymer all the way to substrate could be ascertained when the profilometer trace inside a wide channel smoothed to a surface roughness characteristic of the glass or metal. While this method is still somewhat variable from film to film, the control afforded by the scribing machine has permitted the technique to routinely produce measurable steps with minimum indenture of the substrates.

Device Structure and Instrumentation

It is well known that the growth of thin films, whether by glow discharge polymerization or by chemical vapor deposition, is very dependent on the surface conditions of the substrate. Therefore, an attempt was made to duplicate, as much as possible, the final use conditions when selecting substrates for electrical tests. Also, in the case of the very thin precoat films, consideration must be given to the effect of pores in the selection of the counterelectrode. Figure 1 shows the device geometry chosen for the electrical tests, which consists of measurements of capacitance and dissipation of a thin-film capacitor with the polymer serving as the insulator. As can be visualized from Figure 1, any pore or hole in the polymer allows for the potential problem of the counterelectrode shorting through to the substrate. This parallel path for terminal current will increase the effective dissipation. If the defect consists of a thinning of the film rather than a complete hole, the terminal capacitance will increase, affecting the apparent dielectric constant.

Neglecting fringe effects and assuming the effective parallel capacitance C_p is known, we can calculate the relative dielectric constant ϵ_R from

$$\epsilon_R = dC_p/\epsilon_0 A \tag{1}$$

where d is the thickness of the film, ϵ_0 is the permittivity of free space, and A is the device area.

A volume resistivity $\bar{\rho}$ can be calculated from the measured dissipation D, the results of eq. (1), and

$$\bar{\rho} = 1/\omega\epsilon_R\epsilon_0 D \tag{2}$$

with ω being 2π times the measurement frequency.

The effect of a finite dissipation in the dielectric materials is sometimes represented by expressing the total dielectric constant ϵ as a complex quantity composed of real and imaginary parts:

$$\epsilon = \epsilon' - j\epsilon'' \tag{3}$$

The real part of the dielectric constant ϵ' is that associated with the normal capacitance and can be calculated by using eq. (1) with

$$\epsilon' = \epsilon_R\epsilon_0 \tag{4}$$

Furthermore, it can be shown that [5]

$$D = \epsilon''/\epsilon'. \tag{5}$$

Capacitance and dissipation measurements were taken using four separate bridges to cover the frequency range of interest. The bridges and ranges are as follows: 1 MHz, Boonton model 75A-S8; 100 kHz, Boonton model 74D; 100 Hz–20 kHz, unbalanced transformer bridge (similar to GenRad 1615A); 2×10^{-3}–10 Hz, modified Harris bridge [7]. The unbalanced transformer bridge was directly calibrated with the Boonton bridges by using a high-quality air-core variable capacitor.

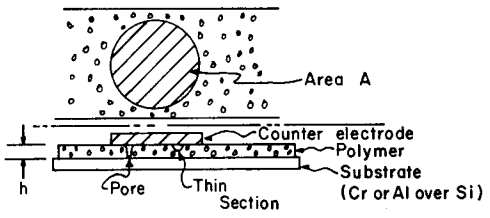

FIG. 1. Cross-section and top view of the test device showing effect of pores and thinning of polymer.

RESULTS AND DISCUSSION

Figure 2(a) shows a typical trace for a narrow channel produced by a plastic stylus on polymethane on a silica glass substrate. Data for this method for four different runs of average thickness of 657 Å produced a standard deviation of 9.3%. Thin bulk overcoat films of Parylene and glow-discharge-polymerized tetrafluoroethylene (GDP-TFE) were also measured with the thickness profilometer. Because of the poor adhesion of the thicker polymers, without precoat, to glass or metal substrates, a single pass of the stylus usually produced a good step. Water slurries were avoided in these circumstances since they have a tendency to cause the films to lift from the substrates. Figure 2(b) shows a typical 1640-Å Parylene N trace.

The effect of the choice of substrate and counterelectrode on the determination of relative dielectric constant and volume resistivity is illustrated in Table I. This table represents measurements on the same run of a polymethane precoat using two different substrates and two different counterelectrodes. Aquadag is a solution of colloidal graphite in water which dries to a highly conductive thick film. The aluminum was a vacuum-deposited thin film applied through a solid mask. While one expects a variation in volume resistivity comparable to the volumes shown, the variation in relative dielectric constant is too large to be ignored. Indeed, the values shown in Table I are very high compared with the

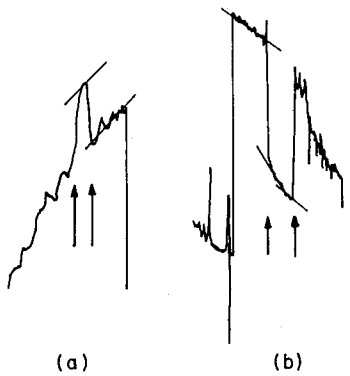

FIG. 2. Thickness profiles for thin polymer films: (a) Polymethane on Al/Si substrate, 1489 Å/in. (b) Parylene N on glass substrate, 1165 Å/in. Arrows indicate edge transition.

TABLE I
Polymethane Precoat

	Chromium substrate		Al/Si substrate	
Electrode	ϵ_R	$\bar{\rho}$ (Ω cm)	ϵ_R	$\bar{\rho}$ (Ω cm)
Aquadag	7.05	0.447×10^6	5.93	1.33×10^6
Aluminum	13.8	2.52×10^6	8.40	1.72×10^6

thicker bulk-type polymers, (conventional and glow discharge), where values of 2–4 as shown below are typical. Also, the standard deviation for the ten measurements of the aluminum counterelectrode appeared to be excessive. It is believed that the high surface energy of the vacuum-deposited aluminum atoms cause this electrode to "wet" the thin portions of the polymer, causing the high variation of dielectric constant from reading to reading and the large average values obtained.

While the aquadag contact produced more typical values, it has the disadvantage that it is difficult to apply in regular shapes of predictable area. A daubing applicator usually produces elliptical contact shapes and these must be measured individually under a metallurgical microscope.

An alternative counterelectrode substrate system that has given the most consistent results has been the use of a mercury probe [6] in conjunction with flat metal substrates made from engraving stock. The probe consists of a column of Hg secured in metallic capillary which presses against the polymer as illustrated in Figure 3. The square flat metal substrate with the polymer side down is secured

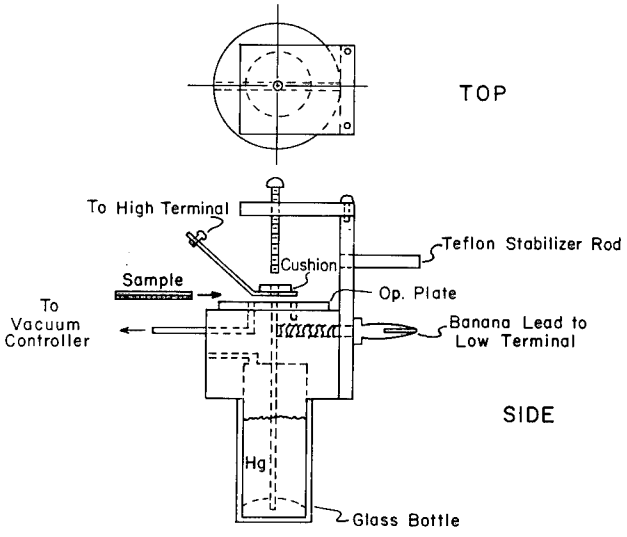

FIG. 3. Drawing of a miniature mercury probe.

against an intermediate Mylar film by an air-suspended cantilever electrode. For the uniformly flat substrate there is sufficient leakage to create a vacuum in the center of the OP plate which causes the Hg in the reservoir to rise. A precisely defined center hole in the Mylar film (OP plate), larger than the capillary aperture, defines the counterelectrode area. Control of the Hg pressure using a vacuum gauge and needle valve further enhances the repeatability of the contact area. This pressure is typically 8 in. Hg. The air-suspended high terminal was found to be particularly important to eliminate shunt dissipation due to the holder itself.

Table II summarizes the results of dielectric measurements using the new Hg probe for ultrathin precoat films, bulk-type thin films and composite films. The values shown here are difficult to compare with other measurements since most of the values that are available in the literature use the NBS standard format. This involves large capacitors composed of pressed powders. Shown also in Table II are specifications given by Union Carbide for Parylene C and N. The match on Parylene C is considered good. Our experience with the C modification is that it is generally more stable and repeatable than the N modification, where our own measurements show large variance from run to run. Parylene N used in this study was synthesized at higher pressure and had a nonuniform surface,

TABLE II
Dielectric Properties of Thin-Film Polymers[a,b]

	1 MHz		1 kHz	
	ϵ'/ϵ_0	$\bar{\rho}$ (Ω cm)	ϵ'/ϵ_0	$\bar{\rho}$ (Ω cm)
Ultrathin films (*<0.1 μm*)				
GDP-methane	6.85	4.4×10^6	5.5	3×10^9
GDP-TFE	6.35	5.1×10^6	4.7	1.5×10^8
GDP-TMDSiO	7.37	1.2×10^7	7.7	8×10^7
Ultrathin Parylene-N (0.05 μm)	3.49	1.37×10^7	. . .	. . .
Thin films (*>0.5 μm*)				
GDP-propylene (1.7 μm)	2.3	1.6×10^9	2.3	5×10^{10}
Parylene N				
Mfgr. Spec.	3.65	6.0×10^9	2.65	6×10^{12}
(0.68–3.8 μm)	3.8 –4.8	8.46×10^7	4.0	7×10^{10}
Parylene C				
Mfgr. Spec.	3.0	3.75×10^7	3.1	3.16×10^{10}
(0.5–2.5 μm)	3.3	3×10^7	3.8	1×10^{10}
Composite GDPM/Parylene N	2.3	4×10^8	3.0	1×10^{11}
Composite GDPM/Parylene C	4.0	1×10^9	3.6	1×10^{11}
Composite GDPM-TFE/Parylene N	4.0	3×10^9	4.7	7×10^{10}

[a]All values for dielectric constant are given relative to the permittivity of free space.
[b]T = 25°C.

as evidenced by SEM. This surface roughness may be partly responsible for the discrepancies in results. It is also interesting to note that a very thin (ca. 200 Å) layer of GDP-TFE or GDP-TMDSiO in the composite films does not change the electrical properties of the bulk overcoat significantly. Also, a thin bulk-type coating of glow-discharge-polymerized propylene behaves similarly to the Parylene coatings of similar thickness.

Figure 4 shows more detailed measurements of the frequency and thickness dependence of the dielectric parameters for Parylene N. Each point represents the average of ten measurements. Shown also on the graph is a curve for glow-discharge-polymerized TFE from Hetzler and Kay [8]. At high frequencies the volume resistivity is seen to increase with thickness. This type of behavior has been attributed to a hopping conduction mechanism [8,9]. The rich detailing in Figure 4 is contrasted to the rather uniform data for Parylene C shown in Figure 5(b). Noteworthy is the fact that the volume resistivity for Parylene C is from one to two orders of magnitude lower than those for Parylene N. Also, for the range of 0.5–2.5 μm the volume resistivity appears to be independent of thickness and approximately linear with frequency as shown in Figure 6.

Alongside Figure 5(b) is a graph with a contracted horizontal scale [Fig. 5(a)] showing several orders of magnitude of the low-frequency behavior of a 9.5-μm Parylene C film. The volume resistivity curve ($\bar{\rho}$) shows a smooth transition from what was a very linear curve from 1 kHz to 1 MHz for this particular sample to a curve tending to saturate at some dc resistivity value. The dielectric constant curve (ϵ') is even more remarkable. The curve shows a general tendency to increase markedly with decreasing frequency, with a slight tendency to saturate at 10^{-1} Hz. The increase in dielectric constant at low frequencies is consistent

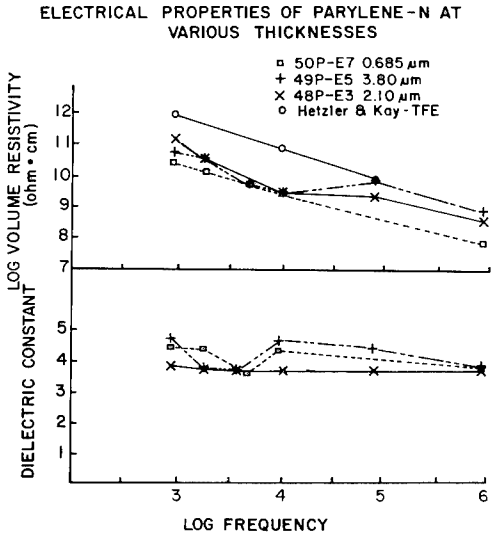

FIG. 4. Dielectric parameters as a function of frequency for Parylene N and GDTFE [8].

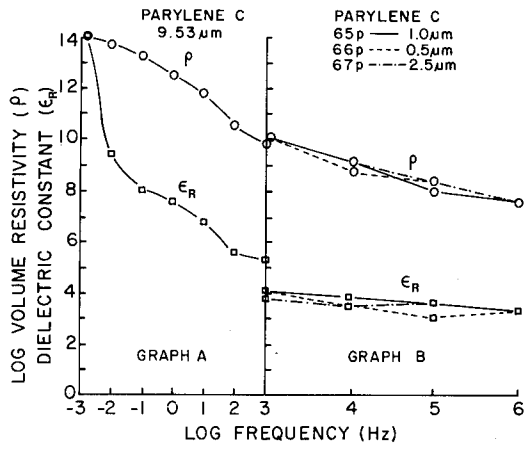

FIG. 5. Dielectric parameters versus frequency for Parylene C.

with the generally accepted theory of a total dielectric constant depending on a classical relaxation mechanism [5]. This theory considers the dielectric to be composed of a distribution of dipole moments with different time constants. At high frequencies a small number of the total dipole moments can respond and the real part of the dielectric constant is low, consistently so for most organic materials and typically in the range of 2–4. However, at low frequencies more and more of the dipole moments with small time constants can respond to the electrical signal, thereby adding to the overall polarizability of the material. The

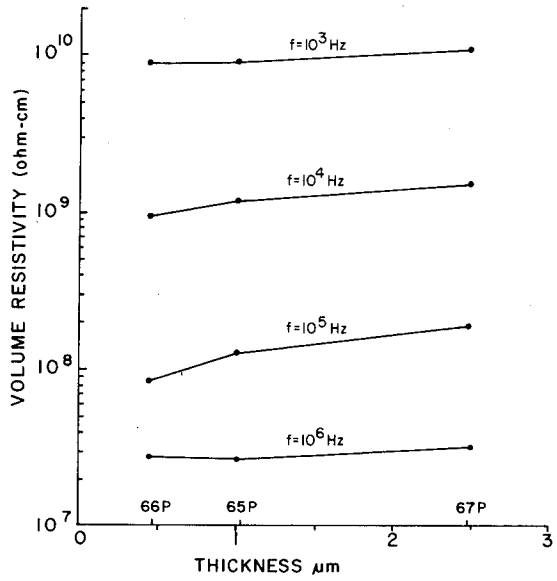

FIG. 6. Volume resistivity versus thickness and frequency for Parylene C.

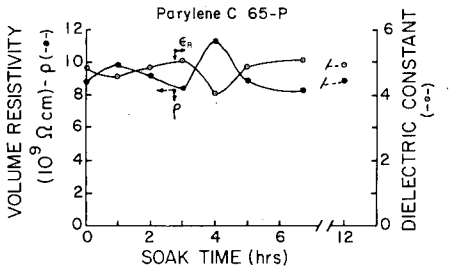

FIG. 7. Dielectric parameters versus soak time in saline solution for Parylene C, 1 kHz.

details of this variation with frequency appears to be dependent on the bulk structure of the films and could potentially be used as the basis of a classification scheme.

The configuration of the substrate and the test protocol in this investigation were designed specifically to accommodate saline soak tests. These tests involve performing multiple-position dielectric measurements on a single polymer on aluminum sample after having been immersed in 0.9% saline (irrigation) solution for a prescribed time. Immediately prior to each test the sample was removed from the solution, rinsed with 12-MΩ semiconductor-quality water and blotted with bibulous paper. Single-frequency tests were performed within a few minutes after which the sample was reimmersed, to be removed again after the next time modulus. Figure 7 shows the dielectric constant and volume resistivity for a 1.02-μm film of Parylene C. Parylene C was chosen for these tests since it has been selected as the primary overcoat for the clinical trials. The cyclic behavior between dielectric constant and volume resistivity versus soak time has been observed by other investigators [10]. GDPM precoats also show this same type behavior with a more extreme variation of volume resistivity (factor of 5).

Figure 8 shows the imaginary part of the dielectric constant versus frequency for 0.47-μm Parylene C film for the frequency range of 100 Hz to 1 MHz. Each

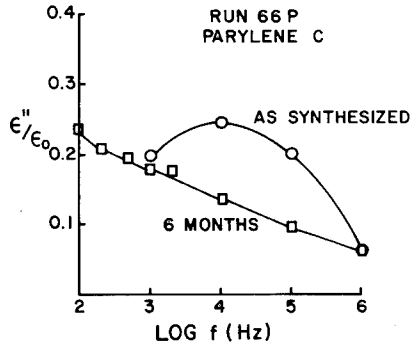

FIG. 8. Changes in the ϵ'' versus frequency plot for Parylene C (○) as synthesized and (□) after six months.

point on the curve represents the average of five measurements. The characteristic maximum at 10 kHz for the as-synthesized curve can be interpreted as a dielectric relaxation loss [11]. This behavior disappears in time to become a normally expected gradual increase in ϵ'' as the frequency decreases. Such a disappearance of ϵ'' peaks usually means that a long-term chemical reaction is taking place, probably involving reduction of the number of free bulk radicals. Such behavior has also been seen in glow-discharge-polymerized TFE [8].

SUMMARY AND CONCLUSIONS

An attempt has been made to solve the difficult problem of electrically characterizing very thin glow discharge precoat polymers alone or in a composite structure. Details are given for a new test protocol involving a miniature Hg probe and flat metallic substrates. This scheme is particularly suited for low-noise measurements of dissipations in the range of 0.001–1 at 1 kHz for thin-film polymers. Electrical characterization of polymers subjected to long-term saline soaks, simulating conditions of chronic implantations, can be performed easily using these methods.

Relative dielectric constants for precoat materials were higher than for thin bulk-type polymers by a factor of 2, with values typically around 6. The thin bulk-type polymers showed wider variability than normally encountered in this parameter, 2.3–4.8, probably resulting from the thin-film configuration of the test device. Composites of ultrathin precoat and thin outer coat tended to have values of dielectric constant intermediate between the two constituents. Ultralow-frequency measurements on Parylene C showed an increasing dielectric constant with decreasing frequency as theoretically predicted.

As was expected, effective volume resistivities varied over a large range from a low of $4.4 \times 10^6\ \Omega$ cm for a precoat material to $1 \times 10^{11}\ \Omega$ cm for a composite material. Variation with frequency followed the usual inverse linear relationship in the range of 1 MHz to 100 Hz. Parylene N films showed a thickness dependence above 10 kHz, suggesting a hopping conduction mechanism. Several of the composite materials involving TFE/Parylene N exhibited very low loss at 1 MHz with volume resistivities greater than $3 \times 10^9\ \Omega$ cm, which was the least measure of the bridge at that frequency. On the other hand, Parylene C showed little variability with thickness and matched values given by the manufacturer. Our experience suggests that the C modification of Parylene is more predictable in electrical properties than the N modification for materials produced in our reactor.

Results of the saline soak tests showed a cyclic variation of volume resistivity and dielectric constant with a period of roughly three hours. While this type of behavior has been reported by other investigators, to our knowledge it has not been explained. Our measurements have ruled out a physical swelling of the film as a contributing factor.

Measurements of the imaginary part of the dielectric constant for Parylene C show a dielectric relaxation loss at approximately 10 kHz which disappears in a matter of months.

This work was supported in part by Contracts No. N01-NS-8-2393 and N01-NS-1-2382 from the National Institute of Neurological and Communicative Disorders and Stroke, NIH, Bethesda, MD.

REFERENCES

[1] N. Morosoff, W. Newton, and H. Yasuda, *J. Vac. Sci. Technol., 13,* 575 (1976); N. Inagaki and H. Yasuda, *J. Appl. Polym. Sci., 26,* 3425 (1981).

[2] R. K. Sadhir, W. J. James, H. K. Yasuda, M. F. Nichols, and A. W. Hahn, *Biomaterials, 2,* 239 (1981).

[3] M. F. Nichols, A. W. Hahn, W. J. James, A. K. Sharma, and H. K. Yasuda, *Biomaterials, 2,* 161 (1981).

[4] W. F. Gorham, *J. Polym. Sci. A-1, 4,* 3027 (1966).

[5] A. R. Blythe, *Electrical Properties of Polymers,* Cambridge U. P., Cambridge, England, 1979.

[6] Model HG-1, MSI Electronics, Inc., Woodside, NY, and modification shown in Fig. 3. A Lederman, *Solid State Technol.* (1981).

[7] W. P. Harris, in *Proceedings of the Conference on Electrical Insulation and Dielectric Phenomena,* National Academy of Sciences, Washington, DC, 1967, p. 72.

[8] U. Hetzler and E. Kay, *J. Appl. Phys., 49* (11), 5617 (1978).

[9] A. K. Jonscher, *Thin Solid Films, 36,* 1 (1978).

[10] E. Hellmuth, personal communication.

[11] R. Pethig, *Dielectric and Electronic Properties of Biological Materials,* Wiley, New York, 1979.

ELECTRICAL CONDUCTION IN PLASMA-POLYMERIZED ORGANOSILICON FILMS: INFLUENCE OF WATER AND OXYGEN

J. TYCZKOWSKI and M. KRYSZEWSKI
Centre of Molecular and Macromolecular Studies, Polish Academy of Sciences, Boczna 5, 90-362 Łódź, Poland

SYNOPSIS

Electrical conductivity of plasma-polymerized organosilicon thin films in the presence of water vapor and oxygen has been investigated. Both these agents cause an increase of conductivity of the electronic type. Taking into account the results of anomalous transient "photocurrents" and direct electrical conductivity as well as water sorption studies, it was found that the observed conductivity increase is related to the activation of some inactive acceptor centers by H_2O molecules. These inactive acceptor centers are situated in the energy diagram at least 2.9 eV above the hole transport band. The proposed conduction mechanism takes into consideration the electronic polarization effect of water molecules associated with acceptor centers. The conductivity increase due to oxygen absorption has been ascribed to the acceptor character of the O_2 molecule.

INTRODUCTION

The electrical properties of plasma-polymerized organosilicon thin films continue to attract much attention [1–4]. Recent studies on the mechanism of their electrical conductivity, taking into consideration among others photoinjection from the metal electrode into films obtained from hexamethyldisilazane, hexamethyldisiloxane, and hexamethyldisilane, have shown that the main role in free-carrier creation is played by bulk generation [5].

The determination of the kind of the generation centers and their density, which consists in investigating an anomalous transient "photocurrent," resulted in the conclusion that these centers are of the acceptor type [6]. Taking into account this fact as well as the results of photoinjection [7] and optical studies, we have proposed a general model of energy levels in these films [8,9]. This

Journal of Applied Polymer Science: Applied Polymer Symposium 38, 149–161 (1984)

CCC 0570-4898/84/010149–13$04.00

model contains the following parameters characterizing the energy structure of these materials: energy gap $E_g = 6.3$ eV, ionization potential $I_p = 7.0$ eV, electron affinity $\chi = 0.7$ eV, bulk work function $W_b = 6.4$ eV, and surface work function $E_s = 4.1$ eV. (The last value is for the polysilazane and polysiloxane films, which without thermal treatment contain surface states whose density is of order 10^{14}–10^{15} cm^{-2} eV^{-1} [7].)

Similar values for these parameters were found for various organosilicon thin films, which suggests that their chemical constitution is similar. It is generally accepted to ascribe to them the general formula Si_xC_y:H [9], which shows that the presence of oxygen atoms or nitrogen atoms in the molecular structure of these films is not important for the basic structure of their energy levels. However, it should be taken into consideration that oxygen and nitrogen atoms have an essential influence on such other properties as the density of surface states [7] and the transport of charge carriers [10]. The above-mentioned model of energy levels seems to be useful in the interpretation of electrical conductivity data and thus it will be used in further discussion.

This article deals with the influence of water and oxygen molecules on the electrical conductivity of thin organosilicon films.

The increased conductivity of various dielectrics under the influence of water has been discussed in many papers, but the basic mechanisms proposed for this effect are very different. The conductivity increase seen in plasma-polymerized siloxane with an increase in humidity during the measurements has been ascribed to ionic currents [11]. Szeto and Hess [2] propose to explain the conductivity rise in these films by assuming a lowering of the contact barriers by dipole structures, e.g., —OH, Si—OH, which arise due to the effect of water; this contributes to increased injection of carriers from the electrode. However, studies of photoinjection of carriers from the electrode into plasma-polymerized organosilicon films, which make it possible to determine the height of the contact barriers, have shown that these do not undergo any substantial changes under the influence of absorption of water molecules in the films [7]. In the case of polyethylene the current rise related to water vapor was assumed to be connected with the removal of deep traps by water molecules, which in turn results in an increase in free-electron concentration [12]. The role of water molecules in electrical conductivity was also based on the assumption that they are active as donors [13].

The conductivity changes due to the presence of oxygen molecules were mainly discussed in terms of their acceptor activity or their role as electron traps. Thus, the reversible decrease of conductivity of plasma-polymerized malononitrile was attributed to this type of activity of the O_2 molecules [14], which in turn leads to the conclusion that the charge carriers are electrons.

Conductivity increase related to absorbed O_2 is occasionally explained by taking into consideration an ionic mechanism of conductivity. This model of electronlike ionic conductivity in the presence of oxygen was applied in the discussion of electrical conductivity of polycarbonate layers [15].

The cited works on the influence of water and oxygen molecules on electrical

conductivity in thin polymer films provide a background for this article, which is an attempt to distinguish between ionic and electronic conductivity of the plasma-polymerized thin films in the presence of water or oxygen as well as to describe the mechanism of their conductivity under these conditions.

EXPERIMENTAL

Thin organosilicon films were obtained by plasma polymerization of hexamethyldisilazane and hexamethyldisiloxane in a flow electrode system using a glow discharge of frequency 20 kHz and current density 2 mA/cm^2. Thin films were deposited on glass substrates (Corning 7059) with a previously evaporated metal (Au) band forming the lower electrode. An upper electrode and guard ring were vacuum deposited on the thin film (effective area of electrodes about 0.1 cm^2). For the vapor sorption measurements, two thin polymer films were deposited on both sides of an aluminum foil of known mass. The thickness of the films was about 1 μm. Electrical property measurements were carried out using the experimental setup schematically presented in Figure 1. The sample was mounted in a temperature-controlled chamber. Stationary currents were determined by connecting the lower electrode with a voltage supply and the upper one with a Takeda Riken TR 8641 electrometer. Anomalous transient "photocurrents" were measured by using a fast operational amplifier, Keithley 301, and an oscilloscope. The sample was illuminated with a 250-W xenon lamp supplied with suitable filters. The details of these measurements and of the determination of generation center density are discussed in our other work [6].

In order to maintain in the measuring chamber a known relative humidity, it was at first evacuated to a vacuum of the order 5×10^{-5} torr and then dry nitrogen (molecular sieves at 77 K) was introduced. At the same time a known amount of water or of heavy water was injected by means of a Hamilton microsyringe. This amount of water introduced near the membrane was heated to increase the rate of water evaporation.

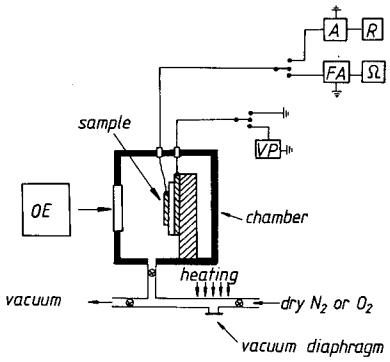

FIG. 1. Schematic diagram of the essential elements of the measuring system: (A) amplifier, (FA) fast operational amplifier, (R) recorder, (Ω) oscilloscope, (VP) voltage supply, (OE) optical system.

In the case of conductivity measurements in oxygen atmosphere, carefully dried O_2 was introduced into the measuring chamber.

The sorption of water and oxygen was determined by using a quartz spiral balance (sensitivity 10^{-5} g).

RESULTS

Figure 2 shows clearly that the increase of relative humidity causes an increase of the current flowing in the polysilazane films. In order to distinguish between the ionic and electronic mechanism of charge transport in these films, the measurements were carried out at various relative contents of heavy water. The results of this study are also presented in Figure 2. The differences between the current values determined in these two experimental conditions are within the limits of experimental error. The course of the $\ln j$ vs. $F^{1/2}$ curves can be approximated by straight lines whose slopes increase with relative-humidity increments.

If before electrical measurements these films were subjected to thermal treatment for 2 h at 350°C in a nitrogen atmosphere with a small amount of oxygen,

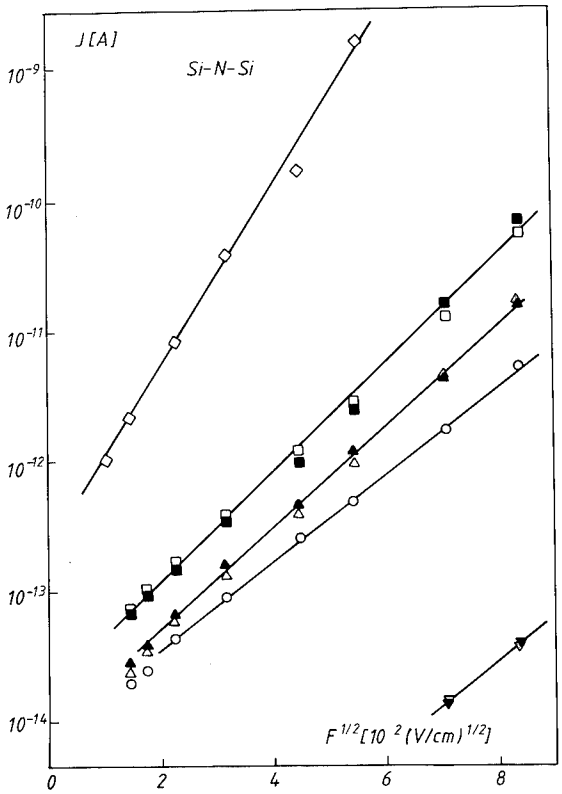

FIG. 2. Dependence of current on square root of field for a nonthermally treated sample of polysilazane: (○) in dry nitrogen, (△) RH = 8%, (▲) RH_{D_2O} = 8%, (□) RH = 36.5%, (■) RH_{D_2O} = 36.5%, (◇) RH = 100%; thermally treated sample: (▽) in dry nitrogen, (▼) RH = 36.5%.

the conductivity values decreased significantly and the presence of water vapor could not be detected (Fig. 2). It seems important to note that such a heat treatment causes a dramatic change in the structure of these films, which manifests itself in the IR absorption spectra (Fig. 3). A similar influence of water vapor on electrical conductivity was observed for thin films obtained from siloxane. Figure 4 shows the dependence of $\ln j$ on $F^{1/2}$ for samples not subjected to thermal treatment (after thermal treatment the conductivity decreases and it is no longer sensitive to the presence of water [11]).

The influence of oxygen absorption on the conductivity of the organosilicon films is presented in Figure 5. The conductivity increase is clearly seen at higher temperatures. The plots of $\ln j$ vs. $1/T$ (Fig. 6) for the films measured in an oxygen atmosphere show at higher temperatures a deviation in slope which is not observed in the oxygen-free atmosphere. A new branch appears to which corresponds an activation energy $E_A \simeq 1.05$ eV. This effect is reversible for polysiloxane and polysilazane subjected to thermal treatment and it disappears rapidly after the removal of oxygen. For nontreated polysilazane samples the disappearance of these deviations in the activation plot is very slow and takes place after several hours of intense pumping at room temperature. The removal of this oxygen influence can be accelerated by heating of the sample in vacuum in mild conditions which does not lead to the changes in molecular structure mentioned above.

The studies on anomalous transient "photocurrents" in thin organosilicon films without thermal treatment show an increase of the density of acceptor centers under the influence of water vapor. Figure 7 represents the dependence of acceptor center density on the relative humidity. Analogous investigations

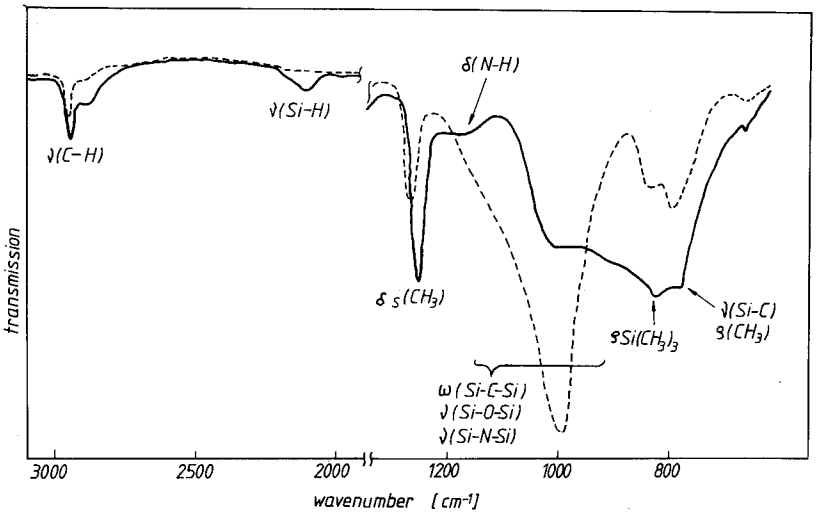

FIG. 3. Infrared ATR spectra of polysilazane film: (—) without thermal treatment, (---) after thermal treatment.

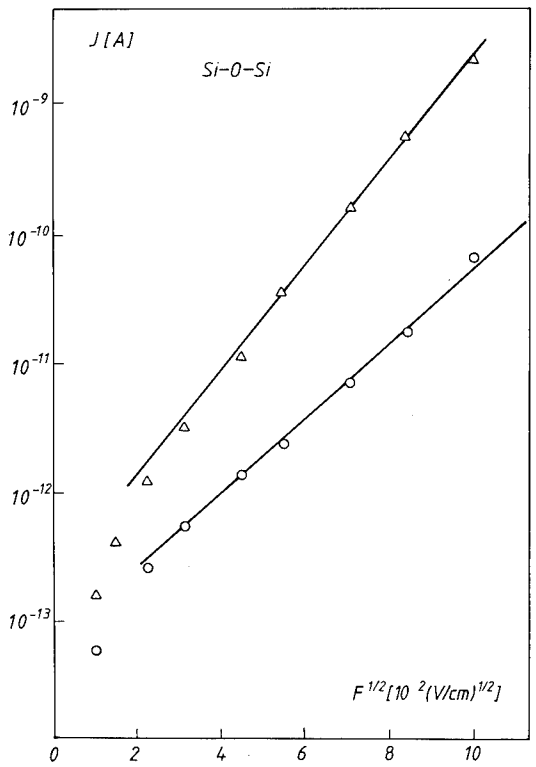

FIG. 4. Dependence of current on square root of field for polysiloxane film: (○) in dry nitrogen, (△) RH = 36.5%

carried out in the presence of oxygen did not demonstrate any change of the acceptor center density.

The water absorption measurements indicated that this effect is quantitatively similar in the case of both thermally treated and nontreated samples. The dependence of the density of absorbed water molecules on relative humidity is depicted in Figure 7. The same type of measurement did not demonstrate any detectable amount of absorbed O_2, but the equipment used for this purpose only allows the detection of an effect of oxygen sorption when the density of absorbed molecules is of the order of 10^{20} molecules/cm^3 or higher.

DISCUSSION

Electrical Conductivity under the Influence of Water Vapor

The lack of systematic differences between the conductivity values of organosilicon films in the presence of water and of heavy water (Fig. 2) point out the electronic character of charge carrier transport. If water molecules were the ion generating species, the conductivity values determined in the presence of

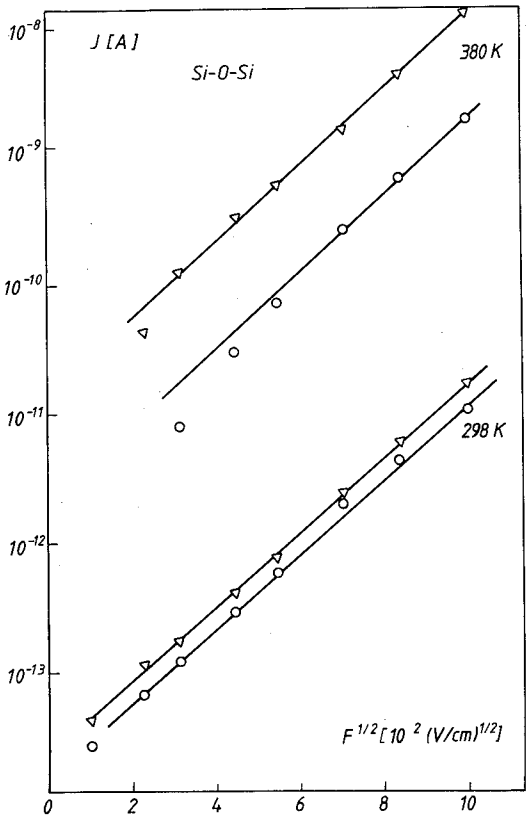

FIG. 5. Dependence of current on square root of field for polysiloxane at two different temperatures: (○) in vacuum 4×10^{-5} torr, (▽) in O_2 at 760 torr.

D_2O should be lower than those found for H_2O. This suggestion is supported by the fact that the mobility of D^+ and OD^- is smaller than that of H^+ and OH^- as well as by the lower dissociation constant of D_2O.

Investigations of ion hopping transport in water have revealed that the mobility of D^+ is 1.4 times lower than that of H^+ and, in the same way, that of OD^- is 1.66 times smaller as compared with OH^-. The ionic product of D_2O is about 5.2 times smaller than that of H_2O [16]. Taking these values into account, one can estimate that electrical conductivity related to D^+ ions would be 3.2 times lower than that connected with H^+ ions (see the values given for solid H_2O and D_2O in [17]).

The electronic mechanism of conductivity in organosilicon films is further supported by the absence of water influence on the conductivity of thermally treated films. Gravimetric measurements show clearly that water vapor is absorbed by these films; thus, it should result in a distinct change of conductivity values in the presence of ionic species at higher concentration.

Proposing an electronic explanation of the observed conductivity, we shall

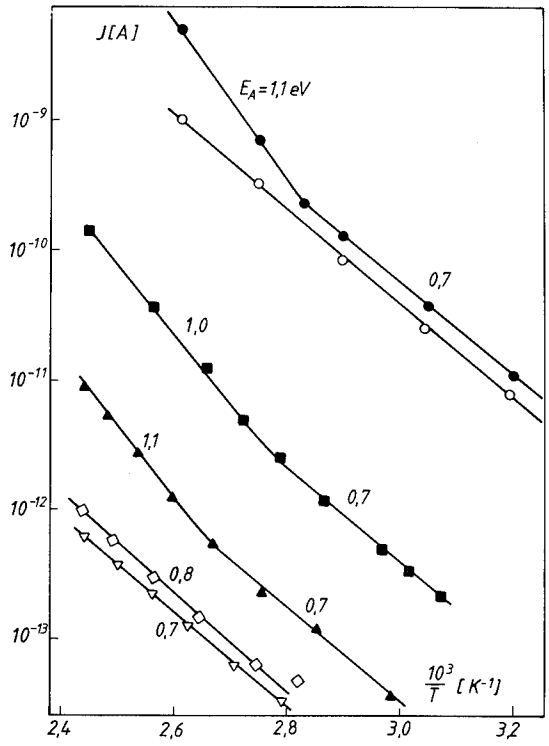

FIG. 6. Current vs. $1/T$ plots for organosilicon films in the presence of O_2 and in vacuum. Polysiloxane: (●) 760 torr O_2, (○) vacuum 5×10^{-5} torr; polysilazane: (■) 760 torr O_2, (◇) vacuum 5×10^{-5} torr (after heating at 300°C for 2 h in vacuum); polysilazane thermally treated: (▲) 760 torr O_2, (▽) vacuum 5×10^{-5} torr.

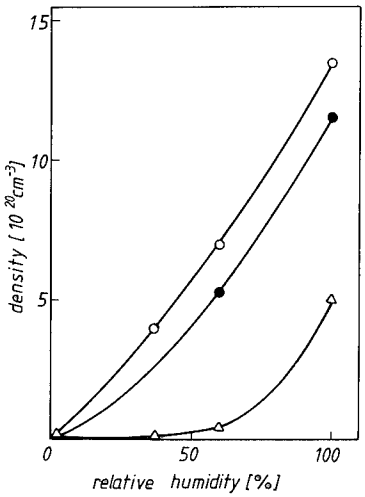

FIG. 7. Acceptor center density and absorbed H_2O molecules density dependence on relative humidity in polysilazane film: (○) density of H_2O molecules in nonthermally treated film, (●) density of H_2O molecules in thermally treated film, (△) density of acceptor centers.

give some detail on the mechanism of this type of charge transport. The detected increase of acceptor center concentration in the films under study (Fig. 7) is evidently correlated with the conductivity increase and with the density of absorbed water molecules. However, one should point out that water molecules are not acceptor sites themselves. If this were the case, similar results would be observed for thermally treated and nontreated layers, which is in contradiction with experimental results. One can explain this behavior considering that water molecules activate primarily inactive acceptor centers existing in the film. During thermal treatment these centers are removed; thus, absorbed water molecules cannot influence the conductivity of such materials. In order to throw some light on the matter, one can use the simplified energy-level model presented in Figure 8. The term inactive centers means that they are not observed in the studies of anomalous "photocurrent". This is due to the fact that these centers are not involved in formation of the depletion layer. Only those centers which constitute the depletion layer can be detected by the anomalous transient photocurrent method and only they are considered in determination of the density of acceptor centers [6]. It follows that they are situated above the Fermi level when calculated from the edge of the hole transport band. Because for the organosilicon films under study the Fermi level corresponds to 0.65 eV and the bands at the surface are bent about 2.25 eV, the inactive centers have to be located 2.9 eV above the hole transport band. As a result their contribution to the electrical conductivity is negligible.

The absorbed water molecules can be attached by hydrogen bonds to inactive centers and are involved in delocalization of the associated hole, which leads to

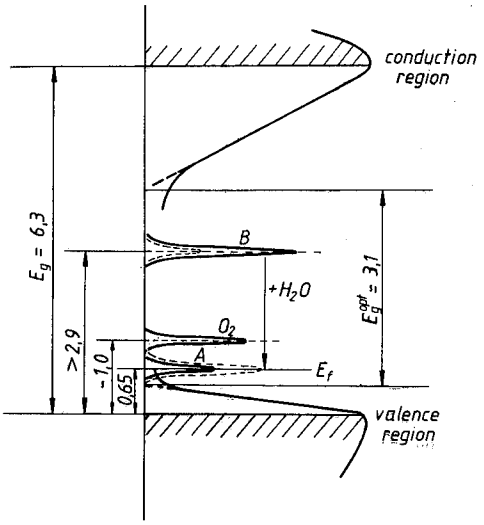

FIG. 8. Scheme of energy-level structure of thin organosilicon films considering the influence of absorbed H_2O and O_2 molecules on their conductivity: (A) intrinsic acceptors responsible for electrical conductivity in absence of water and oxygen; (B) inactive acceptors which can be activated by water molecules; (O_2) oxygen acceptors.

the lowering of their activation energy. The influence of hydrogen bonding on electron delocalization and conductivity is described by Suard-Sender [18].

The exact energy localization of the centers activated by H_2O molecules is difficult to estimate. The dependence of conductivity on temperature in the presence of water, which could be used for activation energy determination, is difficult to interpret in detail. This is due to the fact that two overlapping processes are involved: thermally activated conductivity increase and water-molecule desorption (density of absorbed H_2O molecules decreases) with increasing temperature. The estimation of the activation energy values from isothermal conductivity dependence on field strength, assuming a constant hole mobility in their transport band [10], revealed that the position of water-activated centers in the energy diagram is close to that of the acceptor centers responsible for electrical conductivity in the absence of water.

In the further analysis of water influence on conductivity changes, it seems necessary to compare the density of acceptor centers with that of absorbed water molecules at different relative humidity (RH) values (Fig. 7). The density of absorbed water molecules increases quasilinearly with the relative humidity increment, while the density of acceptor centers increases at first slowly and then at RH $\simeq$ 65% its increment is faster. However, in the whole range of RH variation, its overall percentage change is smaller than that of the H_2O molecule density. This leads one to the conclusion that H_2O molecules are associated not only with inactive acceptor centers but also with other sites of the basic molecular structures of the films under discussion. These sites are present in nonthermally treated as well as in heated samples. They are more susceptible to H_2O molecule association than inactive acceptor centers and are first to react. This can be explained by taking into account the fact that H_2O molecules in structural sites are fixed by hydrogen bonds, while those associated with inactive centers are connected by a weak one-electron bond due to the presence of a hole.

The question of whether several H_2O molecules are needed to activate an initially inactive acceptor center can be also answered by analyzing Figure 7. The different course of the curves characterizing the density of activated centers and that of absorbed H_2O molecules, as well as the ratio of these densities, suggests that several H_2O molecules are involved in such an activation effect.

Further arguments bear on the results of conductivity studies (Figs. 2 and 4) showing that the increase of RH is accompanied by an increment of the slope of $\ln j$ vs. $F^{1/2}$ plots. This slope change can be accounted for by considering the influence of the electrical field on acceptor centers. Besides the barrier lowering (Poole–Frenkel effect [19]), the electrical field will increase the polarization of the active site, consisting of associated H_2O molecules and the delocalized hole. This electronic polarization leads to an initial charge separation. The charge separation distance Δr can be described by a simple relation [20]:

$$\Delta r = eF/\alpha \tag{1}$$

where F is the external field strength, α is the restoring force, and e is the electronic charge. Initial separation has a meaning similar to the concept introduced by Pai [21], bearing on Onsager's theory, which is used, for example, to

explain photogeneration phenomena [22]. Further discussion of these effects should, in fact, be carried out in terms of the Onsager model. However, one can also use a simple Poole–Frenkel model [19], according to which

$$j = A \exp(\beta_{PF} F^{1/2}/kT) \exp(-E_A/kT) \tag{2}$$

where j is the conduction current, β_{PF} is the Poole–Frenkel constant, E_A is the thermal activation energy, and A is a field-independent constant [23]. Initial separation of charges corresponds, in this model, to an additional barrier lowering. Taking into consideration the coulombic relation, one can easily obtain that the actual activation energy, after initial charge separation, will be

$$E_A = \frac{E_A{}^0}{1 + (4\pi\epsilon\epsilon_0 F E_A{}^0/e\langle\alpha\rangle)} \tag{3}$$

where $E_A{}^0$ is the thermal activation energy at $\Delta r = 0$, $\epsilon\epsilon_0$ is the dielectric constant, and $\langle\alpha\rangle$ is the average value of the restoring force.

In substituting eq. (3) into eq. (2) it is convenient to assume that (i) At field $F = 0$ the activated initially inactive acceptor centers are situated at the same position in the dry energy-level diagram, i.e., $E_A = 0.65$ eV. (ii) $\beta_{PF} = 2 \times 10^{-4}$ eV $(\text{cm/V})^{1/2}$ as calculated from $\ln j$ vs. $F^{1/2}$ plots obtained without absorbed water. This value is in agreement with the theoretical value of β_{PF} obtained using $\epsilon_0 = 2.25$ (calculated from refractive index measurements) and assuming the presence of shallow traps for holes [24], which is in agreement with the existence of localized states [8,9]. Thus, one obtains at room temperature

$$j = A \exp\left(7.86 \times 10^{-3} F^{1/2} \exp\left(\frac{25.59}{1 + 1.02 \times 10^7 (F/\langle\alpha\rangle)}\right)\right) \tag{4}$$

where j is given in A, electric field F is in V/cm and $\langle\alpha\rangle$ is in eV/cm^2.

Fitting this equation to the experimental data presented in Figure 2, one can conclude that the increase of relative humidity results in a decrease of $\langle\alpha\rangle$. At RH = 36.5 and 100% the $\langle\alpha\rangle$ values are 1.2×10^{14} and 2.0×10^{13} eV/cm^2, respectively. One can estimate further that for $F = 10^5$ V/cm average values of initial separation are $\langle\Delta r\rangle \simeq 0.1$ Å in the former case and $\langle\Delta r\rangle \simeq 0.5$ Å in the latter, which seems to be a reasonable evaluation. The above-discussed decrease of the average value of the restoring force with RH increase can be correlated with the hole delocalization increment in an activated acceptor center by several H_2O molecules.

This concept of the influence of water on the conductivity of plasma-polymerized organosilicon films has a speculative character and exact calculations are necessary in order to reach a clear understanding of the role of activation of initially inactive centers by H_2O molecules and of the physical sense of initial separation as well as of the influence of external field on its value.

Conductivity under the Influence of Oxygen

The generally accepted conception of the role of oxygen molecules as acceptor centers or trapping centers for electrons seem not to be confirmed by our ex-

periments in a simple way. The lack of acceptor center density changes in films subjected to oxygen atmosphere suggests that O_2 molecules are not active in the generation of this type of site. It was also demonstrated that they are not effective electron traps. If in the films under study there is some concentration of donors then thermally released electrons should lead to a decrease of conduction current due to their recombination with holes. In that case electron traps should oppose such a process and an increase of conductivity should be observed. However, the density of filled electron traps will decrease at higher temperatures, which is in contradiction with experimental results (Fig. 6).

Nor can an electronlike ionic mechanism be accepted to describe the contribution of O_2 molecules to conductivity. According to Barker [15], an O_2 molecule diffusing to a cathode could attract an electron and then transport it in the applied field through the film to the anode. The neutralization process at the electrode results in the release of a neutral molecule which may contribute again to the charge transport process. This concept is based on assumption of a rather high mobility for O_2 molecules in the material under study which seems not to be appropriate for polysilazane films. The rate of diffusion of O_2 in these films is slow as evidenced by the long time needed for degassing. Nevertheless, it should be pointed out that this low mobility of O_2 might be sufficient for elimination of charged molecules from the depletion layer as a consequence of electrostatic repulsion. In that case O_2 molecules could act as acceptors. Their weak bonding with the molecular structure of the organosilicon film ensures their absence from the depletion layer and consequently they do not appear in the studies of anomalous transient photocurrent. The lack of acceptor center concentration change, in agreement with experiment, does not exclude in reality the presence of acceptor-type species in the bulk of the material. A parallel shift of $\ln j$ vs. $F^{1/2}$ curves determined in vacuum and in oxygen atmosphere (Fig. 5) shows that the same general mechanism of conductivity operates in both cases. This suggests that an acceptorlike activity of absorbed O_2 molecules occurs in the plasma-polymerized organosilicon films.

The new branch in the activation plots (Fig. 6) at an activation energy $E_A \simeq 1.05$ eV which appeared in the presence of O_2 at higher temperature defines the average energy level of the bulk oxygen acceptor centers in the energy diagram (Fig. 8). This E_A value seems to be overestimated, but there is no doubt that it must be higher than the activation energy of intrinsic acceptor centers. The increase of the conductivity of plasma-polymerized organosilicon films in the presence of oxygen acceptors appears to confirm the proposed hole mechanism of conductivity derived from optical [8] and anomalous transient photocurrent [6] studies.

CONCLUSIONS

Studies on electrical properties of plasma-polymerized organosilicon thin films have shown an increase in conductivity in the presence of absorbed water and oxygen molecules. The conductivity measurement of virgin thin films and those subjected to water and heavy water vapors have shown that the current flow is

connected with an electronic process. The proposed mechanism of conductivity considers the role of H_2O molecules in activation of initially inactive intrinsic acceptor centers. These acceptors are located in energy diagram at about 2.9 eV above the edge of the hole transport band. Thermal treatment of the plasma-polymerized films results in disappearance of these centers. The proposed mechanism accounts for the water molecules contributing to the initial separation of carriers in those acceptor centers when subjected to electric field. The concept of electrical conductivity in plasma-polymerized organosilicon films presented here seems to explain all basic experimental observations but needs further support by detailed calculations.

The increase of conductivity of these materials in the presence of absorbed oxygen molecules was ascribed to their acceptor-type activity, in agreement with the previously suggested hole conductivity in the materials under study.

REFERENCES

[1] M. Kryszewski, A. M. Wróbel, and J. Tyczkowski, in *Plasma Polymerization,* Am. Chem. Soc. Ser. No. 108, M. Shen and A. T. Bell, Eds., Am. Chem. Soc., Washington, DC, 1979, Chap. 13.
[2] R. Szeto and D. W. Hess, *Thin Solid Films, 78,* 125 (1981); *J. Appl. Phys., 52,* 903 (1981).
[3] J. E. Klemberg-Sapieha, S. Sapieha, M. R. Wertheimer, A. Yelon, *Appl. Phys. Lett., 37,* 104 (1980).
[4] M. Maisonneuve, Y. Segui, and Bui Ai, *Thin Solid Films, 44,* 209 (1977).
[5] J. Tyczkowski, G. Czeremuszkin, and M. Kryszewski, *Phys. Status Solidi A, 72,* 751 (1982).
[6] J. Tyczkowski and M. Kryszewski, *Phys. Status Solidi A, 78,* 259 (1983).
[7] J. Tyczkowski and M. Kryszewski, *J. Phys. D, 14,* 1877 (1981).
[8] J. Tyczkowski, G. Czeremuszkin, and M. Kryszewski, *Mater. Sci., 2,* 372 (1981).
[9] J. Tyczkowski and M. Kryszewski, *J. Phys. D.,* in press.
[10] J. Tyczkowski, J. Sielski, and M. Kryszewski, *Polym. Bull., 8,* 117 (1982).
[11] N. Desbarax, Thèse de Doctorat, Université Paul Sabatier, 1975.
[12] R. Patsch, in *Conference on Electrical Insulation and Dielectric Phenomena,* Annual Report of the National Academy of Science, Washington, DC, 1979, p. 114.
[13] D. D. Eley and D. Leskie, *Adv. Chem. Phys., 32,* 324 (1960).
[14] S. D. Phadke, *Thin Solid Films, 55,* 391 (1978).
[15] R. E. Barker, Jr., *Pure Appl. Chem., 46,* 157 (1976).
[16] A. J. Brodskij, *Chimia Izotopov,* Izd. Akad. Nauk USSR, Moscow, 1957.
[17] R. S. Bradly, *Trans. Faraday Soc., 53,* 687 (1957).
[18] M. Suard-Sender, *J. Chim. Phys., 62,* 79 (1965).
[19] K. C. Kao and W. Hwang, *Electrical Transport in Solids,* Pergamon, New York, 1981, Chap. 5.3.
[20] C. Kittel, *Introduction to Solid State Physics,* Wiley, New York, 1966, Chap. 12.
[21] D. M. Pai, *J. Appl. Phys., 46,* 5122 (1975).
[22] P. J. Melz, *J. Chem. Phys., 57,* 1694 (1972).
[23] M. R. Boon, *Thin Solid Films, 11,* 183 (1972).
[24] J. G. Simmons, *Phys. Rev. 155,* 657 (1967).

MOISTURE BARRIER PROPERTIES OF PLASMA-POLYMERIZED HEXAMETHYLDISILOXANE

E. SACHER, J. E. KLEMBERG-SAPIEHA,
H. P. SCHREIBER, and M. R. WERTHEIMER
Department of Engineering Physics, Ecole Polytechnique, Box 6079, Station A, Montreal, Quebec H3C 3A7, Canada

SYNOPSIS

Organosilicones, in particular hexamethyldisiloxane, have been plasma-polymerized in microwave discharges. Films were formed as functions of both substrate temperature and plasma power. In all cases, 5000-Å coatings cause remarkable decreases in the rate of water permeation, their magnitudes increasing with both substrate temperature and plasma power. This is due to chemical reactions which give both crosslinking and decreased organic content; these, in turn, cause decreases in both diffusion and sorption coefficients. An increase in plasma power is more effective in accomplishing this than is an increase in substrate temperature, and this is shown to be due to a combination of dielectric heating, which is equivalent to an increase in substrate temperature, and increased fragmentation in the plasma.

INTRODUCTION

The present trend in device technology is toward miniaturization. This requires certain characteristics of the thin dielectric films so employed. Among them are (i) strong adhesion to substrates, (ii) low pinhole density, and (iii) chemical stability toward processing and hostile environments. Among the various materials being considered for this application are plasma polymers.

Plasma techniques, which include both plasma deposition and plasma etching, have become widely accepted in the electronics manufacturing industry; plasma polymers have been used as dielectrics for thin-film capacitors [1], MIS devices [2], passivation layers for integrated circuits [3], and photoresists for use in an all-dry lithographic process for VLSI technology [4]. Less directly, plasma polymers have found application as protective coatings for optics [5,6] and metals [7,8], where their barrier properties were employed.

Journal of Applied Polymer Science: Applied Polymer Symposium 38, 163–171 (1984)

CCC 0570-4898/84/010163-09$04.00

Plasma polymers have been the subject of several reviews [9–12], where it was shown that the polymerization of unsaturated monomers under low plasma power results in films whose physical properties are, where comparisons are available [11,12], generally similar to those formed by the straightforward polymerization of unsaturated monomers, suggesting that the extent of fragmentation in such a case is not large. In our opinion, a more fruitful source of plasma polymers results from the fragmentation and selective polymerization of saturated monomers; in particular, we refer to substituted silanes [13–17]. Using hexamethyldisiloxane (HMDSO) as a representative silane, we show how the chemical and physical properties of the resultant plasma polymer may be controlled through their polymerization conditions to produce desirable moisture barrier properties. It should be noted that plasma polymers of both hexamethyldisilazane and silane (SiH_4) gave similar results.

EXPERIMENTAL

Spectral grade HMDSO was purchased from PCR Research Chemicals, Inc., and used without further purification. Plasma polymerization took place in the large-volume microwave plasma generator (LMP) previously described [15,16].

Plasma coatings of various thicknesses were polymerized onto 40-mm × 40-mm × 51-μm samples of Du Pont Kapton type H polyimide film, at a pressure of 0.2 torr. Kapton was chosen as the substrate because it is known to be thermally stable, for short periods of time, to at least 450°C [19], the highest substrate temperature used here. In addition, the moisture permeation properties of Kapton were previously evaluated in [20,21], where it was found that the presence of moisture in this material causes such an increase in its ionic conductivity as to completely obscure its electronic conductivity [22].

Prior experience [15] has shown the importance of both substrate temperature and plasma power on the structure of HMDSO plasma polymers, and both variables were employed here in order to study their effects on moisture permeation. In addition, because of the known effect of film thickness on permeation [23], it, too, was chosen as a variable.

Two methods were used to evaluate moisture permeation: (i) routine measurements, used for comparative data, were evaluated by ASTM E96-53T (Water Vapor Transmission of Materials in Sheet Form): A small dish, 30 mm in diameter and specially made for this purpose, was filled with $CaCl_2$, covered with the sample, and placed in a controlled atmosphere at 37.8°C/90% RH (ASTM test procedure E). The weight gain was monitored over a period of 24 h by a Sartorius model 2600 microbalance. (ii) More precise data were obtained on a Dohrmann Envirotech model PPA-1 Polymer Permeation Analyzer, which was extensively modified as previously described [20]. The permeant flow was maintained at 55°C/50% RH.

In both methods, the plasma polymer coating faced the permeant flow, although initial experiments showed no difference, beyond experimental error, whichever side faced the flow.

RESULTS

The ASTM method revealed that the weight gain ΔW was linear with time and highly reproducible. Plots of the weight gain in 24 h, ΔW_{24}, were thickness dependent, as seen in Figure 1. These data were used to evaluate the permeation coefficient of the substrate as it varied with thickness.

The overall permeation coefficient was calculated as

$$P = \frac{\Delta W}{t}\frac{L}{A}\frac{1}{C_{H_2O}} \tag{1}$$

where t is the time, L the sample thickness, A the surface area (= 7.07 cm^2), and C_{H_2O} the water vapor pressure (= 90% RH at 37.8°C, or 4.425 cm Hg). Using a single thickness of Kapton, 51 μm, various thicknesses of plasma polymer, up to 0.5 μm, were deposited at 200 W, 0.2 torr, and 300°C. The permeation coefficients of the composite were then evaluated at 37.8°C/90% RH, using method (i) in the Experimental section. The permeation coefficients of the two layers were then separated as

$$1/P = l_K/P_K + l_P/P_P \tag{2}$$

where the subscripts K and P refer to Kapton and plasma polymer, respectively, and l_i is the fractional thickness of layer i. Typical permeation data for the plasma polymer are found in Table I, where a noticeable change is seen over the thickness range.

Such a change suggests a surface barrier to permeation [23,24], which was evaluated by the equation derived by Kammermeyer and co-workers [23]:

$$1/P(L) = 1/P_\infty + r/L \tag{3}$$

where $P(L)$ is the permeation coefficient measured under a constant set of conditions at thickness L, P_∞ is the permeation coefficient at infinite thickness as evaluated from the intercept of the linear plot of $1/P(L)$ vs. $1/L$, and r is the surface layer resistance as obtained from the slope of the plot. The data in Table

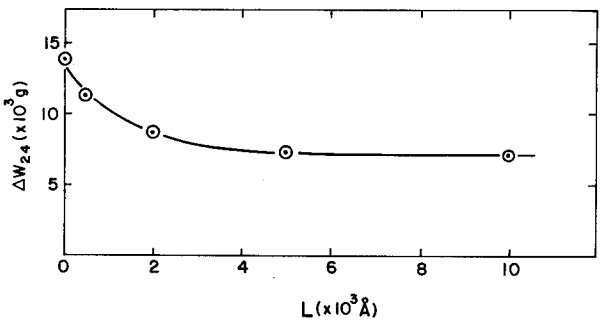

FIG. 1. 24-h water uptake through plasma-polymerized HMDSO/Kapton composites, as a function of plasma polymer thickness, at 37.8°C/90% RH.

TABLE I
Permeation Coefficient of the Plasma-Polymerized HMDSO Layer, as a Function of Thickness, after Deposition at 200 W, 0.2 torr, and 300°C

Thickness (μm)	Fractional thickness	$P_P \times 10^{10}$ [cm³ (STP) cm/cm³ s cm Hg]
0.05	0.001	2.23
0.25	0.005	2.81
0.5	0.01	3.08_5

I were evaluated by this method to give $P_\infty = 3.12 \times 10^{-10}$ cm³ (STP) cm/cm² s cm Hg and $r = 6.50 \pm 0.96 \times 10^7$ cm² s cm Hg/cm³ (STP); the plot is linear to a statistical significance of >97.5%, as determined by both t test and correlation coefficient. All plasma polymers tested exhibited such small, but significant, surface barriers to permeation, indicating that the surface of the plasma polymer was, to some extent, different than the bulk.

The plot in Figure 1 showed that ΔW_{24} was constant at thicknesses > 0.5 μm. For this reason, we chose to continue our optimization study after fixing L = 0.5 μm.

Values of ΔW_{24} were obtained as functions of (i) substrate temperature T_s at a constant power p of 200 W and (ii) p at a T_s setting of 200°C. These are found in Figure 2. In fact, temperature calibration with temperature-sensitive materials showed that the actual value of T_s was substantially higher during plasma deposition, owing to dielectric heating by the applied microwave field. This calibration is seen in Figure 3.

Thus, an increase in p simultaneously increases T_s. Therefore, the lower curve in Figure 2 indicates the change in ΔW_{24} due to both. It is important to note that this leads to a reduction in ΔW_{24} by more than tenfold.

These measurements were repeated on the polymer permeation analyzer, using method (ii) in the Experimental section and 55°C/50% RH as the standard measurement conditions; these conditions were chosen for reasons given in a

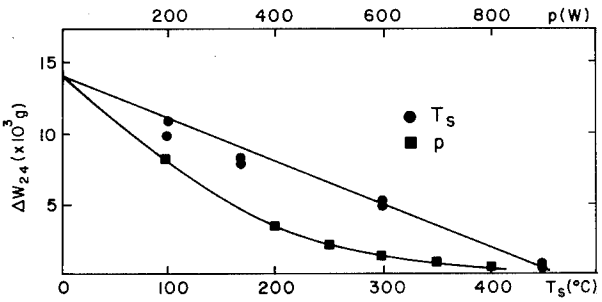

FIG. 2. 24-h water uptake through 5000-Å-thick plasma-polymerized HMDSO/Kapton composites, as functions of substrate temperature (●) and microwave power (■), at 37.8°C/90% RH.

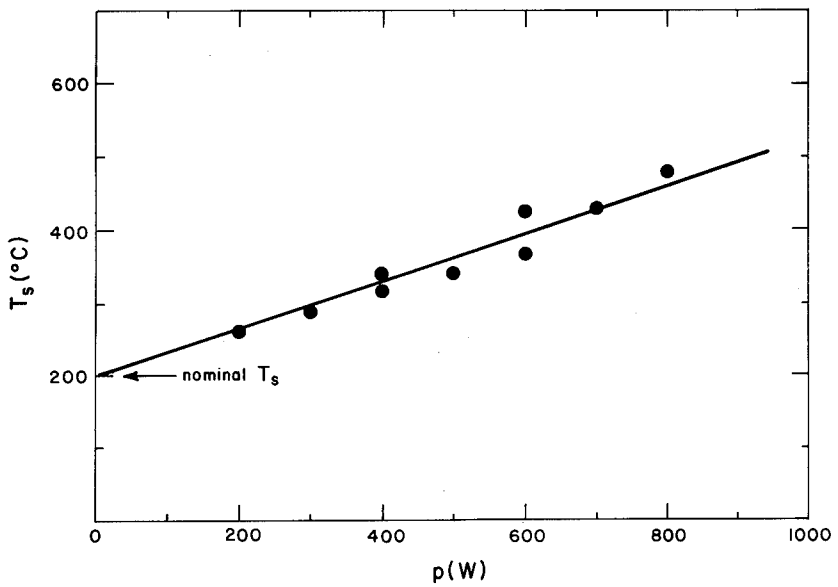

FIG. 3. Dielectric heating of 51-μm-thick Kapton Du Pont Polyimide film type H, as a function of microwave power.

previous study on polyimide permeation [20]. The permeation data for the plasma polymer/Kapton composite are plotted in Figure 4. As seen here, P decreases logarithmically with T_s at constant p. The data fit the equation

$$\ln P \pm 0.169 = (-0.00526 \pm 0.00047)T_s - 16.42 \quad (4)$$

with a statistical significance of >99.95%, as determined by both t test and correlation coefficient. A previous study [16] found that increasing T_s resulted in increases in both crosslinking and inorganic content, revealed by both density and IR measurements. We have found that the densities ρ determined there, in g/cm^3, vary with T_s as

$$\ln \rho \pm 0.00173 = (0.000147 \pm 0.000007)T_s + 0.5518 \quad (5)$$

again to a statistical significance of >99.95%. It appears, then, that this increase in density of the plasma polymer is related to the observed decrease in permeation coefficient of the plasma polymer/Kapton composite. They fit the equation

$$\ln P \pm 0.168 = (-35.69 \pm 4.70)\ln \rho + 3.269 \quad (6)$$

also to a statistical significance of >99.95%.

Figure 4 also reveals that P decreases logarithmically with increasing p and, as with eq. (4), does so to a statistical significance of >99.95%. The data fit the equation

$$\ln P \pm 0.245 = (-0.00457 \pm 0.00036)p - 16.71 \quad (7)$$

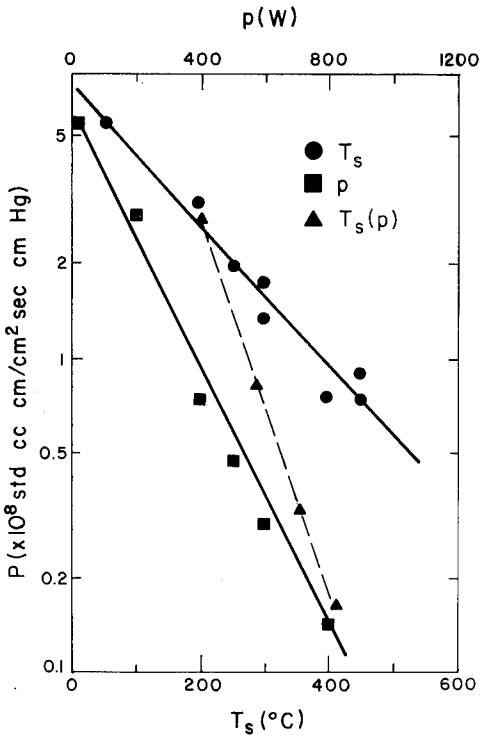

FIG. 4. Permeation coefficient of 5000-Å-thick plasma-polymerized HMDSO/Kapton composites, as functions of substrate temperature (●), microwave power (■), and substrate temperature due to dielectric heating (▲), at 55°C/50% RH.

The effect of p in increasing T_s was shown in the following way: Values of T_s were recalculated for various values of p, and the ln P vs. p data were recast as ln P vs. $T_s(p)$. They are also plotted in Figure 4 and reveal that, at low power, the permeation is related almost entirely to dielectric heating. However, as the power is increased, greater fragmentation, leading to more and more "inorganic" film structures, plays an increasingly important role. While the expected increase in density with power was not determined in the present case, it undoubtedly does so, leading to an equation similar to eq. (5). The associated increases in crosslinking and inorganic content are the probable reasons for the decrease in the ability of the water to permeate. This will be further considered in the Discussion section.

DISCUSSION

In our experience, unlike plasma-polymerized unsaturated hydrocarbons or fluorocarbons, PPHMDSO is very effective as a barrier to moisture permeation. The barrier effect increases with both T_s and p, and is related to the structure

TABLE II
Representative Permeation Parameters of the Plasma-Polymerized HMDSO/Kapton Composite, as a Function of Plasma Power, after Deposition at 200°C, 0.2 torr

Power (W)	$P \times 10^8$ [cm^3 (STP) cm/cm^3 s cm Hg]	$D \times 10^9$ (cm^2/s)	S [cm^3 (STP)/cm^3 cm Hg]
200	2.78	6.24	4.46
500	0.471	3.20	1.47
800	0.139	1.84	0.756

of the resultant plasma polymer film: Increases in both density and inorganic character [16] result in a vitreous silicalike structure which is highly crosslinked and extremely rigid.

Any free-standing film is able to swell on sorption of a permeant, thereby relieving the stresses due to the sorption process. An inability to strain, such as with a strongly adhering conformal coating, will cause a decrease in the diffusion coefficient D [21,25–27]. This also holds true for materials crosslinked both chemically [28–31] and with radiation [32–34] because, by virtue of their three-dimensional chemical bonding, they also lose the ability to strain. In addition, crosslinking also decreases the sorption coefficient S.

In our present materials, which are crosslinked by virtue of the very nature of the plasma polymerization process [11], we also expect decreases in D and S. This is indeed the case, as seen in Tables II and III*: Both D and S decrease with increasing crosslinking and inorganic content. These data, and those in Figure 4, suggest that very subtle changes in chemical structure have a profound influence on the permeation parameters.

The surface barrier to resistance, as calculated from the ΔW_{24} data, was earlier found to have a value of 6.50×10^7 cm^2 s cm Hg/cm^3 (STP). This is concep-

TABLE III
Representative Permeation Parameters of the Plasma-Polymerized HMDSO/Kapton Composite, as a Function of Substrate Temperature, after Deposition at 200 W, 0.2 torr

T_s (°C)	$P \times 10^8$ [cm^3 (STP) cm/cm^2 s cm Hg]	$D \times 10^9$ (cm^2/s)	S [cm^3 (STP)/cm^3/cm^3 cm Hg]
200	2.78	6.24	4.46
300	1.29	4.16	3.47
400	0.70	3.23	2.18

*While one may evaluate the permeation coefficient of the plasma polymer through the use of eq. (2), this separation cannot be made for either the diffusion or the sorption coefficient. We prefer to list the values for the composite in Tables II and III, as well as in Figure 4, to illustrate the extent of *reduction* in water permeation through Kapton, as provided by these thin plasma polymer layers. In actual fact, P_P approaches 1×10^{-11} cm^3 (STP) cm/cm^2 s cm Hg at elevated temperatures.

tually [20] the pressure necessary for the flow of unit flux across the surface, and shows that the surface offers a greater barrier to permeation than does the bulk. This in turn indicates that the surface is structurally different from the bulk, a fact [16] which has recently been confirmed by elastic recoil detection profiles of the deposited films [35]. Presumably, the lower-density outer layer contains more dipolar material, which may then retard the water molecules through dipole–dipole interactions.

The authors wish to thank John Susko for the use of his polymer permeation analyzer and Patricia Lazarou for obtaining the permeation data on it. This work was supported by the Natural Sciences and Engineering Research Council of Canada and by the Ministry of Education of Quebec.

REFERENCES

[1] A. Bradley, *Ind. Eng. Chem. Prod. Res. Dev., 9,* 101 (1970).
[2] M. Maisonneuve, Y. Segui, and B. Ai, *Thin Solid Films, 33,* 35 (1976); M. Aktik, Y. Segui, and B. Ai, *J. Appl. Phys., 51,* 5055 (1980).
[3] W. Kern and R. S. Rosler, *J. Vac. Sci. Technol., 14,* 1082 (1977).
[4] S. Hattori, J. Tamano, M. Yamada, M. Ieda, S. Morita, K. Yoneda, and S. Ishibashi, *Thin Solid Films, 83,* 189 (1981).
[5] J. R. Hollahan, T. Wydeven, and C. C. Johnson, *Appl. Opt., 13,* 1844 (1974).
[6] F. G. Yamagishi, D. D. Granger, A. E. Schmitz, and L. J. Miller, *Thin Solid Films, 84,* 435 (1981).
[7] H. P. Schreiber, Y. B. Tewari, and M. R. Wertheimer, *Ind. Eng. Chem. Prod. Res. Dev., 17,* 27 (1978).
[8] H. P. Schreiber, M. R. Wertheimer, and A. M. Wróbel, *Thin Solid Films, 72,* 487 (1980).
[9] V. M. Kolotyrkin, A. B. Gilman, and A. K. Tsapuk, *Russ. Chem. Rev., 36,* 579 (1967).
[10] M. Millard, in *Techniques and Applications of Plasma Chemistry,* J. R. Hollohan and A. T. Bell, Eds., Wiley-Interscience, New York, 1974, Chap. 5.
[11] M. Shen and A. T. Bell, in *Plasma Polymerization,* Adv. Chem. Ser. No. 108, M. Shen and A. T. Bell, Eds., Am. Chem. Soc., Washington, DC, 1979, p. 1.
[12] H. Yasuda, *J. Polym. Sci. Macromol. Rev., 16,* 199 (1981).
[13] A. M. Wróbel, M. Kryszewski, and M. Gazicki, *Polymer, 17,* 673, 678 (1976).
[14] T. Hirotsu, *J. Appl. Polym. Sci., 24,* 1957 (1979).
[15] A. M. Wróbel, M. R. Wertheimer, J. Dib, and H. P. Schreiber, *J. Macromol. Sci. Chem., 14,* 321 (1980).
[16] A. M. Wróbel, J. E. Klemberg, M. R. Wertheimer, and H. P. Schreiber, *J. Macromol. Sci. Chem., 15,* 197 (1981).
[17] S. K. Varshney and C. L. Beatty, *Org. Coat. Appl. Polym. Sci. Proc. 46,* 127 (1982).
[18] R. G. Bosisio, M. R. Wertheimer, and C. F. Weissfloch, *J. Phys. E: Sci. Instrum.* 628 (1973).
[19] Du Pont Kapton Polyimide Film Bulletin H-2.
[20] E. Sacher and J. R. Susko, *J. Appl. Polym. Sci., 23,* 2355 (1979).
[21] E. Sacher and J. R. Susko, *J. Appl. Polym. Sci., 26,* 679 (1981).
[22] E. Sacher, *IEEE Trans. Electr. Insul., EI-14,* 85 (1979).
[23] S.-T. Hwang and K. Kammermeyer, in *Permeability of Plastic Films and Coatings,* H. B. Hopfenberg, Ed., Plenum, New York, 1974, p. 197, and references cited therein.
[24] E. Sacher, *J. Polym. Sci. Lett. 21,* 111 (1983).
[25] J. Crank, *J. Polym. Sci., 11,* 151 (1956).
[26] G. Astarita and G. C. Sarti, *Polym. Eng. Sci., 18,* 388 (1978).
[27] G. C. Sarti, *Polymer, 20,* 827 (1979).
[28] A. S. Carpenter and D. F. Twiss, *Rubber Chem. Technol., 13,* 326 (1940).

[29] G. J. van Amerongen, *Rubber Chem. Technol., 20,* 479 (1947).
[30] R. M. Barrer and G. Skirrow, *J. Polym. Sci., 3,* 549, 564 (1948).
[31] G. J. van Amerongen, *Rubber Chem. Technol., 37,* 1065 (1964).
[32] I. Sobolev, J. A. Meyer, V. Stannett, and M. Swarc, *J. Polym. Sci., 17,* 417 (1955).
[33] H. A. Bent, *J. Polym. Sci., 24,* 387 (1957).
[34] H. J. Bixler, A. S. Michaels, and M. Salame, *J. Polym. Sci. A, 1,* 895 (1963).
[35] R. Groleau, P. Depelsenaire, M. R. Wertheimer, and J. F. Currie, unpublished.

PREPARATION OF POLYACRYLONITRILE REVERSE OSMOSIS MEMBRANE BY PLASMA TREATMENT

T. SHIMOMURA, M. HIRAKAWA, I. MURASE, M. SASAKI, and T. SANO

Central Research Laboratory, Sumitomo Chemical Co., Ltd., 40, 2-Chome, Tsukahara, Takatsuki City, Osaka, Japan 569

SYNOPSIS

In order to prepare a reverse osmosis (RO) membrane, the surface plasma treatment of porous acrylonitrile copolymer (PAN) films by using non-plasma-polymerizable gases was investigated. An excellent RO membrane having high water flux and high salt rejection was obtained. Extremely thin and crosslinked active skin layers were produced on the top surface of porous PAN films by this plasma treatment. The relationship between plasma discharge conditions and RO properties was described in terms of plasma treatment time, gas pressure, discharge wattage, type of gases, and so on. From ATFT-IR and ESCA analyses of the membrane surface it is concluded that hydrophilic groups such as >C═O, —OH, and >NH have been incorporated onto the surface after the plasma treatment. The characteristics of RO membranes thus obtained are also reported. A tubular module with this plasma-treated PAN membrane has successfully been produced on the basis of these fundamental studies, and the first plant having a daily capacity of 15 m^3 of permeate water, which is for the effluents from an electrocoloring bath, has been working smoothly without any troubles for more than three years.

INTRODUCTION

In the past 20 years, RO membranes have been well developed because of their usefulness in industry. In the preparation of RO membranes, it is very important how fine and how thin a skin layer which separates solutes from solvent can be made. From this point of view, the plasma polymerization of organic monomers onto porous substrates has been investigated by many workers. An investigation done by Yasuda and Lamaze [1] revealed that membranes exhibiting high water flux and high salt rejection can be obtained with nitrogen-containing monomers such as 4-vinylpyridine and 3,5-lutidine. Another paper

Journal of Applied Polymer Science: Applied Polymer Symposium 38, 173–183 (1984)

CCC 0570-4898/84/010173-11$04.00

by Bell et al. [2] demonstrated that an excellent RO membrane can be prepared by plasma polymerization of allylamine. The big advantages of this technique over conventional casting methods are that the resulting membranes can be pinhole free and the rejecting layers can be made very thin, thereby producing membranes possessing high water fluxes. However, from the practical point of view, it seems to be very difficult to produce a uniform membrane at a good reproducibility by plasma polymerization, because this technique is highly dependent on the design of a discharge vessel [3], monomer configurations [4], discharge conditions, and so on.

It is well known that polymer surfaces can be modified when treated in a plasma without using organic gases, but we have found no papers or patents dealing with the preparation of RO membranes by plasma treatment so far. Therefore, we have studied the direct surface treatment of polymer films and have found that thin RO membranes can be prepared by the plasma treatment of water-soluble polymers [5]. In addition, we have found that out of many candidates plasma-treated porous PAN films show especially good RO properties.

This article discusses the influence of the preparation conditions on the RO characteristics of the final PAN membranes, taking a flat membrane as an example.

EXPERIMENTAL

The porous PAN films used for this study were prepared by casting on a glass plate or fabrics from *N,N*-dimethylformamide (DMF) solutions. The evaporation, coagulation in water, annealing in hot water, and drying were carried out in various conditions. The dried porous films ready for the plasma treatment were asymmetric and highly porous (50–70%) and exhibited no selectivity with respect to low-molecular-weight solutes such as NaCl. From electron micrographs, pores in the top surface could not be detected clearly and consequently they were estimated to be less than 100 angstrom in diameter.

The plasma reactor is illustrated in Figure 1. It consists of a 30-cm-diam glass bell jar containing two parallel disk electrodes. The discharge was sustained by a neon transformer by using low-frequency (60-Hz) ac.

A membrane was prepared by placing a 10-cm disk of dried porous films on a sample holding unit. The bell jar was evacuated to a base pressure of 0.01 torr. Then the desired flow of non-plasma-polymerizable gases was introduced. Once a stable pressure was established inside the system, the discharge was initiated by turning on the neon transformer. The discharge was then allowed to operate at a fixed condition, after which air was admitted.

Thus, obtained plasma-treated membranes were immersed in 1–12N of a mineral acid such as phosphoric acid, sulfuric acid, hydrochloric acid, etc. for 1–20 h to enhance water flux prior to RO testings. As a result of this acid treatment water fluxes of plasma-treated membranes increased by a factor of 2–10 while salt rejections remained unchanged. The details of the acid treatment have been described elsewhere [6].

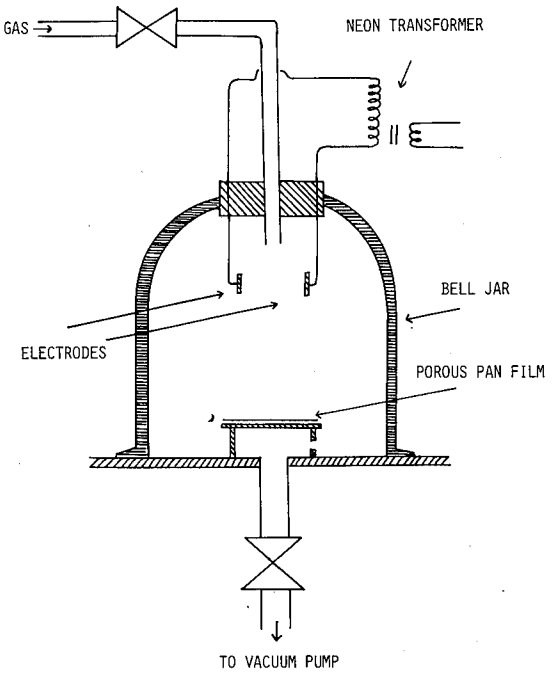

FIG. 1. Plasma reactor.

The RO tests were carried out in a test cell (membrane area = 13 cm^2) connected to a high-pressure (operating pressure = 50 kg/cm^2) brine (NaCl) recirculation loop. In all experiments the brine concentration was maintained at 0.5 wt % (π = 4 kg/cm^2) and the temperature of the brine was kept at 25°C. Each membrane was allowed to operate for a minimum of 20 h before the first sample of effluents was collected for the determination of water flux and salt rejection.

Water flux and salt rejection were determined by:

$$\text{Water flux (L/m}^2\text{ h)} = \text{Volume permeated/Membrane area/Time}$$

$$\text{Rej (\%)} = (1 - \text{Conc. permeate/Conc. feed}) \times 100$$

Chemical characterization of the membrane surfaces was obtained by ATFT-IR and ESCA. ATFT-IR and ESCA spectra were measured with a DIGILAB-FTS 15 spectrometer and a Shimadzu ESCA-650 B, respectively.

RESULTS AND DISCUSSION

Porous PAN Films and RO Properties

In the plasma polymerization the RO property of a plasma-deposited membrane is highly dependent on both starting porous substrate properties and plasma

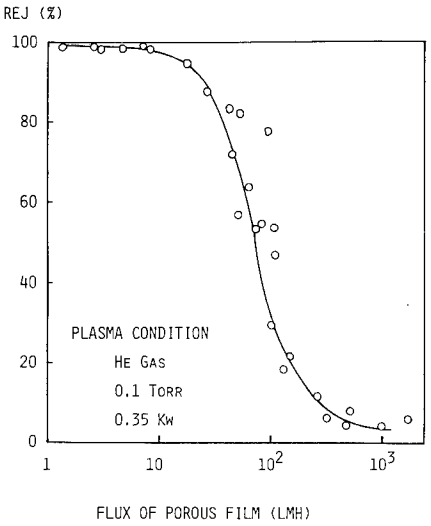

FIG. 2. Relation between water flux of starting porous PAN film (measured with distilled water at 25°C and 10 kg/cm^2) and salt rejection of resulting membrane after plasma treatment (obtained with 0.5% NaCl at 25°C and 50 kg/cm^2).

treatment conditions [1]. Therefore, in this study we have investigated the relationship between starting porous film properties and RO properties after plasma treatment. In the course of this study, we have found that regardless of the casting conditions of porous films there exists a good relationship between the pure water flux of porous films measured with distilled water under 10 kg/cm^2 at 25°C and the salt rejection of plasma-treated membranes under given plasma conditions although there are many factors in the casting process affecting the basic properties of the porous films. An example is given in Figure 2. This curve was obtained with He gas at 0.1 torr and 0.35 kW. By measuring the pure water flux of a given porous film at 10 kg/cm^2 we can estimate the salt rejection of the resulting RO membranes with this curve without doing the plasma treatment. In other words, Figure 2 shows that in order to obtain RO membranes exhibiting salt rejections greater than 98%, for example, under these plasma conditions, porous films having pure water fluxes less than 10 L/m^2 h (LMH) should be submitted to plasma treatment. Without the plasma treatment, these porous films show only slight salt rejections of around 10%.

Plasma Discharge Conditions

Plasma discharge conditions are also very important.

Experiments were carried out in various discharge conditions in order to establish the optimum conditions for RO membranes. For this purpose porous PAN films having a pure water flux of less than 10 LMH were used.

The water flux and salt rejection of the final membranes are shown in Figure

3 as a function of plasma treatment time. With the plasma treatment time the salt rejection first increases and then levels off around 98–99%. On the other hand, the water flux passes through a maximum during this course. Extended plasma treatment times have negative effects on the rejection of the final membranes. The results shown in Figure 3 can be explained by postulating the existence of three regions. In region 1 the hydrophilicity of plasma-treated surfaces increases remarkably and at the same time the crosslinking reaction begins to occur gradually, resulting in enhancement of both water flux and salt rejection. This is supported by the ESCA spectrum analysis, which is discussed below. In region 2 the incorporation of hydrophilic groups levels off and the thickness of surface crosslinked layer increases to depress the water flux. In region 3 the water flux increases suddenly and the salt rejection decreases remarkably, which indicates that the skin layer of the surface is etched off and a sublayer whose pore size is a little bit large compared with the initial surface is coming up to the surface.

Figure 4 shows the water flux and salt rejection of final membranes as a function of He gas pressure. In this case the water flux increases gradually and passes through a maximum and the salt rejection decreases slightly at higher pressures. The electric current is kept constant in this experiment and consequently the discharge wattage increases with decreasing discharge gas pressure. We thus conclude that with increasing discharge wattage, the incorporation of hydrophilic groups into polymer surfaces becomes an important factor in imparting high water flux and high salt rejection. And this is gradually replaced by the crosslinking reaction to result in the decrease in water flux.

What kind of gases are employed for this study is also very important. Figure 5 shows RO performance when some other non-plasma-polymerizable gases are utilized. According to this graph, H_2 and He are preferable because discharge

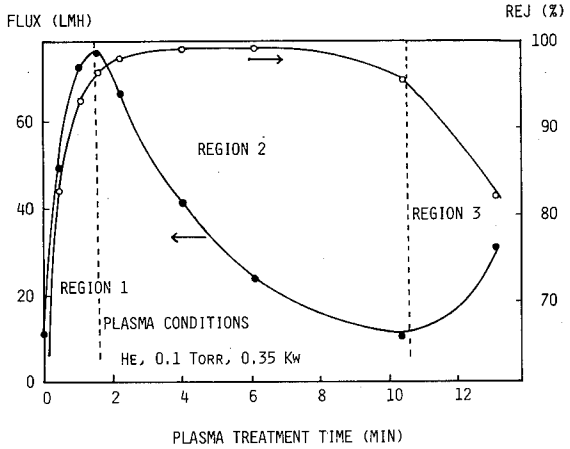

FIG. 3. Change of water flux and salt rejection as a function of plasma treatment time (RO operating conditions; 0.5% NaCl, 25°C, 50 kg/cm^2).

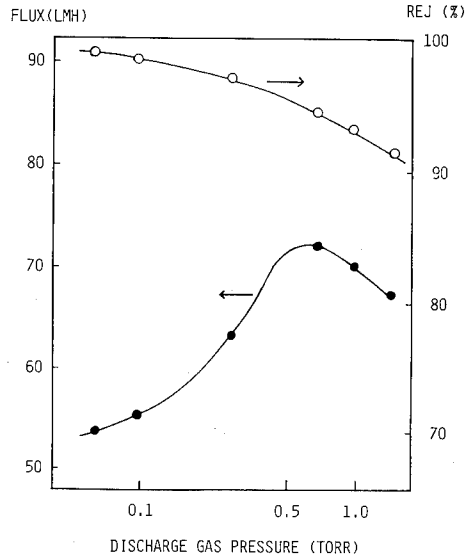

FIG. 4. Change of water flux and salt rejection as a function of He discharge pressure (RO operating conditions: 0.5% NaCl, 25°C, 50 kg/cm^2).

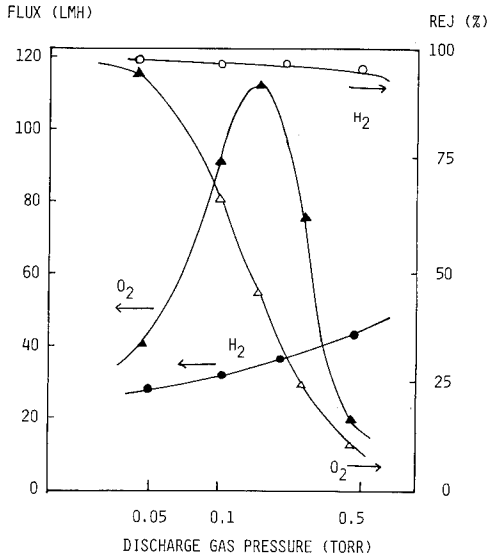

FIG. 5. Change of water flux and salt rejection as a function of discharge gas pressure in case of H_2 and O_2 gases (RO operating conditions: 0.5% NaCl, 25°C, 50 kg/cm^2).

conditions have only a slight effect on RO properties with these gases. However, in the case of O_2, air, and some other gases, RO properties are greatly affected by discharge gas pressure and also by discharge wattage. Of course we can fix the optimum conditions in these cases by experimentation. In other words, we can obtain RO membranes exhibiting high salt rejection by changing plasma conditions whatever gases may be employed. This means that in our cases plasma-excited gas molecules do not play an important role with respect to the surface modification of porous PAN films.

In this study it has been found that the different types of RO membranes with salt rejections ranging from 0 to nearly 100% can be easily prepared by changing the casting conditions and the plasma discharge conditions.

Crosslinking and Degradation

In general, it has been found that the plasma reaction is limited to a very thin surface layer of materials and that the crosslinking and the degradation of polymers seem to be involved [7,8]. Our plasma-treated membranes left thin and insoluble layers when immersed in DMF after treatment with gas plasma, indicating that a certain number of crosslinks were introduced by the plasma treatment. The thickness of the crosslinked layer was calculated by weighing the DMF-insoluble portion after it had dried. The crosslinked thickness increases with treatment time, as shown in Figure 6. This is coincident with the fact described already that the water flux goes down with plasma treatment time. Weight loss also increases linearly with plasma treatment time, which is a good indication that the degradation of the substrate surfaces is occuring at the same

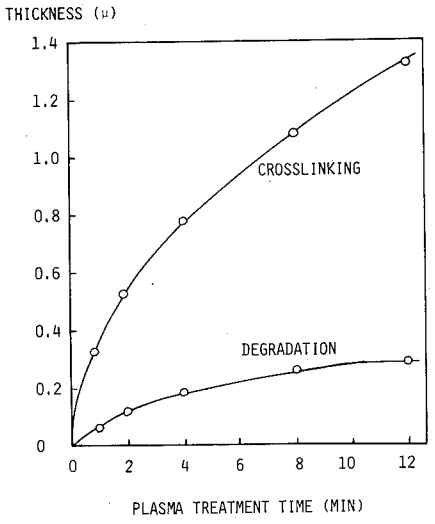

FIG. 6. Crosslinking and degradation as a function of plasma treatment time; plasma conditions: He gas, 0.1 torr, 0.35 kW.

time during the plasma treatment. When plasma discharge was initiated in our experiment, the pressure increase was always observed. This is also a good indication of the occurrence of surface degradation. The formation of a cross-linked layer in glow discharge under the conditions of this study can be considered as simultaneous reaction of plasma degradation and plasma-induced deposition of degraded gases.

Surface Analysis

The ATFT-IR spectra for porous PAN film (untreated substrate), plasma-treated membrane, and final membrane exhibiting salt rejection of 98% or more at fairly high water flux (after acid treatment) are shown in Figure 7. The spectrum of the plasma-treated membrane is quite similar to that of the final membrane. When the spectrum of the final membrane is compared with that of the porous PAN film, these two can be seen to differ appreciably; the following features are particularly notable: (i) a new absorption band appears at 1680 cm^{-1} which is attributed to >C═O and >C═N— stretchings, (ii) an absorption at 2240 cm^{-1} attributed to —C≡N stretching decreases remarkably, and (iii) a 3200–3600 cm^{-1} broad band assigned to —OH and >NH stretchings appears.

Examination of the plasma-treated membrane surface by ESCA indicates that oxygen increases with the plasma treatment time. This is shown in Figure 8. It is difficult to determine exactly where the oxygen incorporated at the membrane surface comes from, but it must be partly from the PAN itself, since our co-polymer consists of acrylonitrile and vinyl acetate, and partly from oxygen in

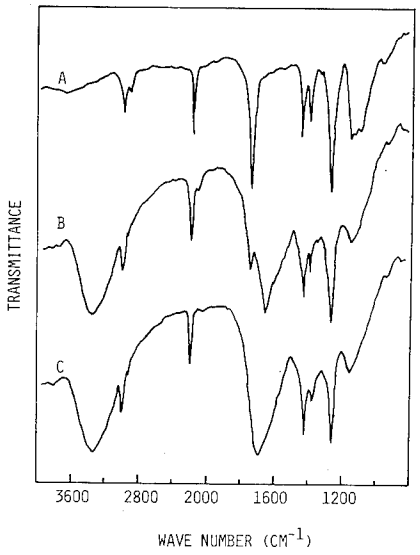

FIG. 7. ATFT-IR spectra of porous PAN film: (A) untreated substrate, (B) plasma-treated membrane, and (C) final membrane (after acid treatment).

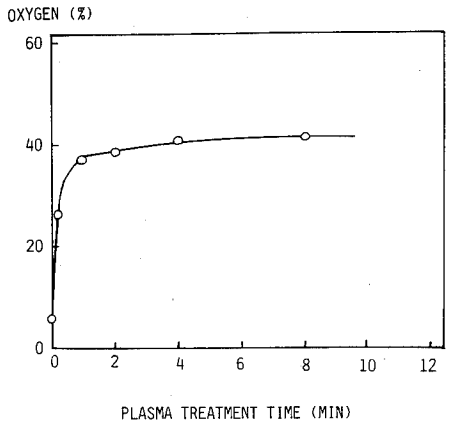

FIG. 8. Change of weight fraction of oxygen at the plasma-treated membrane surface calculated from ESCA spectra as a function of plasma treatment time; plasma conditions: He gas, 0.1 torr, 0.35 kW.

air introduced after the plasma treatment. However, the increase in oxygen at the surface observed by ESCA must be closely related to the IR bands, i.e., >C═O and —OH, newly appeared at 1680 and 3200–3600 cm^{-1}, respectively.

From ATFT-IR and ESCA analyses of membrane surfaces it is concluded that such hydrophilic groups as >C═O, —OH, and >NH have been introduced onto the substrate film, which seems to be responsible for the RO property.

Thin films obtained by plasma polymerization are said to change chemically with time [9]. But our plasma-crosslinked PAN membrane remains chemically and mechanically unchanged in atmosphere.

Membrane Characteristic Features

The final membrane thus obtained by the new method described above is characterized by high water flux and high salt rejection and has characteristics superior to those of conventional cellulose acetate membranes with respect to chemical resistance, heat resistance, organics removal, membrane compaction, and biological attack. In particular the membrane can reject all kinds of organic solutes with a molecular weight of more than 100 at above 90% rejection. Details of the membrane characteristics have been presented in a previous paper [10].

Recently, we have successfully produced a tubular module by applying this plasma technique to tubular membranes [10]. The tubular module is shown in Figure 9 and the module specifications are given in Table I. The tubular membrane is on the outer surface of a porous supporting tube (1 cm diam × 105 cm long) and the module, of external-pressure type, consists of 36 tubular membrane elements connected in series. For the plasma treatment of tubular membrane elements a 40-cm-diam × 130-cm-long cylinder containing a pair of pipe electrodes was used. The discharge conditions in this case were almost the same as

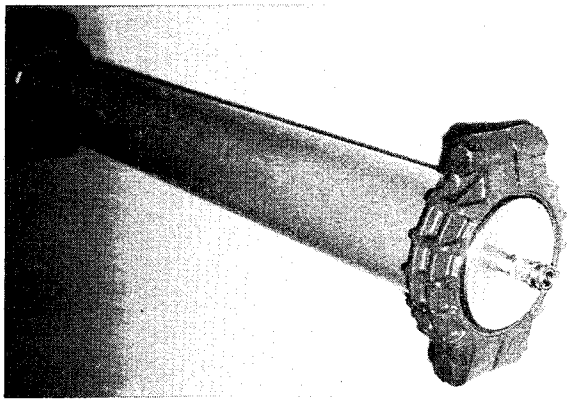

FIG. 9. Tubular module of plasma-treated PAN membrane.

those with the bell-jar-type reactor. For instance, power intensities were in the range of 0.1–0.7 kW. As far as the RO property of the standard tubular membrane is concerned, the water flux is now 60–70 LMH and the salt rejection is 98% when measured with 0.5% NaCl at 25°C and 50 kg/cm^2.

Since our plasma-treated PAN membrane has characteristics superior to those of conventional membranes, we have already constructed several commercial plants. The first one having a daily capacity of 15 m^3 of permeate water is for the effluents from an electrocoloring bath (see Fig. 10) and has been working smoothly for more than three years.

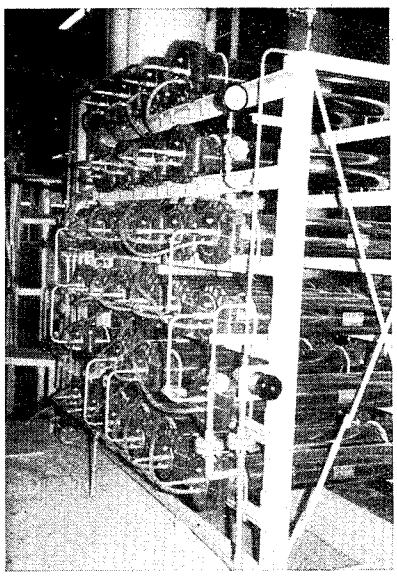

FIG. 10. Commercial plant of tubular modules of plasma-treated PAN membrane for effluents from an electrocoloring bath.

TABLE I
Module Specifications

Dimensions	1190 × 211 × 269 mm
Maximum operating pressure	70 kg/cm^2
Maximum operating temperature	45°C
pH range	1–10
Permeate productivity[a]	1.6–1.8 m^3/day
Salt rejection[a]	98%

[a]These two values were determined with 0.5% NaCl at 25°C and 50 kg/cm^2. The permeate productivity is larger than this when membranes of lower salt rejection are used.

REFERENCES

[1] H. Yasuda and C. E. Lamaze, *J. Appl. Polym. Sci., 17,* 201 (1973).
[2] A. T. Bell, T. Wydeven, and C. C. Johnson, *J. Appl. Polym. Sci., 19,* 1911 (1975).
[3] H. Yasuda and T. Hirotsu, *J. Polym. Sci. Polym. Chem. Ed., 16,* 313 (1978).
[4] H. Yasuda and T. Hirotsu, *J. Polym. Sci. Polym. Chem. Ed., 15,* 2749 (1977).
[5] T. Sano, T. Shimomura, and M. Sasaki, presented at the 9th Symposium on Plasma Chemistry, Osaka University, 1979.
[6] T. Sano, T. Shimomura, and I. Murase, U.S. Pat. 4,268,662 (May 18, 1981).
[7] H. Yasuda, C. E. Lamaze, and K. Sakaoku, *J. Appl. Polym. Sci., 17,* 137 (1973).
[8] R. H. Hansen, J. V. Pascal, T. De Benedicts, and P. M. Rentzepis, *J. Polym. Sci. A, 3,* 2205 (1965).
[9] H. Yasuda, M. O. Bumgarner, H. C. Marsh, and N. Morosoff, *J. Polym. Sci. Polym. Chem. Ed., 14,* 195 (1976).
[10] T. Sano, *Chem. Econ. Eng. Rev., 12* (5), 22 (1980).

PLASMA POLYMER COATINGS FOR INDOOR CORROSION PROTECTION

W. O. FREITAG*
Materials Research, Sperry Univac, P.O. Box 500, Blue Bell, Pennsylvania 19424

H. YASUDA and A. K. SHARMA†
Graduate Center for Materials Research, University of Missouri–Rolla, Rolla, Missouri 65401

SYNOPSIS

Plasma polymers of methane, acetylene, tetrafluoroethylene, and tetramethylbisiloxane were applied as protective coatings for magnetic alloys in office and room environments. The *W/FM* parameter, i.e., energy input per mass unit of monomer, was found to be a critical parameter as far as the corrosion resistivity of the coating is concerned. A remarkable increase of this resistivity was observed when *W/FM* exceeded 10^{10} J/kg. Methane is the most practical monomer in such applications, i.e., applications which require high *W/FM* values, since owing to its very low molecular weight it can be polymerized in relatively higher-energy inputs.

INTRODUCTION

One of the advantages of plasma polymers as protective coatings for metals and alloys is the possibility that an extremely thin layer (<1 μm) of coating having a good corrosion resistance can be applied in a flawless and uniform manner. Coatings of conventional polymers at this level of thickness hardly provide protection against corrosion due to flaws inherent in ultrathin films and to the difficulty of obtaining good adhesion of films to metallic surfaces.

The potential of plasma polymers as corrosion protection coatings had been explored in the early stage of the recognition of technology known today as

*Present address: InterFact Associates, Ltd., 1613 Kenmare Dr., Dresher, PA 19025.
†Present address: Applied Membrane Technology, Inc., 11558 Encore Circle, Minnentonka, MN 55343.

Journal of Applied Polymer Science: Applied Polymer Symposium 38, 185–191 (1984)

CCC 0570-4898/84/010185-07$04.00

plasma polymerization [1,2]; however, no convincing superiority of a plasma polymer coating over conventional coatings was demonstrated in those early studies. Perhaps the first demonstration of the superiority of plasma polymer coatings over conventional polymers was described by Schreiber, Tewari, and Wertheimer [3], who showed that a plasma polymer of thiophene deposited by microwave plasma on carbon steel and Monel protected the substrate from corrosion by an alkali medium ($10^{-4}M$ LiOH) at a temperature of 300°C. In a recent study, Schreiber, Wertheimer, and Wróbel [4] reported corrosion protection characteristics of plasma polymers of organosilicone monomers under a simulated sea environment.

One application of the plasma polymer coatings which is closely related to our interests has been recently reported by Harada [5]. In an attempt to improve the durability of the Ni–Co–P films chemically deposited on magnetic computer disks, Harada applied plasma polymers from toluene-2,4-diisocyanate, α-pyrrolidone, tetrafluoroethylene, and hexafluoropropylene. A thickness heterogeneity of less than 5% over a 140-cm^2 area was obtained by proper choice of plasma conditions. It was found that very thin (1000–1500 angstrom) plasma polymer coatings can impart good abrasive durability to magnetic disks, without causing any magnetic deterioration or instability.

Plasma-polymerized styrene and acetylene, 250 angstrom thick, have been described for wear and corrosion protection in experimental video disks, and overcoats in this thickness range could prove useful in magnetic recording systems [6,7].

This article discusses plasma polymers of methane, acetylene, tetrafluoroethylene, and tetramethyldisiloxane, prepared under various conditions of plasma polymerization as protective coatings for magnetic alloys in office and computer room environments.

EXPERIMENTAL

Preparation of Coatings

The substrates used for coating were 1-in.-diam glass wafers coated with sputtered 20 Fe–80 Ni alloy films 2000–4000 angstrom thick. Plasma polymerization was conducted in a bell jar reactor using aluminum electrodes approximately 320 cm^2 in area separated by an electrode gap of 7.7 cm. The details of the reactor geometry were reported earlier [8]. A magnetically enhanced plasma was used. The electrodes were cleaned and dried each time in order to ensure the reproducibility of the results. The samples were examined in an optical microscope (in order to see the integrity of the inorganic coatings) and blown with dust cleaner prior to mounting on a circular, perforated, aluminum substrate holder. The latter was rotated in between the two electrodes by magnetic coupling to a motor placed outside the bell jar reactor. The plasma was created by passing monomer vapors from the group of monomers (methane, acetylene, tetrafluoroethylene, and tetramethyldisiloxane) selected for this study. Power was sup-

plied to the system by a Crown model M-600 amplifier at a fixed audio frequency of 10 kHz. Three different thicknesses, 200, 400, and 800 angstrom, of each monomer were deposited under widely varying plasma polymerization conditions.

A quartz crystal thickness monitor (Kronos, Inc., OM-301) placed close to the substrate holder inside the bell jar reactor was used for this purpose. The effect of an inert-gas plasma pretreatment was also studied. The monomer flow rate, discharge power, and reactor pressure, although varied from run to run, were always in the range of 0.1–10.0 cm^3/min, 10–200 W, and 1–100 mtorr, respectively. After polymer deposition, the bell jar was reevacuated for 2–10 h then vacuum released and samples subjected to corrosion testing.

Corrosion Testing

Plasma-coated and uncoated wafers were exposed to an accelerated indoor atmosphere consisting of 300 ppb SO_2 and 300 ppb NO_2 in air at 75% RH and 20.0°C. Total air flow through the 1-L chamber was about 1.5 L/min. This system has been shown [9] to provide an acceleration factor of about 100–300 compared with an average indoor office area.

The degree of corrosion was estimated by measuring the amount of light scattered normal to the sample surface when the sample is illuminated by two light beams incident at 45°. With uncorroded samples, specular reflection predominates and very little light is scattered. When surface roughness appears due to corrosion, each irregularity contributes to light scatter. A scheme similar to this was used by Phipps [10].

The fixture for this measurement is shown in Figure 1. A Dolan–Jenner Fiberlite source was fitted with a Y fiber optic light pipe, the ends of which were mounted in a hollow aluminum block. A pair of 12-mm-focal-length simple lenses focused the beam to illuminate the sample area, about 25 mm diameter. An image of the sample was focused onto the silicon photovoltaic cell of a power meter (Coherent Radiation Labs model 212) by a 28-mm-focal-length $f/2.8$ lens; this measured the intensity R of the light scattered from the 14-mm-diam central area of the sample. The intensity of the light source was adjusted to give a standard reading (300 μW in the present case) from an Al_2O_3 wafer placed in the sample position.

The scattered light intensity R_t was measured as a function of time t in the corrosion system and plotted as $R_t - R_0$ vs. t. Surface imperfections in the sputtered film, such as scratches or defects in the glass substrate, contributed a constant intensity to R_0 and R_t since they did not change during corrosion. Hence the difference $R_t - R_0$ was chosen to characterize the corrosion rather than their ratio. Uncorroded samples typically had $R_0 = 0.3$–0.8 μW and those readings were reproducible within ±0.01 μW.

The onset of corrosion was marked by a very rapid rise in $R_t - R_0$ after some induction time. By the time $R_t - R_0$ exceeded about 0.05 μW, the slope was quite steep. Unprotected metal samples reached $R_t - R_0$ values of 1–3 μW in

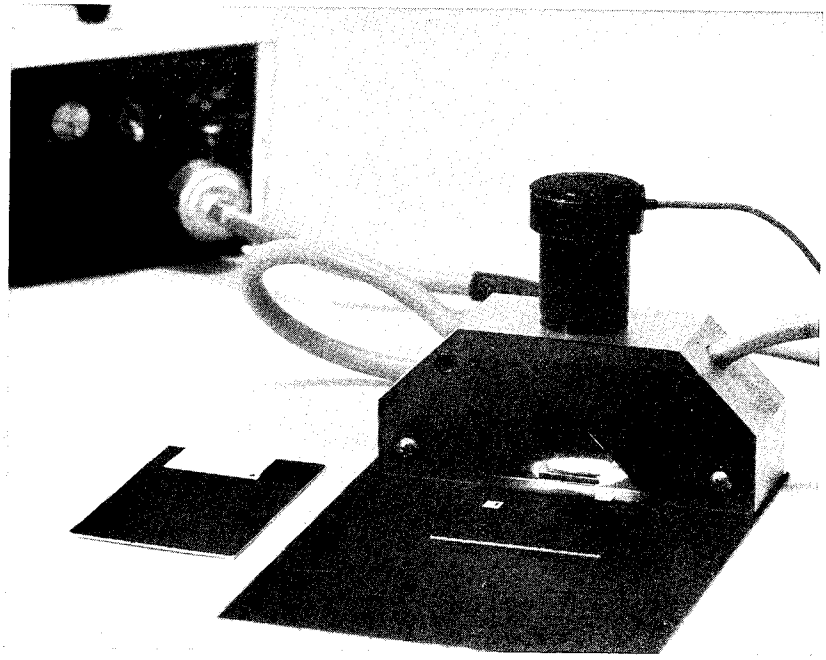

FIG. 1. Fixture used to measure light scattered by sample surface. Fiber optic illuminators are mounted at 45°; lens and detector are in the cylinder on top. Sample is shown in place in illuminated cavity; Al_2O_3 standard is at left.

about 10 h, but most experiments were not carried much beyond the induction time. Samples could be stored in a desiccator for extended periods of time with no change in R. This was true even for partially corroded wafers.

RESULTS AND DISCUSSION

Plots of $R - R_0$ versus exposure time for typical measurements are shown in Figure 2. As seen in the figure, a distinctive initiation time τ characteristic of plasma polymer coatings can be estimated.

Where films of well-defined thickness ranges prepared under nearly identical plasma polymerization conditions were available, τ is shown to increase with film thickness l as shown in Figure 3.

It should be noted that the time lags of diffusion, which is given by $l^2/6D$, for gases and water vapor through 1000-angstrom-thick film are expected to be less than a second (even in the case of $D = 10^{-10}$ cm^2/s). Therefore, the corrosion initiation times τ, which are on the order of hours, are not a direct reflection of the diffusional time lags of corrosive gases and water vapor. Under these circumstances, it seems reasonable to think that the corrosion initiation time τ is related in a more complex manner to the total flux of gases and water vapor which is given by $\Sigma(P_i/l)$, where P_i is the permeability constant of the ith

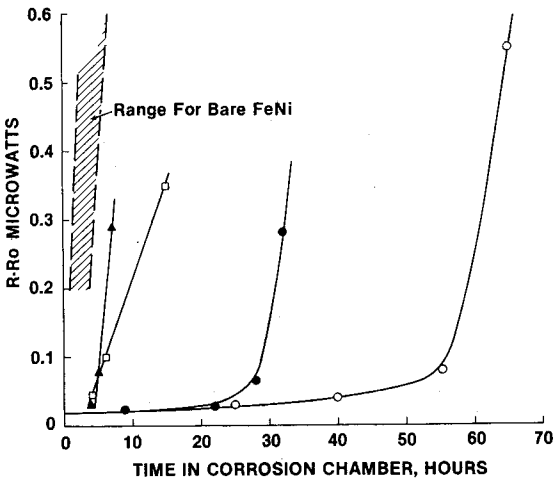

FIG. 2. Change in the intensity of light scattered by FeNi samples covered by various plasma films, with time in the corrosion chamber: (○) methane, 1050 Å, (●) acetylene, 950 Å, (□) TMDSiO, 1000 Å, (▲) TFE, 330 Å.

component and l is film thickness. Thus, it is anticipated that τ is proportional to the film thickness. As shown in Figure 3, for plasma polymers prepared under similar conditions with different thicknesses τ increases with l.

In order to find the correlation between τ obtained under different thickness and plasma polymerization conditions, τ/l is taken as the specific corrosion resistance parameter in this study.

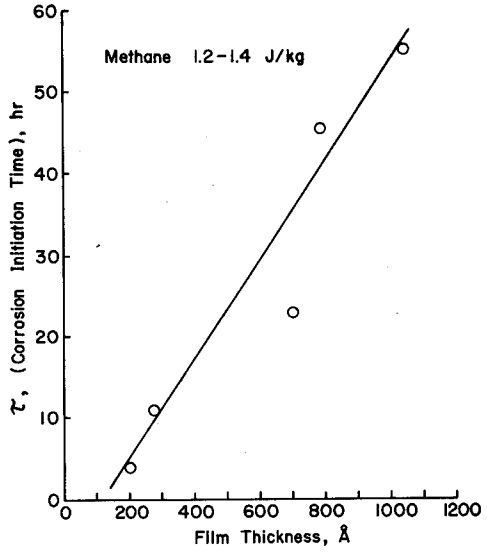

FIG. 3. Dependence of corrosion initiation time on the coating thickness; methane, 1.2–1.4 J/kg.

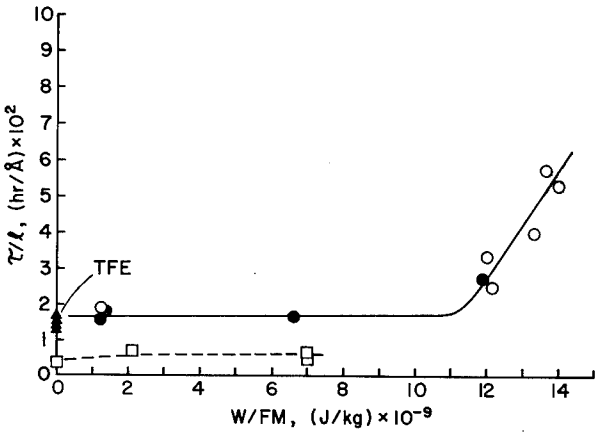

FIG. 4. Dependence of specific corrosion resistance τ/l of plasma polymers on the energy input parameter W/FM (in J/kg): (○) methane, (●) acetylene, (□) TMDSiO, (▲) TFE.

Studies of the gas permeability of plasma polymers comparable to ones used in this study indicate that the permeation of small gas molecules through plasma polymers is not truly represented by a solution diffusion mechanism but by one of flow through a porous medium [11]. Although the permeability constants of some plasma polymers are very low, their pressure dependence and permeability ratios, e.g., $P(CO_2)/P(O_2)$, $P(O_2)/P(N_2)$, etc., suggest very little contribution of solubility, indicating a lack of mobility of polymer segments. Thus the increase of film thickness is seen as an effective increase of permeation path length through a rigid polymer matrix.

Assuming the linear dependence of τ on the film thickness, the characteristic corrosion resistivity of plasma polymer coatings may be represented by a parameter τ/l.

In Figure 4, the values of τ/l are plotted against the value of W/FM expressed in J/kg, where W is wattage, F is monomer volume flow rate, and M is molecular weight of monomer. The parameter W/FM is considered an important parameter of plasma polymerization and represents the energy input per unit mass of monomer [12].

A remarkable increase of corrosion resistivity is observed as the W/FM value exceeds 10^{10} J/kg. Below this level, the resistivity is marginal (less than 2×10^{-2} h/angstrom) and depends little on W/FM or monomer type. It is interesting to note that acetylene and methane behave in a nearly identical manner. An advantage of methane is seen in that high W/FM values can be obtained practically at relatively low levels of wattage owing to the small value of M. Because of the limitations of the equipment, higher W/FM values for TFE, TMDSiO, and acetylene could not be obtained in this study.

REFERENCES

[1] R. M. Brick and J. R. Knox, *Mod. Packag.*, 123 (1965).
[2] T. J. Williams, *J. Oil Colour Chem. Assoc.*, *48*, 936 (1965).

[3] H. P. Schreiber, Y. B. Tewari, and M. R. Wertheimer, *Ind. Eng. Chem. Prod. Res. Dev., 17*(1), 27 (1978).
[4] H. P. Schreiber, W. R. Wertheimer, and A. M. Wróbel, *Thin Solid Films, 72,* 487 (1980).
[5] K. Harada, *J. Appl. Polym. Sci., 26,* 3707 (1981).
[6] D. L. Ross, *RCA Rev., 39, 136,* 161 (1978).
[7] G. Kaganowicz, J. W. Robinson, and H. Yasuda, U.S. Pat. 4,137,550.
[8] N. Morosoff, W. Newton, and H. Yasuda, *J. Vac. Sci. Technol., 15,* 1815 (1978).
[9] W. O. Freitag, in *Atmospheric Corrosion,* W. H. Ailor, Ed., Interscience, New York, 1982.
[10] P. B. P. Phipps, *IEEE Trans. Magn.,* M-15(6), 1839 (1979).
[11] T. Haraguchi and H. Yasuda, unpublished data.
[12] H. Yasuda and T. Hirotsu, *J. Polym. Sci. Polym. Chem. Ed., 16,* 743 (1978).

MODIFICATION OF PAPER SURFACE PROPERTIES BY MICROWAVE PLASMAS

M. F. BOTTIN and H. P. SCHREIBER*
Department of Chemical Engineering, Ecole Polytechnique, P.O. Box 6079, Station A, Montreal, Québec H3C 3A7, Canada

J. KLEMBERG-SAPIEHA and M. R. WERTHEIMER
Department of Engineering Physics, Ecole Polytechnique, P.O. Box 6079, Station A, Montreal, Québec H3C 3A7, Canada

SYNOPSIS

A large-volume microwave plasma (LMP) apparatus has been used to polymerize organosilicone and styrene vapors onto paper substrates. Polymerization rates were established in the active glow of the plasma and in the dark, downstream volume of the reactor. Rates decrease from about 70 Å/s in the former to about 1 Å/s in the latter space. Surface modifications of paper substrates were studied by measurements of contact angles, of resistivity, and of charge retention properties. Plasma–polymer layers increased water contact angles from about 45° for control paper samples to >110° for plasma-treated specimens. Resistivity was increased by up to four orders of magnitude, and the charge retention of coated papers was increased significantly. Controlled variations of the environment into which materials were placed immediately after plasma polymerization led to changes in the property balance of paper, confirming that plasma–polymer surfaces remain in active states for some time following quenching of the plasma.

INTRODUCTION

Plasma processes are the subject of increasingly intensive fundamental study, and equally of efforts to find useful applications for their effects. In these laboratories work has been concentrated on both aspects of plasmas sustained by microwave power, in a large-volume microwave (LMP) apparatus [1,2]. In recent months several studies have been conducted to show the range and potential usefulness of surface modifications brought about by LMP treatments of nu-

*To whom all correspondence should be addressed.

Journal of Applied Polymer Science: Applied Polymer Symposium 38, 193–200 (1984)

CCC 0570-4898/84/010193-08$04.00

TABLE I
Examples of Plasma-Induced Surface Modifications

Substrate	Plasma treatment	Effect	Reference
Steel, Monel, and other alloys	Thiophene, aniline, perfluorobutene-2	Passivation of alkali to 400°C	3
Mica	NH_3, C_2H_4, others	Control of surface wettability	1
Mica	C_2H_4, styrene	Improved reinforcement in polyolefins and polyblends	2
$CaCO_3$	Butyl alcohol, butyl amine	Control of dispersion, reinforcement in PVC	4
Kapton	Organosilicone	Reduced water transport in membranes	5

merous substrates. An abridged overview of this work, given in Table I, shows some of the organic and inorganic vapors used in plasma treatments, the substrates involved, and the advantages sought by the plasma route.

The present study was intended to modify selected surface properties of paper. The quest to alter some of the more deficient properties of cellulosic materials is a pervading one, grafting, *in situ* polymerization, interfacial polymerization, and encapsulation being among the techniques applied to this end [6]. One interesting approach, followed by Fisa, Revol, and Marchessault [7], encapsulated paper in linear polyethylene by performing the Ziegler–Natta polymerization of the olefin with catalysts deposited on the cellulose fibers. Distinct modification of mechanical and optical properties could be carried out in this manner. Although the principles of the earlier approach [7] differ greatly from those involved here, there is a general similarity in the ends sought; that is, to modify selected properties of paper substrates in a controlled manner. The present work thus reports on a brief exploration in which LMP treatments were applied to paper substrates to modify wetting and electrical properties, and to establish the feasibility of depositing on paper, plasma polymers of organosilicone, and styrene monomers. Also reported is additional information on polymer deposition kinetics in LMP apparatus, and on the modification of plasma–polymer properties through control of the environment to which the freshly formed polymer is exposed after the plasma is extinguished.

EXPERIMENTAL

The principles of the LMP apparatus and our procedures have been reported earlier [1–3]. In the present case, a tubular quartz reactor, about 4 cm in diameter and 110 cm long, was employed. A glass scale was placed along the length of the vessel to allow precise location of substrate samples. As before, the apparatus was operated from a 2.5-kW microwave power source (2.45 GHz). The reactor was placed over the slow-wave structure of the assembly so as to give a uniform

glow discharge over the initial 30 cm length of the tube. Paper substrates ca. 3 × 5 cm were plasma treated in the active glow as well as in the downstream dark space. A conductivity base paper (cbp) and a standard xerographic paper (sp) served as substrates.

Hexamethyldisiloxane (HMDSO) and styrene (S) vapors were used in LMP reactions, the former at ca. 0.5 torr, the latter near 1-torr pressure. Substrate temperatures T_s ranged from room temperature to 110°C. Following extinction of the plasma, the still-active surface of specimens was conditioned for several hours in one of three ways: condition A: air was admitted at once to the reactor; condition B: the reactor was flooded with He gas at 1 atm for several hours prior to removing substrates; condition C: the reactor was let down to the saturation vapor pressure of monomer prior to removing substrates. As in previous work [8,9] plasma polymers were analyzed by internal reflectance IR, and deposition rates were determined by gravimetric measurements.

PLASMA-MODIFIED-PAPER PROPERTIES

Wettability

Contact angles for water, diiodobenzene, nitrobenzene, and for aqueous solutions of propionic acid were determined photographically, following the method described by Carré and Schreiber [10]. Contact angles were then used to compute the critical surface tension γ_c by applying the familiar Zisman method [11].

Electrical Properties

Initial results on the surface resistivity of specimens are reported by way of illustrating the effects attainable. The resistivity was calculated from experimental data of applied voltage and current flowing from specimens of known geometry. A Keithley 610 C electrometer was used.

Charge retention properties were evaluated by exposing paper samples to a corona discharge from a sharp point in dry air and with a total potential difference of 4 kV. Surface-charged samples were transferred to a Monroe Instruments Isoprobe apparatus, in a closely controlled procedure, maintaining constant transfer time. The initial charge on samples clearly varied, but this was entirely due to inherent properties of the materials and not to random effects of the experimental procedure. The Isoprobe was operated at 25°C and 50% relative humidity; a strip chart recorder followed charge decay to steady states, generally over periods ranging from less than 2 min for control samples to more than 60 min for plasma-modified substrates.

RESULTS AND DISCUSSION

The chemical characteristics of P–PHMDSO, as inferred from IR measurements, were very similar to those reported earlier [3,4] for glass and metal

substrates. Principal absorption peaks for polymers made in the active glow discharge were observed at 800 cm^{-1} [ν(Si—C) in $Si(CH_3)_2$], 840 cm^{-1} [ν(Si—C) in $Si(CH_3)_3$], 1000–1100 cm^{-1} [ν_{as}(Si—O—Si)], 1260 cm^{-1} [$\delta(CH_3)$ methylsilyl], 2120 cm^{-1} [ν(Si—H)]. Clearly the polymers are of unusual structure and warrant their plasma prefix. Further evidence of this uniqueness lies in the high inorganic content in plasma-polymerized organosilicones, as reported previously [8,9]. The plasma polymerization mechanism for these monomers appears to be little affected by the chemistry of the substrate, at least in the later stages of polymerization, producing polymer thickness in the range above 10^3 Å.

The effect of substrate position on reaction kinetics in the LMP apparatus is demonstrated by the results of Figure 1. Rates of polymerization in the active glow of the plasma were measured to be 70 Å s^{-1}, once again in very satisfactory agreement with earlier measurements [8,9]. As the paper substrates were moved downstream, a systematic decrease in polymer buildup was observed, the rate falling to about 2 Å/s some 40 cm downstream from the glow portion of the plasma. Evidently the decay rates of reactive species are such as to strongly reduce their population outside the visible glow portion of the reaction space. Film thicknesses obtained in experiments with substrates placed in the dark space were not sufficient to provide accurate analytic information as to structure or properties. It is expected, however, that significant changes in the composition of plasma constituents occur and, as a result, that corresponding changes take place in polymerization mechanisms and in the chemical composition of the product. These aspects of LMP processes are under ongoing study.

The profound influence exerted by the presence of thin plasma–polymer films on paper surface properties is illustrated qualitatively in Figure 2. This compares the contact angle of water on cbp before and after the deposition of a ca. 1000-angstrom-thick layer of P–PHMDSO. A more detailed survey of results is given in Table II. This shows contact angles for the polar water molecule and for diiodobenzene, a much less polar species, as well as listing calculated γ_c values and surface resistivities.

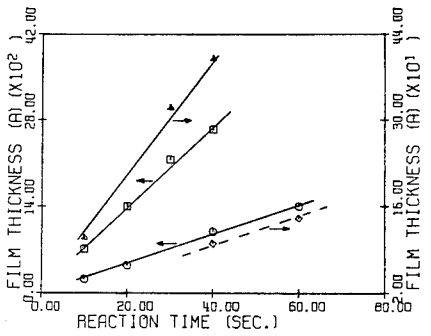

FIG. 1. Variation of P–PHMDSO deposition rates with placement of paper substrates in reactor: (□) active glow space, (○) 10 cm downstream, (△) 25 cm downstream, (◇) 40 cm downstream.

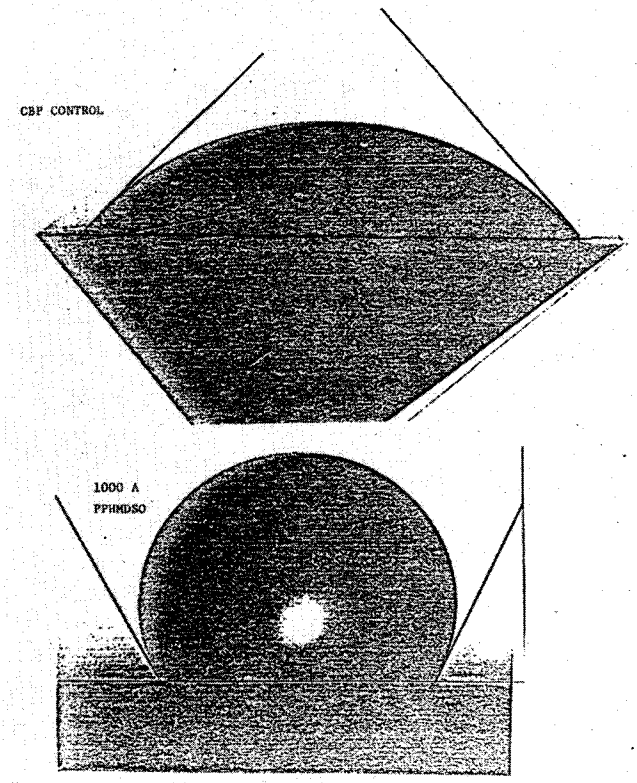

FIG. 2. Contact angles of water droplet on unmodified conductivity-base paper, and after deposition of plasma polymer.

The contact angle for water on cbp substrates is greatly increased by the presence of hydrophobic plasma polymers based on HMDSO and styrene. Comparatively, the contact angles of organic liquids on plasma-modified cbp are influenced much less, as illustrated in the case of diiodobenzene. In the Zisman procedure, fitting a linear section to the experimental data therefore produces relatively little change in the γ_c value for this material. The sp substrate, on the other hand, being inherently hydrophobic, responds much more strongly to plasma treatment in terms of its wettability by the less polar fluids. Consequently, γ_c here is changed appreciably, while the water contact angle simply remains near or at the experimental limit of measurement. Evidently, the effects of plasma treatment on hydrophobic–hydrophilic property balances depend both on the characteristics of the substrate and on the choice of monomer to be polymerized on that substrate.

The surface resistivity of paper is also strongly influenced by plasma treatment. Typically, increases of the order of 10^2–10^4 occur. In this regard, for example, the resistivity of cbp overcoated with P–PHMDSO becomes the rough equivalent of standard paper, while the latter is readily raised by such treatment into the range 10^{12} $\Omega/\square$.

TABLE II
Summary of Wetting and Surface Resistivity: Plasma-Modified Paper

	Contact angles (deg)			
	Water	DIB	γ_c (dyn cm^{-1})	ρ ($\Omega/\square$)
Control cbp	52	40.5	48.5	3.38×10^6
P–PHMDSO (1000 Å)				
T_s = amb.				
Cond. A	100	39.5	42.0	2.7×10^8
Cond. B	115	37.5	38.0	6.3×10^9
Cond. C	>120	37.5	41.5	2.0×10^9
T_s = 100°C				
Cond. A	103	39.5	42.5	4.4×10^8
Cond. B	>120	37.5	41.0	5.2×10^9
Cond. C	>120	36.5	41.0	
P–PS (ca. 1000 Å)				
Cond. B	107	36.5	44.0	7.7×10^8
Control sp	110	36	46.5	2.1×10^9
P–PHMDSO (1000 Å)				
T_s = amb.				
Cond. A	120	31.5	40.0	1.3×10^{10}
Cond. B	>120	29.0	39.0	3.0×10^{12}
Cond. C	>120	28.0	36.0	6.5×10^{12}
T_s = 100°C				
Cond. A	115	30.0	41.5	1.4×10^{10}
Cond. B	>120	28.5	37.0	4.4×10^{12}
Cond. C	>120	28.5	34.5	8.0×10^{12}

Particularly interesting in Table II are the effects of post-plasma treatment. It is known that surfaces retain appreciable reactivity for some time after plasma treatment as free radicals and other reactive species respond to their environment. Reactions with atmospheric gases, oligomerization, and crosslinking may be proposed as typical post-plasma occurrences. The data in Table II indicate the apparent effects of these reactions. Condition A should promote surface oxidation, as suggested particularly by the lower resistivity of specimens and by a lower H_2O contact angle than is obtained under conditions B and C. The averaging effects of the Zisman procedure, however, again are such as to make γ_c relatively insensitive to these effects. Slight differences between conditions B and C are discerned in resistivity, however. These observations could be accounted for if greater surface porosity (and surface area) were produced under condition B. The supposition seems reasonable, as under the other post-plasma-treatment conditions this porosity is more likely to be moderated. The effect of T_s on measured surface properties seems slight; we have shown previously, however, that much stronger adhesion and cohesion of plasma–polymer films is obtained at higher reaction temperatures, and suggest a similar consequence in this case.

TABLE III
Comparison of Charge Retention Behavior

	Decay parameter (s)		
	τ_1	τ_2	τ_3
Control sp	0.11	0	0
P–PHMDSO			
T_s = amb. Cond. A			
1000 Å	0.12	2.74	205
2000 Å	0.68	10	278
Cond. B			
1000 Å	0.14	3.04	218
2000 Å	0.72	11	285
P–PS			
T_s = amb. Cond. A			
2000 Å	0.86	14	343

Charge retention characteristics were measured for sp substrates only, because of limitations imposed by available experimental facilities. As noted, the initial surface charge on substrates could not be determined accurately; nevertheless reproducible evidence was obtained to show that charge retention also is very strongly enhanced by LMP treatments. Charge loss rates were followed for extended times, generating smooth decay curves that could be fitted by an expression of the type

$$V = V_0 e^{-t/\tau_1} + V_1 e^{-t/\tau_2} + V_2 e^{-t/\tau_3}$$

where τ_1, τ_2, τ_3 are charge-decay parameters; t is the decay time (s); and V_0, V_1, V_2 are voltage parameters. Values of τ are given in Table III. These show that initial charge decay, as indicated by τ_1, is significantly reduced by P–PHMDSO; furthermore, subsequent decay is greatly attenuated, as shown by the τ_2 and τ_3 values. In general, thicker plasma–polymer layers improve charge retention; postpolymerization controls also affect the performance. Since P–PHMDSO is a largely inorganic polymer with appreciable polar group content, P–PS may be a more effective surface coating for paper when attenuated charge decay is sought. The single datum available at this writing is consistent with the expectation.

CONCLUSION

Appreciable control over surface wetting, and electrical properties of paper can be exercised by depositing plasma–polymer layers on paper substrates. Surface resistivity and charge decay in particular can be varied to a large extent by this means. Plasma polymerization is readily carried out on paper and proceeds at rates comparable to those measured on metal, glass, and other substrates.

The authors thank Xerox Research Center of Canada Ltd. for their financial and material support of this work; additional support was received from the Natural Sciences and Engineering Research Council of Canada. They also thank Dr. S. Sapieha for useful comments.

REFERENCES

[1] A. Bialski, R. St.J. Manley, M. R. Wertheimer, and H. P. Schreiber, in *Plasma Chemistry of Polymers,* M. Shen, Ed., Dekker, New York, 1976, pp. 241–250.
[2] H. P. Schreiber, M. R. Wertheimer, and A. U. Sridharan, in *Plasma Polymerization,* ACS Symp. Ser. 108, M. Shen and A. T. Bell, Eds., Am. Chem. Soc., Washington, DC, 1979, pp. 287–298.
[3] H. P. Schreiber, Y. B. Tewari, and M. R. Wertheimer, *Ind. Eng. Chem. Prod. Res. Dev., 17,* 27 (1978).
[4] H. P. Schreiber, M. R. Wertheimer, and M. Lambla, *J. Appl. Polym. Sci., 27,* 2269 (1982).
[5] E. Sacher, J. Susko, J. Klemberg-Sapieha, H. P. Schreiber, and M. R. Wertheimer, in *Proceedings, American Chemical Society Symposium on Plasma Chemistry,* Kansas City, 1982, Am. Chem. Soc., Washington, DC, 1982.
[6] B. Fisa and R. H. Marchessault, *J. Appl. Polym. Sci., 18,* 2025 (1974).
[7] B. Fisa, J. F. Revol, and R. H. Marchessault, *Tappi, 59,* 88 (1976).
[8] A. M. Wróbel, M. R. Wertheimer, J. Dib, and H. P. Schreiber, *J. Macromol. Sci. Chem., 14,* 321 (1980).
[9] A. M. Wróbel, J. Klemberg, M. R. Wertheimer, and H. P. Schreiber, *J. Macromol. Sci. Chem., 15,* 197 (1981).
[10] A. Carré and H. P. Schreiber, *J. Coat. Technol., 54,* 31 (1982).
[11] W. A. Zisman, *Adv. Chem. Ser., 43,* 1 (1964).

EFFECTS OF GLOW DISCHARGES ON FIBERS AND FABRICS

TAKESHI YASUDA
Department of Textile Science, Mukogawa Women's University, Nishinomiya, Japan

MACIEJ GAZICKI and H. YASUDA
Graduate Center for Materials Research, University of Missouri–Rolla, Rolla, Missouri 65401

SYNOPSIS

The effect of plasma treatment on different fibers and fabrics has been studied. Four nonpolymerizing gases were used: helium, air, nitrogen, and tetrafluoromethane. It has been found that in some cases the etching of the fiber was accompanied by the implantation of the specific atoms onto its surface. The model studies performed with nylon 6 have shown that plasma treatment similar to plasma polymerization may be carried out in the power-deficient range as well as in the gas-deficient range. Finally, the wettability of many hydrophilic fabrics has been substantially decreased by using tetrafluoromethane plasma treatment.

INTRODUCTION

Modification of polymer surfaces by means of plasma treatment has been studied for at least two decades. Usually two different processes are referred to as plasma treatment of polymer surfaces. One is plasma polymerization, i.e., the deposition of the thin, highly crosslinked polymer film on the surface of the material, and the other is the surface modification of the structure of the material itself (such as surface crosslinking for instance) under the influence of the glow discharge. The above distinction is somewhat simplified since, owing to ablation, both of these phenomena occur simultaneously in the case of polymeric substrates. Which of the processes is predominant, however, strongly depends on the nature of the gas or the vapor used in the glow discharge. Most of the

Journal of Applied Polymer Science: Applied Polymer Symposium 38, 201–214 (1984)

CCC 0570-4898/84/010201-18$04.00

organic, organosilicone, or organometallic vapors tend to form thin films on the surfaces subjected to the glow discharge, and the deposition of these films is the main factor modifying the polymer surface in these cases. On the other hand, glow discharges of nonpolymerizing gases such as noble gases, nitrogen, oxygen, hydrogen, ammonia, or water vapor, for example, modify polymer surfaces through processes such as oxidation, ablation, crosslinking, and perhaps grafting. It should be recognized, however, that ablation supplies the gas phase with various chemical species, some of which may be able to form deposits, especially in mixtures with such nonreactive gases as hydrogen or ammonia.

Many polymer properties such as permeability, friction coefficient, surface energy (wettability), or biocompatibility of conventional polymers can be controlled by the appropriate application of a plasma treatment. The very advantage of these techniques is the fact that plasma treatment usually changes surface properties of the polymer without interfering with the bulk properties simply because of the very low range of its penetration. However, when the surface-to-volume ratio of material increases significantly, as it does in the case of the fibers, this is not necessarily true. That is why, perhaps, in the studies of plasma modification of polymer surfaces, much more effort has been concentrated on the films and other products rather than fibers. It is known that the properties of the fibers, especially natural ones such as wool, depend strongly on their delicate morphological structure, and in many instances plasma treatment may simply be too rough. There are only a few publications dealing with the plasma modification of fibers. Wróbel et al. [1] studied the plasma treatment of poly(ethylene terephthalate) fabrics using various nonpolymerizing gases, and they reported significant changes in surface structure as well as in the wettability of these fabrics depending on the type of gas and the treatment conditions. The electron scanning micrographs of similar poly(ethylene terephthalate) fibers etched by oxygen plasma were reported by Blakey and Alfy [2]. As far as natural fibers are concerned, Ward et al. [3] investigated plasma modification of cellulose and its derivatives and characterized such structural modifications of their surfaces as changes in elemental composition, introduction of free radicals, and formation of carbonyl groups. To our best knowledge, however, no one has so far reported a broad, comparative study concerning plasma treatment of a wide range of fibers including both natural and synthetic materials. The purpose of this work was, therefore, to perform such a comparative study of plasma treatment of many different fibers using four kinds of gases belonging to the nonpolymerizing group. These gases were helium (a noble gas), air (an oxidizing gas), nitrogen, and tetrafluoromethane (a substance which does not polymerize itself, but does form films while in mixtures with other nonpolymerizing gases such as hydrogen).

EXPERIMENTAL

Twenty different natural and synthetic fibers were examined in this work including cotton, wool, silk, ramie, and others. Some of the materials, like nylon 6, were subjected to more detailed investigation. Plasma treatment was carried

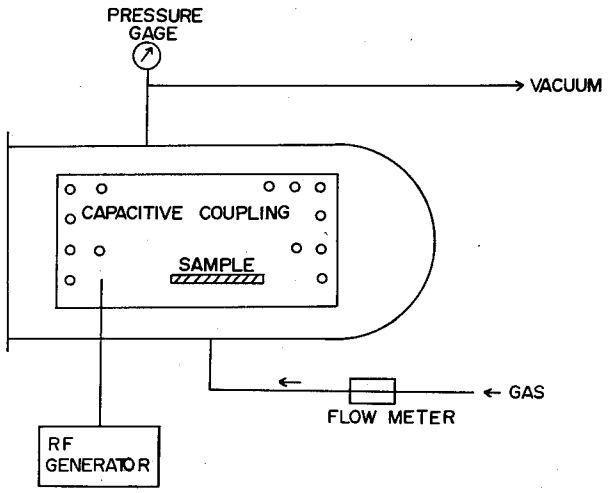

FIG. 1. Schematic view of the plasma equipment used for the surface treatment of the fibers.

out either on the fibers themselves or on fabrics woven out of these fibers. The schematic picture of the equipment used for the treatment is presented in Figure 1. It is a capacitively coupled flow system supplied by a 13.5-MHz power source (IPC-1000, International Plasma, Inc.). The volume of this system is approximately 2 L. The fiber samples, about 0.1 g, were loosely wound and laid on the quartz dish avoiding tight adherence to each other. In the case of the fabrics, the size and the number of the fibers in the unit length of the sample were selected so that different types of fibers could be compared in approximately similar conditions of the treatment.

The temperature measurements were performed using thermochromic paints (Tempile Division, Big Three Industry). The respective fibers were coated by the paint and then subjected to the discharge. It was found that the temperature increase during the treatment was practically independent of the kind of fiber used.

Electron micrographs were obtained using a Jeol JSM-35CF scanning electron microscope, tensile tests were performed on a Shimadzu IS-500 multipurpose tensile tester, and ESCA measurements were carried out with a Shimadzu model 750 spectrometer using the K_α line of aluminum.

RESULTS AND DISCUSSION

Temperature Changes during Plasma Treatment

Since the decomposition (weight loss) of the fibers under plasma conditions was one of the major effects studied in this work, a temperature increase inside the reactor was measured in each case in order to evaluate the possibility of the thermal decomposition of these fibers as the side effect. Figures 2 and 3 present

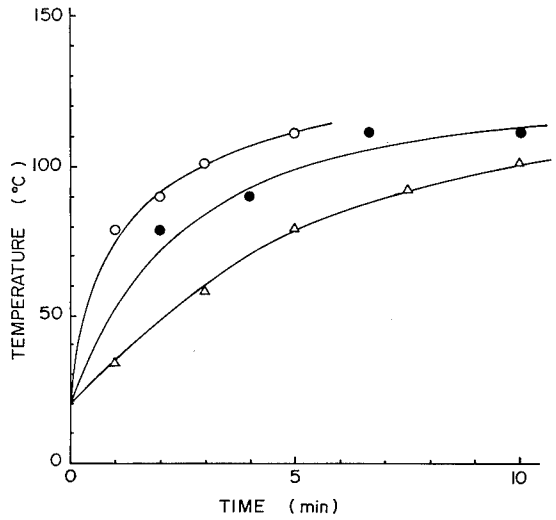

FIG. 2. Temperature inside reactor as a function of time for CF_4 plasma. Discharge conditions: (○) power 150 W, flow rate 50 sccm; (●) power = 100 W, flow rate = 50 sccm; (△) power = 50 W, flow rate = 100 sccm.

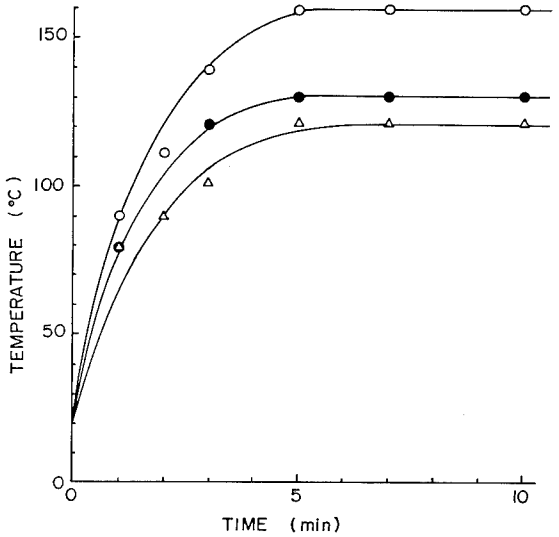

FIG. 3. Temperature inside reactor as a function of time for air plasma. Discharge conditions: (○) power = 70 W, flow rate = 180 sccm; (●) power = 50 W, flow rate = 120 sccm; (△) power = 30 W, flow rate = 100 sccm.

the change of the temperature with time for CF_4 plasma and air plasma, respectively. These examples are characteristic for the whole study. In most cases, the temperature inside the reactor reached a saturation level, usually lower than 130°C, and remained relatively constant during the whole experiment. Air plasma treatment was accompanied with a slightly higher temperature increase, which might be attributed to the evolution of the heat of oxidation. Nevertheless, the temperatures of the treatments were always far below the thermal decomposition regions for the respective polymers so the possibility of the pyrolysis of the fibers accompanying their plasma degradation should be ruled out. One should remember, however, that in certain cases the evolution of the low-molecular-weight species from the bulk of the fiber may be expected in elevated temperatures, and this phenomenon, although not significant, may contribute somewhat to the total weight loss.

Weight Loss during Plasma Treatment of the Fibers

The weight loss of the fibers as a function of plasma treatment time was not strictly linear owing to the fact that the surface area changed with time. However, the initial slope and the area-corrected loss rate yielded a reasonably constant weight loss rate, characteristic for the given fiber under a given plasma treatment condition. Figure 4, presenting the weight loss of nylon 6 treated with air, nitrogen, or tetrafluoromethane plasmas, is an example of such area-corrected data. It is also obvious from this figure that the weight loss rate in the case of air plasma treatment is much higher than for any other gases. This finding is

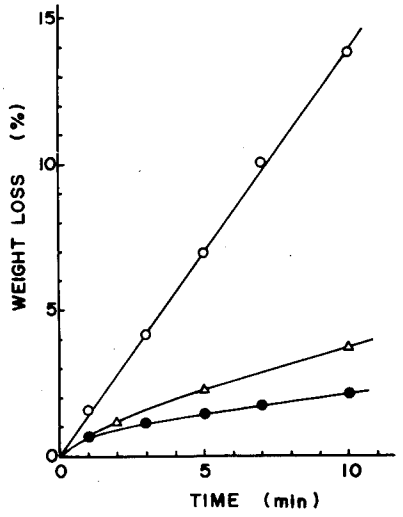

FIG. 4. Weight loss of nylon 6 fiber by plasma treatment. Air and N_2 plasmas, discharge power = 50 W, flow rate = 10 sccm; CF_4 plasma, discharge power = 150 W, flow rate = 50 sccm: (○) air, (●) N_2, (△) CF_4.

quite consistent with the fact reported several times [4,5] that oxygen plasma has a marked tendency to cause ablation of the polymeric materials. The same is generally known about tetrafluoromethane plasma, which is used as an etching tool in the preparation of microelectronic circuitry. However, according to the competitive ablation and polymerization (CAP) mechanism proposed by Kay [6] and Yasuda [7], CF_4 plasma can also be used to implant fluorine-containing moieties on the surface or to form thin film containing fluorine, if only H_2 is present in the system. Since H_2 is generated in most of the cases here, the polymerization part of the model actually comes into the competition, and the resulting weight loss rate is much lower than in the case of air plasma treatment.

As far as the plasma parameters are concerned, the molar flow rate of the gas and the discharge power play the major roles in determining the effect of the treatment. As shown in Figure 5, weight loss increases with flow rate at every discharge wattage in the low-flow-rate region. As the flow rate further increases, however, the weight loss deviates from linearity and starts to decrease. The initial increase with the flow rate can be explained by the increase of the number of reactive species, particularly of O and O_3 in air. The deviation from linearity and the further decrease occur at lower flow rates when the lower wattage is applied. It is obvious from the picture that at the higher flow rate the concentration of the active species decreases despite the increase in gas flow rate. By plotting the same data against W/F, which is proportional to the energy input per molecule, this situation can be clearly shown, as in Figure 6. All the points which were off from the linear dependence in Figure 5 now fall on the straight line. These two figures (Figs. 5 and 6) strongly indicate that plasma treatment can be performed under two distinctly different sets of conditions: (i) insufficient

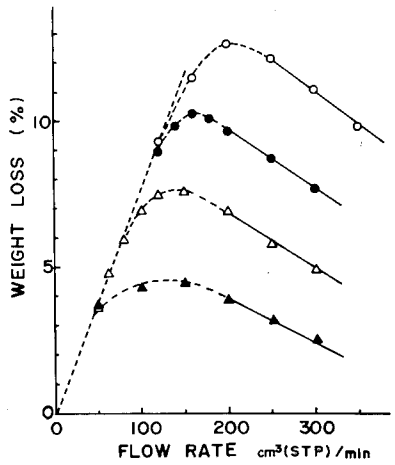

FIG. 5. Effect of the gas flow rate on weight loss of nylon 6 treated by air plasma for 5 min: (○) plasma discharge at 100 W, (●) 70 W, (△) 50 W, (▲) 30 W.

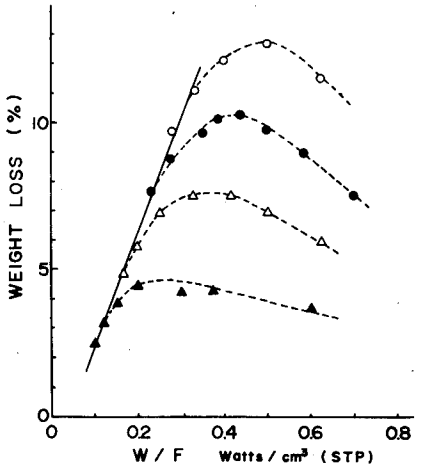

FIG. 6. Relation between values of W/F and weight loss for nylon 6 treated by air plasma for 5 min: (○) plasma discharge at 100 W, (●) 70 W, (△) 50 W, (▲) 30 W.

amount of gas with ample wattage, and (ii) insufficient wattage with ample amount of gas. In the first case, the mass flow rate becomes the rate-determining factor, while in the second case, the discharge power becomes the rate-determining factor. Thus these two ranges of plasma conditions can be described as the gas-deficient range and the power-deficient range, respectively. It seems, therefore, very reasonable to also apply the W/FM parameter used in plasma polymerization [8] to plasma treatment processes in which the ablation of polymer surface takes place rather than the formation of thin films.

A comparative study of a number of different fibers was also done, and the respective weight losses for various fibers in air plasma treatment are shown in Figure 7. These weight losses may be used to compare the plasma susceptibility of the polymers which constitute the corresponding fibers. In order to make such a comparison, however, one must correct the data considering the differences in the total area exposed to plasma since a wide variety of fiber sizes is available, and it is sometimes difficult to obtain fibers of the same diameter. The weight loss rates per unit area obtained with various kinds of polymers are summarized in Table I. The following general trends can be emphasized based on these results: (i) The presence of oxygen in the polymer structure makes it more susceptible to plasma, and the presence of nitrogen seems to have the opposite effect. The same trend was observed before as the in–out rule of thumb in plasma polymerization of organic compounds [9]. (ii) The most plasma-susceptible structure is the aliphatic polyether, which contains oxygen in its backbone. (iii) The second most plasma-susceptible structure is polyether with cyclic rings such as polysaccharide and its derivatives. (iv) The presence of O is somewhat protected when the polymer contains aromatic structure of N adjacent to oxygen, and oxygen is the pendant moiety. (v) The least susceptible polymers are either

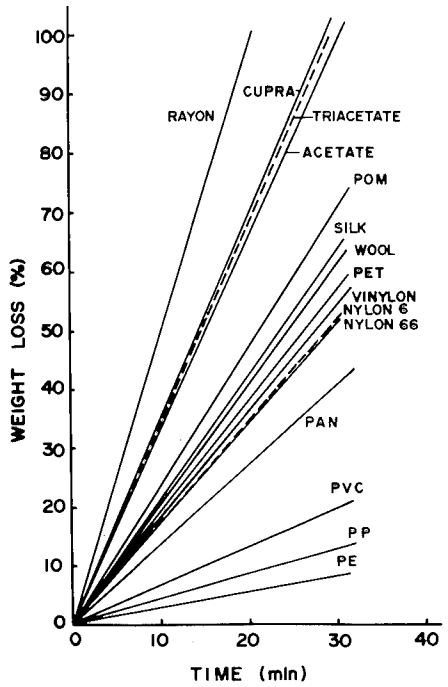

FIG. 7. Weight loss of various fibers by air plasma treatment. Discharge power 50 W, flow rate 100 sccm.

TABLE I
Plasma Susceptibility of Fibers

Type	Schema	Structural formura	Fiber	Weight loss rate (mg cm^{-2} min^{-1} x 10^3)							
				Air (50W, 1.0 Torr)		He (5W, 1.5 Torr)		CF_4 (5W, 1.0 Torr)		He (30W, 0.1 Torr)	
1.	—O—	—O—	POM	68.5	68.5	2.4	2.4	8.0	8.0	17.0	17.0
	—O—C(=O)—		Triacetate	18.3	16.2	0.8	1.4	0.7	1.3	—	—
			Cupra	15.7		2.4		2.0		—	
			Acetate	14.7		1.1		1.2		—	
			PET	9.3	9.3	0.5	0.5	0.8	0.8	1.7	1.7
	C(=O)—O	C(=O)—O	Vinylon	11.3	11.3	0.4	0.4	1.8	1.8	9.4	9.4
2.	C(=O)—N—	C(=O)—N—	Nylon 6	8.9	8.9	1.0	0.9	1.1	1.3	1.1	1.1
			Nylon 66	8.9		1.0		0.8		—	
			Silk	8.8		0.8		2.0		—	
	C(=N)—N	C(=N)—N	PAN	5.1	5.1	0.1	0.1	0.5	0.5	—	—
3.	——	——	PE	8.1	5.5	0.7	0.4	1.9	0.9	1.2	1.0
			PP	3.4		0.3		0		0.8	
			PVC	5.1		0.3		0.7		—	

hydrocarbon polymers like polypropylene or those which contain nitrogen but not oxygen. (vi) All the above trends were found for both air and He plasma treatment, although the magnitudes of He plasma susceptibilities were an order of magnitude lower than the corresponding oxygen plasma susceptibilities.

Morphology and Tensile Strength of Plasma-Treated Fibers

The scanning electron micrographs of selected fibers treated with all four different kinds of plasmas are shown in Figure 8. The reference (untreated) samples are not presented here, but since samples treated with helium plasma show very few morphological differences, and in certain cases, like silk, no differences at all from untreated ones, they should serve very well as a reference.

Generally it is obvious from the photographs that air plasma treatment is the most severe one. The example of cotton, where the fiber has been thinned significantly by such treatment, is a very suggestive one. Another interesting case is the air-plasma-treated acrylic fiber, which develops cracks perpendicular to its axis, making it look similar to an empty corn cone. Nitrogen plasma treatment is the second most destructive one, and all the features of air plasma treatment are followed in this case, only to a lower degree. The two least destructive treatments were performed by helium and CF_4 plasmas. The reasons for this are, however, totally different. In the case of helium, it is just the low ablation efficiency of this noble gas. The influence of CF_4 is much more complicated, where ablation is accompanied by the deposition of a thin fluorocarbon film on the surface of the fiber.

The very general conclusion drawn from Figure 8 concerns the fact that ablation of the fiber never takes off layers of material like a grinding or polishing process. Instead, it develops the surface of the fiber, introducing different kinds of holes, cracks, and fissures. The example of the air-plasma-treated acrylic fiber, with its corn-cone-like structure, is the most pronounced, but not the only one. It seems as though certain spots at the fiber surface are more susceptible to the etching and that is where the cracks begin to develop.

The tensile strength of the air-plasma-treated fibers were also measured as the function of weight loss. Since, however, in the process of plasma treatment the diameter of the fiber drops with the time of treatment, the tensile strength was always calculated based on the actual diameter of the treated sample and not on the initial diameter of the fiber. Figure 9 presents the resulting dependence of the tensile strength of the air-plasma-treated fibers on the weight loss caused by the treatment. As can be seen, the majority of the fibers show relatively small changes due to plasma treatment. There are some natural fibers among the exceptions, such as ramie for instance, which exhibit a very distinct decrease of tensile strength with the treatment time. As said before, the properties of natural fibers depend strongly on their delicate microscopic structure, which is usually much more elaborate than that of synthetic fibers. This structure can be destroyed by plasma treatment, and this is the reason why some of the natural fibers lose their tensile strength when subjected to the plasma treatment.

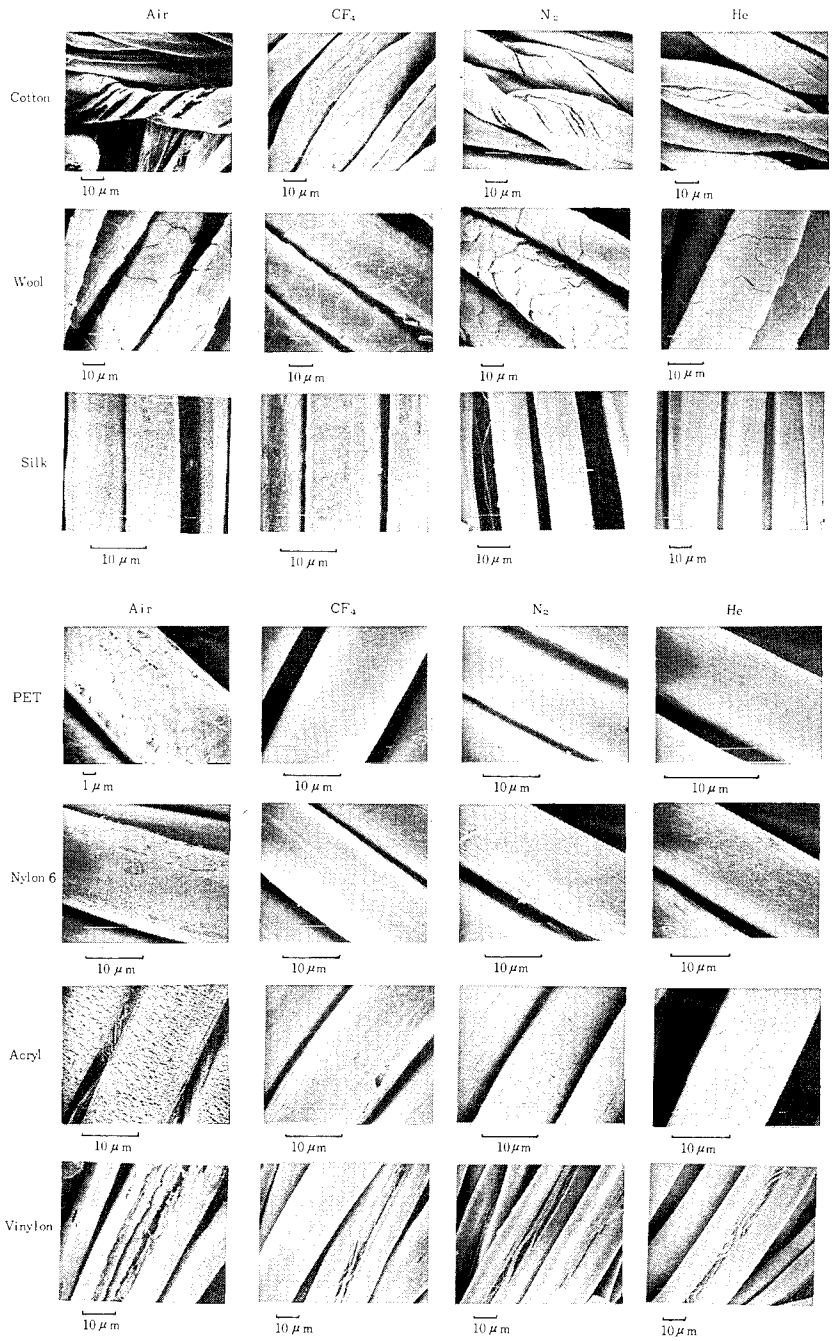

FIG. 8. Scanning electron micrographs of selected fibers plasma treated by four different gases. Discharge conditions: time = 10 min, power = 50 W, flow rate = 100 sccm in each case.

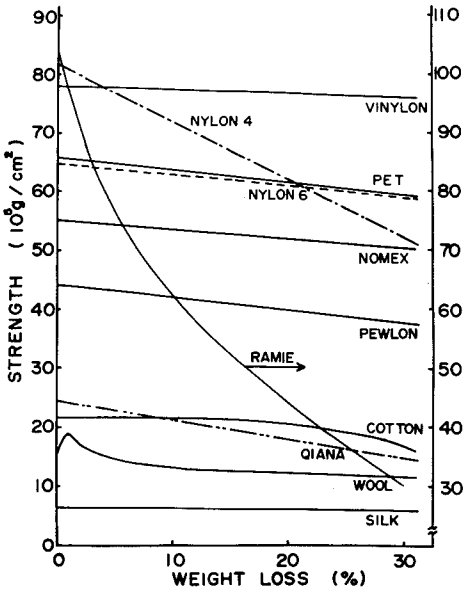

FIG. 9. Effect of glow discharge on the tensile strength of the fibers. Air plasma treatment, power = 50 W, flow rate = 100 sccm.

Wettability Studies: The Effect of CF_4 Plasma Treatment

As has been said before, tetrafluoromethane plasma is usually used for ablation purposes as in the preparation of microelectronic printed circuitry, for instance. In the cases, however, when hydrogen is present in the gas phase of the system, fluorine atoms are actually implanted into the surface of the material, thus changing its properties. Fluorine-containing polymers, on the other hand, are known to exhibit extremely hydrophobic surfaces. Therefore, if any implantation of fluorine-containing moieties takes place in the case of CF_4 plasma treatment of the fibers, it should be reflected in the change of the contact angle of water. Table II presents the results of water contact angle measurements. For obvious reasons the samples used in these measurements were the fabrics rather than the fibers. One should remember, however, that owing to the porosity of the fabrics, the contact angles do not correspond to those on the respective polymeric films. Unless fibers are very hydrophobic, water penetrates through the fabric and it is impossible to measure the contact angle. Such a situation is represented by zero contact angle in Table II. It is clear from the results presented that CF_4 plasma treatment decreases dramatically the wettability of all the hydrophilic fabrics and can be used to impart the excellent water repellence characteristic of these materials. In other words, this treatment modifies the surfaces of traditionally wettable fabrics such as cotton or silk to the extent of placing them among the best water-repellent materials such as wool.

The hypothesis that it is an implantation of fluorine atoms into the surface of

TABLE II
Water Contact Angle of CF_4 Plasma Treated Fabric, Right After Treatment, and After 10 Days of Exposure to the Atmosphere (Wore)

Fabric	Contact Angle θ degree		
	Untreated	Plasma Treated	Wore
Cotton	0.0	129.5	112.7
Wool	129.0	134.0	123.3
Silk	0.0	136.0	111.0
PET	124.0	136.0	128.3
Nylon 6	0.0	141.0	132.0
Vinylon	0.0	132.5	125.5

the fiber which is responsible for these dramatic changes of wettability was fully confirmed by ESCA studies of the respective fibers. Figure 10 presents characteristic O_{1s} and C_{1s} ESCA signals for selected fibers (the same as those used for wettability studies) treated by CF_4 plasma. In this case, ESCA not only confirmed the presence of fluorine atoms at the surface of the fiber, but also enabled the distinction between different fluorine-containing groups. The energy range of 285–295 eV corresponds to C_{1s} electrons and the chemical shifts due to the presence of fluorine atoms are large enough to permit such a distinction. Thus, typically a carbon peak without any attached fluorine atoms appears at 286 eV, whereas the CF group corresponds to 289 eV, CF_2 corresponds to 293 eV, and CF_3 corresponds to 295 eV [10]. All the untreated samples exhibited strong carbon peaks at 286 eV with no fluorine shifts. During the treatment, all three kinds of fluorine-containing groups are introduced to the surface, but which one is predominant largely depends on the fiber itself. Difluoromethylene groups are the main species for most of the treated samples, but in the case of silk, for instance, monosubstituted systems are predominant rather than disubstituted systems. Trifluoromethyl groups are also present in each case as indicated by the distinct, although not very large, irregularity of a CF_2 peak in the energy region of 295 eV.

It is also evident from Figure 10 that the extent of the surface fluorination is much higher in the case of synthetic fibers than for the natural ones. The unsubstituted C_{1s} signal (286 eV) is still the predominant one in the spectra of wool and silk, whereas in all the remaining cases this peak is overshadowed by strong signals corresponding to fluorine-substituted groups.

CONCLUSIONS

The purpose of this study was to modify the properties of fibers by means of plasma treatment of nonpolymerizable gases. Plasma polymerization is not a

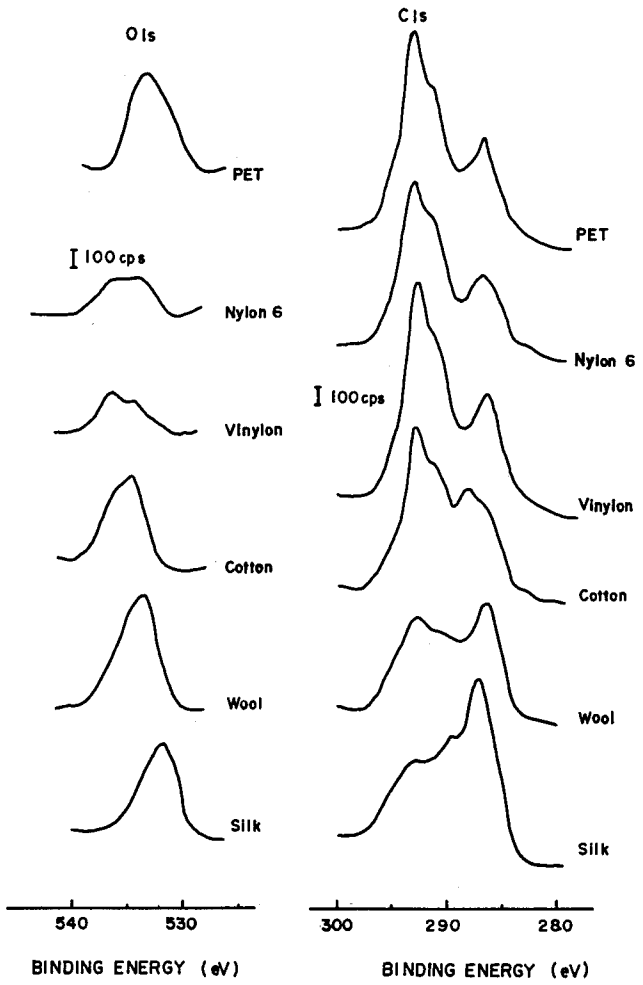

FIG. 10. O_{1s} and C_{1s} ESCA signals of selected fibers treated by CF_4 plasma. Discharge conditions: time = 10 min, power = 50 W, flow rate = 100 sccm.

major phenomenon in such processes. In many cases, however, owing to ablation, the gas phase is enriched with species able to polymerize in the mixtures with the primary plasma gas (as it is in the case of H_2 and CF_4, for example) and the weight loss is actually accompanied by the implantation of specific atoms onto the surface or even the deposition of thin films. In other words, in the plasma treatment of polymeric materials the transport of mass usually takes place in both directions; i.e., atoms migrate not only from the surface to the gas phase (ablation) but also in the reverse direction, from the gas phase to the surface (polymerization). This finding implies the possible applicability of the CAP model [6,7] to plasma treatment as well as to plasma polymerization processes. Pure plasma ablation and pure plasma polymerization are the extreme cases and

probably occur rarely. In most of the cases, the final effect is the result of a competition between these two phenomena.

The second major conclusion drawn from the above work is the fact that, similar to plasma polymerization processes, plasma treatment of polymer surfaces can be performed either in the gas-deficient range of conditions or in the power-deficient range of conditions and these two regions should stimulate different changes in the polymer surface introduced by plasma treatment. As a consequence, the W/FM parameter, which has been so successfully applied to plasma polymerization processes [8], can also be very helpful in describing plasma treatment.

A last and very practical conclusion to be drawn from this work concerns the possibility of changing the water contact angles of many fabrics by means of CF_4 plasma treatment, which can lead to the production of water-repellent fabrics from the highly hydrophilic fibers as cotton, for instance. It is also important to note that the durability of such treatment is promising, at least as indicated in Table II by short time measurements.

REFERENCES

[1] A. M. Wróbel, M. Kryszewski, W. Rakowski, M. Okoniewski, and Z. Kubacki, *Polymer, 19,* 908 (1978).
[2] P. R. Blakey and M. O. Alfy, *J. Text. Inst., 69,* 38 (1978).
[3] T. L. Ward, H. Z. Jung, O. Hinojosa, and R. R. Benerito, *J. Appl. Polym. Sci., 23,* 1987 (1979).
[4] H. Yasuda, in *Proceedings, 3rd IUPAC International Round Table on Plasma Polymerization and Plasma Treatment,* Limoges, France, 1977.
[5] M. Gazicki and H. Yasuda, in *Proceedings of the 184th ACS National Meeting, Symposium on Plasma Polymerization and Plasma Treatment,* Kansas City, Am. Chem. Soc., Washington, DC, 1983, p. 308.
[6] E. Kay, in *Proceedings, 3rd IUPAC International Round Table on Plasma Polymerization and Plasma Treatment,* Limoges, France, 1977.
[7] H. Yasuda, in *Plasma Polymerization,* ACS Symp. Ser. No. 108, M. Shen and A. T. Bell, Eds., Am. Chem. Soc., Washington, DC, 1979, p. 37.
[8] H. Yasuda, in *Thin Film Processes,* J. L. Vossen and W. Kern, Eds., Academic, New York, 1978, p. 314.
[9] H. Yasuda and C. E. Lamaze, *J. Appl. Polym. Sci., 17,* 1533 (1973).
[10] D. T. Clark and W. J. Feast, *J. Macromol. Sci. Rev. Macromol. Chem., 12*(2), 191 (1975).

SURFACE FLUORINATION WITH INORGANIC FLUORIDES IN GLOW DISCHARGE

TOSHIHARU YAGI and ATTILA E. PAVLATH

Western Regional Research Center, Agricultural Research Service, U.S. Department of Agriculture, Berkeley, California 94710 and Daikin Kogyo Co., Ltd. Osaka 564, Japan

SYNOPSIS

The utilization of glow discharge for the surface fluorination of organic polymers was extended by using volatile inorganic fluorides as a source of fluorine. These fluorinating agents are generally inert materials in the absence of water, but provide fluorine radicals in glow discharge. A high level of fluorination was observed with NF_3, SiF_4, and BF_3 using polyethylene, polypropylene, polystyrene, and poly(methyl methacrylate) as substrates. The fluorination was evident already at short exposure times, 1–2 s. The fluorinated layers obtained were highly resistant to extraction with CF_2ClCCl_2F. The critical surface tension of these surfaces approached that of the polytetrafluoroethylene.

INTRODUCTION

Polytetrafluoroethylene has very desirable surface properties; consequently, a wide range of research efforts have been undertaken to add these surface characteristics to less expensive polymers where bulk properties are of secondary importance [1]. Elementary fluorine reacts very violently with most organic surfaces. Various successful methods have been developed to tame this reaction, but the average chemist still considers elementary fluorine as a dangerous and cumbersome fluorinating agent. Polymerization of fluorinated organic monomers in glow discharge is an easy and safe technique which results in instantaneous deposition of fluoropolymer coatings on exposed surfaces [2,3]. However, the solvent resistance of these depositions are highly dependent on the method. In our experiments, a large amount of this deposited coating was eliminated by extraction with $CF_2C1CFCl_2$ [3]. In later attempts, to make durable coatings, we studied various saturated fluorocarbons in glow discharge using high-density

Journal of Applied Polymer Science: Applied Polymer Symposium 38, 215–223 (1984)

Published by John Wiley & Sons, Inc. CCC 0570-4898/84/010215-09$04.00

polyethylene as substrate [4]. These experiments were more successful, but depending on the fluorine compound and the reaction conditions varying amounts of fluoropolymers were still lost during extraction.

When unsaturated fluorocarbons are injected in glow discharge, they form biradicals which rapidly polymerize in the vapor phase, frequently before they can react with any free radicals also created by the glow discharge on the organic surface. Such polymer can precipitate onto the surface without bonding covalently to it; thus the deposit is subject to extraction. When saturated fluorocarbons are used, monoradicals are the major products in the vapor phase, and they remain capable of surface bonding. For example, in case of carbon tetrafluoride, a simple dissociation is the first step:

$$CF_4 \rightleftharpoons CF^{\cdot} + F^{\cdot} \tag{1}$$

These radicals then react with a free radical or even a chemical bond on an organic polymer surface, resulting in fluorinated surfaces:

$$F\cdot + C\cdot \longrightarrow C{-}F \tag{2}$$

$$F\cdot + C{-}H \longrightarrow C{-}F + H\cdot \tag{3}$$

$$CF_3\cdot + C{-}H \longrightarrow C{-}CF_3 + H\cdot \tag{4}$$

Such surfaces should be unextractable. Nevertheless, as mentioned above, experiments showed that a certain amount of the fluoropolymer was removed by extraction [4]. This could have been caused by at least two other possible reactions: (a) the glow discharge, a very powerful activating medium, further activated a monoradical to form a biradical (in case of $CF_3\cdot$, a difluoromethylene, CF_2: radical) which then polymerized rapidly; (b) the fluorocarbon radicals recombined with one another to form longer chains. It has been shown that CF_3CF_3 can be obtained by the action of glow discharge in CF_4 [5]. Excitation of these longer chains will create new fluorocarbon radicals which then could undergo the same process. At certain lengths, these molecules deposited on the surface without any grafting. These new ungrafted surfaces competed with the original organic surface in the regular grafting process, described in eq. (2)–(4), and thus decreased the amount of firmly grafted fluoropolymer not subject to solvent removal. Experiments showed the amount of this extractable polymer varied with the starting material and the reaction conditions, but in general it was only the smaller part of the main reaction.

Regardless of the actual side reaction involved in the formation of the extractable deposits, the latter could be minimized or entirely eliminated if the fluorinating agent could not form either biradicals or longer chains. Practically, all fluorocarbons can form one or the other, but the situation is completely different with inorganic fluorides. The first step would be the same:

$$XF_n \rightleftharpoons XF_{n-1}\cdot + F^{\cdot}, \quad X = \text{As, B, M, S, etc.} \tag{5}$$

The forming $F\cdot$ would have the same reactivity as the $F\cdot$ formed by the dissociation CF_4. However, the reactivity of the $XF_{n-1}\cdot$ radical is quite different from that

of $CF_3\cdot$ or other fluorocarbon radicals. In some cases, dimeric compounds, such as N_2F_4, may be formed, but these compounds are more likely to redissociate again instead of growing into longer chains. The only possible side reaction is the formation of C—XF_{n-1}, (C—)$_2XF_{n-2}$, etc. Such compounds, with the exception of (C—)$_nX$, are generally unstable in the presence of nearby C—H bonds. Only perfluorinated structures may be expected to form.

We wish to report here a convenient and safe method to obtain practically unextractable fluorocarbon surface layers using gaseous inorganic fluorides in glow discharge.

EXPERIMENTAL

Glow discharge was created in a cylindrical glass reactor using a 13.56-MHz generator. The reactor was identical to the one described in a previous publication [6]. A nearly homogeneous field was achieved with capacitive coupling using quarter-cylindrical electrodes. The sample was placed on a glass plate in the center of the glow and the reactant inorganic fluorides were introduced through a flowmeter immediately above the sample. The flow rate was regulated in such way that the pressure was between 0.5 and 1 torr and a stable glow could be maintained already at 10 W. The inorganic fluorides reported in this article, BF_3, NF_3, and SiF_4, were from commercial sources and used without any purification. Commercial polymer samples of high-density polyethylene (HDPE), polypropylene (PP), polystyrene (PS), and poly(methyl methacrylate) (PMMA) were cleaned in an ultrasonic cleaner using $CF_2ClCFCl_2$ under conditions similar to those used in extracting fluoropolymer coatings [4]. There was no evidence of any attack by $CF_2ClCFCl_2$ on the above-listed polymers themselves. After the glow discharge treatment the surface of the sample was analyzed by x-ray photoelectron spectroscopy (ESCA) to determine the fluorine to carbon ratio. Finally, the sample was treated with $CF_2ClCFCl_2$ to extract any loose deposit and the ESCA analysis was repeated. Both before and after extraction, the carbon and fluorine 1*s* spectra were measured. A normalization factor of 3.85 was used to divide the area under the fluorine 1*s* spectra before calculating the F/C ratios. The carbon 1*s* ESCA spectra were deconvoluted to determine the presence and ratio of CF_3 (293–294 eV), CF_2 (291–292 eV), and CF (288.5–289.5 eV) groups [7]. Surface wettability studies were carried out to measure the critical surface tension (CST) to compare the surface properties of these experimental samples to those of polytetrafluoroethylene. The test liquids were C_{10}–C_{16} hydrocarbons. CST was determined by measuring the advancing contact angle ϕ, then extrapolating $\cos\phi$ vs. surface tension line to $\cos\phi = 1$ as described by Zisman [8].

RESULTS AND DISCUSSION

The validity of the theory was tested with three readily available gaseous inorganic fluorides, NF_3, BF_3, and SiF_4 and compared with the reactions of CF_4 and C_2F_4 under identical conditions. Table I summarizes the fluorine to carbon

TABLE I
Fluorine to Carbon Ratios in Glow-Discharge-Treated Polyethylene (25 W, 5 min) Samples Before (BE) and After (AE) Extraction with $CF_2ClCFCl_2$

Reactant	F/C ratio		Loss (%)
	BE	AE	
NF_3	1.92	1.90	1
BF_3	1.12	0.93	17
SiF_4	1.12	0.92	19
CF_4	1.50	1.05	30
C_2F_4	1.44	0.63	57

ratios as determined by ESCA measurements on the surface of polyethylene treated in glow discharge with these fluorine compounds. The absolute value of the F/C ratio before extraction does not necessarily show the superiority of the inorganic fluorides, but the differences between the before and after extraction values clearly demonstrate it. With NF_3 there was practically no change; the difference was within the limits of the experimental error. In the case of BF_3 and SiF_4 there was some loss, but it was relatively small. It might be hypothesized that during the fluorination some bond fracturing occurred in the polymer and these lower-molecular-weight polymers were eliminated by the extraction, but further experimentation is needed to prove this theory. A thorough ESCA analysis was carried out to determine whether the fluorinated surface included any C—X bonding, but no evidence was found.

The structure of the fluorinated layers obtained with inorganic fluorides also differed from those forming from fluorocarbons in glow discharge. In the latter case various compounds C_xF_y could form; therefore the carbon 1*s* ESCA spectrum was generally a wide peak extending from 285 eV (CH_2) to 294 eV (CF_3). Its deconvolution indicates the presence of all possible groups (e.g., CF_3, CF_2, CF)

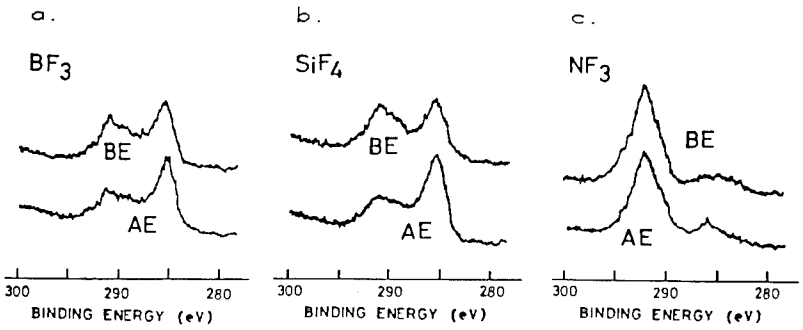

FIG. 1. Carbon 1*s* spectra of glow-discharge-treated polyethylene (at 25 W for 5 min) with (a) boron trifluoride, (b) silicon tetrafluoride, and (c) nitrogen trifluoride (BE = before, AE = after extraction with $CF_2ClCFCl_2$).

[4]. Using NF_3, an easily distinguishable peak was present in the 292 eV (CF_2) range with a small peak around 285 eV, characteristic for nonfluorinated carbon atoms [see Fig. 1(c)]. The latter peak was more evident with BF_3 and SiF_4, since fluorination under these conditions was less complete, as shown in Figure 1. However, deconvolution of these curves again indicated the presence of mostly a CF_2 group together with some partially fluorinated —CHF— structures.

As Table I indicates, NF_3 was the most efficient fluorinating agent in glow discharge. This can be explained by the fact that under these conditions, the compound decomposed in a slow, regulated way to form its gaseous components, fluorine and nitrogen, without any residue. This controlled release of elementary fluorine brought about the uniform fluorination of the organic surface. Decomposition was not a self-maintaining chain reaction—it stopped as soon as the glow was extinguished. Figure 2 illustrates the amount of fluorination obtained as a function of the applied power. At 3-s residence time using 10 W (the minimum input required to maintain a glow discharge under the given conditions) fluorination was already evident. Increasing the power resulted in rapidly increasing F/C ratios approaching 2.0, which is the F/C ratio for tetrafluoroethylene. The differences between the values before and after extraction were quite small. At higher power input the difference was slightly larger and there was also a small drop in the F/C ratio, probably caused by fragmentation of the polymer chain.

Maximum fluorination could be obtained at lower power inputs by increasing exposure. As Figure 3 illustrates, fluorination was already evident at 1-s exposure to NF_3 in glow discharge. The peak was still wide and included both CF_2 and CF (at 292 and 290 eV, respectively), but it was clearly separated from the CH_2 peak around 285 eV. With increasing exposure time, the peak sharpened and shifted to 292 eV, while the CH_2 group gradually disappeared. Deconvolution of the spectrum indicated almost exclusively —CF_2— structure. Figures 4 and 5 show the F/C ratios before and after extraction at two power levels as a function of time, again demonstrating that the major reaction, independent of time and power, was surface fluorination. In previous experiments with fluoro-

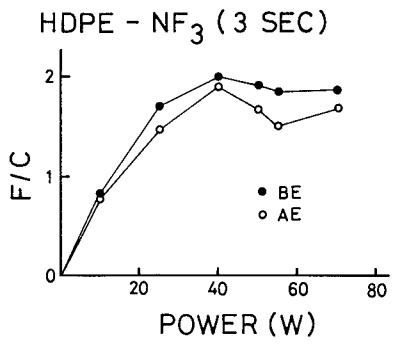

FIG. 2. Fluorine to carbon ratio versus input power on the surface of NF_3 glow-discharge-treated polyethylene (HDPE); exposure time 3 s; BE = before, AE = after extraction with $CF_2ClCFCl_2$.

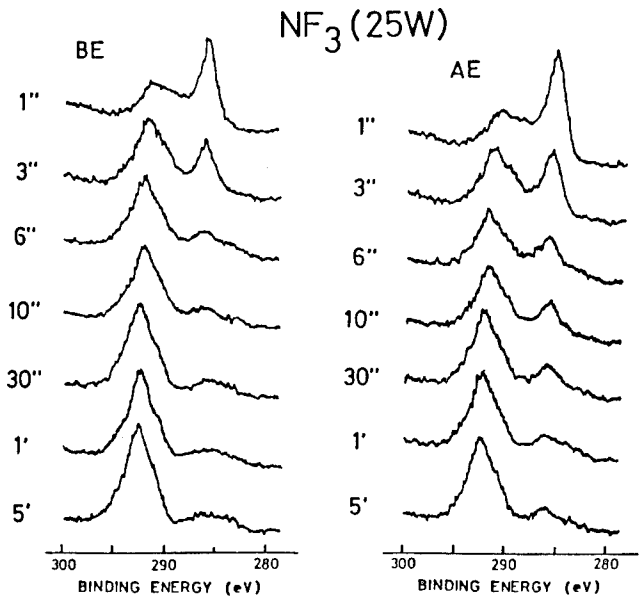

FIG. 3. Carbon 1*s* ESCA spectra of NF_3 glow-discharge-treated (25 W) polyethylene samples at various exposure times; BE = before, AE = after extraction with $CF_2ClCFCl_2$.

carbons [4], increasing exposure to glow discharge narrowed the gap between the curves for extracted and unextracted surfaces. This was attributed to a cross-linking side reaction of the deposited but not grafted fluorinated layers, which decreased their solubility in the extractant. If this phenomena had not occurred, the difference between F/C values before and after extraction should have been minimal and independent of exposure time, just as in Figures 4 and 5.

Surface fluorination with inorganic fluorides could be applied to other polymers too. Table II compares the results obtained with NF_3 in the case of four

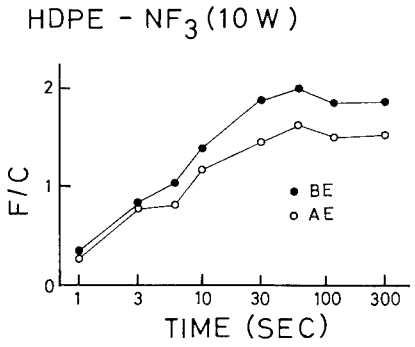

FIG. 4. Fluorine to carbon ratio versus exposure time on the surface of NF_3 glow-discharge-treated (10 W) polyethylene (HDPE); BE = before, AE = after extraction with $CF_2ClCFCl_2$.

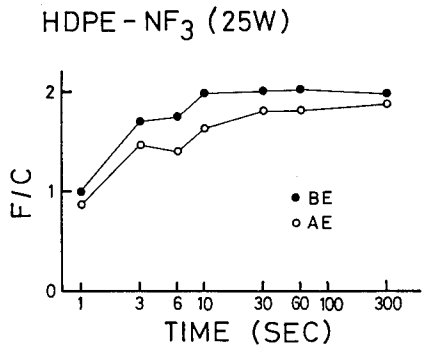

FIG. 5. Fluorine to carbon ratio versus exposure time on the surface of NF_3 glow-discharge-treated (25 W) polyethylene (HDPE); BE = before, AE = after extraction with $CF_2ClCFCl_2$.

different polymers. Maximum fluorination was obtained in each case, but the F/C ratio in poly(methyl methacrylate) showed a drop of 45% after extraction, though the amount of fluorination retained was still considerable. The carbon 1*s* ESCA spectra are shown in Figure 6. For polypropylene the fluorinated peak was slightly wider than for polyethylene, indicating the fluorination of the CH_3 groups. The spectrum of polystyrene was almost identical with that of polyethylene. Major changes, both qualitative and quantitative, could be seen in the spectrum of fluorinated poly(methyl methacrylate) after extraction. This behavior might be rationally explained by the formation of $CF_3\cdot$ radicals through the breakup of the ester linkage and consequent formation of ungrafted fluorinated deposits as observed with fluorocarbons. No experimental proof can be presented at this time to support this hypothesis.

The ultimate purpose of surface fluorination is to obtain surface properties similar to those of polytetrafluoroethylene. The critical surface tension (CST) values for these fluorinated surfaces, determined by surface tension measurements [8], approached 18.5 dyn/cm, which is the CST for polytetrafluoroethylene. The CST values for the untreated samples were over 30 dyn/cm. Numerical values of the measurements of surface properties are summarized in

TABLE II
Fluorine to Carbon Ratios in Various Polymer Samples Treated in Glow Discharge (NF_3, 25 W, 30 s) Before (BE) and After (AE) Extraction with $CF_2ClCFCl_2$

Polymer	F/C ratio		Loss (%)
	BE	AE	
Polyethylene	2.00	1.82	9
Polypropylene	1.85	1.70	8
Polystyrene	1.90	1.55	18
Poly(methyl methacrylate)	2.06	1.14	45

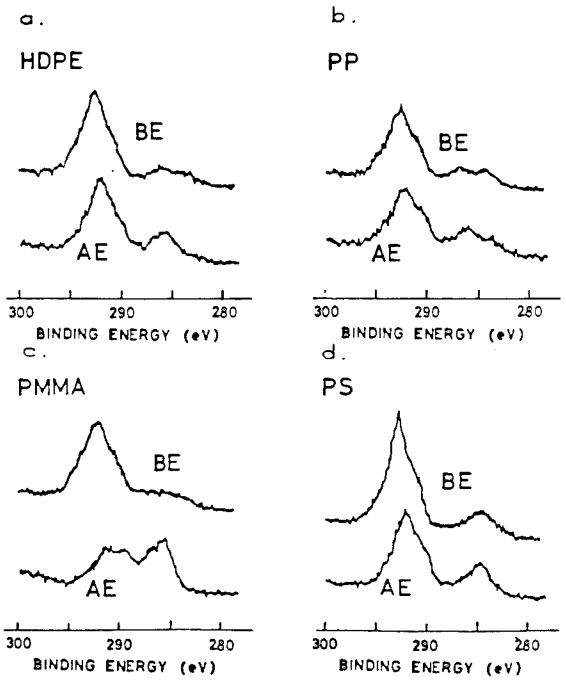

FIG. 6. Carbon 1*s* ESCA spectra of NF_3 glow-discharge-treated (25 W, 30 s) samples: (a) polyethylene, (b) polypropylene, (c) poly(methyl methacrylate), and (d) polystyrene; BE = before, AE = after extraction with $CF_2ClCFCl_2$.

Table III and Figure 7. It is interesting to note that glow-discharge-treated poly(methyl methacrylate) became hydrophilic after extraction, even though its CST value was comparable to those of the other similarly treated polymers. This would again point toward the possibility of breaking the ester linkages, which might result in hydrophilic carboxyl-type surface structures.

TABLE III
Contact Angles with Water and CST Values for Glow-Discharge-Treated Samples (NF_3, 25 W, 30 s) Before (BE) and After (AE) Extraction with $CF_2ClCFCl_2$

	Contact angle (with water, deg)			CST (dyn/cm)	
Polymer	BT[a]	BE	AE	BE	AE
Polyethylene	89	109	114	18.6	20.8
Polypropylene	109	126	126	19.6	22.4
Polystyrene	87	112	112	19.4	21.4
Poly(methyl methacrylate)	90	108	(Wet)	18.3	21.6

[a]Before glow discharge treatment. The CST was higher than 30 dyn/cm for all materials before glow discharge treatment and could not be determined by the available test liquids.

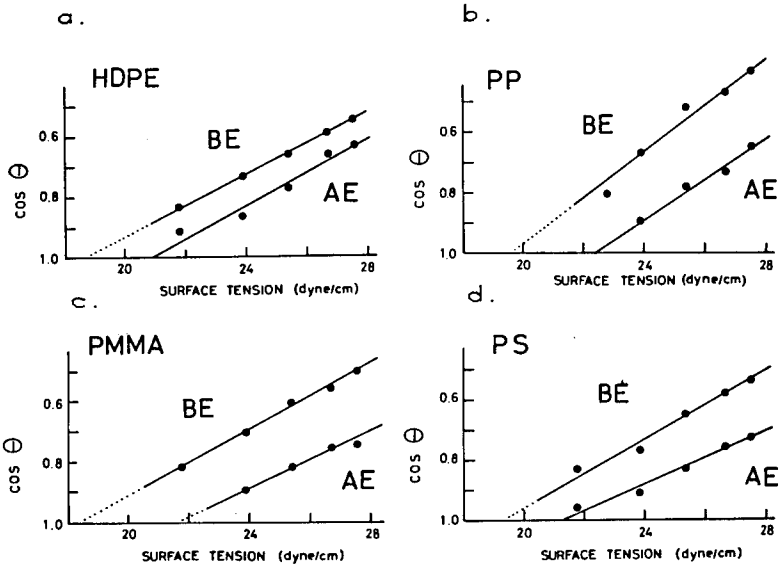

FIG. 7. Wettability results of NF_3 glow-discharge-fluorinated polymer surfaces (25 W, 30 s): (a) polyethylene, (b) polypropylene, (c) poly(methyl methacrylate), and (d) polystyrene; BE = before, AE = after extraction with $CF_2ClCFCl_2$.

CONCLUSION

Nitrogen trifluoride, boron trifluoride and silicon fluoride are convenient surface fluorinating agents in glow discharge. These materials, as well as other gaseous inorganic fluorides which can dissociate and produce F· radicals without forming polymer depositions, can cause the same reactions as observed with elementary fluorine, but in a safe and controllable way suitable for easy laboratory application. Since the reaction lacks the potential violence of elementary fluorine, the reaction conditions can be appropriately modified so that little or no bond fracture occurs in the polymer chain. The fluorination of certain polymers containing more easily breakable bonds might require special conditions. The properties of surfaces obtained by this method approach those of polytetrafluoroethylene.

REFERENCES

[1] A. G. Pittman, in *High Polymers, XXV. Fluoropolymers,* L. Wall, Ed., Interscience, New York, 1972, Chap. 13.
[2] D. F. O'Kane and D. W. Rice, *J. Macromol. Sci. Chem., 10,* 567 (1976).
[3] A. E. Pavlath and A. G. Pittman, in *Plasma Polymerization,* ACS Symp. Ser. No. 108, M. Shen and A. T. Bell, Eds., Am. Chem. Soc., Washington, DC, 1979, Chap. 11.
[4] T. Yagi, A. E. Pavlath, and A. G. Pittman, *J. Appl. Polym. Sci. 27,* 4019 (1982).
[5] E. A. Truesdale and G. Smolinsky, *J. Appl. Phys., 50,* 6594 (1979).
[6] M. M. Millard, J. J. Windle, and A. E. Pavlath, *J. Appl. Polym. Sci., 17,* 2502 (1972).
[7] A. E. Pavlath and M. M. Millard, *Appl. Spectrosc., 33,* 456 (1979).
[8] W. A. Zisman, *Adv. Chem. Ser. 43,* Am. Chem. Soc., Washington, DC, 1964, Chap. 1.

CONTINUOUS PLASMA POLYMERIZATION INVESTIGATED BY MEANS OF A MAGNETICALLY ENHANCED GLOW DISCHARGE WITH MOVING SUBSTRATES

A. K. SHARMA,* Y. MATSUZAWA, and H. YASUDA
Department of Chemical Engineering and Graduate Center for Materials Research, University of Missouri–Rolla, Rolla, Missouri 65401

SYNOPSIS

Parameters to operate a continuous plasma polymerization in a scaled-up system were investigated in terms of discharge power, monomer flow rate, and electrode design, as well as the electrode status. A magnetron discharge system (magnetically enhanced glow discharge) was found to play an important role in the continuous operation of plasma polymerization because of the uniform plasma zone in the interelectrode space where substrates to be coated move. It was also found that conditioning of electrodes (to establish coated–uncoated zones on the electrode) is a significant factor in obtaining a continuous and stable glow discharge. In other words, once the electrode surface has been conditioned, fluctuation of electrical parameters, voltage and current, decreases, resulting in a stable discharge. The change of properties of the deposited allylamine polymer was negligibly small in its reverse osmosis performance when the plasma polymer is formed above a threshold value of the composite discharge parameter W/FM (flow-rate-controlled case). The overall process is reproducible when these parameters are well maintained in the flow-rate-controlled region.

INTRODUCTION

Plasma polymerization can be carried out by a number of different methods utilizing electric power sources ranging from direct current to alternating current in the gigahertz range (microwave). Various kinds of reactor design can be applied to accommodate advantageous features of each range of power source. On the other hand, it has become quite evident that plasma polymerization is a highly system-dependent process and phenomenon, and plasma polymerization of a

*Present address: Applied Membrane Technology, 11558 Encore Circle, Minnentonka, MN 55343.

Journal of Applied Polymer Science: Applied Polymer Symposium 38, 225–234 (1984)

CCC 0570-4898/84/010225-10$04.00

monomer such as styrene cannot be discussed in general terms extending beyond the limitations of the system used.

From the viewpoint of application of plasma polymerization on an industrial scale, this aspect is a drawback in that experimental data obtained in a laboratory reactor might not be transferred to a larger-scale application. Therefore, any laboratory experiment which has a definite goal for larger-scale use in mind should be carried out in a reactor which can be scaled up in a straightforward manner.

In the application of plasma polymerization in which a continuous operation of plasma polymerization [1,2] is employed, the difference between a batch operation and a continuous operation becomes an important factor. There are several effects due to uncontrolled factors of typical batch-type plasma polymerization processes. For instance, the effect of heat created in a plasma might cause a serious problem, such as curling of the membrane due to thermal stresses [3]. The effect of monomer adsorbed on the surfaces within a reactor [4,5] and the post-plasma polymerization of some monomers on the surface of plasma-deposited polymers [5,6] often affect the reproducibility of the process. Such effects are associated with phenomena which occur before and after the plasma polymerization process and which may occupy significant portions of a batch operation. Furthermore, the dimension and form of the substrate is extremely restricted in a batch system as far as the uniformity of the plasma polymer coating is concerned.

A continuous plasma polymerization process with a moving substrate system can be utilized in order to minimize or eliminate these uncontrollable factors associated with batch systems. This moving substrate system plays an important role in the continuous plasma polymerization process as a part of process control. This method ensures the uniformity of the coating as well as the process reproducibility since the substrate to be coated moves [1,2].

Magnetically enhanced glow discharge by internal electrodes (using an audio-frequency power source) has several advantageous features particularly suited to continuous operation of plasma polymerization applied to continuously fed moving substrates [7]. Some factors which influence a prolonged operation of plasma polymerization were investigated by using reactors which utilize magnetron discharge and have been described previously [8,9].

EXPERIMENTAL

Two different types of plasma reactors were used in this study. Magnets attached to electrodes used for both systems were specially designed to modify the distribution of the power density in the glow zone [9].

The bell jar system used is a conventional type using an audio frequency of 10 kHz [5,8]. The details of the other reactor used for the continuous plasma polymerization of allylamine were described elsewhere [1].

The deposition patterns on the aluminum electrodes were obtained by methane plasma polymerization in the bell jar system. A pair of clean aluminum electrodes

were placed 3 in. apart in the middle of the reactor. Then the methane plasma polymerizations were performed under different discharge conditions, i.e., different flow rates and discharge powers. After the plasma polymerization, the electrode surface was carefully observed to determine the pattern of depositions on the electrodes. In this bell jar system, a substrate is placed on a rotatable plate attached to an electric motor. Thus the substrate can be continuously rotated in the electrode gap during the plasma polymerization process. This rotating substrate method used as one of the moving substrate systems was satisfactory to ensure the uniformity of the plasma coating [10].

On the other hand, the continuous plasma polymerization of allylamine to prepare a composite reverse osmosis membrane was carried out in a tandem reactor [1] using an audio frequency of 10 kHz. A thermocouple was installed in the glow zone to measure the ambient temperature of the plasma. Electron temperature T_e and numbers of positive ions, n_p, were measured by a probe installed in the plasma zone [11]. Six-strand hollow fiber (polysulfone) (12–15 m) used as the substrate was loaded into the system to prepare the composite reverse osmosis membrane. During the continuous plasma polymerization process, the current and voltage were periodically adjusted to maintain a constant discharge power and the moving substrate speed was controlled by an electric-motor-driven spool to obtain a uniform coating.

The reverse osmosis performance of the resulting fibers was tested in a specially designed reverse osmosis system for hollow fibers (details described in [1]). The test conditions used for the reverse osmosis performance were applied pressure 1300 psi and concentration of NaCl feed solution 2 wt %.

RESULTS AND DISCUSSION

Overall Phenomena in a Reactor System

Because a magnetic field exists in the vicinity of an electrode surface, the movement of electrons is largely restricted and localized. As a consequence of this localized electron movement, glow appears as an intense doughnut-shaped ring near the surface of an electrode. Accordingly, the plasma energy density is very uneven across the surface of an electrode. This uneven distribution of plasma energy density is reflected in the uneven distribution of polymer deposition onto the electrode surface, and under certain conditions ablation of materials placed on the electrode surface right beneath the intense ring-shaped glow is observed [12].

On the other hand, the measurement of electron temperature T_e and numbers of positive ions, n_p, by the plasma probe method revealed that the plasma which occupies the majority of space between two electrodes is very uniform except the space very close to the electrodes [12]. In the reactors used in this study, substrates on which polymer deposition occurred move through this uniform plasma zone. Because of the uniformity of plasma in this zone and of the movement of substrates controlled by an electric-motor-driven spool, a very

uniform deposition of polymer is obtained. Because of the flow pattern of polymer-forming plasma, polymer deposition onto a stationary substrate is generally not uniform, and in nearly all cases a visible interference pattern due to variation of thickness develops. The deposition of plasma onto moving substrates employed in this study is completely free of such a pattern, indicating high uniformity of coating thickness.

Thus, the magnetron discharge system employed has characteristic features of (i) very uneven plasma energy density near the electrode surfaces and (ii) uniform plasma zone in the interelectrode space. Because of the nonuniformity of the plasma, a portion of the electrode surface remains uncoated with plasma polymer and under certain conditions sputtering of electrode material occurs. The establishment of the coated–uncoated zones on the electrode surface plays an important role in continuous operation of plasma polymerization.

FACTORS WHICH INFLUENCE CONTINUOUS PLASMA POLYMERIZATION

Electrode Surface

Perhaps the most dramatic display of the competitive ablation and polymer formation (CAP) mechanism can be seen in the pattern that develops on the electrode surface after a plasma polymerization is completed. The patterns on the electrode surface reflect the nature of plasma processes occurring at the surface of electrodes and vary from intense etching of the electrode material (sputtering) to deposition of a polymeric film. The most intense changes are often observed in the surface area corresponding to the intense ring-shaped glow. Figure 1 shows such patterns observed with aluminum electrodes after polym-

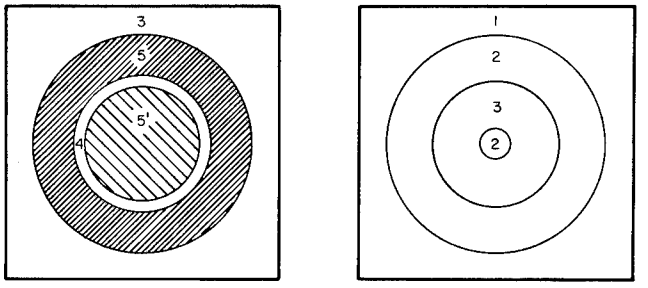

FIG. 1. Schematic representation of electrode surface after plasma polymerization of methane expressed by the following codes: (1) original; (2) clean, shiny Al; (3) original Al with yellow or blue tinge; (4) yellow, blue, or brown tinges repeated alternately; (5) dark coating which is difficult to remove; (5′) dark coating which is easy to remove. (a) 3.40 cm^3 (STP)/min, 80 W, $W/FM = 1.97 \times 10^9$ J/kg; (b) 0.26 cm^3 (STP)/min, 90 W, $W/FM = 2.90 \times 10^{10}$ J/kg.

erization of methane in the bell jar reactor. In general, in polymerization at relatively low W/FM (e.g., 10^8–10^9 J/kg) deposited materials cover the majority of electrode surface, although the nature of deposition varies depending on location as shown in Figure 1(a). Polymerization at higher levels of W/FM (e.g., 10^{10} J/kg) generally results in plasma etching of electrodes with little or no polymer deposition as shown in Figure 1(b). In many cases, the patterns that develop on electrodes are between these two extreme cases; i.e., a portion of electrode in the shape of a circular band remains uncoated and various depositions occur in circular bands inside and outside of the uncoated zone.

How and what kind of patterns develop on the electrodes are important factors which influence the current–voltage (C–V) relationship of the glow-discharge polymerization process. When plasma polymerization is started using a clean electrode surface, the C–V curve obtained for a plasma polymerization system is dependent on (i) the type of monomer, (ii) the flow rate, and (iii) the state of the electrode surface. Examples of the change of C–V relationship for plasma polymerization performed by maintaining a given discharge wattage are shown in Figures 2 and 3. Figure 2 represents change of current and voltage when plasma polymerization of allylamine was carried out using a clean stainless electrode. Shortly after plasma is initiated, rather sharp drops of voltage and increase of current are generally observed. This initial change may be due in part to the rising of the temperature of the electrode. The initial change tends to level off within 30 min and a reversal of the changes starts to take place, i.e., increase of voltage and decrease of current. The second trend continues, under

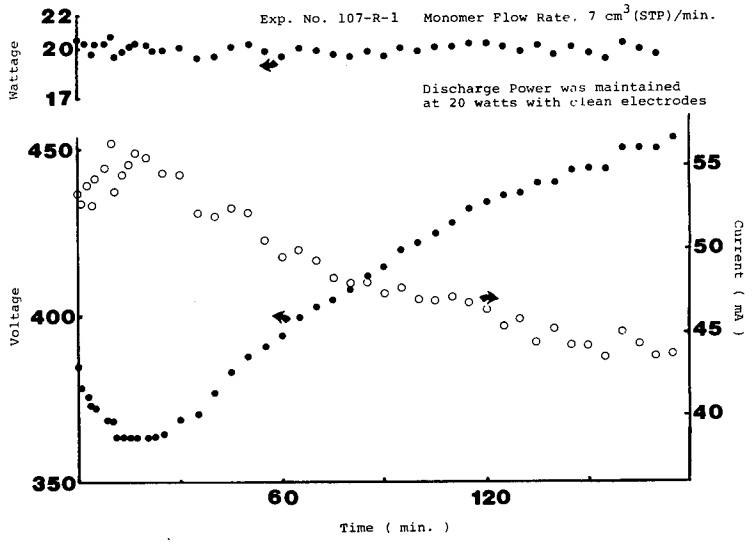

FIG. 2. Change of discharge voltage and current to maintain a constant discharge wattage of plasma polymerization of allylamine with the operation time. The operation was initiated with cleaned electrodes; discharge power was maintained at 20 W with clean electrodes; monomer flow rate 7 cm³ (STP)/min.

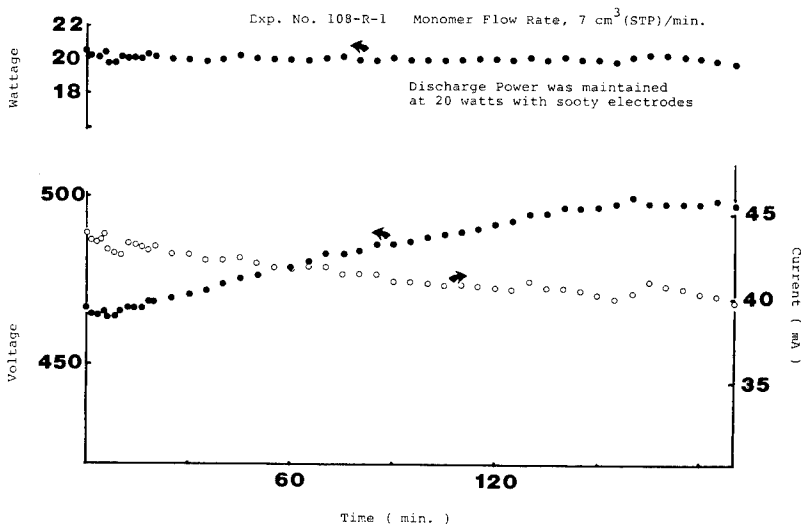

FIG. 3. Continuation of plots shown in Fig. 2. The operation was initiated using the same electrodes on the following day; discharge power was maintained at 20 W with sooty electrodes.

a given set of conditions, for up to approximately 3 h. This change seems to be due to partial covering of the electrode surface by plasma polymer deposition decreasing the effective area of electrode surface to sustain plasma. When plasma polymerization is started again using the same electrodes, after the system has been cooled down overnight, the *C–V* relationship appears as if plasma polymerization had continued, as shown in Figure 3, and the changes become smaller and smaller with time, finally reaching a dynamic steady state in which no change in current and voltage (to maintain a given wattage) is observed. The initial value (for clean electrodes) of 380 V and 53 mA changed to 500 V and 40 mA in the steady state. If such a set of conditioned electrodes is used for plasma polymerization under different conditions, reconditioning of electrodes takes place and the *C–V* relationship changes with time. The change in such a case may be similar to that shown in Figures 2 and 3 or in opposite direction, i.e., decrease of voltage and increase of current, depending on whether the new set of conditions allows more deposition of polymer on the electrode or exposes more metal surface compared to the steady state obtained by the previous set of conditions. It is obvious that the process of electrode conditioning due to the extent of coverage of the electrode surface significantly affects the control of plasma polymerization process.

Ambient Temperature of Plasma

The results of ambient-temperature measurements taken by inserting a thermocouple into the interelectrodes space, where deposition of plasma polymer onto moving substrates occurs, during the plasma polymerization of allylamine are summarized in Figure 4. The ambient temperature of plasma increases in

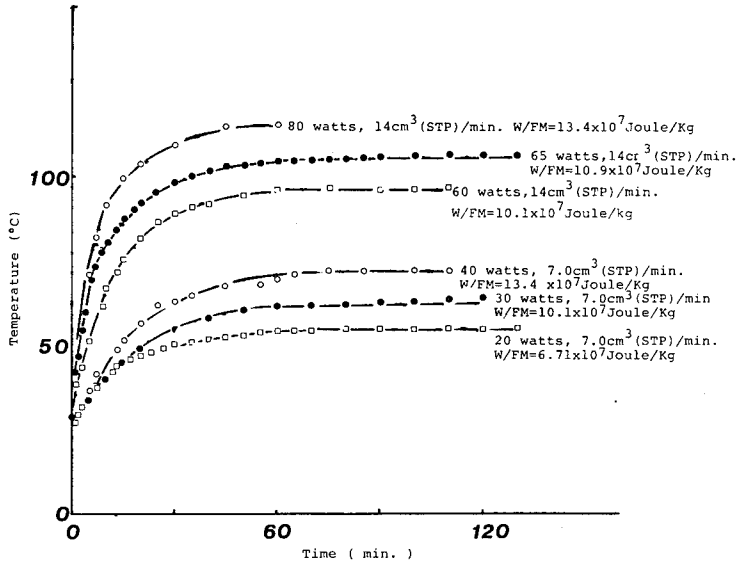

FIG. 4. Change of ambient temperature of plasma measured by a thermocouple with operation time: *upper plots:* (○) 80 W, 13 cm^3 (STP)/min, $W/FM = 13.4 \times 10^7$ J/kg; (●) 65 W, 14 cm^3 (STP)/min, $W/FM = 10.9 \times 10^7$ J/kg; (□) 60 W, 14 cm^3 (STP)/min, $W/FM = 10.1 \times 10^7$ J/kg; *lower plots:* (○) 40 W, 7.0 cm^3 (STP)/min, $W/FM = 13.4 \times 10^7$ J/kg; (●) 30 W, 7.0 cm^3 (STP)/min, $W/FM = 10.1 \times 10^7$ J/kg; (□) 20 W, 7.0 cm^3 (STP)/min, $W/FM = 6.7 \times 10^7$ J/kg.

the early stage of plasma polymerization and reaches a steady-state value in approximately 30–60 min depending on the conditions of plasma polymerization. The temperature rise due to plasma polymerization in the steady state is proportional to the discharge wattage as shown in Figure 5. While the polymerization in plasma is dependent on the composite parameter W/FM, the ambient tem-

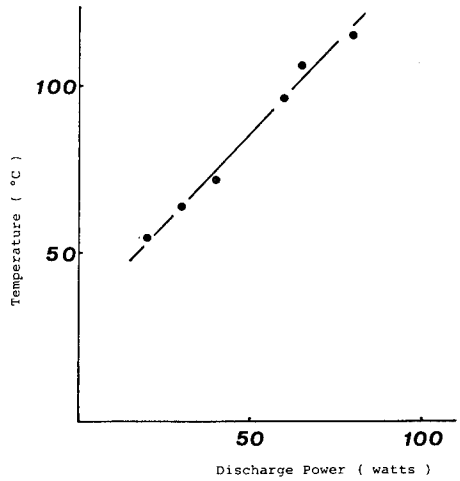

FIG. 5. Dependence of ambient plasma temperature on discharge wattage.

perature of plasma is dependent on W. In a nonequilibrium plasma, electron temperature (e.g., 60,000 K) is not in equilibrium with the temperature of positive ions and neutral species. Therefore the true meaning of such a temperature measurement is difficult to interpret. It has been observed, however, that when high wattage is employed, the hollow fiber substrates used for membrane preparation often break, indicating that thermal effects at high wattage indeed play an important role.

It should be noted that plasma polymerization at relatively high W/FM can be accomplished without excessive temperature rise by employing a lower flow rate at reduced wattage to avoid excessive heating of delicate substrates.

EFFECT ON PROPERTIES OF PLASMA POLYMERS

The C–V relationships as a function of time shown in Figures 2 and 3 are taken under the conditions necessary to maintain a constant wattage. If plasma polymerization is carried out by maintaining discharge current, then the drift of discharge wattage results. How these changes in discharge conditions affect the properties of plasma polymers is important for their continuous operation. Perhaps the most important factor in this respect is whether plasma polymerization is carried out in (i) wattage-controlled or (ii) flow-rate-controlled domains. Plasma polymerization can be generally divided into the two above-mentioned cases. In the first case, there are plenty of monomers available in a reactor system and

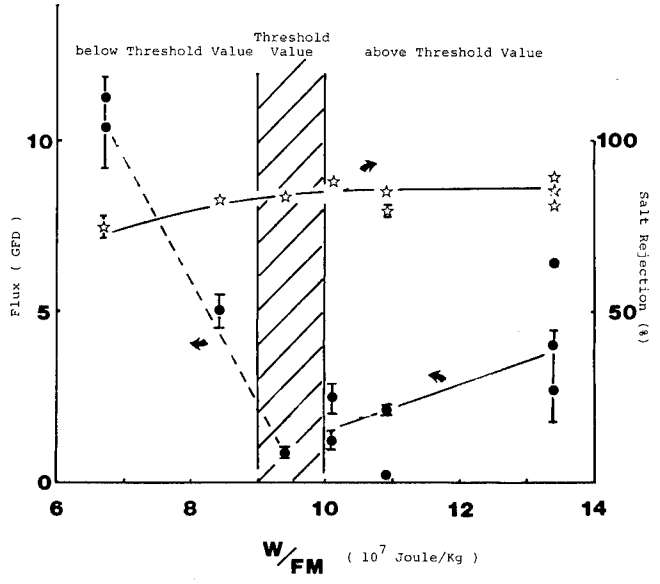

FIG. 6. Reverse osmosis characteristics of plasma polymer of allylamine as a function of operating parameter given by W/FM, where W is wattage and FM is mass flow rate of monomer. The left side of the threshold value represents the discharge-power-controlled region and the right side is the flow-rate-controlled region.

the discharge wattage is the rate-determining step. In the latter case, provision of sufficient monomer by the mass flow rate is the rate-determining step in plasma polymerization. These situations can be easily identified by observing the dependence of deposition rate or system pressure on discharge wattage; i.e., these parameters are dependent on wattage in the former case and independent of wattage in the latter case. In between these cases there is usually a transitional zone which can be identified by a threshold value with a certain range of W/FM. Some properties of plasma polymers are highly dependent on whether polymers are prepared under wattage-controlled or flow-controlled conditions. In Figure 6, the dependence of reverse osmosis characteristics of plasma polymers of allylamine deposited on porous hollow fibers of polysulfone by a semicontinuous method on the parameter W/FM is shown [2]. While the salt rejection tends to increase monotonically with increasing W/FM, the water flux has completely different dependence in these two zones of plasma polymerization conditions; i.e., an above-threshold value corresponds to the flow-rate-controlled (wattage-independent) case.

The effect of change of discharge conditions with time on the properties of plasma polymers largely depends on (i) whether polymerization is in a wattage-controlled region or a flow-rate-controlled region, and (ii) whether the change occurs crossing the zones. In other words, if polymerization is performed in the flow-rate-controlled case and the change of discharge conditions is within the range of the case, the effect on the properties is generally negligibly small. In the wattage-controlled case, the changes in discharge conditions cause fluctuation of properties and it is more difficult to obtain high reproducibility of plasma polymerization.

CONCLUSION

These results indicate that a continuous operation of plasma polymerization provides much higher consistency of the process than does batch operation. The often feared inconsistency of plasma polymerization is largely due to uncontrollable or difficult-to-control factors associated with batch operation of plasma polymerization which can be virtually eliminated in continuous operation.

REFERENCES

[1] P. J. Heffernan, K. Yanagihara, Y. Matsuzawa, E. E. Hennecke, E. W. Hellmuth, and H. Yasuda, *Ind. Eng. Chem. Prod. Res. Dev.*, to appear.
[2] Y. Matsuzawa and H. Yasuda, *Ind. Eng. Chem. Prod. Res. Dev.*, to appear.
[3] A. Morinaka and Y. Asano, *J. Appl. Polym. Sci., 27,* 2139 (1982).
[4] P. J. Dynes and D. H. Kaelble, in *Plasma Chemistry of Polymers,* M. Shen, Ed., Dekker, New York, 1976.
[5] N. Inagaki and H. Yasuda, *J. Appl. Polym. Sci., 26,* 3557 (1981).
[6] S. Yamaguchi, G. Sawa, and M. Ieda, *Kobunshi Ronbunshu, 38,* 623 (1981).
[7] R. L. Cormia, K. N. Tsujimoto, and S. Andresen, U.S. Pat. 4,013,532 (1977).
[8] N. Morosoff, W. Newton, and H. Yasuda, *J. Vac. Sci. Technol., 15*(6), 1815 (1978).

[9] H. Yasuda and N. Morosoff, in *Plasma Polymerization,* ACS Symp. Ser. No. 108, M. Shen and A. T. Bell, Eds., Am. Chem. Soc., Washington, DC, 1979.
[10] N. Inagaki and H. Yasuda, *J. Appl. Polym. Sci., 26,* 3425 (1981).
[11] K. Yanagihara and H. Yasuda, unpublished data.
[12] H. K. Yasuda, in *Plasma Polymerization,* ACS Symp. Ser. No. 108, M. Shen and A. T. Bell, Eds., Am. Chem. Soc., Washington, DC, 1979.

Author Index

Published Applied Polymer Symposia

1965	No. 1	High Speed Testing, Vol. V Co-Chaired by A. G. H. Dietz and Frederick R. Eirich
1966	No. 2	Thermoanalysis of Fibers and Fiber-Forming Polymers Edited by Robert F. Schwenker, Jr.
	No. 3	Structural Adhesives Bonding Edited by Michael J. Bodnar
1967	No. 4	Weatherability of Plastic Materials Edited by Musa R. Kamal
	No. 5	High Speed Testing, Vol. VI: The Rheology of Solids Co-Chaired by Rodney D. Andrews, Jr. and Frederick R. Eirich
	No. 6	Fiber Spinning and Drawing Edited by Myron J. Coplan
1968	No. 7	Polymer Modification of Rubbers and Plastics Edited by Henno Keskkula
1969	No. 8	International Symposium on Polymer Modification Edited by K. A. Boni and F. A. Sliemers
	No. 9	High Temperature Resistant Fibers from Organic Polymers Edited by J. Preston
	No. 10	Analysis and Characterization of Coatings and Plastics Edited by Claude A. Lucchesi
	No. 11	New Polymeric Material Edited by Paul F. Bruins
	No. 12	High Speed Testing, Vol. III: The Rheology of Solids Co-Chaired by Rodney D. Andrews, Jr. and Frederick R. Eirich
1970	No. 13	Membranes from Cellulose and Cellulose Derivatives Edited by Albin F. Turbak
	No. 14	Silicone Technology Edited by Paul F. Bruins
	No. 15	Polyblends and Composites Edited by Paul F. Bruins
1971	No. 16	Scanning Electron Microscopy of Polymers and Coatings Edited by L. H. Princen
	No. 17	Mechanical Performance and Design in Polymers Edited by O. Delatycki
	No. 18	Proceedings of the Fourth International Wool Textile Research Conference Edited by Ludwig Rebenfeld
1972	No. 19	Processing for Adhesives Bonded Structures Edited by Michael J. Bodnar
1973	No. 20	United States—Japan Seminar on Polymer Processing and Rheology Edited by D. C. Bogue, M. Yamamoto, and J. L. White
	No. 21	High-Temperature and Flame-Resistant Fibers Edited by J. Preston and J. Economy
	No. 22	Polymeric Materials for Unusual Service Conditions Edited by Morton A. Golub and John A. Parker
1974	No. 23	Scanning Electron Microscopy of Polymers and Coatings. II Edited by L. H. Princen
	No. 24	Technological Aspects of Mechanical Behavior of Polymers (Witco Award Symposium) Edited by R. F. Boyer
	No. 25	Acrylonitrile in Macromolecules Edited by E. M. Pearce

1975	No. 26	Polymerization and Polycondensation Processes Edited by N. A. J. Platzer
	No. 27	Fiber and Yarn Processing Edited by J. L. White
	No. 28	Proceedings of the Eighth Cellulose Conference (Part I, 1975; Part II, 1976; Part III, 1976) Edited by T. E. Timell
1976	No. 29	New and Specialty Fibers Edited by J. Economy
1977	No. 30	Cationic Graft Copolymerization Edited by J. P. Kennedy
	No. 31	Fiber Science Edited by M. Lewin
	No. 32	Durability of Adhesive Bonded Structures Edited by M. J. Bodnar
1978	No. 33	Fiber Structure and Properties Edited by J. L. White
	No. 34	Polymer Analysis Edited by T. K. Wu and J. Mitchell, Jr.
1979	No. 35	Long-Term Properties of Polymers and Polymeric Materials Edited by B. Rånby and J. F. Rabek
1981	No. 36	Commodity and Engineering Plastics Edited by N. Platzer
1983	No. 37	Proceedings of the Ninth Cellulose Conference (Parts I and II) Edited by A. Sarko
1984	No. 38	Plasma Polymerization and Plasma Treatment Edited by H. K. Yasuda
	No. 39	Wood Adhesives—Present and Future Edited by A. Pizzi
	No. 40	Chemistry and Technology of Rubber Edited by J. B. Donnet and A. Vidal

All of the above symposia may be individually purchased from the Subscription Department, John Wiley & Sons, Inc.